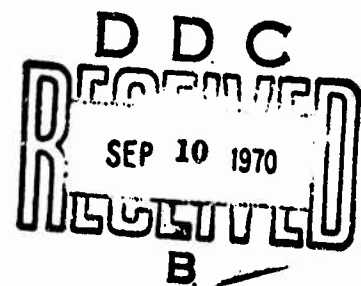Report No. FAA-NO-70-10

SONIC BOOM MODELING INVESTIGATION OF TOPOGRAPHICAL AND ATMOSPHERIC EFFECTS

A.B. Bauer and C.J. Bagley
Douglas Aircraft Company
McDonnell Douglas Corporation
Long Beach, Calif. 90801

JULY 1970

FINAL REPORT

Prepared for

214

The contents of this report reflect the views
of the Douglas Aircraft Company which is
responsible for the facts and the accuracy of
the data presented herein. The contents do not
necessarily reflect the official views or policy
of the Department of Transportation. This report
does not constitute a standard, specification or
regulation.

1. Report No. FAA-NO-70-10	2. Government Accession No.	3. Recipient's Catalog No.
4. Title and Subtitle SONIC BOOM MODELING INVESTIGATION OF TOPOGRAPHICAL AND ATMOSPHERIC EFFECTS		5. Report Date July 1970
		6. Performing Organization Code
7. Author(s) A.B. Bauer and C.J. Bagley		8. Performing Organization Report No. MDC-J0734/01
9. Performing Organization Name and Address Douglas Aircraft Company McDonnell Douglas Corporation Long Beach, California 90801		10. Work Unit No.
		11. Contract or Grant No. FA 69WA-2114
12. Sponsoring Agency Name and Address Department of Transportation Office of Noise Abatement Washington, D.C. 20005		13. Type of Report and Period Covered Final Report June 1969 - July 1970
		14. Sponsoring Agency Code

15. Supplementary Notes

16. Abstract

An experimental program has been undertaken to study the effects of topographical and structural shapes on sonic boom focusing and to study the effects of atmospheric turbulence on sonic boom signatures. These effects were modeled by firing projectiles and by allowing the projectile N waves to interact with model shapes and with turbulent jets. The wave interactions were studied by means of shadowgraph pictures and microphone pressure records. The boom focusing parameters were related to the work of Ting and Pan. A canyon model showed wave amplification factors as large as 14 for a special shape and a particular wave direction of propagation. A large amount of statistical information was obtained from the turbulence interactions. This information was studied and found to be in essential agreement with the theory of Crow, but the mechanisms of the shock front breakup and of certain nonlinear features are not understood. Turbulence scaling parameters are developed and used to relate the model results to full scale.

17. Key Words sonic boom turbulence atmosphere topography	18. Distribution Statement Availability is unlimited. Document may be released to the Clearinghouse for Federal Scientific and Technical Information, Springfield Virginia 22151, for sale to the public.
19. Security Classif. (of this report) Unclassified	20. Security Classif. (of this page) Unclassified	21. No. of Pages	22. Price

Form DOT F 1700.7 (8-69)

PREFACE

During the course of this work the authors have benefited from contact with several colleagues. Dr. Bradford Sturtevant and Dr. Anatol Roshko have been of particular help in offering suggestions for the test program and in relating other sonic boom studies to the present work. Dr. John Laufer has offered valuable suggestions for the generation and measurement of turbulent flows. Mr. A.M.O. Smith has encouraged the work from its earliest stages and has offered his guidance throughout the program.

TABLE OF CONTENTS

Page

3

LIST OF ILLUSTRATIONS

5

LIST OF TABLES

LIST OF ABBREVIATIONS AND SYMBOLS

The list below gives definitions for the more important symbols. Variables that are defined and used in only one section are excluded from the list below because it is felt that the need to refer to a list of definitions for such variables will seldom arise. In several instances where it seemed the chances for confusion were slight, a symbol is given one meaning in one section and another meaning in another section. For example, I is used to denote hot-wire current in Appendix D and to denote the value of an integral in section 6. In each instance I is used immediately after it is defined and nowhere else. Thus I does not appear in the list below.

c	speed of sound
e_1	root-mean-square value of wave analyzer output
E_1	spectral energy distribution function
f	longitudinal correlation coefficient
f_{ij}	longitudinal correlation coefficient between points i and j
g	transverse correlation coefficient
H_i	normalized pressure fluctuation, see equations (6) through (10)
H_{MAX}	peak overpressure divided by overpressure of basic N-wave for zero turbulence
IF	boom intensification factor
L	turbulence integral scale
L_s	signature length measured along the ground plane
M	Mach number
N	number of signatures
n	frequency of turbulent fluctuations
P	probability
P_i	boom pressure signature amplitude, $i = 1, 2, 3, 4,$ or 5 corresponding to times t equal to $0, 5, 10, 20,$ or 40 percent t_s, respectively

11

P_{io} P_i for basic signatures having zero turbulence interaction, $i = 1, 2, 3, 4,$ or 5 corresponding to times t equal to 0, 5, 10, 20 or 40 percent t_s, respectively

P_{MAX} maximum value of boom pressure signature

R radius of Crow's paraboloid

t time measured as defined in Figure 19; $t = 0$ corresponds to τ seconds after the start of the boom disturbance wherein τ is defined as the time for the measuring instrument to respond to a square wave passing by the instrument in a direction normal to the wave front

t_c critical time derived by Crow

t_i time t corresponding to pressure P_i or P_{io}

t_{MAX} time t for peak pressure P_{MAX}

t_s signature time between leading and trailing shocks

U fluid velocity in the x-direction

$\bar{U}$ mean value of U

u fluctuating component of U

u' root-mean-square value of u

x coordinate axis

y coordinate axis

z coordinate axis

δ turbulent layer thickness

λ_f turbulent dissipation scale

$\langle \psi^2(t) \rangle$ ensemble average of H_i

1. INTRODUCTION

The introduction of the Supersonic Transport (SST) into commercial service promises a major technical advance as great as that provided by the advent of the present jet transport a decade ago. The feasibility of routine SST operations will be largely a function of the severity of the sonic boom problem.

This problem is compounded by interactions between the sonic boom and atmospheric turbulence. Interactions between the sonic boom and topographical features such as canyons or buildings are also important. Several schemes have been proposed for studying these interactions on a model scale. The topographical interactions are no doubt much simpler to understand and to model because these interactions are the result of the reflection of weak shock and expansion waves which are well understood. On the other hand, the turbulence interactions are not at all well understood; in fact, the atmospheric turbulence itself is far from being fully understood. A turbulence interaction theory has been put forth by Crow (Reference 1). This theory presents a rough physical picture of how the observed pressure fluctuations are connected with earlier shock-turbulence interactions along the surface of a "paraboloid of dependence", but the theory fails to give a finite answer for the pressure fluctuations or the perturbed shock structure at the leading and trailing shock waves in the distorted boom N wave. George (Reference 2) has developed a mathematical theory of shock thickening at the leading part of the boom N wave, and he suggests that his analysis can be coupled with Crow's theory to give the complete explanation of observations. Pierce (References 3 and 4) has studied the focusing and defocusing of wave fronts by turbulence using the methods of geometrical acoustics; this leads to the consideration of caustics and multiple fronts.

Several laboratory methods are possible for studying boom-turbulence interactions. Perhaps the most obvious one and the one that is reported on here is to fire model projectiles in order to create a sharp sonic boom and to allow the boom to pass through modeled atmospheric turbulence. A second scheme would be to build a very large, low-pressure shock tube which could be used easily to generate the first half of an N wave. The wave could then be passed through a turbulent region in the shock tube. The problem with the shock tube is that very long tube lengths are required for a sharp front to develop on the weak wave; therefore, the tube must be designed to produce

13

fairly clean and sharp waves at the outset. Then wave interactions with turbulence will give rise to pressure fluctuations that will not be confused with irregularities in the basic wave.

The McDonnell Douglas Aerophysics Laboratory Ballistic Range has been used to fire projectiles of diameters between 0.22 inches and 1.50 inches at Mach numbers between 1.3 and 3.0. The resulting sonic booms were reflected from a "ground plane" located 15 feet from the projectile path. The boom overpressures were measured by special high-frequency microphones. This experimental setup is discussed in section 2. The results of boom interactions with topographical models are reported in section 3 and analyzed in section 4. The results of boom interactions with turbulent jets are reported in section 5 and analyzed in section 6. The model results are related to the full-scale problem insofar as is possible. A discussion of scaling laboratory sonic boom work is given in section 7. Conclusions are given in section 8, and references to related work are given in section 9.

The experimental work was organized into a series of four tasks. Tasks I and II have been concerned with the boom interactions with turbulence, as reported in section 5. Tasks III and IV have been concerned with the boom interactions with topographical models, as reported in section 3. Tasks I and III were carried out in October 1969 for the purpose of demonstrating the validity of the testing techniques; these were followed by the much more extensive Tasks II and IV in February and March 1970. Most of the data used to obtain the conclusions reported in section 8 were taken during the course of Tasks II and IV.

2. EXPERIMENTAL ARRANGEMENT

The experiments were performed in the ballistic range at the McDonnell Douglas Aeorphysics Laboratory at El Segundo. The ballistic range was modified by erecting a barricade at the end of the range. The purpose of the barricade was for housing the pressure sensors, the topographical models, and the turbulence generation equipment at a distance of approximately 15 feet from the projectile path. This distance was chosen so that the N-wave overpressures generated by the projectiles would not be too large. A significantly larger distance was not available without extensive range modifications, and a shorter distance would have increased the overpressure. For the 15 foot distance the ground plane reflected overpressures ranged from about 0.12 to 0.50 psi, which are much larger than the 0.02 psi typical for the SST. The scaling of this data is discussed further in section 6.

A. Ballistic Range, Barricade, and Projectile Descriptions.

Figure 1 is a plan view showing a portion of the ballistic range tank and the barricade. The inside dimensions of the barricade room are 22 by 23 feet with a ceiling height of more than 10 feet. The projectile path is 5 feet from the floor. A plywood diagonal wall was built and hinged about the point 0 so that the angle β_w could be varied. In the test program β_w was set at the angle $\sin^{-1}(1/M)$, where M was the projectile Mach number, so that the projectile shock cones would be approximately perpendicular to the wall. However, since it was determined that the observed sonic boom signatures were not significantly affected by the angle β_w, for the later testing β_w was maintained at about 23°, corresponding to M = 2.5.

Along the north wall a vertical flat surface, hereafter called the "ground plane", was constructed for the purpose of holding the microphone and aspirating probe sensors. The sonic boom from the projectile was reflected from the ground plane, which corresponded to the reflection of a full-scale sonic boom over the ground surface. The ground plane was 15 feet from the projectile path, and 18 possible sensor locations were provided. Virtually all of the testing was performed using microphones located at points I, II, and III in figure 1. These were located at the same height above the floor, 5 feet, as the projectile path; the ground plane extended from 3 feet to 7 feet above the floor. Location II is 90 inches from the barricade east wall
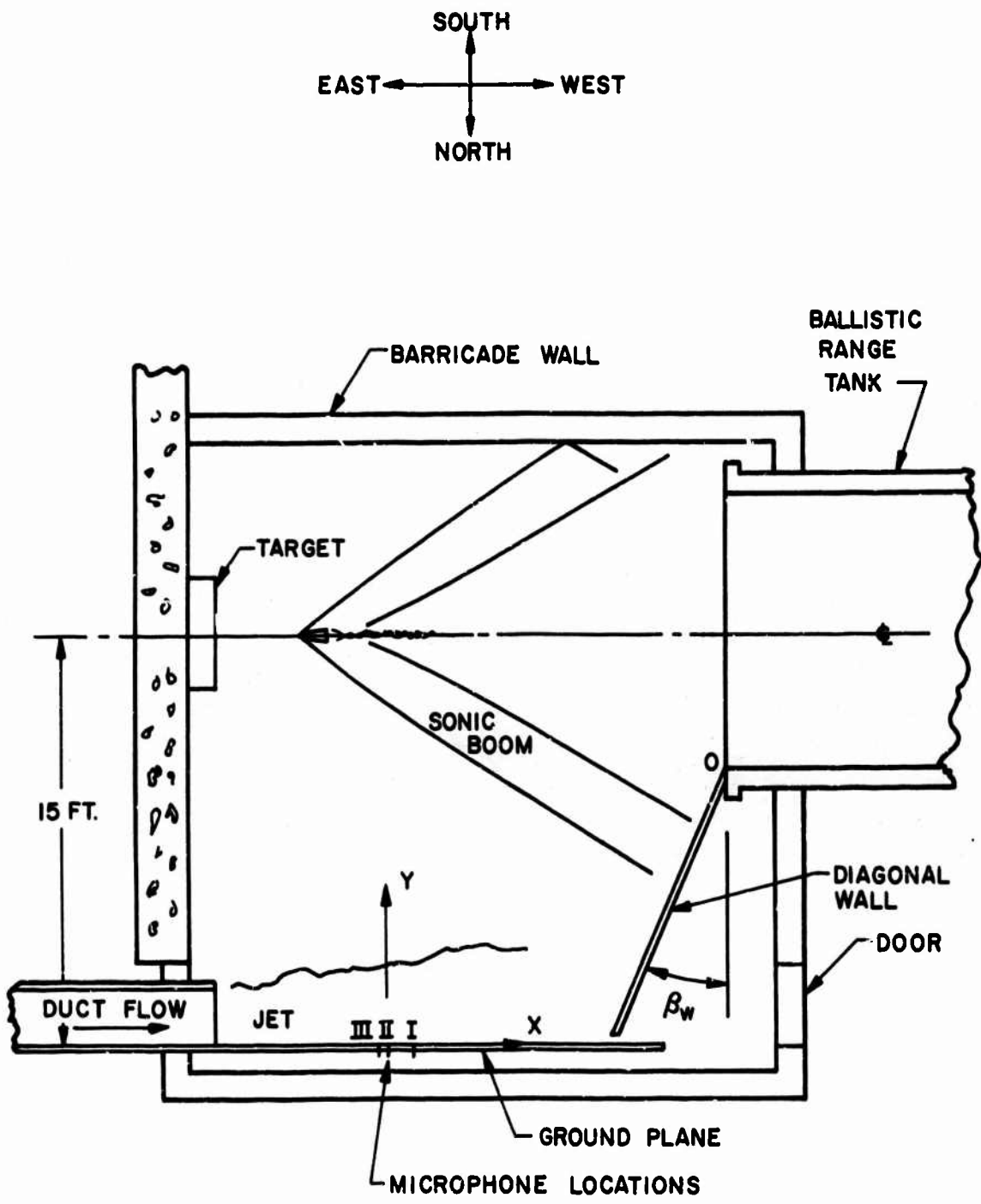
Figure 1 Plan view of barricade.

16

and 78 inches from the end of the blower duct. Locations I and III were
6 inches and 2 inches from location II, respectively.

The ground plane was constructed of 1/4-inch aluminum plate backed by
2-inch by 4-inch wood braces for rigidity. This assembly was screwed to short
projections from the vertical wall of the barricade. This produced a smooth
and rigid surface for the reflection of boom waves.

Shadowgraph pictures were taken by using a spark light source located
72 inches above the microphone locations, at the coordinate station $z = 72$ in.,
and at the coordinates x,y as shown on figure 1. The plane of the photo-
graphic film was 26 inches below the microphone locations, or $z = -26$ inches.
Therefore, flow-field features at the height of the microphones were magnified
by a factor of 98/72 by the light rays. The conical sonic boom wave fronts
which appear on the shadowgraphs are, of course, only those portions of the
wave approximately tangent to the spark light rays. These tangency points were
approximately 5 feet above the floor for wave fronts undistorted by turbulence.

The barricade was sufficiently dark and light-tight for taking shadowgraph
pictures. The barricade was built with double plywood walls filled with sand
for safety against any stray projectile which failed to hit the target area.
The target area was built of plastic foam, plywood, and mild steel sheets for
the purpose of catching and holding the projectiles.

The various projectiles used are shown in figure 2. The A projectiles
were fabricated from a Fansteel tungsten alloy having a specific gravity of
17, and from lexan plastic in such a manner as to keep the projectile center
of gravity as far forward as possible for aerodynamic stability. These pro-
jectiles had a mass of about 365 grams. When fired from the ballistic range
light gas gun, the projectiles proved to have remarkable armor-piercing ability.
Some difficulty was experienced at first in getting the lexan to retain its
shape during the gun launch, but this was overcome. The remaining projectiles
shown in figure 2 were rifle launched without difficulty. The projectile Mach
numbers were controlled by varying the powder charges appropriately.

17

5.055

3.375

TANGENT

1.5 DIA.

7.97 R.

"A"
MACHINED
PROJECTILE

1.540

1.028

2.43 R.

0.457 DIA.

"B"
MACHINED PROJECTILE

0.741

0.493

0.22 DIA.

"C"
MACHINED PROJECTILE

1.17 R.

NOTE:
DIMENSIONS ARE
IN INCHES

1.1

0.30 DIA.

"D"
0.30 CALIBER MILITARY
BULLET

1.33

0.46 DIA.

0.46 CALIBER
BULLET

0.71

0.22 DIA.

0.22 CALIBER
BULLET
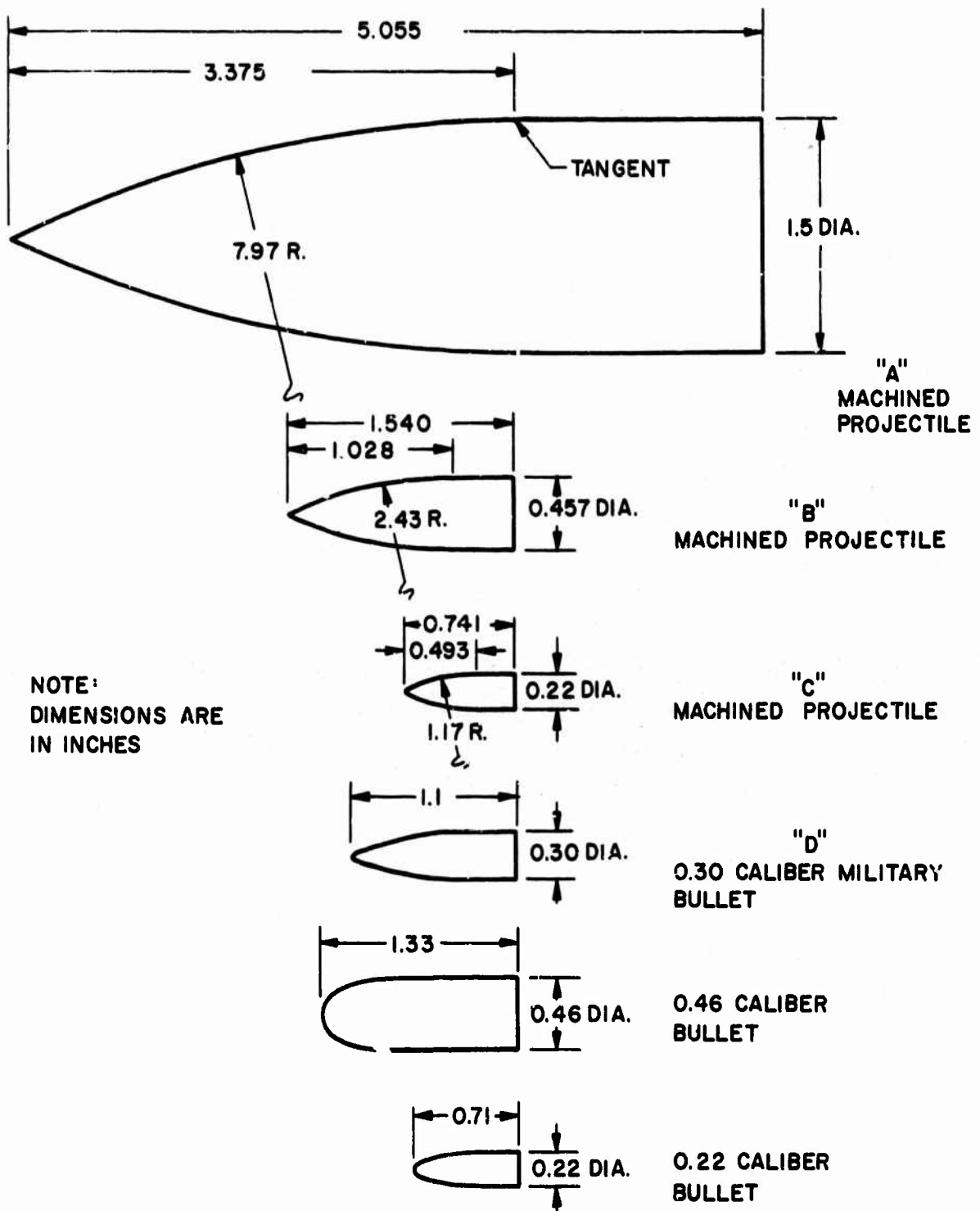
Figure 2 Projectile shapes

18

B. Topographical Model Description.

The topographical models used in the Task IV testing are shown in figures
3, 4, and 5. For Task III testing models essentially the same as shown in
figure 3a and in figure 4 for $\theta_c = 90^\circ$ were built. The Task III models were
built of wood. Later, when the Task IV models of figures 3 and 4 were built,
aluminum was used, which brought about a significant gain in quality. The
aluminum models had sharp corners and smooth flat surfaces to within about
0.002 inches of perfection. The canyon model shown in figure 5 was built from
wood and plaster of paris covered with several coats of grey lacquer; this
model was shaped to within about 1/32 inch of perfection except for corners
which were somewhat rounded.

The models of figure 3 were essentially two-dimensional with a length of
18 inches normal to the figure. They were mounted one at a time on the ground
plane (see figure 1) so that they extended 9 inches above and 9 inches below
the center of the ground plane at z = 0. For shadowgraph pictures, which were
meaningful only with the two-dimensional models, the spark source was aligned
with the corner marked V. Because of the divergence of the spark light rays,
the other corners of the models appeared as lines rather than points on the
shadowgraph film. The dots IV, V, and VI denote microphone locations which
were also at the center of the 18-inch model length. On the overhang model,
the overhang ℓ_m could be changed to 1, 2, 3, or 4 inches.

Figure 4 shows the corner models and microphone locations. One corner
model had the angle θ_c equal to 90°; the other had $\theta_c = 45^\circ$.

The canyon model, figure 5, was shaped by hollowing out the interior of
the rectangular shape to the surface defined by

$$x_c = \frac{1}{8} (y_c^2 + z_c^2)$$

where all lengths are measured in inches. This equation defines a paraboloid
of revolution. The microphone locations VII, VIII, and IX had the x_c, y_c,
z_c coordinates in inches of (8, 0, -8), (3.125, 0, -5), and (1.125, 0, -3),
respectively. The X, XI, and XII locations were (1, 0, 0), (2, 0, 0), and
(3, 0, 0), respectively.

19

DIRECTION OF PROJECTILE FLIGHT

NOTE: DIMENSIONS ARE
      IN INCHES

(a) STEP MODEL

GROUND PLANE

(b) PARALLEL
    WALL MODEL

(C) OVERHANG
    MODEL
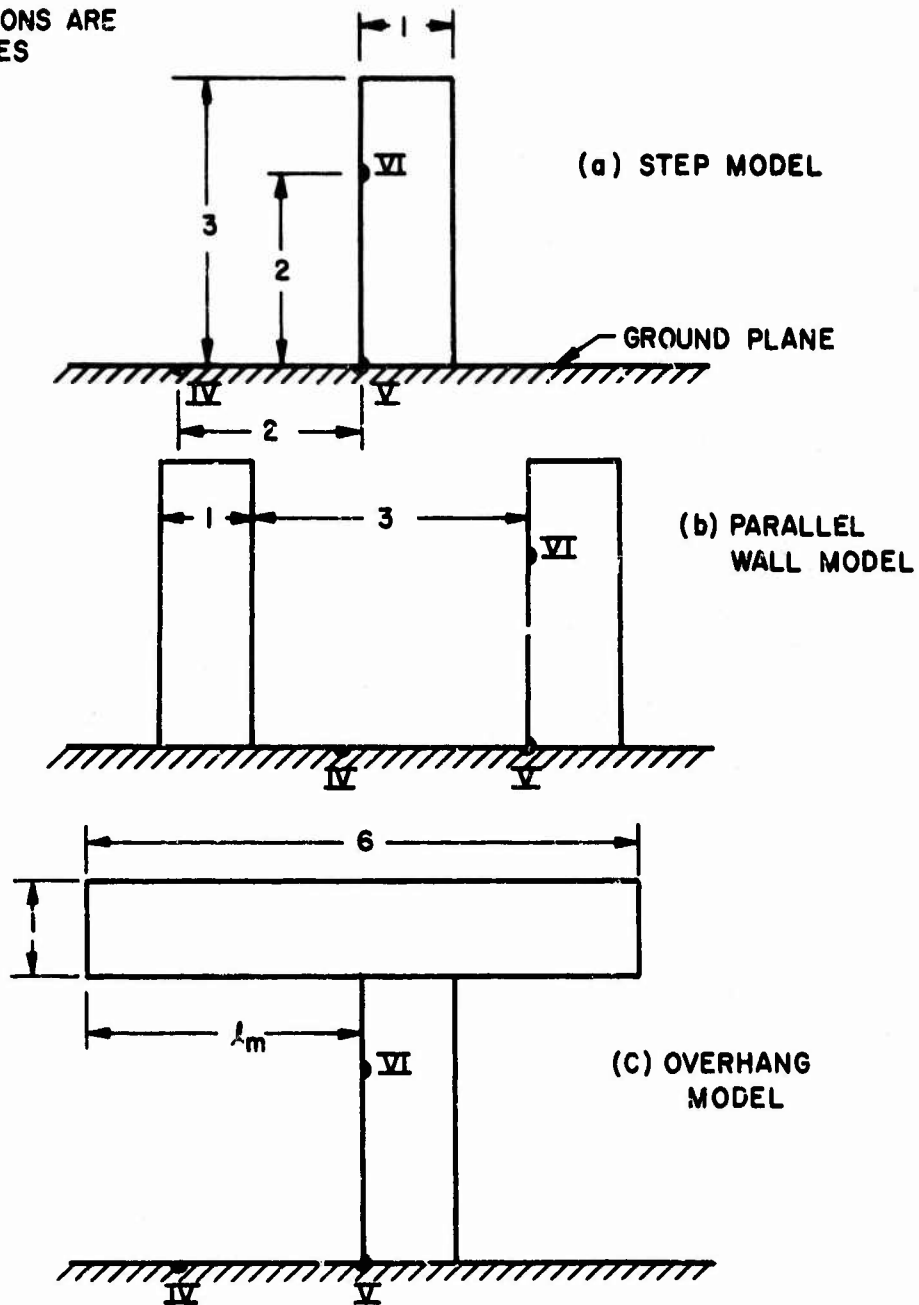
Figure 3 Two-dimensional topographical models as viewed looking in the +z
direction.

DIRECTION OF PROJECTILE FLIGHT

TOP VIEW

12

θ_c

IV •

V AND VI

NOTE:
DIMENSIONS ARE
IN INCHES

1

SIDE VIEW
LOOKING IN THE
+Z DIRECTION

3

VI

IV   V

GROUND PLANE
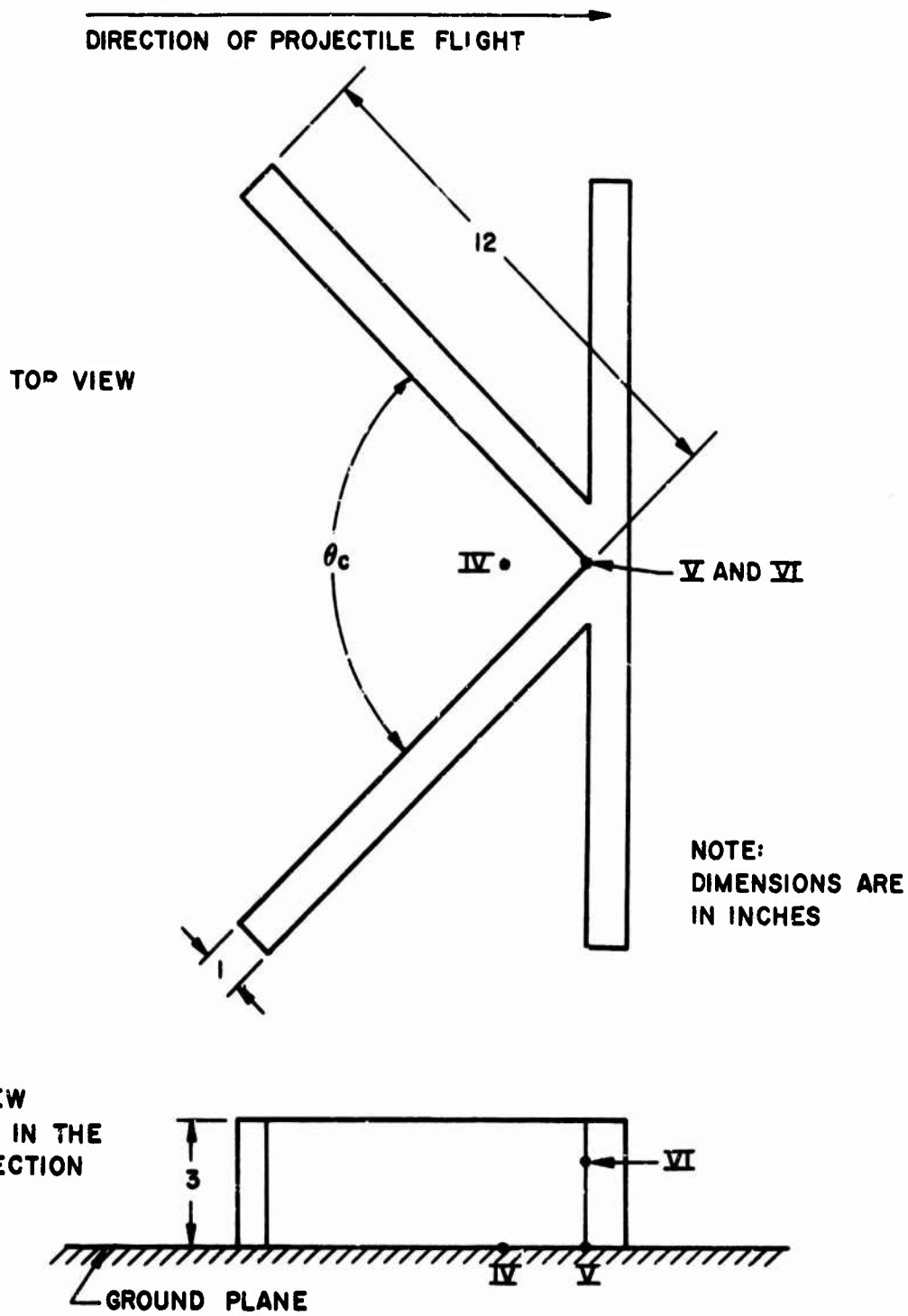
Figure 4   Corner topographical models.

TOP VIEW

NOTE: DIMENSIONS ARE
IN INCHES

SIDE VIEW,
LOOKING IN THE
+Z DIRECTION
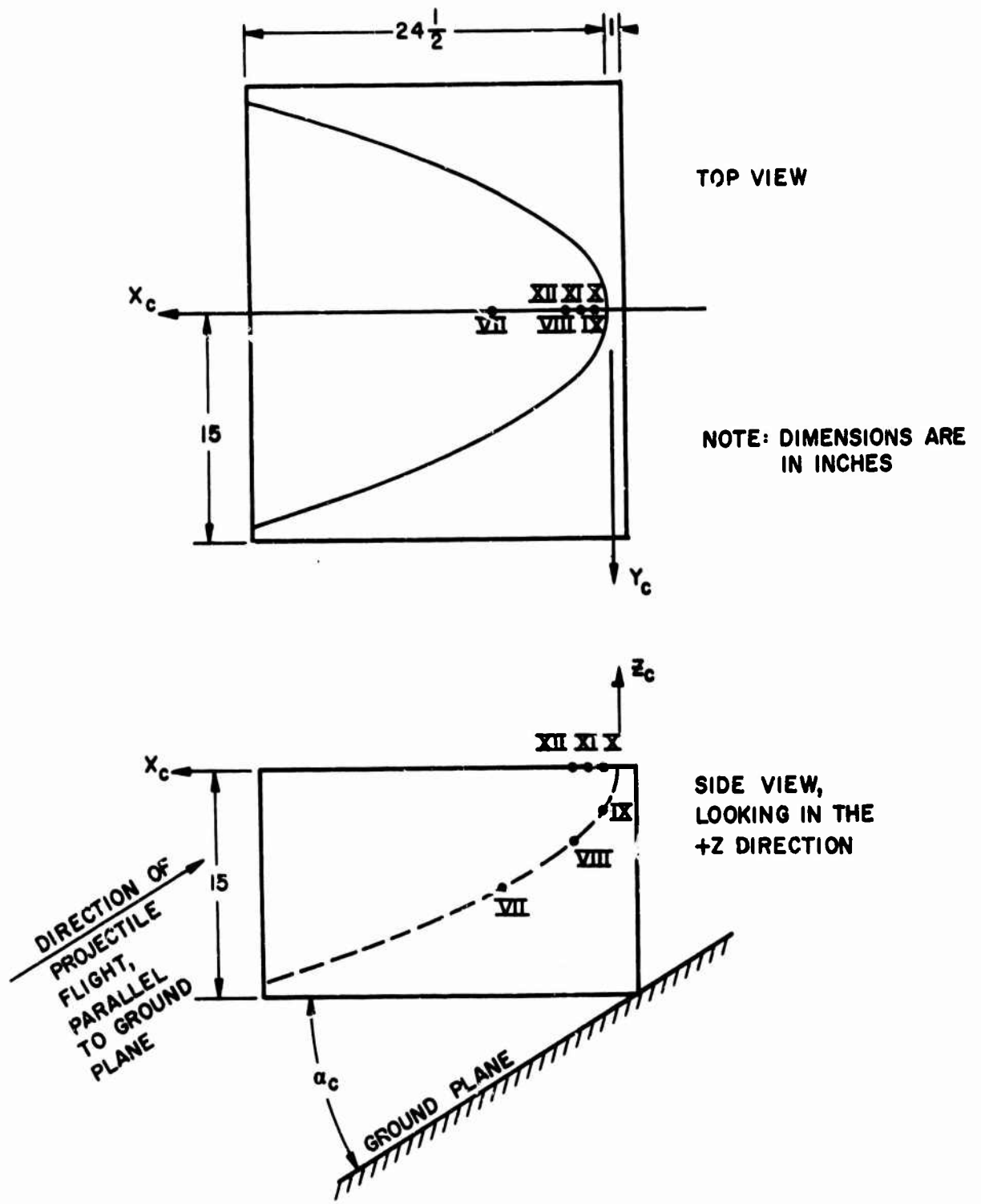
Figure 5 Canyon model.

C.   Turbulence and Thermal Generators.

Figure 1 shows the blower duct which was used to generate a turbulent jet. The duct cross section is 2 feet by 2 feet and hence the jet cross section was somewhat larger as given in section 5. The height of the duct and jet center-line above the floor was 5 feet, which corresponds to $z = 0$. Hence the sonic boom N wave was forced to travel through the turbulent stream before reaching the microphone locations.

The west end of the blower duct extended one foot inside the barricade. The other end of the 18-foot duct was attached to the output side of a large blower, which was driven by a 40-horsepower electric motor. Since the motor and blower speeds were constant, whereas the duct and jet velocities were intended to be variable, the duct was fitted with a large bypass valve so that only a fractional part, continuously variable from 0 to 1, of the blower air was used to form the jet. This arrangement was used throughout Task I. After Task I, Dr. John Laufer suggested that perhaps the bypass valve could contribute to flow nonuniformity and large-scale, low-frequency velocity fluctuations. He further suggested that the jet speed be regulated by constricting the air inlet to the blower. This was done for the Task II tests by a large constrictor plate just ahead of the blower inlet. The plate hole diameter was 24 inches; this plate was replaced as needed by one of three other plates having hole diameters of 20 inches, 16 inches, and 12 inches, respectively. The resulting duct velocities were 79, 66, 43, and 25 feet/sec., respectively, over all but the boundary-layer portions of the duct cross section. These speeds could be varied continuously by placing a solid plate over all or any part of the inlet plates. When the inlet plates were entirely removed the duct speed was 103 feet/sec. The blower evidently served as a turbulence generator in addition to the turbulence which arose naturally in the duct and the jet shear layers.

For the experiments this duct configuration was termed the "24-inch nozzle." Four other nozzles configurations were also used in the Task II program. Each of the additional configurations was obtained by adding an extension onto the basic duct or 24-inch nozzle. These additions are sketched in figure 6.

23

a) 4 INCH NOZZLE

GRID MADE UP FROM
3/4 IN. DOWELS ON
4 IN. CENTERS

b) 6 INCH NOZZLE

HONEYCOMB GRID
WITH 6 IN. CELLS

c) HI—SPEED NOZZLE NO. I

d) HI—SPEED NOZZLE NO. 2
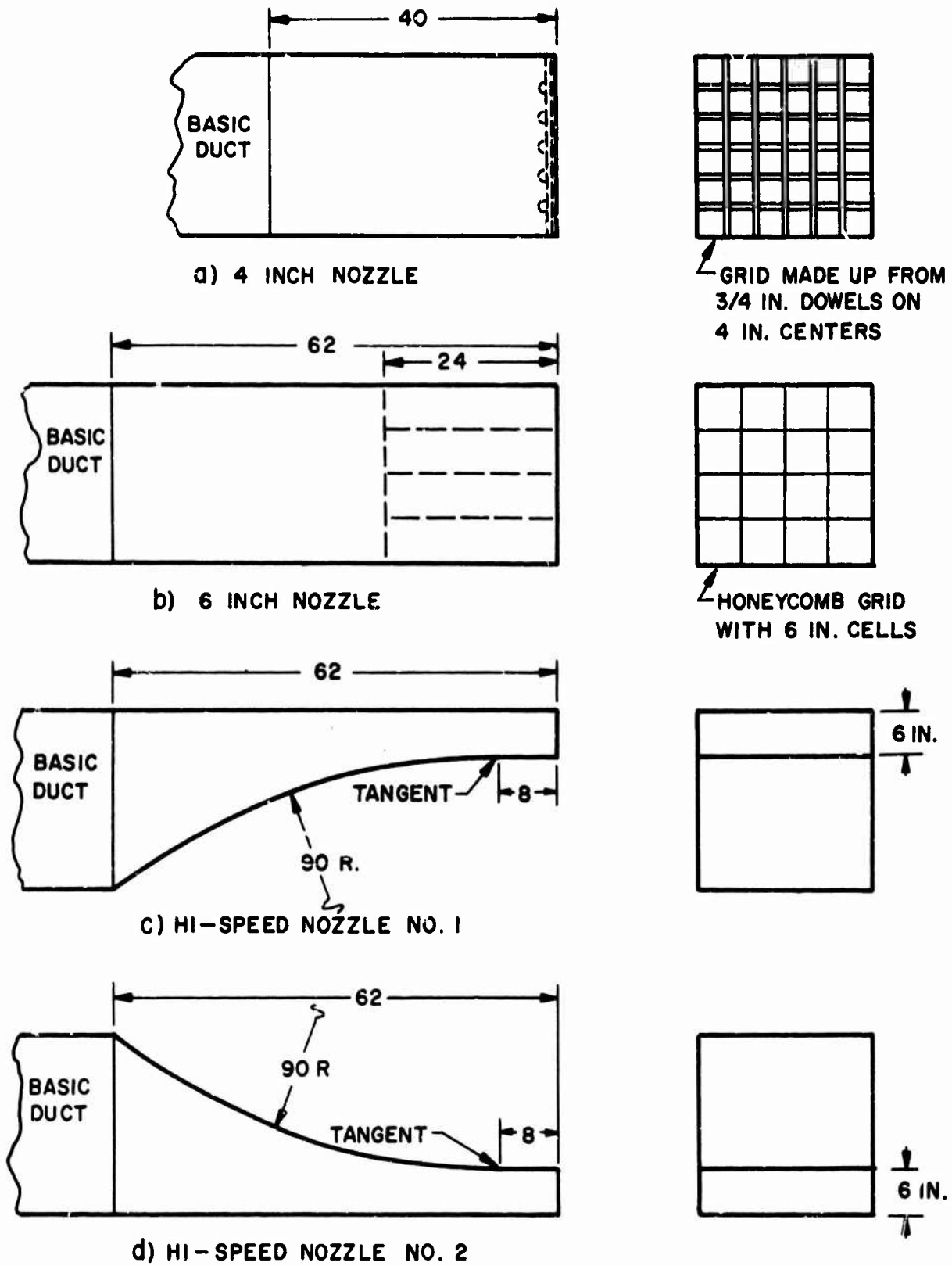
Figure 6   Duct extensions used in the task II program.

The 4-inch nozzle was so-called because of the grid of 3/4-inch dowels on 4-inch centers at the nozzle exit. The exit came within 38 inches of the plane x = 0 of figure 1.

The 6-inch nozzle was so-called because of the 6-inch grid honeycomb as shown in figure 6b. The honeycomb extended 24 inches upstream into the nozzle. The nozzle exit plane was 16 inches from the plane x = 0.

With the 4-inch and with the 6-inch nozzles the jet flow velocities were much the same as for the 24-inch nozzle. This was largely a result of the constant 2-foot by 2-foot cross section used in these nozzles. In contrast, the two nozzles shown in figures 6c and in 6d were designed with a 4-to-1 contraction ratio; at the exit plane these nozzles have a 2-foot by 0.5-foot cross section. At this cross section the flow speeds were 204 feet/sec. using the 24-inch inlet on the blower and 82 feet/sec. using the 12-inch inlet on the blower. Actually, only one high-speed nozzle was built; the two different configurations shown in figure 6 were obtained by orienting the one nozzle as shown before attaching it to the basic duct. The high-speed nozzle exit plane was located 16 inches from the plane x = 0.

The essential difference between the high-speed nozzle 1 and nozzle 2 is that in nozzle 1 the jet is separated from the ground plane and in nozzle 2 the jet flows as a wall jet along the ground plane. Originally plans were made for a third high-speed nozzle with a geometry intermediate between those of nozzles 1 and 2. This would have generated a jet closer to the wall than in the case of nozzle 1, but it would not have been a wall jet. As pointed out by Dr. Laufer, the jet from such a nozzle would not scatter a sonic boom differently than would the jet from nozzle 1. Therefore, the third nozzle was not built.

The characteristics of the various turbulent jets were measured and are reported in section 5. The various nozzles were designed, after consultation with Dr. John Laufer, to obtain several different turbulent scales and at the same time to generate a high turbulent intensity in relation to the jet speed. Since most of the literature on turbulent flows is concerned with homogeneous turbulence which is best obtained at a large distance downstream from a grid placed in the airstream, the turbulent intensity for most of the carefully recorded data is rather small compared to the stream speed. Therefore, not much

25

information on flows with a large turbulent intensity is available. This fact was somewhat of a hindrance to the nozzle designs, but the turbulence characteristics of the nozzles tested turned out to be essentially what was desired.

The design of the thermal generators also presented a unique challenge. In the proposal for this work the thermal generators are shown simply as an electrical heater surrounded by a box-like duct for channeling the heated air upward. As soon as design calculations for such a generator were started, the results showed that if the goal of air heated $200^{\circ}F$ above ambient were reached, then the upward velocity of natural convection would be so large that the jet diameter would be necessarily small compared to the dimensions of the boom signature scale. This was done under the assumption of limiting the heat input to less than one kilowatt. As a result, the heated jet would rapidly mix with the surrounding cold air and the jet column would be cooled so that not much interaction would be obtained between the warmed air and the boom. A large upward velocity was also undesirable from the point of view of possibly acting as a shear layer interaction rather than a thermal interaction with the sonic boom. The final solution to these problems was to design the generators as illustrated in figure 7.

The box illustrated in figure 7 is used to house the electrical heater whose output is variable between 0 and 750 watts. A commercial laboratory hot plate was used and ten large aluminum fins were added to the hot plate for good transfer of the heat to the air inside the box. The box exterior was insulated to minimize heat loss. At the top of the box was placed a stack of 52 parallel aluminum tubes each with an inside diameter of 0.444 inches, an outside diameter of 0.500 inches, and a length of 12 inches. The stack was welded together to form an approximately hexagonal cross section as shown. This size of tubing was calculated so that the upward mean speed of the convection currents through the tubes would be only about 3 feet/sec. with a 750 watt input.

Above the stack natural convection results in an increased thermal velocity, but the total heat flux in the thermal should remain constant at any height. Measurements showed that when the generator was turned up full the temperature of the air at the top of the stack was uniform at about $216^{\circ}F$ above ambient. At ten inches above the center of the stack the temperature

26

TOP VIEW OF TUBING
SHOWING TUBE
ARRANGEMENT

|←— 4 IN. —→|

CROSSECTIONAL VIEW
OF INSULATION,
TUBING, BOX, AND
HEAT TRANSFER
FINS

SIDE VIEW OF TUBING

10 HEAT TRANSFER
FINS OF 0.090 IN.
ALUMINUM, 6 IN. TALL
AND 10 IN. WIDE.

12 IN.

INSULATION

BOX

HOT PLATE
HEATER

CONVECTED AIR
ENTERS HERE AND
ON OTHER THREE
SIDES OF HEATER.
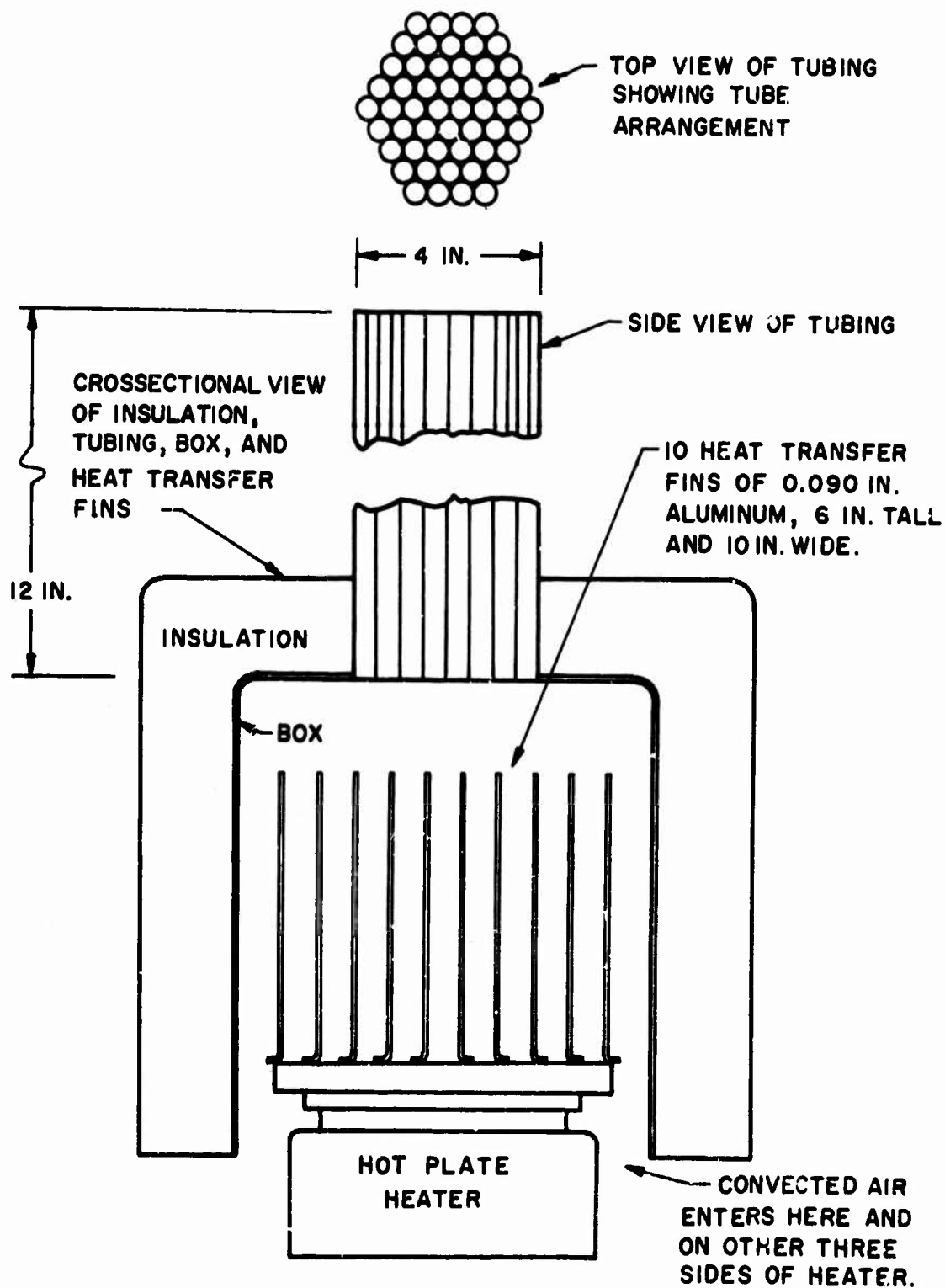
Figure 7   Thermal generator design.

27

was about 200°F above ambient; at 20 inches it was about 104°F above ambient. Above 8 or so inches the temperatures were difficult to measure with a thermometer; when a hot-film sensor was used the reason for the difficulty was found to be some unsteadiness in the thermal location which resulted in fluctuations in the temperature measured at any given point.

Two such thermal generators were built and used in the experiments.

Experiments related to the thermal work were performed using a rising column of helium instead of heated air. The helium was injected vertically upward from a nozzle with a 0.031-inch inside diameter and a 0.50-inch length attached to a small plenum chamber. The chamber pressure was maintained at 10 psig. The low molecular weight of the helium was exptected to alter the boom in much the same way as the hot air. The advantage of the helium setup was in the small size of the nozzle as compared to the large size of the thermal generator. This permitted the helium nozzle to be placed directly above the shadowgraph plate without loss of a significant portion of the shadowgraph picture.

D.   Instrumentation.

The projectile flights were detected by two lightscreen photocell devices located ten feet apart near the east end of the ballistic range tank. These were used to trigger a counter which measured the time of flight between lightscreens so that the projectile speeds and Mach numbers could be calculated. The lightscreen devices were also used for triggering both horizontal view and vertical view photographs of the projectile flight attitudes. At one lightscreen station a shadowgraph system was used to observe the projectile and the associated shock wave and wake features. At the other station radiogram pictures of the projectile were taken. In general the projectile flights were at zero angle of attack; projectile stability was a problem only for flight speeds less than Mach 1.35 with the 0.46 caliber shots and less than Mach 1.9 with the 0.22 caliber shots. Each time that the projectile size or speed was changed a series of pictures were taken to check the projectile stability; when the stability was satisfactory for several flights no more pictures of the flight were taken.

28

The sonic boom signatures were recorded on the ground plane and on the topographical models through the use of B and K model 4138 microphones. These microphones are 1/8 inch in diameter and were mounted either flush with the surrounding surface or up to an estimated 0.007 inch below the surrounding surface. This distance had to be estimated with the aid of a magnifying glass as the microphone diaphragm was too delicate to be touched by any measuring instrument. At the start of Task I a microphone failed to operate after a short length of time. Inspection of the diaphragm under the microscope revealed what appeared to be slight indentations which may have been caused by an occasional sand grain entrained by the blower airflow and blown across the microphone face. For this reason the remaining microphones were mounted several thousandths of an inch below the surrounding surface whenever the blower was used.

For the topographical models the microphones were not exposed to the blower airflow and could be mounted flush with the surface. Whenever a microphone was mounted along a corner such as those shown in figures 3 and 4, the diaphragm center was located along the line defining the corner, and a small volume of the model was cut away so that the diaphragm could be fully exposed.

The microphones were each connected to a B and K model 2615 cathode follower by means of a B and K adapter. The model 2615 power was obtained from a B and K model 2801 power supply. The cathode follower has an output impedance of 750 ohms; this output was first fed into the 200 foot long cables which led to the oscilloscopes in the ballistic range control room. The cable capacitance resulted in a slight distortion of the signal because of the 2 microsecond time constant of the system. This problem was overcome by using an amplifier, a Thermo-Systems, Inc., model 1057, to amplify the signal by a factor of 10 before putting the signal into the 200 foot cable. Since the output impedance of this amplifier is only 20 ohms, the system time constant was quite small, and the system operated without any apparent difficulty.

The microphone signals were fed to Tektronix oscilloscopes and were photographed by polaroid cameras. Model 502, 555, and 556 oscilloscopes were used. Because of the better quality of the model 556 oscilloscopes, this model was used for most of the data recording in Tasks II and IV. The oscilloscopes were triggered by using the signal obtained from a B and K model 4136 microphone system. The model 4136 microphone was located on or near the

29

ground plane. Time delay circuits were used as required to delay the start of each oscilloscope trace by the time needed so that the boom signature would be displayed properly.

Four different model 4138 microphones were used. Since there exist some differences in sensitivity and frequency response from one microphone to another, the various boom signatures are labeled A, B, C, or D according to the microphone used.

The shadowgraph spark located at $z = 72$ inches also was triggered by the signal from the model 4136 microphone. The film, located in the plane $Z = -26$ inches, was 16 inches by 20 inches in size, extending 16 inches outward from the ground plane, $y = 0$. This outward edge was sufficiently far removed from the microphones at $z = y = 0$ that shock waves reflected from the film plane were sufficiently delayed so as not to interfere with the boom signature.

The various jet turbulence characteristics were measured using two Thermo-Systems, Inc. (TSI) hot film cylindrical gages of 0.002 inches diameter. TSI 1050 and 1050A anemometers and power supplies were used to drive the film gages. The anemometer outputs were linearized using TSI 1055 linearizer modules. This system was calibrated using a Hewlett Packard digital voltmeter, a TSI 1125 calibration unit, and a sensitive manometer. The manometer was also used with a pitot-static tube to measure mean velocities in the jet flows.

The linearized anemometer outputs were fed into a TSI 1015C correlator and a TSI 1060 true RMS voltmeter for measurements of correlation coefficients and turbulence microscales based on the differentiated film output. The turbulent energy spectra were measured using a Hewlett Packard 302A wave analyzer and 297A sweep drive; the measurements were recorded using the RMS voltmeter and a Mosely 7005B X-Y plotter.

A few of the sonic boom signatures were recorded by using the above TSI anemometer units, a vacuum pump, and an aspirating-probe type of sensor. This system offered a higher frequency response capability than the B and K microphones at the expense of a smaller signal-to-noise ratio. The aspirating probe system also suffered because of the fragility of the probe wire and because of dust contamination of the wire. For these reasons, the aspirating probes were used for only a very few signature measurements. Since the development of these probes was quite detailed, this development is presented in Appendix D.

30

3. EXPERIMENTAL RESULTS FOR TOPOGRAPHICAL MODEL AND SONIC BOOM INTERACTIONS

Experimental sonic boom signature measurements are tabulated in Appendix A, and shadowgraph pictures of the interactions are shown in Appendix B. In Appendix A, figure A1 shows the "basic" N-wave signature shapes obtained during the course of Tasks I and III. The word basic is used to denote the N-wave shape obtained in the absence of any turbulent or topographical interactions. Basic N-wave shapes obtained during the course of Tasks II and IV are shown in figures A2 through A5. Signature shapes with topographical interactions are shown in figures A8 and A9 as obtained from the pilot shots of Task III and in figures A59 through A65 for the shots of Task IV. The figures show the microphone locations, the particular microphone used for each signature, the sensitivity of that microphone in psi per division of the oscilloscope scale, and the horizontal sweep speed in microseconds per division. The shot number is placed at the bottom of each picture.

For Task IV the various shots were numbered from 101 through 157. Some of the shots duplicated the signatures obtained for the same conditions on earlier shots; but these duplicate shots were not wasted. The duplicate shots served two purposes: (1) they proved that confidence could be placed in the results from the earlier shots, and (2) they made it possible to obtain shadowgraph histories at several different times during the boom-topographical model interaction. Figures B11 through B13 of Appendix B show three successive moments in the N-wave and step model interaction. Other interactions are shown in figures B14 through B19. Duplicate pictures were eliminated in presenting the Task IV interaction data.

For shots 101 through 157 only the B projectiles were used since it was decided that the basic N-wave amplitude and duration variations obtainable through the other projectiles would not significantly affect the results. This consistency in projectile size simplifies the comparison of results from the several different topographical models. The maximum overpressure measurements come from the microphones placed at location IV on the two corner models. Since the peak overpressures were obtained immediately after the first shock of the N-wave touched the corner, the N-wave duration had very little to do with these overpressures. Also, since sonic boom waves overpressures are very

31

weak compared to an atmosphere, the corner interaction overpressures would be expected to be linear with the basic N-wave amplitude. Hence variations in either the amplitude or the duration of the basic N-waves should not affect the peak boom intensification factors measured at the corner locations.

A. Comments on Boom Signature Measurements.

The horizontal time scale shown on figures A60 and A61 for the overhang models was 200 microseconds/division. Notice that shot 115 on figure A59 is a duplicate of shot 116 on figure A60 except that the timing on shot 115 was delayed by an additional 300 microseconds. The other time scales on figures A59 through A65 were 100 microseconds/division except for shot 130 on figure A62. Note that shot 130 is a duplicate of shot 128 except for the time scale difference.

B. Problem Areas in Using Ballistic Range Facilities for Studies of Boom and Topographical Model Interactions.

In general not many problem areas existed. The undisturbed booms generated by the projectiles were quite clean, as shown by the shocks viewed on the shadowgraph pictures. The pictures also demonstrate that the shocks reflected quite cleanly from the surfaces of the topographical models. The main problem was the frequency response limit of the microphones, but this could be overcome by using larger topographical models located at a much greater distance from the projectile path. Then the microphone time scale would be much smaller in comparison to the time for the N-wave to traverse a given portion of the topographical model. The main limit on placing the models at a greater distance from the projectile path is the cost of the room or barricade to house the experiment. The barricade is not really essential since one could run the experiment in open air if one were willing to wait the length of time required to obtain a day wherein the surrounding atmosphere were sufficiently quiet to not interfere with the test. From a cost point of view, it is probably better to build the barricade than to wait for a calm day. The barricade will also improve the quality of the data. Furthermore, shadowgraph pictures cannot be taken without the barricade, which serves as a darkroom.

32

4. ANALYSIS OF TOPOGRAPHICAL MODEL RESULTS

The incidence of sonic boom N-waves on structures has been studied by
Ting and Pan (Reference 5). Ting has developed a procedure for the determina-
tion of transient pressure distributions on two-dimensional structures, but
the general three-dimensional problem is much more complicated and has not
been solved. Ting does give a few results for corner regions on three-
dimensional models.

Shadowgraph figures B11 through B15 show patterns of diffracted waves
similar to those shown by Ting and Pan's figure 1. In fact, on the 16-inch
by 20-inch original of figure B11 the half-circle shape of the diffracted wave
given by the interaction of the incident wave with the first model corner can
be viewed faintly; on figure B11 only the stronger portions of this wave are
visible. Figures B11, B12, and B13 are at successive instants in time for M
equal to 2.55. Figures B14 and B15 show the same thing for M equal to about
1.4. Figures B16 and B17 show similar results with the added feature of an
overhang roof. In figures B18 and B19 the added feature is a second wall
parallel to the first.

Figures A59 through A62 show pressure time histories at locations IV, V,
and VI on the two-dimensional models. The results for the corner, location V,
show the approximate N-wave shape and intensification factor "IF" as calculated
by Ting and shown in his figure 5. The figures show a rather complicated series
of wave interactions; such interactions are discussed by Ting.

Figures A62 through A65 show pressure time histories on three-dimensional
models. The corner models had large overpressures, but the canyon overpres-
sures were much smaller until the paraboloidal canyon was rotated through
angle α_c with respect to the ground plane in an attempt to focus the waves.
For α_c such that the canyon x_c axis was perpendicular to the waves, the
canyon overpressure peaks were larger than given by the two-dimensional models.

A. Data Analysis

The peak overpressures were judged to be the most critical signature
factors and are given in Tables 1 and 2 in terms of the intensification
factor IF, where IF is defined as the ratio of the peak overpressure to the

33

TABLE 1. — BOOM INTENSIFICATION FACTORS PRODUCED BY TOPOGRAPHICAL MODELS

Task	Shot No.	Model	Projec-tile	M	Intensification Factors Measured at Station		
					IV	V	VI
III	1-3	Step	D	2.5	--	3.70	1.72
III	3-3	Step	D	1.4	--	3.04	1.56(-1.66)
III	7-3	Step	B	2.6	--	3.22	1.78
III	4A-3	90° Cor.	D	2.5	--	4.14	2.80
III	5-3	90° Cor.	D	1.4	--	4.78	2.76
III	6B-3	90° Cor.	B	2.6	--	3.18	3.00
IV	104	Step	B	2.56	1.78	3.78	2.00
IV	111	Step	B	1.40	1.86	3.68	1.70
IV	133	90° Cor.	B	2.57	1.80(-2.40)	4.24	4.16
IV	137	90° Cor.	B	1.46	2.84(-3.06)	7.54	3.48
IV	138	45° Cor.	B	2.57	2.56(-2.74)	5.62	5.24
IV	142	45° Cor.	B	1.40	3.60(-3.94)	10.52	8.08
IV	122	1 in.O.H.	B	2.56	1.94	2.86	1.48(-1.80)
IV	121	2 in.O.H.	B	2.56	1.86	2.62	1.24(-1.58)
IV	127	3 in.O.H.	B	2.56	1.41	2.75	1.44
IV	124	4 in.O.H.	B	2.57	1.32	1.80(-1.92)	1.02(-1.04)
IV	123	1 in.O.H.	B	1.39	1.80	3 78	1.36(-2.42)
IV	116	2 in.O.H.	B	1.40	1.86	3.28	1.02(-1.51)
IV	126	3 in.O.H.	B	1.40	1.86	2.34	2.22(-2.34)
IV	125	4 in.O.H.	B	1.36	2.06	1.86(-1.88)	1.96
IV	128	Parallel	B	2.56	1.10(-1.16)	3.88	1.90
IV	131	Parallel	B	1.47	1.18	2.42	1.82

TABLE 2. — BOOM INTENSIFICATION FACTORS PRODUCED BY CANYON MODEL

Shot Numbers	M	α_c (Degrees)	Intensification Factors Measured at Station					
			VII	VIII	IX	X	XI	XII
144, 146, 149, 150	2.57	0	2.68	3.70	2.14	1.04	1.04	1.14
145, 147, 148, 151	1.40	0	3.32	3.18	1.96(-2.42)	1.10	1.14	1.18
152, 154	2.56	66		2.28(-2.98)	3.48(-3.82)		13.8	
156	1.40	45		2.58(-3.18)	3.08(-3.88)		12.8	

pressure rise P_{10} of the incident wave. The appropriate values of P_{10} were measured from the basic N-waves given in figures A1 and A2. Since these waves were reflected from the ground plane, the amplitudes of the waves as shown were divided by 2. This assumes a perfect reflection from the ground plane. The plane surface was 1/4-inch aluminum plate supported well by 2-inch by 4-inch wooden beams; the shadowgraph pictures indicate that the waves reflected from the ground plane with apparently undiminished amplitude. In some cases the amplitudes of the negative peaks were larger than the amplitudes of the positive peak overpressures. These negative peak IF values are placed in parenthesis in the tables.

Notice that the above definition of IF gives a factor of 2 for a sonic boom reflection from a rigid, flat surface such as flat portions of the earth's surface.

The IF values recorded during the Task III test program are somewhat smaller than corresponding values from Task IV. This is attributed to the fact * that the Task III models were wooden rather than aluminum, and to the fact that the wooden models were less perfectly constructed. The wooden models were lacquered; the corners were somewhat rounded; and the models were slightly warped so that about 0.020-inch clearance existed between the models and the ground plane. This clearance was helpful in preventing microphone damage during the model installations. For Task III, microphones were in short supply; this is the reason that a microphone was not placed at location IV.

Ting and Pan predict a peak IF of 4 at the corner location V on a step model. Shots 104 and 111 gave IF's of 3.78 and 3.68 at the corner.

The overhang and parallel wall models also show the largest IF's at this corner. The measured IF was 3.88 for the parallel wall model and $M = 2.56$; this IF decreased to 2.42 when M was reduced to 1.47. From the geometry it is clear that the second wall would be better able to shield location V from an incident wave at $M = 1.47$ than the more nearly-horizontal wave at $M = 2.56$. On the other hand, the overhang configurations do the better job of protecting location V when the incident wave is at $M = 2.56$. In this case the $M = 2.56$ or more-nearly horizontal wave is evidently refracted to a greater degree by the overhang than is the $M = 1.4$ wave; the location V IF is 2.86 for the former case and 3.78 for the latter. These are for overhangs of only one inch. As the overhang distance is increased, these IF values decrease.

Ting and Pan calculate an IF of 8 for a corner model with $\theta_c = 90°$ and a solid angle of $\pi/2$. Table 1 shows an IF of 7.54 for M = 1.46; this falls off to IF = 4.24 for M = 2.57. When $\theta_c = 45°$ the Ting and Pan results would give IF = 16. Table I shows corresponding values of 10.52 and 5.62 at M = 1.40 and 2.57, respectively. The reason for these differences is not understood.

The canyon model is in the form of a paraboloid of revolution with a focal point at $x_c = 2.00$ in., $y_c = z_c = 0$, which is location XI. With the canyon in its normal position at $\alpha_c = 0°$, the largest IF was at location VIII; this IF was about the same as obtained at location V of the step model. When the canyon was rotated through angle α_c so as to make the incident waves perpendicular to the x_c axis of the paraboloid, measurements at the focal point, station XI, showed IF's of 13.8 and 12.8 for M = 2.56 and 1.40, respectively. These pressure peaks, shown on figure A65, are quite sharp and show a tendency for two peaks to appear close together. These results show that the proper combination of canyon shapes and orientation can dramatically increase the IF.

B. Derived Guidelines on Topographical Features Which Could Result in Boom Focusing

With the aid of the above results, several statements can be made about sonic boom focusing:

1. The IF for a plane, rigid surface is 2. This serves as a standard for evaluating other shapes.

2. The maximum IF on a two-dimensional structure with right-angled corners is 4.

3. Additions such as parallel or overhanging walls reduce the maximum IF on a structure.

4. Corner structures having a solid angle of $\pi/2$ can have an IF as large as 8; larger IF's can occur with smaller solid angles.

5. Large IF's can be obtained from concave topographical shapes such as a paraboloid of revolution. These IF's may be of the order of 12 or greater and are high dependent on the orientation of the shape with respect to the incident wave.

36

6. Imperfections in the above structural or topographical shapes will reduce the IF.

7. Because of wave reflections, the topographical models usually increase the duration of the boom disturbances by a factor of two or more as compared to that heard on a plane, rigid surface.

8. The peak IF is found at the inside corner of models such as the step or overhang models; as one goes away from this corner the maximum IF falls off somewhat if the signature length is long compared to the distance from the corner. When the signature length is of the same order as the distance from the corner, the maximum IF tends to be greatly reduced.

5. EXPERIMENTAL RESULTS, TURBULENCE AND SONIC BOOM INTERACTIONS

All the experiments were carried out in the barricade shown in figure 1. Measurements first were made of the various turbulent jet configurations; then boom N-wave measurements were made in the absence of turbulence. Finally, a large number of boom signatures were obtained with the turbulent jets operating.

A. Turbulence Measurements

Measurements of the jet mean velocity $\bar{U}$ and of the turbulent intensity u' are given in figures 8 through 13. Also given are values of the turbulent dissipation scale λ_f calculated from u', $\bar{U}$, and measurements of the velocity derivative $\overline{(\partial U/\partial t)^2}$; this was done using the Taylor hypothesis and the assumption of homogenous turbulence as discussed in Reference 6. Figures 8, 9, and 10 are for the 4-inch, 6-inch, and 24-inch nozzles using the 24-inch inlet on the blower to regulate the maximum $\bar{U}$ to about 80 ft/sec. For all three nozzles u' is near 5 ft/sec. across the interior of the jet, but in the intermittent zone at the edges of the jet u' rises to more than 10 ft/sec. Notice that the 6-inch nozzle flow dividers appear in figure 9 as reductions in $\bar{U}$ and u' at 6-inch intervals. The results for the 24-inch nozzle in figure 10 are closely related to those in figures 11 and 12 for the same nozzle but with the bypass configuration on the blower duct used instead of the 24-inch inlet restriction to regulate the jet speed. The bypass arrangement was used throughout Task I, whereas the inlet restriction was used for Task II measurements. Figure 12 shows the near uniform-flow conditions which exist 3 inches from the nozzle; in contrast, at the plane $x = 0$, 78 inches from the nozzle exit plane, the jet as shown in figure 11 has developed rounded $\bar{U}$ and u' profiles because of the turbulent mixing of the jet and the ambient air. Figure 13a shows results for the high-speed nozzle 1; again u' is only about 5 ft/sec. at the jet center at $y = 23$ in., but u' increases greatly at the jet edges. Figure 13b is like figure 8 except that the mean velocities $\bar{U}$ have been reduced by a factor of about 0.27 by changing the blower inlet diameter from 24 inches to 12 inches. The result is a reduction in u' by the same factor within the accuracy of the measurements; λ_f is reduced by a factor of about 0.64.
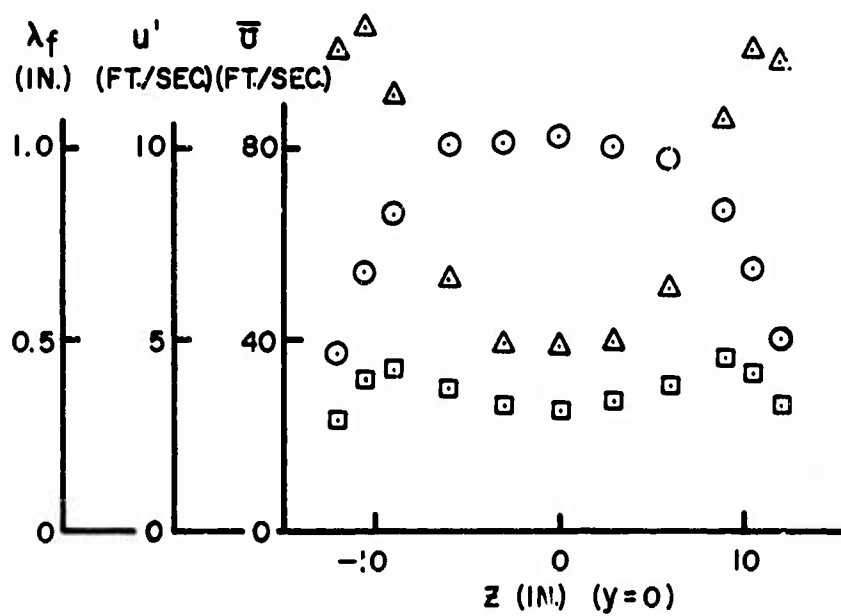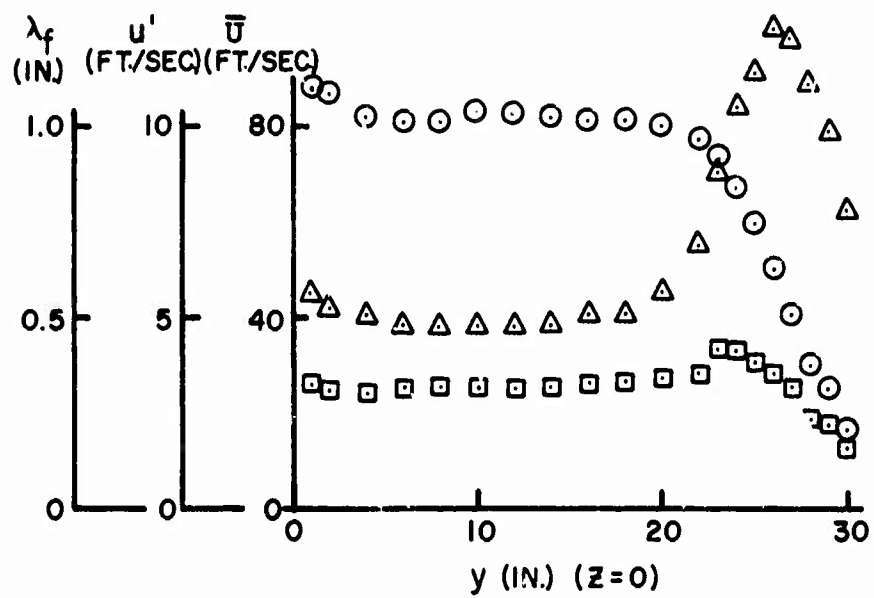
Figure 8 Four-inch nozzle jet parameters measured in the plane x = 0 with 24-inch blower inlet.

39
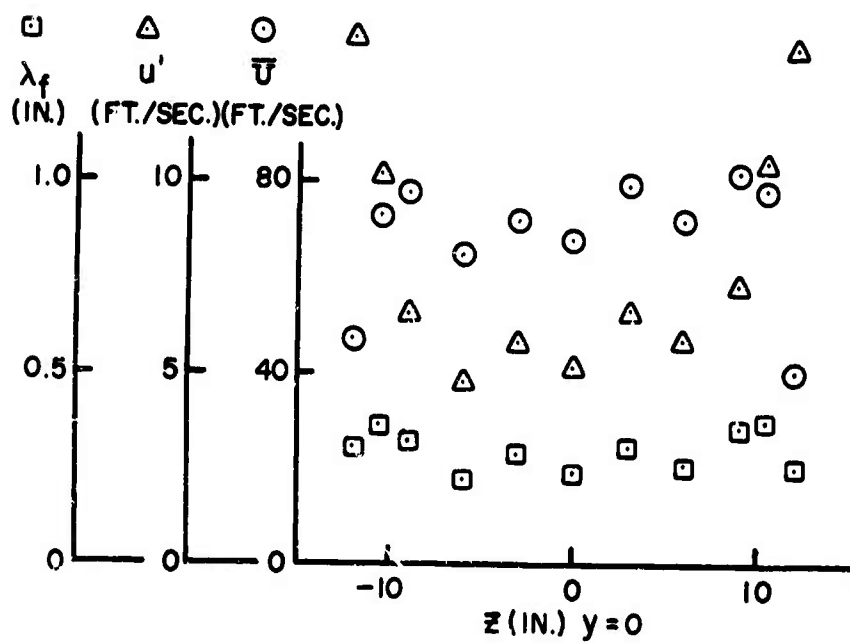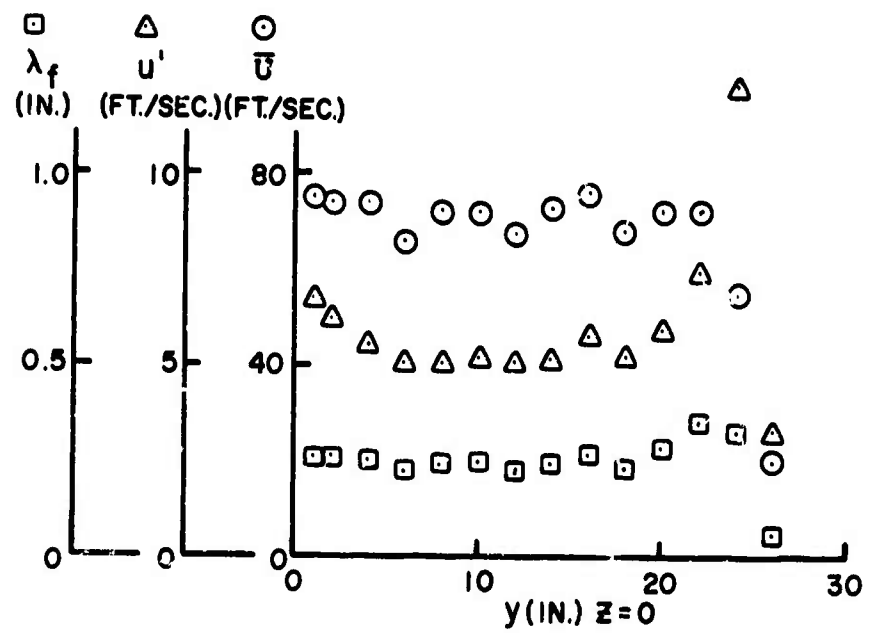
Figure 9   Six-inch nozzle jet parameters measured in the plane   x = 0   with
24-inch blower inlet.
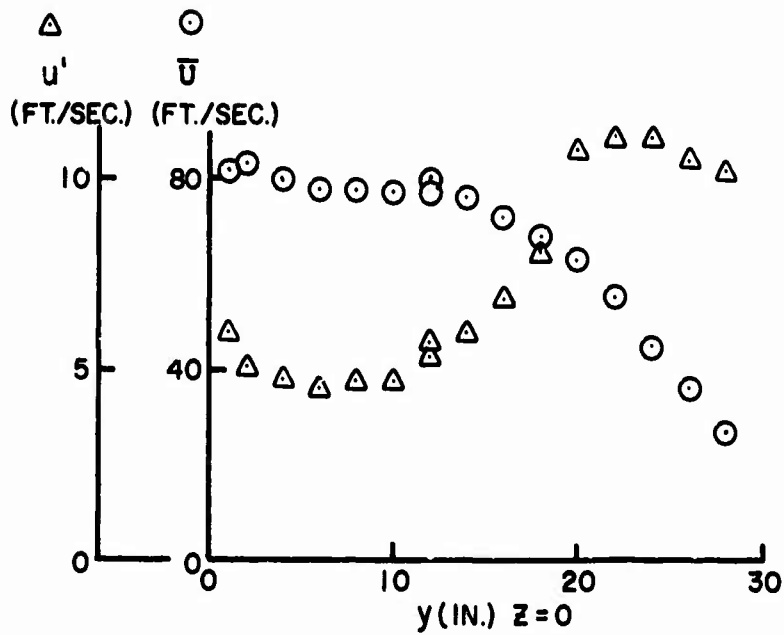
NOTE: NO DATA WERE TAKEN FOR y = 0 AND z VARIABLE.
SEE FIGURE II FOR RELATED DATA.
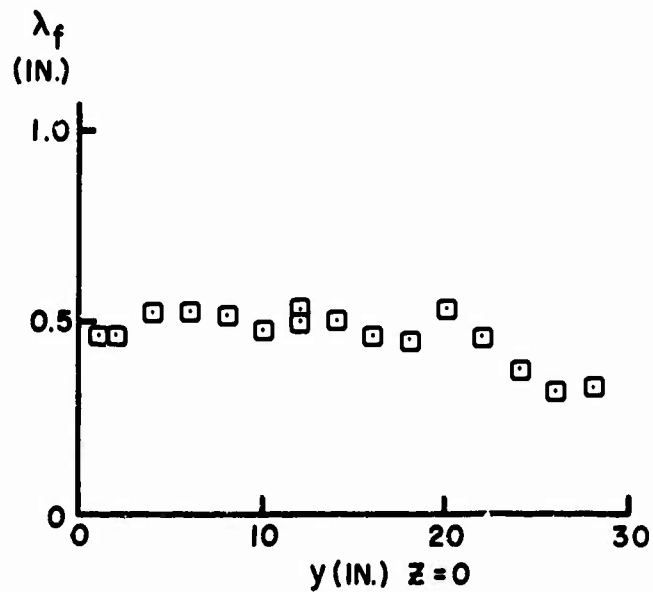
Figure 10   24-inch nozzle jet parameters measured in the plane   x = 0   with
24-inch blower inlet
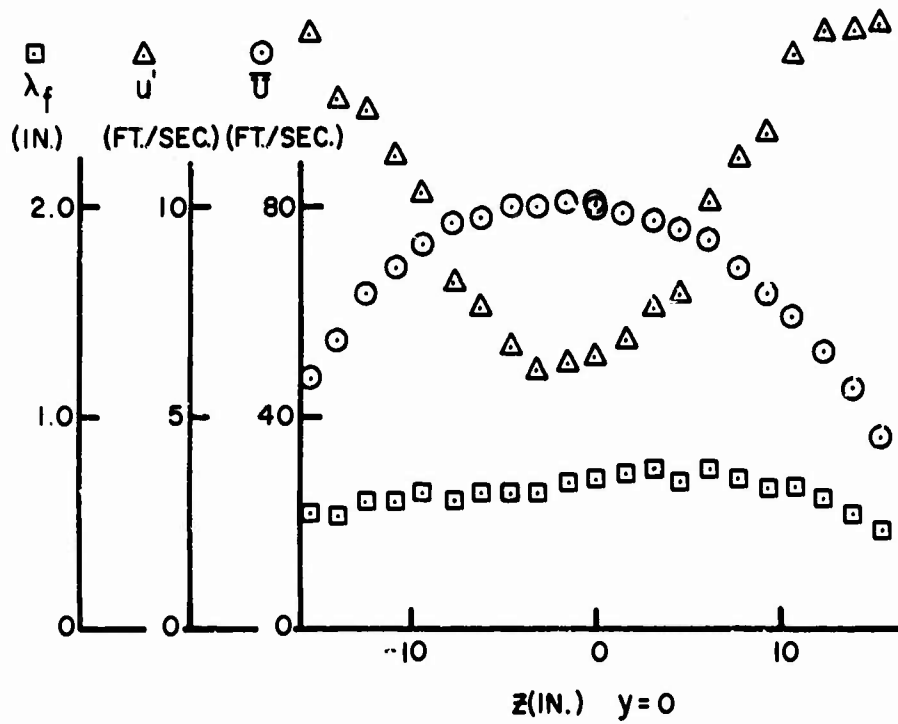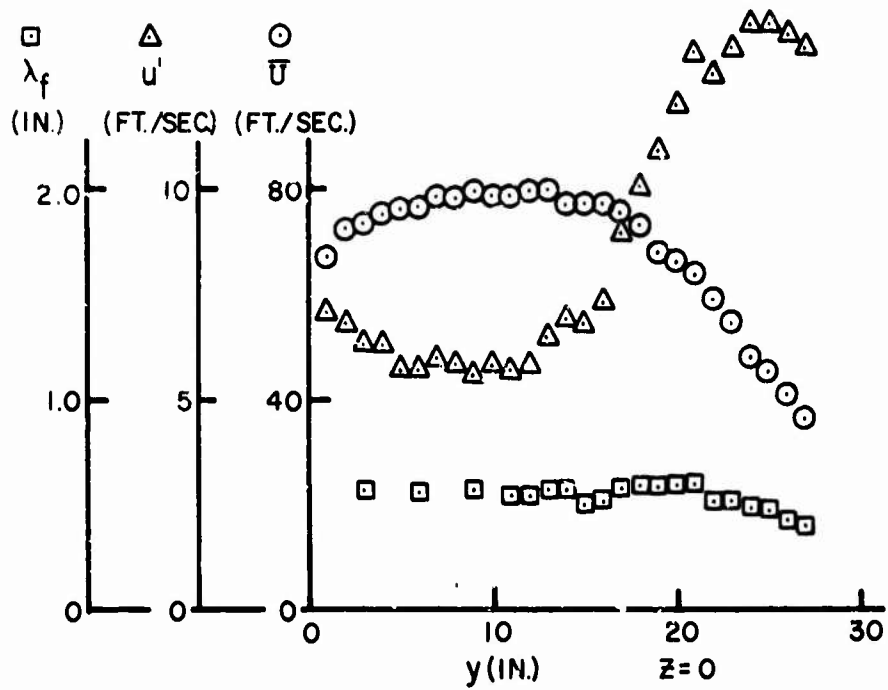
Figure 11   24-inch nozzle jet parameters measured in plane   x = 0   with bypass in blower duct.
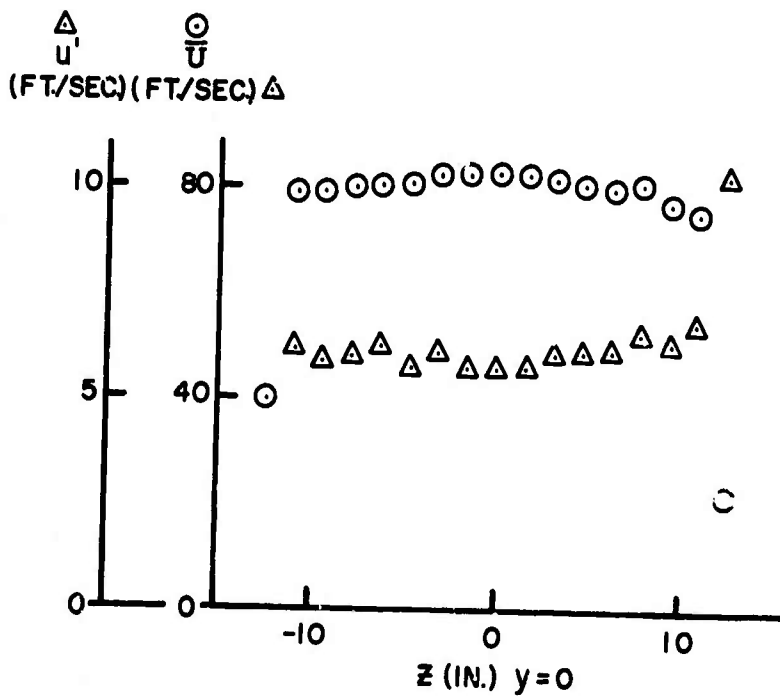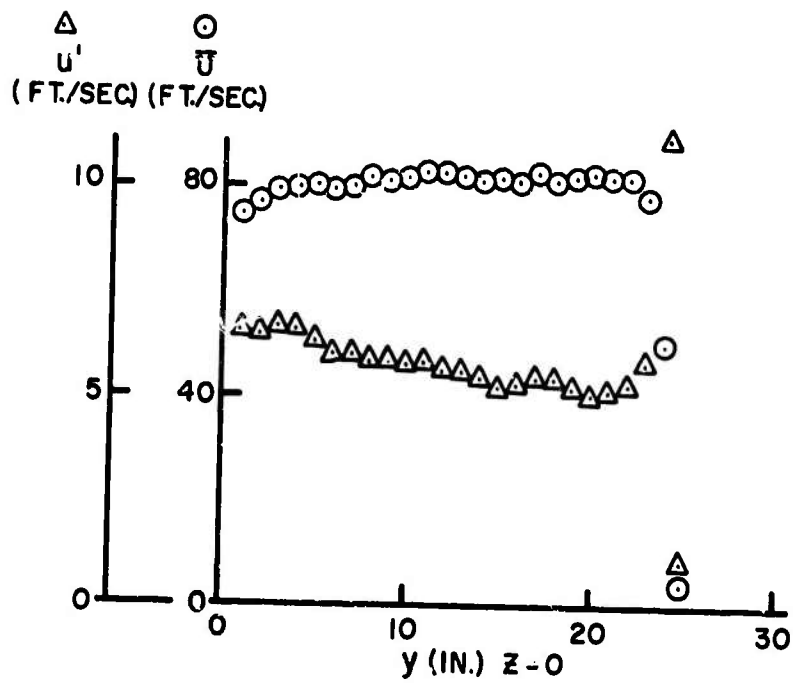
Figure 12 24-inch nozzle jet parameters measured 3 inches from nozzle (x = -75 in.) with bypass in blower duct
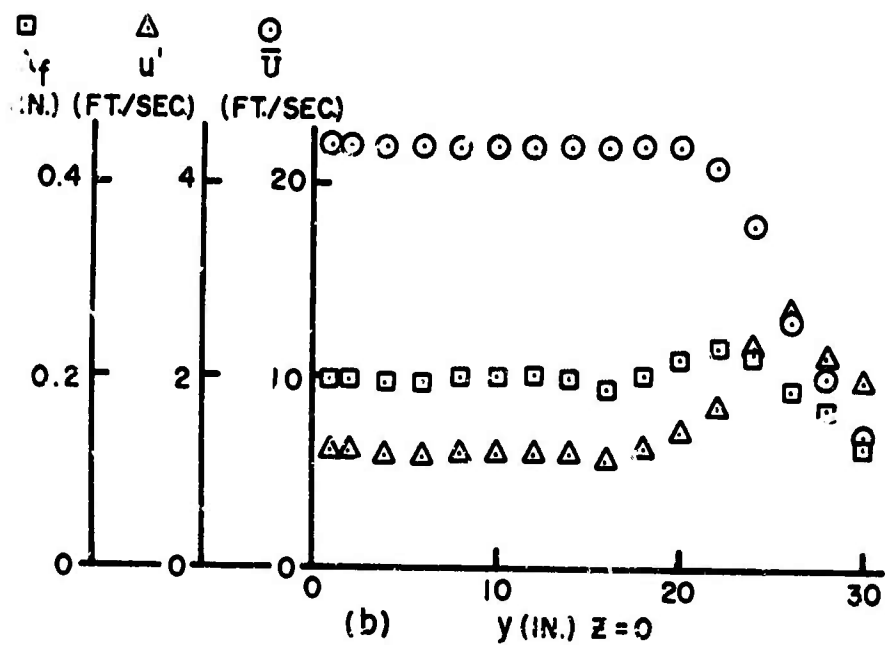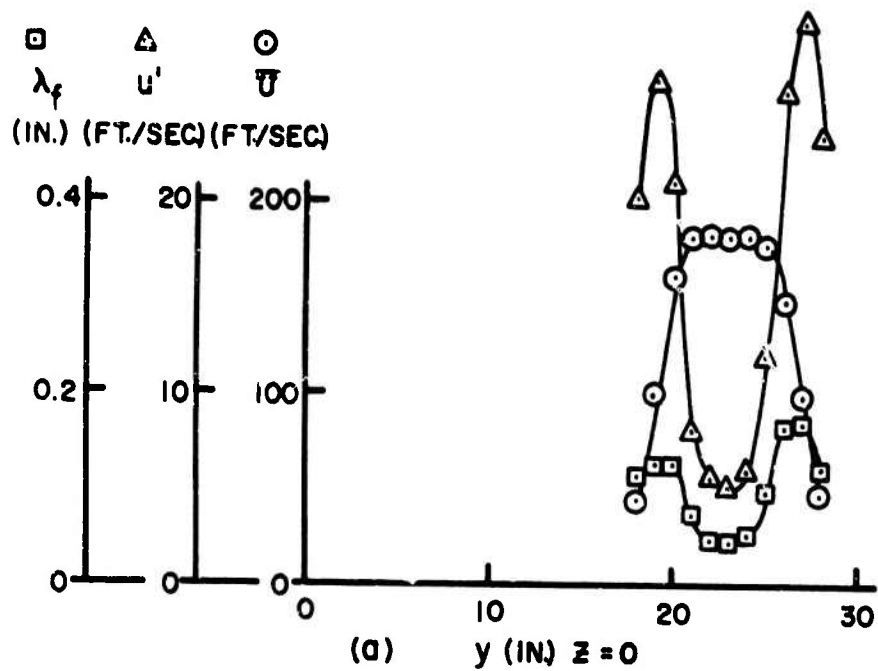
Figure 13 Jet parameters measured in the plane x = 0.   (a) For high-speed nozzle No. 1 and 24-inch inlet.   (b) For 4-inch nozzle and 12-inch inlet.

44

These turbulent jet experiments were on such a scale that $u'/\bar{U}$ was not expected to vary significantly as $\bar{U}$ was varied; figures 8 and 13b confirm this expectation. For the same reason it was expected that the turbulence integral scale L would be independent of $\bar{U}$, whereas the dissipation scale λ_f, which depends on the turbulent Reynolds number, would vary with $\bar{U}$.

The jet turbulence characteristics were studied in greater detail by measuring the energy spectra shown in figures 14 and 15 for the various nozzles. The spectra were taken at $x = 0$, $y = 12$ in., and $z = 0$, which is essentially along the jet centerlines. The bandwidth f_b of the spectrum analyzer was 6.0 hertz; and the analyzer output e_1 is based on the hot-film gage output U_1 which had a scale factor H of 30 ft./sec./volt. Since the energy distribution function $E_1(n)$ must satisfy the integral

$$u'^2 = \int_0^\infty E_1(n)\,dn \tag{1}$$

we must have

$$u'^2 = \int_0^\infty \frac{e_1^2(n)H^2}{f_b}\,dn \tag{2}$$

where

$$E_1(n) = \frac{H^2}{f_b}\,e_1^2(n) \tag{3}$$

The spectrum analyzer bandwidth f_b was determined through equation (2) and measurements of u', $e_1(n)$, and H. This was first done for the 6-inch nozzle which had a constant e_1 from $n = 20$ hertz to about 100 hertz. Since the analyzer does not cover the range 0 to 20 hertz, $e_1(n)$ was extrapolated to $n = 0$ so that the integral (2) could be carried out. As shown on pages 55 through 61 of Reference 6, e_1 or E_1 is generally constant for sufficiently low frequencies. Also, the integral scale is

$$L = \frac{\bar{U}}{4u'^2} \lim_{n \to 0} E_1(0) \tag{4}$$

so that L is determined by $E_1(0)$.
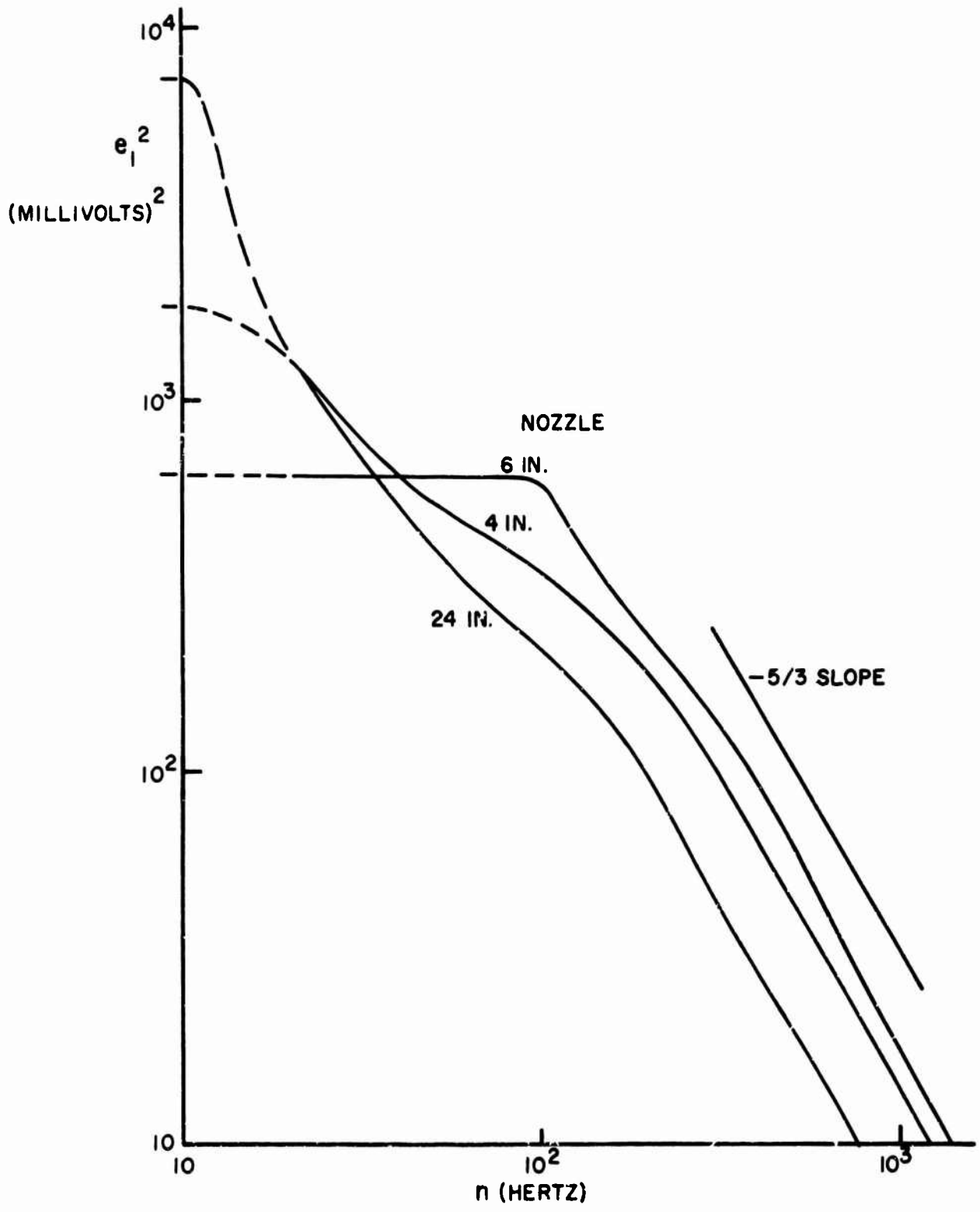
Figure 14 Spectral energy distribution of jets at x = z = 0, y = 12 inches.
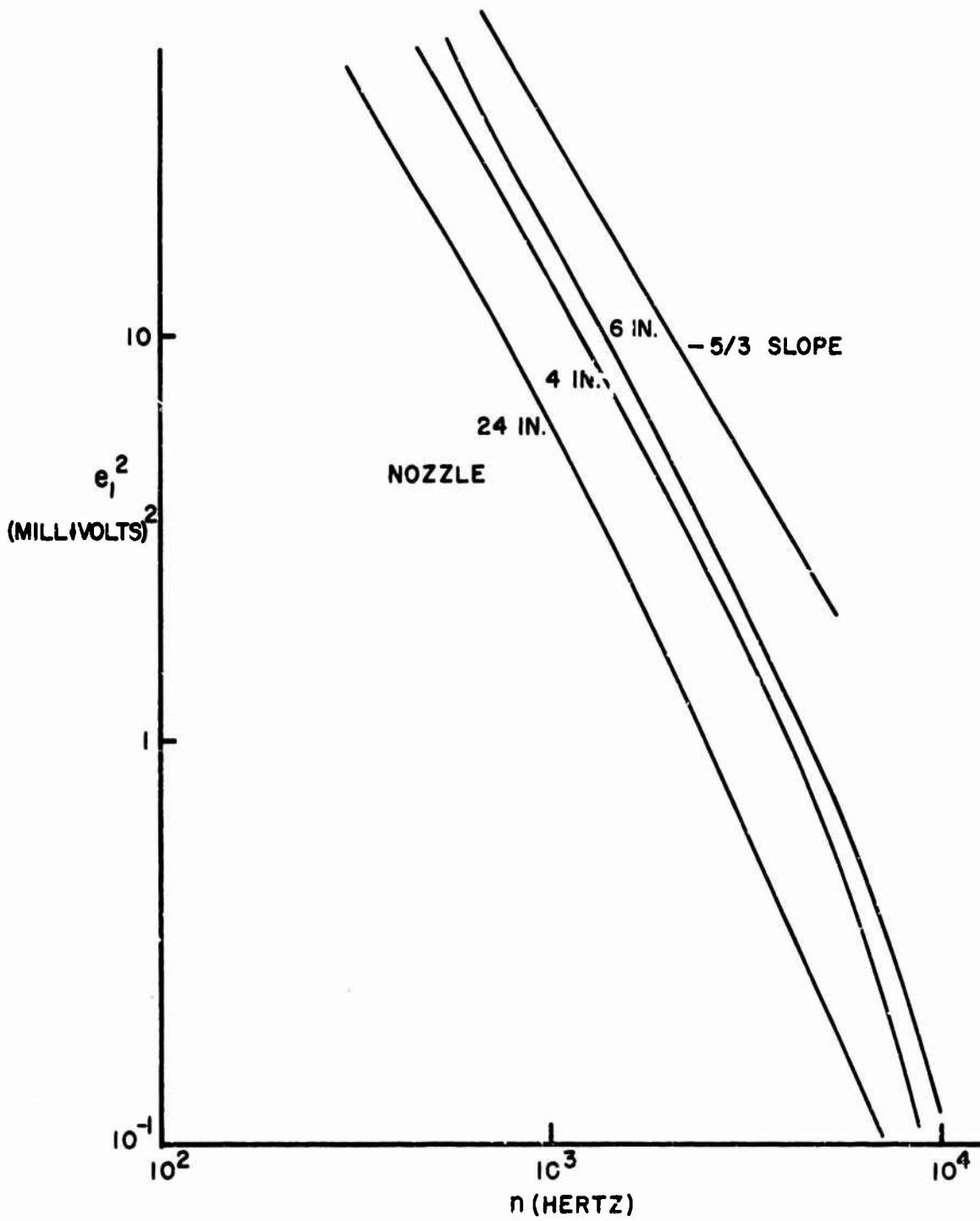
Figure 15 Spectral energy distribution of jets at x = z = 0, y = 12 inches.

Two-point correlation measurements were made in the jets in an attempt to determine L. When this was done the correlation function $g(r)$ was well-behaved for small values of r, but g refused to go to less than 0.2 for values of r as large as 20 inches. Even for small r, g was difficult to measure with good accuracy. Because of these difficulties and because it is clear that the jet turbulence is not homogeneous, L was determined from the energy spectra.

For the 6-inch nozzle, L was 0.74 inch. For the 4-inch and 24-inch nozzles $e_1(n)$ was extrapolated from $n = 20$ to $n = 0$ hertz on the basis of the 6.0 hertz bandwidth and the requirement that equation (2) be satisfied. These extrapolations are shown on figure 14 in dotted lines. In both cases e_1 was assumed to be constant for n smaller than 10 hertz. With this work $L = 2.7$ in. for the 4-inch nozzle, and $L = 8.9$ in. for the 24-inch nozzle.

Figures 14 and 15 show at the higher frequencies that the slope of e_1^2 versus n is somewhat steeper than the 5/3 power spectrum law of Kolmogoroff (see Reference 6). Hence, the spectra are in this sense well-behaved. Also, notice for these high frequencies that the 6-inch nozzle has the largest amplitude, the 4-inch nozzle is second, and the 24-inch nozzle has the smallest amplitude. Thus, in this region e_1^2 is largest for the nozzle with the smallest L and vice versa. This is in spite of the fact that u' is almost the same for these nozzles. As soon as this e_1^2 change without a corresponding change in u'^2 was found experimentally, the results were checked by carefully repeating the measurements. The repeated measurements confirmed the earlier ones. Since the integral over n as given in equation (2) must be satisfied, the spectra with the largest e_1^2 at the high frequencies would tend to have the lowest e_1^2 at the low frequencies, which is just what figures 14 and 15 show. This reasoning and the measurement checks add confidence to validity of the integral scales.

As shown by Reference 6, the correlation function $f(x)$ and the energy spectrum are Fourier transforms. The transform

$$f(x) = \frac{1}{u'^2} \int_0^\infty E_1(n) \cos \frac{2\pi n x}{\bar{U}} \, dn \qquad (5)$$

48

was used to calculate $f(x)$ for the three nozzles, as shown in figure 16. These may be compared with the two point correlation measurements $g(y)$ and $g(z)$ shown in figure 17. In general, $f(x)$ and $g(y)$ or $g(z)$ should be related between the three nozzles so that the nozzle with the largest integral scale L has the largest f or g at a given value of x or y or z and vice versa. In figures 16 and 17 such is the case. Therefore, the two-point correlation measurements are in general agreement with the $f(x)$ calculated from the spectral measurements.

B.   Boom Signature Measurements without Turbulence

As already discussed in section 3, "basic" boom signatures, signatures without turbulent or topographical interactions, are presented in figures A1 through A5 of Appendix A. The signatures on figure A1 were taken first during the performance of Tasks I and III of Reference 5. Figures A2 through A5 were obtained during the Task II and IV test programs. These signatures are discussed in more detail in section 6C..

C.   Boom Signature Measurements with Turbulence

The boom signature measurements with turbulence are of two basic types, those generated by jet interactions and those generated by thermal interactions.

1.   Boom Signature Measurements with Turbulent Jet Interactions

Figure A6 shows turbulent signatures taken for various projectiles during the Task I program. These records first demonstrated the feasibility of obtaining distorted boom signatures with features similar to those obtained from full-scale flight.

During the Task II program a large number of turbulent signatures were obtained. Figures A10 through A54 show over 600 such signatures displayed on more than 300 photographs. Each photograph contains an upper and a lower signature; the upper one was taken with microphone B at location I; the lower one was taken with microphone D at location II, just 6 inches from location I. Although these microphones were only 6 inches apart, no readily apparent correlation exists between signatures at the two locations.

49
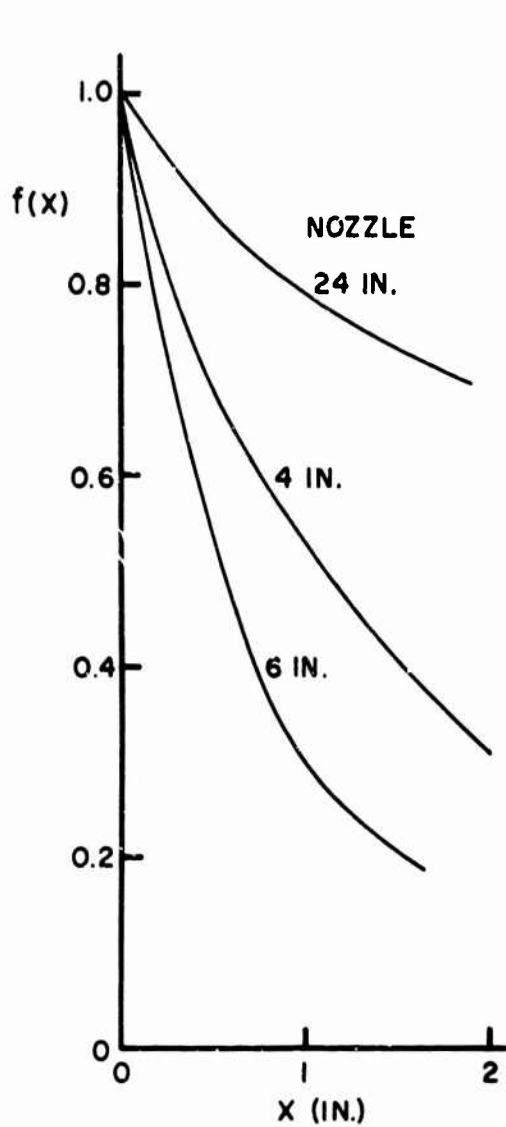
Figure 16 Two-point longitudinal correlation coefficients calculated from energy spectrum measurements.
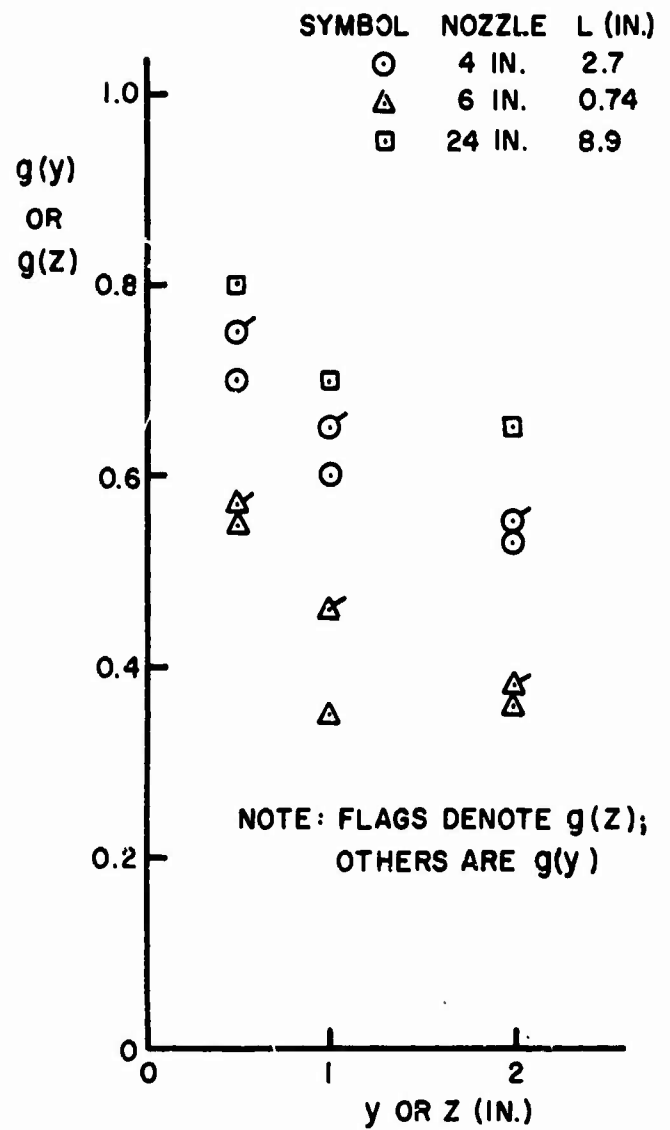
Figure 17 Two-point transverse correlation coefficients determined by direct measurements.

These signatures are classified into 22 different groups according to the projectile size, the Mach number, the nozzle, and the blower inlet constrictor size. Each group is identified by three digits. This group code is defined as follows:

First digit:

    1 means $M = 1.40$ and a B projectile.

    (Sometimes M is significantly different from 1.40 and is so noted.)

    2 means $M = 2.55$ and a B projectile.

    3 means $M = 3.0$ and an 0.22 caliber bullet.

    4 means $M = 2.15$ and an 0.46 caliber bullet.

Second digit:

    1 means the 4-inch nozzle.

    2 means the 6-inch nozzle.

    3 means the 24-inch nozzle.

    4 means the high-speed nozzle No. 1.

    5 means the high-speed nozzle No. 2.

Third digit:

    1 means the 12-inch blower inlet size.

    2 means the 16-inch blower inlet size.

    3 means the 20-inch blower inlet size.

    4 means the 24-inch blower inlet size.

    5 means no restrictor on the inlet blower.

Thus, the group 314 signifies a $M = 3.0$, 0.22 caliber bullet, the 4-inch nozzle, and the 24-inch inlet constrictor. For this group over 100 shots were fired with the object of obtaining good quality statistical data.

The large number of shots was carried out on the recommendation of the consultants, Professors John Laufer, Anatol Roshko, and Bradford Sturtevant, who arrived at this conclusion independently. The large number of smaller projectiles were fired rather than a smaller number of the large A sized projectiles (which were much more difficult to fire) so as to obtain a large number of signature data points. The A projectiles also had the disadvantages of a large overpressure of the basic wave (see figures A1 and A6), which was many times larger than the full-scale value, and apparently a rather low

51

sensitivity to turbulence. The A projectiles also were much more dangerous to fire than the small projectiles.

The projectile signature length L_s may be defined as the distance between the N-wave leading and trailing shocks as measured on the ground plane. Then the ratio L_s/L may be tabulated for the several different groups of data as given below in table 3.

TABLE 3. -- RATIOS OF L_s/L FOR BOOM TURBULENCE INTERACTIONS

Group First Digit	Group Second Digit	L_s (in.)	L (in.)	L_s/L
1	1	5.84	2.7	2.2
1	2	5.84	0.74	7.9
1	3	5.84	8.9	0.65
2	1	9.01	2.7	3.3
2	2	9.01	0.74	12.2
2	3	9.01	8.9	1.0
3	1	6.41	2.7	2.4
3	2	6.41	0.74	8.7
3	3	6.41	8.9	0.72
4	1	8.80	2.7	3.3
4	2	8.80	0.74	11.9
4	3	8.80	8.9	1.0

Hence, the ratios L_s/L for the shots in Appendix A cover the range 0.65 to 12.2.

Figures B1 through B8 are shadowgraph pictures of turbulence shots. These pictures show that the conical shock fronts are greatly distorted so that a number of lines appear instead of single shock lines as illustrated in figures B11 through B18. The following table correlates the shadowgraphs and the boom traces in Appendix A.

TABLE 4. — CORRELATION OF SHADOWGRAPH PICTURES AND BOOM SIGNATURES

Shadowgraph Number	Group Number	Shot Number	Signatures on Figure Number
B1	212	226	A14
B2	214	199	A16
B3	415	218	None
B4	222	294	A18
B5	224	239	A19
B6	232	229	A22
B7	234	174	A24
B8	314	347	A28

2. Boom Signature Measurements with Thermal Interactions

The boom signature measurements with thermal interactions are shown in figure A7 and in figures A55 through A58. The tops of the stacks of the thermal generators were located in the plane $z = -20$ in.

Figure 18 is a view of the tops of two thermal generators and the ground plane as seen by one looking in the $+z$ direction. This is the same type of view presented in the shadowgraph figures B9 and B10. Notice that the two lines passing through the center of the two generators at an angle normal to the shock direction intersect the ground plane. These two locations are designated by $y = 0$ and by $x = x_{h1}$ and $x = x_{h2}$. Since the shocks travel in a direction normal to themselves, the portion of the shocks perturbed by the thermals will intersect the ground plane in the vicinity of x_{h1} and x_{h2}.

In table 5 below is listed the shot numbers, figure numbers, x and y coordinates of the thermal generators, the thermal strengths, and the x_{h1} and x_{h2} coordinates for all the thermal generator shots. The shots shown on figure A7 were made during Task I using a D projectile at $M = 2.5$. The shots on figures A55 through A58 were made during Task II using 0.46 caliber bullets at $M = 2.16$.

53
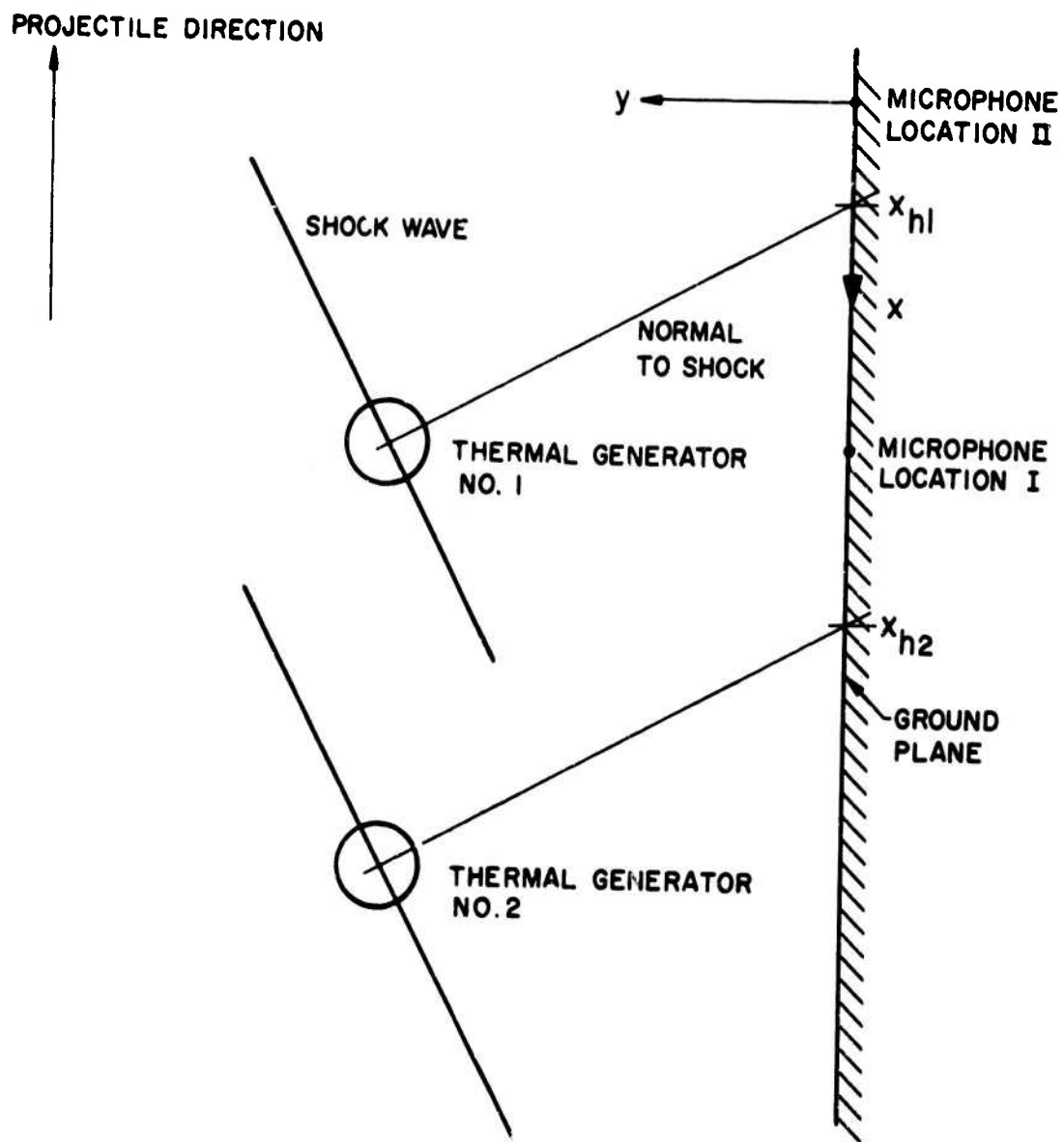
Figure 18 Relationship between the thermal generators, the shock waves, and the ground plane looking in the +z direction.

TABLE 5. -- CONFIGURATIONS USED FOR THERMAL GENERATOR SHOTS

Shot No.	Figure No.	x Generator No. 1 (in.)	y Generator No. 1 (in.)	x Generator No. 2 (in.)	y Generator No. 2 (in.)	Thermal Strength (°F)	x_{h1} (in.)	x_{h2} (in.)
4A	A7	4.0	9.0	10.0	23.0	200	0.1	0
4A1	A7	4.0	9.0	10.0	23.0	200	0.1	0
4B	A7	1.0	9.0	20.0	23.0	200	10.1	10.0
4C	A7	-6.0	9.0	0	23.0	200	-9.9	-10.0
4D	A7	8.0	18.0	23.0	18.0	200	0.1	15.1
250	A55	4.0	8.0	19.2	8.0	100	-0.2	15.0
251	A55	4.0	8.0	19.2	8.0	100	-0.2	15.0
252	A55	4.0	8.0	19.2	8.0	100	-0.2	15.0
253	A55	1.0	8.0	16.2	8.0	100	-3.2	12.0
254	A55	-2.0	8.0	13.2	8.0	100	-6.2	9.0
255	A55	-5.0	8.0	10.2	8.0	100	-9.2	6.0
256	A55	-17.0	8.0	-1.8	8.0	200	-21.2	-6.0
257	A55	-14.0	8.0	1.2	8.0	200	-18.2	-3.0
258	A56	-11.0	8.0	4.2	8.0	200	-15.2	0
259	A56	-8.0	8.0	7.2	8.0	200	-12.2	3.0
260	A56	-5.0	8.0	10.2	8.0	200	-9.2	6.0
261	A56	-2.0	8.0	13.2	8.0	200	-6.2	9.0
262	A56	1.0	8.0	16.2	8.0	200	-3.2	12.0
263	A56	4.0	8.0	19.2	8.0	200	-0.2	15.0
264	A56	6.0	12.0	21.2	12.0	200	-0.3	15.0
265	A56	3.0	12.0	18.2	12.0	200	-3.3	12.0
266	A57	0	12.0	15.2	12.0	200	-6.3	9.0
267	A57	-3.0	12.0	12.2	12.0	200	-9.3	6.0
268-272	A57	None	None	5.4	10.2	200	None	0
273	A58	None	None	9.1	17.3	200	None	0
274-275	A58	None	None	9.1	17.3	200	None	0
276-278	A58	None	None	5.4	10.2	Helium	None	0
279-281	A58	None	None	9.1	17.3	Helium	None	0

Notice that shots which are repeated, such as 268 through 272, do not produce identical signature shapes. This indicates the somewhat turbulent nature of the thermals. Figures B9 and B10 are shadowgraphs of shots 270 and 275. In B9 the turbulent nature of the thermals is indicated. The thermals cause the shock front to accelerate in the warm air; thereafter there exist a series of bulges in the shock front. In B9 the first shock of the N-wave has gone some 6 inches from the center of the generator; in B10 the distance is about 19 inches. At the larger distance the perturbed portion of

the shock is somewhat longer, but the amplitude of the bulge is about the same as for the shorter distance.

For shots 276 through 281 the helium nozzle located at z = -25 in. was substituted for the thermal generators. This produced an effect similar to the thermal generator effect but with a much smaller amplitude. Shadowgraphs of this effect showed shock bulges with an amplitude of about 0.08 inches.

D. Problem Areas in Using Ballistic Range Facilities for Studies of Boom and Turbulence Interactions

The main problem in using the ballistic range facility for these studies has been the limitation in frequency response of the microphones. The microphone response time to a square wave or shock input has been about 5 microseconds to 2/3 of the full amplitude and 9 microseconds to essentially full amplitude. The microphone manufacturer quotes an upper limit of 140 kilohertz for the response. This limitation could be overcome by conducting the boom measurements at a larger distance from the projectile path and by an appropriate increase in the turbulence scales. Then the microphone response would give greater detail in the boom signatures.

The microphone response limitation affects the data quantitatively by clipping off the sharper peaks of the signatures. Such peaks may be of prime interest because such peaks may be psychologically more annoying than the lower frequency wave components. A few such peaks have evidently been clipped from the data presented in this report. This problem is discussed in more detail in the second paragraph of section 6C.

6. ANALYSIS OF TURBULENT INTERACTION RESULTS

An analysis of the boom-turbulence interaction is not easy because of the great complexity of the phenomena. Turbulence itself is far from being fully understood even though it has been studied in detail for more than 30 years. Nevertheless, some overall comments can be made through a study of the statistical character of the boom signatures when these signatures are segregated into the several groups discussed earlier. This enables one to develop some implications for full-scale flight.

A. Preliminary Comments on Shadowgraphs and Signature Shapes

A brief study demonstrates that the signature shapes are quite varied. For example, group 214, figures A15 and A16, begins with signature 190-1 (location I trace of shot 190) being peaked whereas 190-2 is not significantly peaked or rounded. Signature 193-1 is rounded while 193-2 has a small peak. The peak in 200-1 is very large. Similar comments can be made for all the signatures.

Signature 347-1 in figure A28 shows a very large peak whereas 347-2 is quite rounded. Yet when the shadowgraph of shot 347 is viewed (figure B8) there is no great contrast between the shock lines approaching location I and those approaching location II.

One feature that the signatures show in common with full-scale flight results is the sameness of the pressure perturbations added to the leading shock as compared to the perturbations at the trailing shock. This phenomenon has been discussed by Crow (Reference 1).

There are several significant points to be seen on the shadowgraphs:

(1) The features appearing on the pictures are all remarkably parallel. Thus, they are probably disturbances that propagate with essentially the same path length as the undisturbed waves and are probably wrinkles on the original wave fronts.

(2) In almost every picture two sharp features identifiable as the front and rear shocks are visible. These features are separated by a distance corresponding to that indicated by the pressure history. In some cases they don't seem to be the leading disturbance on the

N-wave but this spurious effect can always be attributed to a) curvature of the conical wave front and/or b) divergence of the light rays in the optical system.

(3) The fuzzier features on the shadowgraphs have evidently been amplified more (and therefore are further from the film plane) than the sharper ones. They also tend to occur farther away from the ground plane than the sharper features; note that this is consistent with their being further from the film plane and on the conical wave fronts.

(4) There is a remarkable correspondence between features near the front shock and those near the rear shock. For example, the curved feature on the front shock of figure B7 can also be seen on the rear shock. The separation of these features (measured from the picture) compared to the known length of the N-wave gives the amplification factor, and therefore the distance of the feature (and presumably the disturbance that caused it) from the film plane.

Thus it is concluded that most of the features observed on the shadowgraphs are wrinkles on the original conical wave fronts.

B.   Comments on Signatures with Thermal Interactions

In shots 250 through 252 in figure A55 the x_{h1} (refer to figure 18) from thermal generator 1 is at microphone location II. This can be seen as a rounding in the lower traces of shots 251 and 252, whereas the lower trace of shot 250 is slightly peaked and then rounded. Meanwhile, the upper traces are not greatly affected because neither x_{h1} nor x_{h2} is near location I. By shot 255 x_{h2} becomes 6.0 inches and the upper signature responds with a peak.

For the series of shots 256 through 263 the thermal generators are turned on full so that the signature perturbations become larger. This is fully evident in shot 258 as the lower signature responds by rounding in correlation with $x_{h2} = 0$. By shot 260 the lower signature has regained its basic N-wave shape, but the upper signature is somewhat rounded in response to $x_{h2} = 6.0$ inches. Signature 263-2 is somewhat rounded in response to $x_{h1} = -0.2$ inch. The same can be said for 264-2. The next signature that is so rounded is 267-1. In

58

shots 268 through 272 we see five variations in the lower signature in response to $x_{h2} = 0$, whereas the upper signature is not greatly affected. Shots 273 through 275 again show rounding of the lower signature because x_{h2} is 0. Shots 276 through 281 show little effect from the helium injection.

The above results are not nearly so clear cut as was obtained in shots 4A, 4A1, 4B, and 4C of figure A7 wherein the x_h's of both generators were the same; when the x_h's were near 0 a large rounding of the signature occurred, whereas for the x_h's at +10 inches or -10 inches the effects were very slight.

C.   Turbulent Signature Data Reduction Process

In order to obtain statistical information on the signatures, a procedure was established for reading the signatures at the stations illustrated in figure 19. The figure illustrates a basic signature; the microphone rise time to full amplitude τ is 9 microseconds. The signature length is defined as time t_s, and amplitudes P_{10} through P_{50} have been read at times corresponding to 0, 5, 10, 20, and 40 percent t_s, respectively. For the turbulent signatures the amplitudes P_1 through P_5 were read at the corresponding times. The beginning station was always defined at time τ after the corner defining the start of the signature.

A few of the turbulent signatures had a very fast rise; the lower signature of shot 438, figure A38, is a good example of this. Apparently this is the result of an extremely large pressure peak which decays before the microphone can give an output that is more than some fraction of the peak value. This would result in a recorded first peak which might appear to the left of the line $t = 0$ in figure 19. Hence, in this case lack of microphone response probably prevents us from seeing some extremely large overpressures. In establishing a P_1 value for such situations, P_1 was always taken to be either as shown in figure 19 or as the amplitude of the first peak; the larger of these values was used.
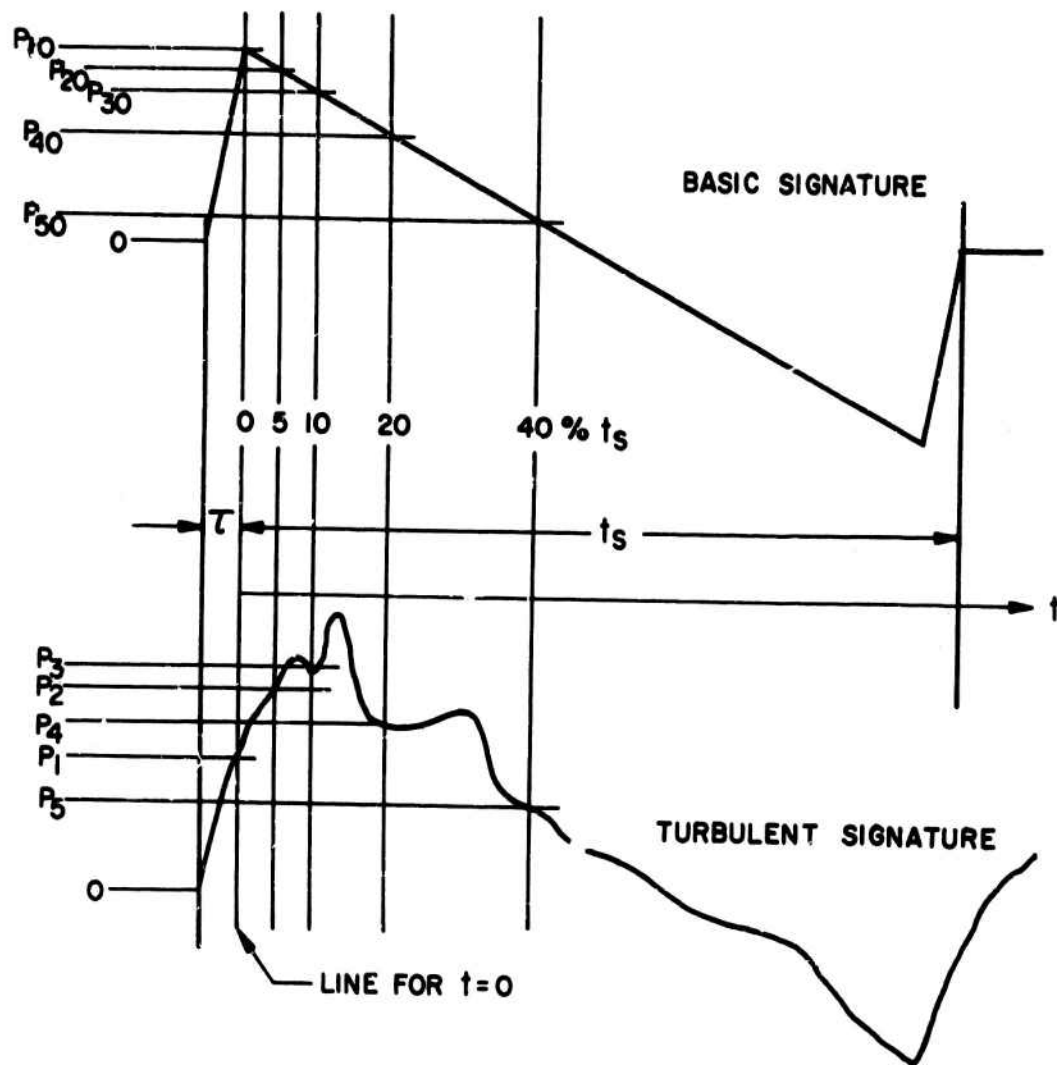
Figure 19   Sketch showing measurement stations and amplitudes for a basic
N-wave signature and for a turbulent signature.

60

From these definitions five nondimensional amplitudes were established for each signature:

$$H_1 = \frac{P_1 - P_{10}}{P_{10}} \tag{6}$$

$$H_2 = \frac{P_2 - P_{20}}{P_{10}} \tag{7}$$

$$H_3 = \frac{P_3 - P_{30}}{P_{10}} \tag{8}$$

$$H_4 = \frac{P_4 - P_{40}}{P_{10}} \tag{9}$$

$$H_5 = \frac{P_5 - P_{50}}{P_{10}} \tag{10}$$

In Appendix C these H_i's and P_i's are listed under the appropriate group and shot number, but the computer output does not lower the subscripts 1, 2, 3, 4, and 5. A 1 or a 2 follows each shot number to signify either the upper signature, from microphone B, or the lower signature, from microphone D, respectively. Table 6 below gives the values of P_{10} through P_{50} that were used together with the P_i's in equations (6) through (10) to compute the H_i's. The values of P_{10} through P_{50} were taken from the appropriate basic shots. All the P's here and in the appendix were measured in terms of the divisions which represented centimeters on the oscilloscope screen.

TABLE 6. — PARAMETERS READ FROM BASIC SIGNATURE SHOTS

Mach Number	Projectile	Microphone	t_s (sec. x 10^6)	P_{10}	P_{20}	P_{30}	P_{40}	P_{50}
1.4	B	B	317	0.95	0.85	0.68	0.43	-0.02
1.4	B	D	317	0.88	0.81	0.65	0.45	0.04
2.55	B	B	268	1.14	1.00	0.86	0.64	0.15
2.55	B	D	268	1.02	0.92	0.79	0.58	0.09
3.0	0.22 bullet	B	162	1.85	1.62	1.40	0.96	0.23
3.0	0.22 bullet	D	162	1.50	1.35	1.20	0.78	0.12

On each signature the peak amplitude P_{MAX} and the time at which this peak occurred in terms of percent of t_s were tabulated. These are also listed in Appendix C as P_{MAX} and TPK. Also listed is the quantity $H_{MAX} = P_{MAX}/P_{10}$. The computer was used to compute root-mean-square values of H_{MAX} and H_1 through H_5 for each group of data shots. These are listed as HRMS in the appropriate column.

Correlation coefficients F12, F13, F14, F15, F23, F24, F25, F34, F35, and F45 for the signature fluctuations between the various stations were calculated from the formula

$$f_{ij} = \frac{\sum_{k=1}^{k=n} H_{ik} H_{jk}}{n\, H_{iRMS} H_{jRMS}} \tag{11}$$

where n is the number of signatures in the group and H_{ik} and H_{jk} are simply the k-th values of H_i and H_j. H_{iRMS} and H_{jRMS} are the root-mean-square values of the n H_i's and the n H_j's, respectively. These correlation coefficients can range only from perfect correlation at +1.0 to a perfect negative correlation at -1.0.

For each group of signatures the computer was also used to list the variables TPK, H_{MAX}, H_1, H_2, H_3, H_4, and H_5 in columns starting with the largest number of each variable of the group and then proceeding to the next largest value and repeating this until all n values of each variable were listed. This tabulation was then used to calculate the probability P of exceeding each of these particular variable values through the formula

$$P = \frac{n_1 + n_2/2}{n} \tag{12}$$

where n_1 is the number of signatures in the group wherein the variable was larger than the particular value in question, and where n_2 is the number of signatures having the variable equal to the particular value in question.

An examination of Appendix C shows that a large number of statistical data points are available. Some of these are plotted and presented in section 6E.

Appendix C does not contain information for groups 114, 124, and 144. These were omitted because the variability of the Mach numbers obtained within these groups was so great that the above procedure could not be used. A total of 19 other groups of shots are presented in the appendix.

D.   Comments on the Number of Shots Required for Reliable Data

Crow, in Reference 7, has stated that for N sonic boom signatures the probable fractional error in the experimental value of a parameter such as $\overline{H_2^2}$ will be about $(2/N)^{1/2}$. Then the probable error in H_{2RMS} will be about $(1/2N)^{1/2}$. It is interesting to examine a few values of H_{2RMS} as a function of N starting with N = 1 for the first signature in the group and proceeding in the order that the shots were fired. For example, from several groups we obtain:

\ Group 234			Group 214			Group 134		
N	H_{2RMS}	fract.error	N	H_{2RMS}	fract.error	N	H_{2RMS}	fract.error
1	0.175	2%	1	0.123	17%	1	0.141	30%
3	0.138	23%	11	0.180	22%	7	0.280	37%
5	0.190	7%	20	0.142	4%	21	0.236	16%
7	0.164	8%	24	0.148	0%	41	0.225	10%
10	0.176	1%				61	0.220	8%
16	0.159	12%				81	0.214	5%
22	0.178	0%				101	0.219	7%
						121	0.212	4%
						141	0.217	6%
						161	0.210	3%
						181	0.219	7%
						207	0.204	0%

The above errors were calculated on the assumption that the last H_{2RMS} is correct.

According to Crow, the H_{2MAX} fractional error should be about:

$\underline{N}$	Fractional Error
10	22%
20	16%
100	7%
200	5%

The above group tabulations appear to support this order of fractional error.

E.   Data Presentation

Log normal probability distributions of the signature pressure peaks are shown in figures 20 and 21. These show that the lowest peaks come with the 6-inch nozzle, which has the smallest intergral scale, $L = 0.74$ in. The highest peaks were found for the 24-inch nozzle which has the largest integral scale, $L = 8.9$ in. The intermediate nozzle or 4-inch nozzle with $L = 2.7$ in. gave intermediate results in figure 21 and close to the largest peaks in figure 20.

Figure 20 is drawn for B projectiles at $M = 2.55$ and $L_s = 9.01$ in., whereas figure 21 is for 0.22 caliber bullets at $M = 3.0$ and $L_s = 6.41$ in. Since figure 20 has the larger normalized pressure peaks, this implies that H_{MAX} tends to increase with L_s. Thus figures 20 and 21 imply that H_{MAX} increases with the parameter L_s/L; these figures cover an L_s/L range of 0.72 to 12.2.

Somewhat smaller values of L_s/L are associated with group 124, shown in figure A11, but these data shots are difficult to evaluate because M was not sufficiently close to 1.4 to make the data useful.

The slopes on figures 20 and 21 are generally less negative than shown in the corresponding data at $M = 1.6$ for full-scale flight results as shown in figure 9 of Reference 8. This means that the experimental turbulence intensity was such as to create somewhat larger perturbations on the model scale than for the full scale results. Of course, the model scale perturbations were reduced as $\bar{U}$ was reduced, and the full scale results depend on the weather.

64
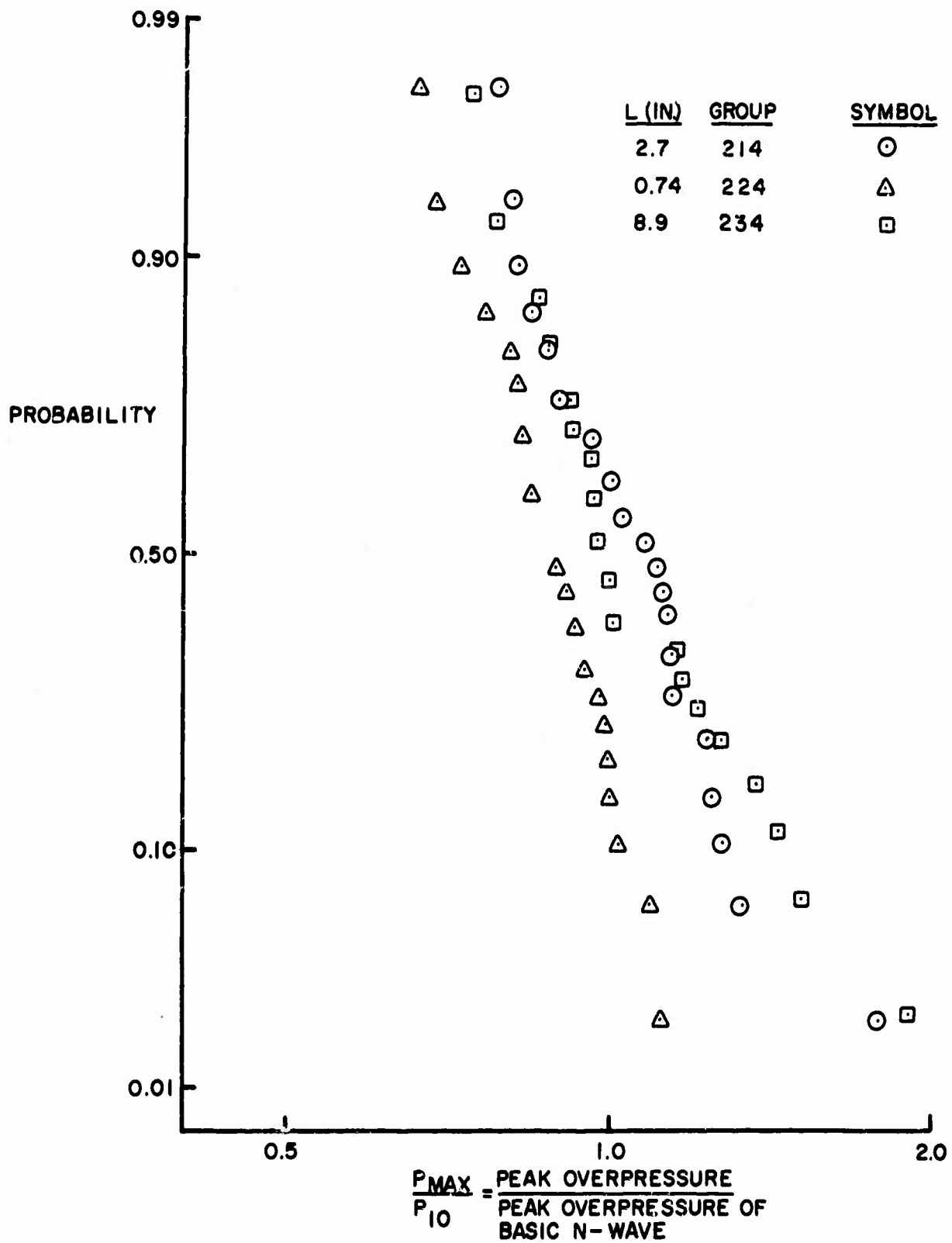
Figure 20 Probability of exceeding p_{MAX}/p_{10}. M = 2.55, B projectile.
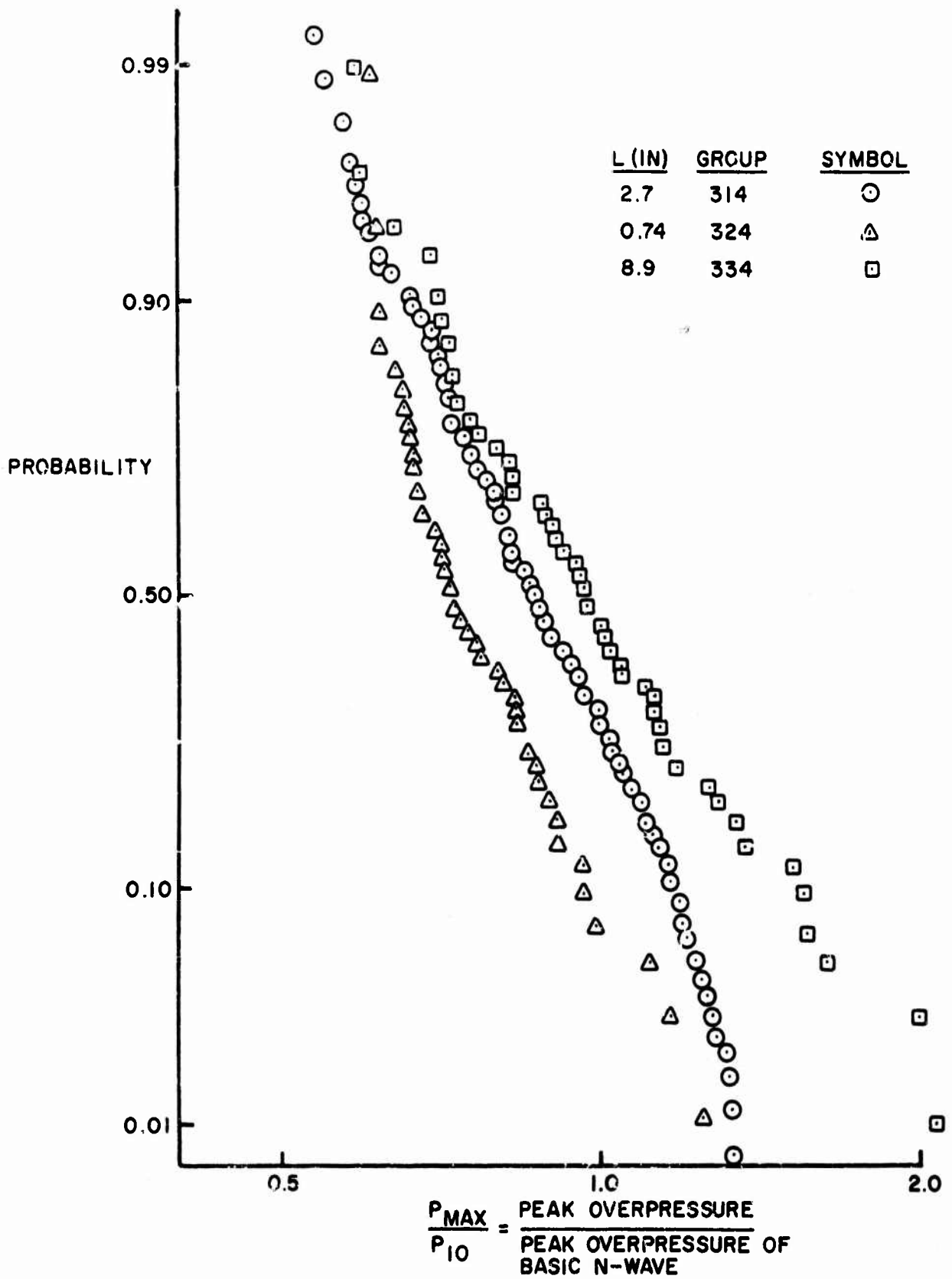
Figure 21 Probability of exceeding p_{MAX}/p_{10}. M = 3.0, 0.22 caliber bullet.

Normal probability distributions of t_{MAX}/t_s = TPK are given in figures 22 and 23. These show that the time to peak amplitude, t_{MAX}, increases as L decreases so that t_{MAX}/t_s increases as L_s/L increases for a fixed L_s. On the other hand, a comparison of figures 22 and 23 indicates that increasing L_s for a fixed L causes t_{MAX}/t_s to decrease. Apparently t_{MAX} does not vary with L_s. Therefore, t_{MAX}/t_s cannot be correlated with only L_s/L.

In figures 24, 25, and 26 the most probable values of H_1 through H_5 are plotted with respect to a normalized N-wave pressure distribution. This gives the most probable shape of the turbulent signature. The figures show that a change in nozzle such that $1/L$ is increased causes an increase in the rounding of the leading part of the N wave.

This rounding is compensated for later when the most probable shape rises above the N-wave; again the departure from the N-wave increases as $1/L$ increases.

These departures from the basic N-wave shape are larger in figure 25 than in figure 24; therefore, these departures do not correlate with the parameter L_s/L.

Figures 24 and 26 document the expected result that the departures decrease as $\bar{U}$ and u' are decreased.

F. Comparison of Experimental Results and Crow Theory

In Reference 1 Crow predicts that under the assumption of homogeneous turbulence the ensemble average of the normalized and squared boom pressure fluctuations should follow a 7/6 power law in the form

$$\langle \psi^2(t) \rangle = \left(\frac{t_c}{t}\right)^{7/6} \tag{13}$$

In the absence of thermal effects, Crow's expression for the time t_c is

$$t_c = \frac{1}{c} \left[\frac{M}{(M^2 - 1)^{1/2}}\right]^{11/7} \left[\int_0^\infty \frac{(1.33)y^{5/6}\epsilon_u^{2/3}}{c^2} \, dy\right]^{6/7} \tag{14}$$

67
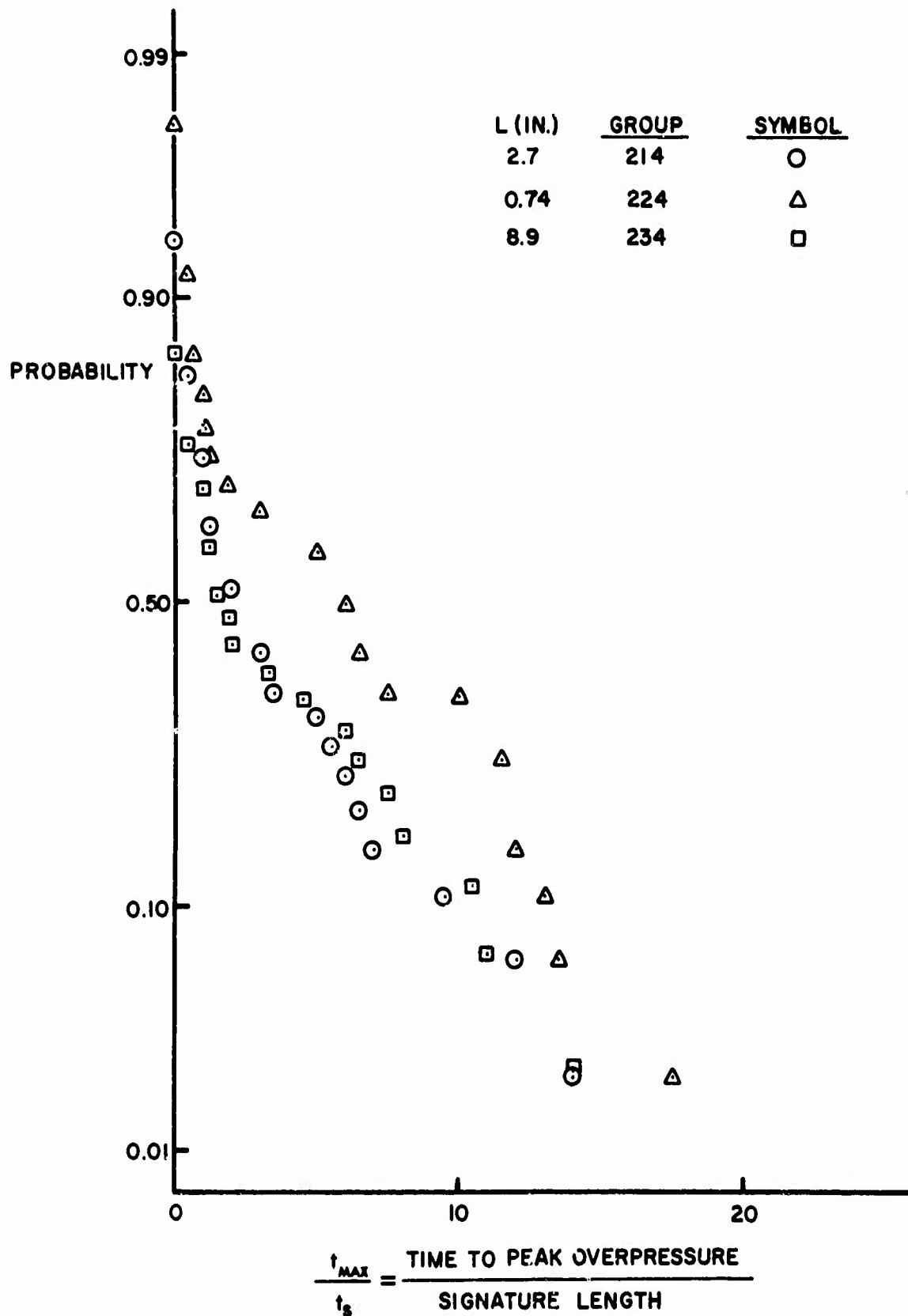
Figure 22 Probability of exceeding t_{max}/t_s . M = 2.55, B projectile.
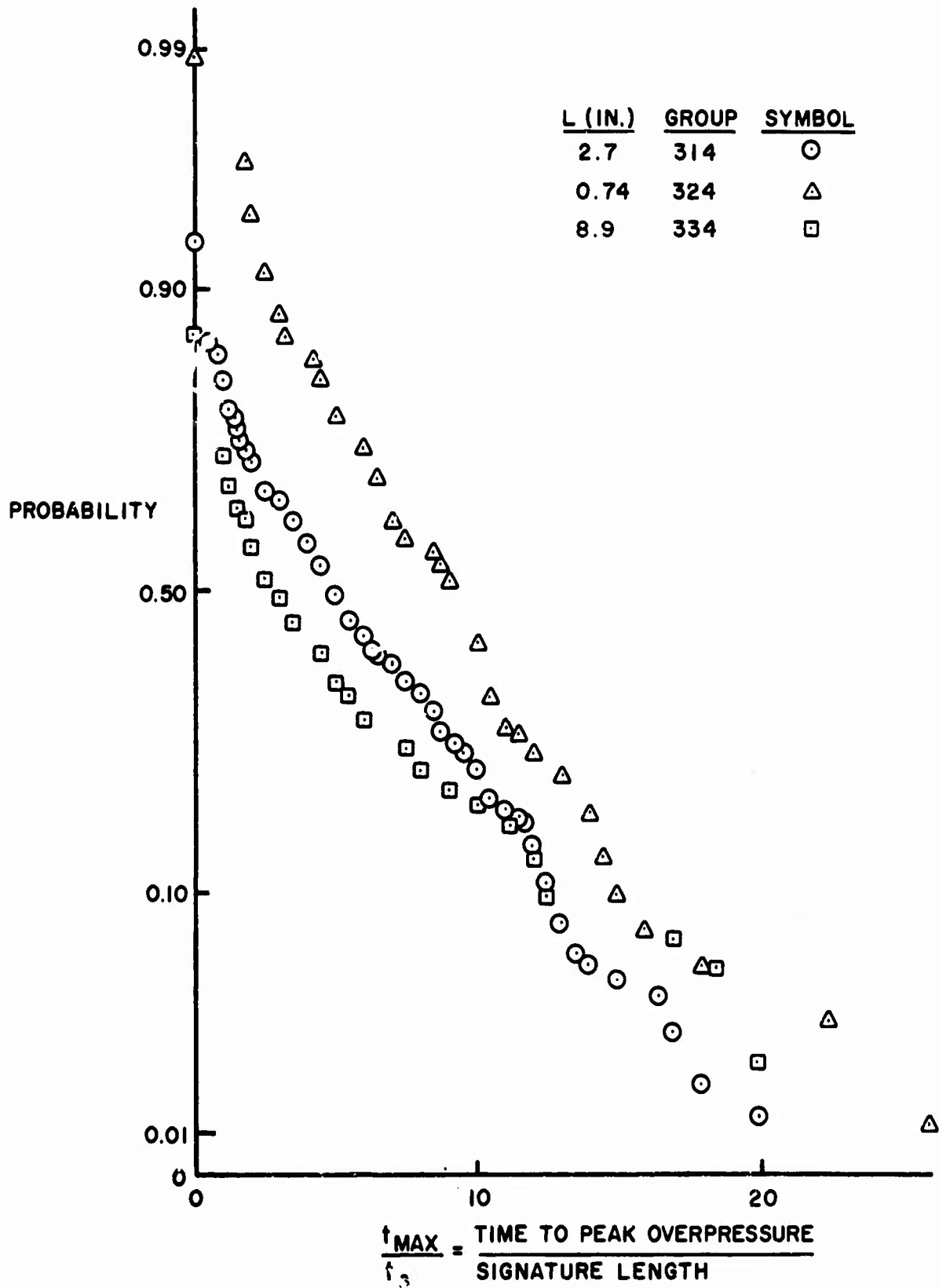
Figure 23 Probability of exceeding t_{MAX}/t_s. M = 3.0, 0.22 caliber bullet.

69
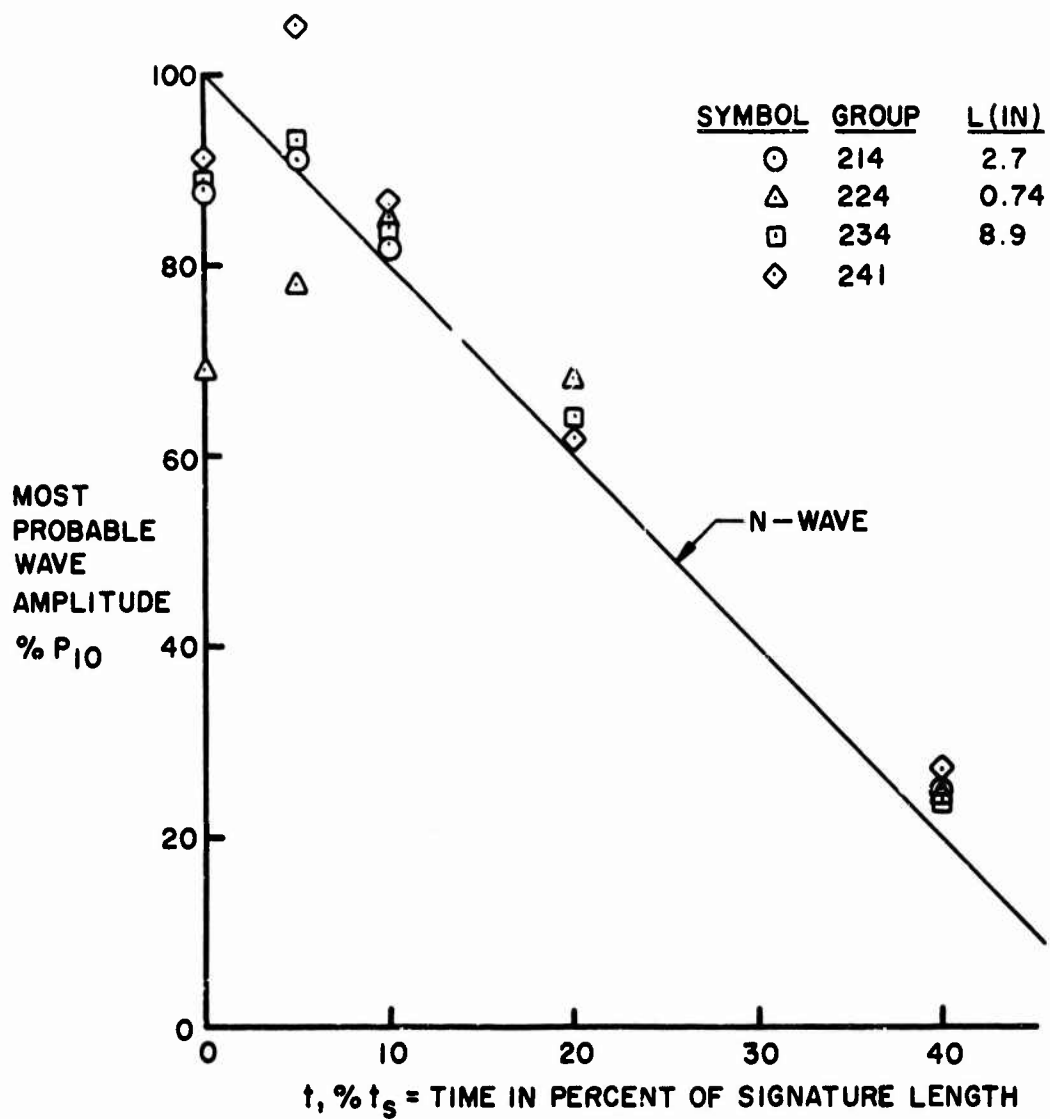
Figure 24 Comparison between an N-wave and the most probable wave amplitude. M = 2.55, B projectile.
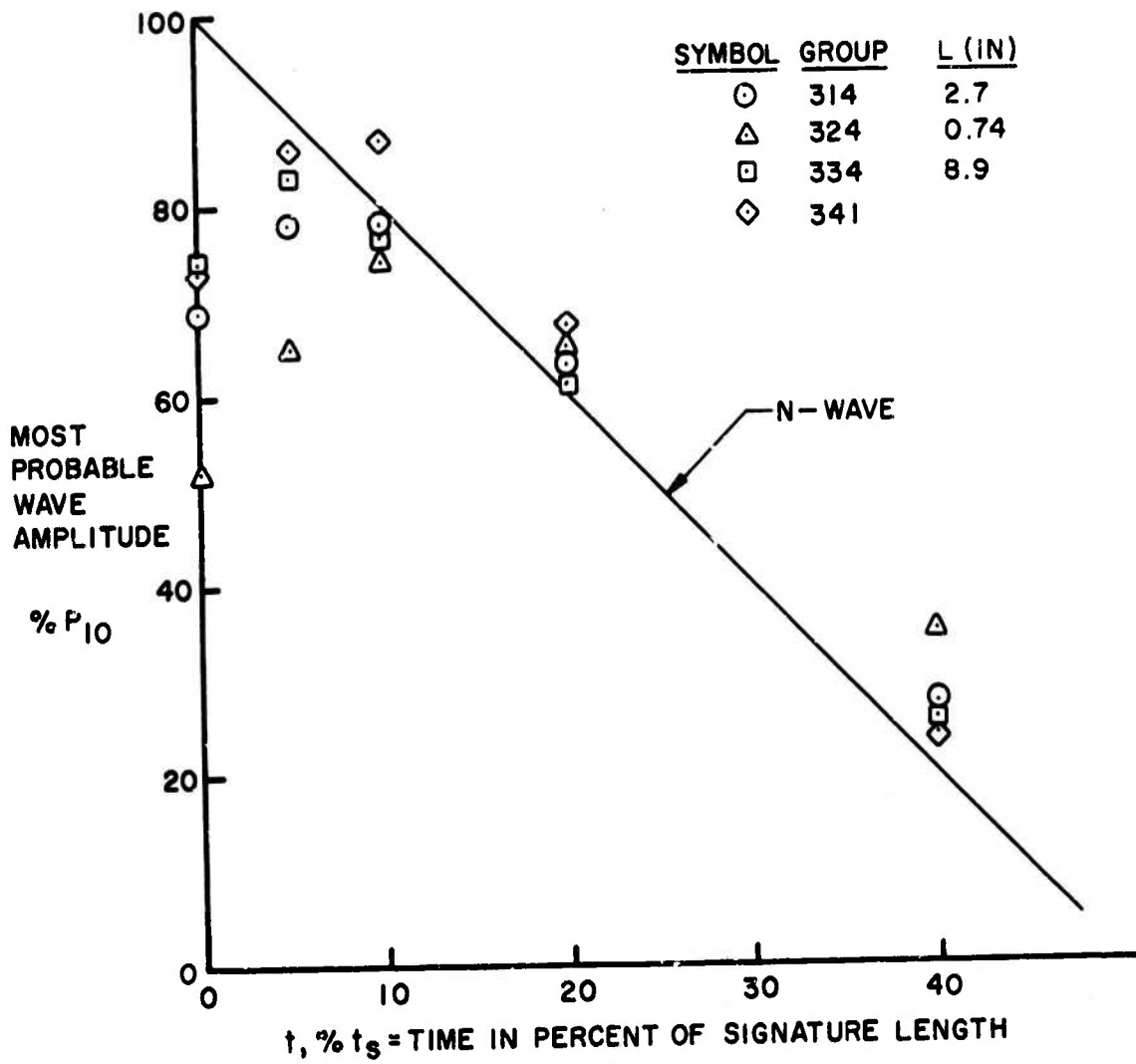
Figure 25 Comparison between an N-wave and the most probable wave amplitude. M = 3.0, 0.22 caliber bullet.
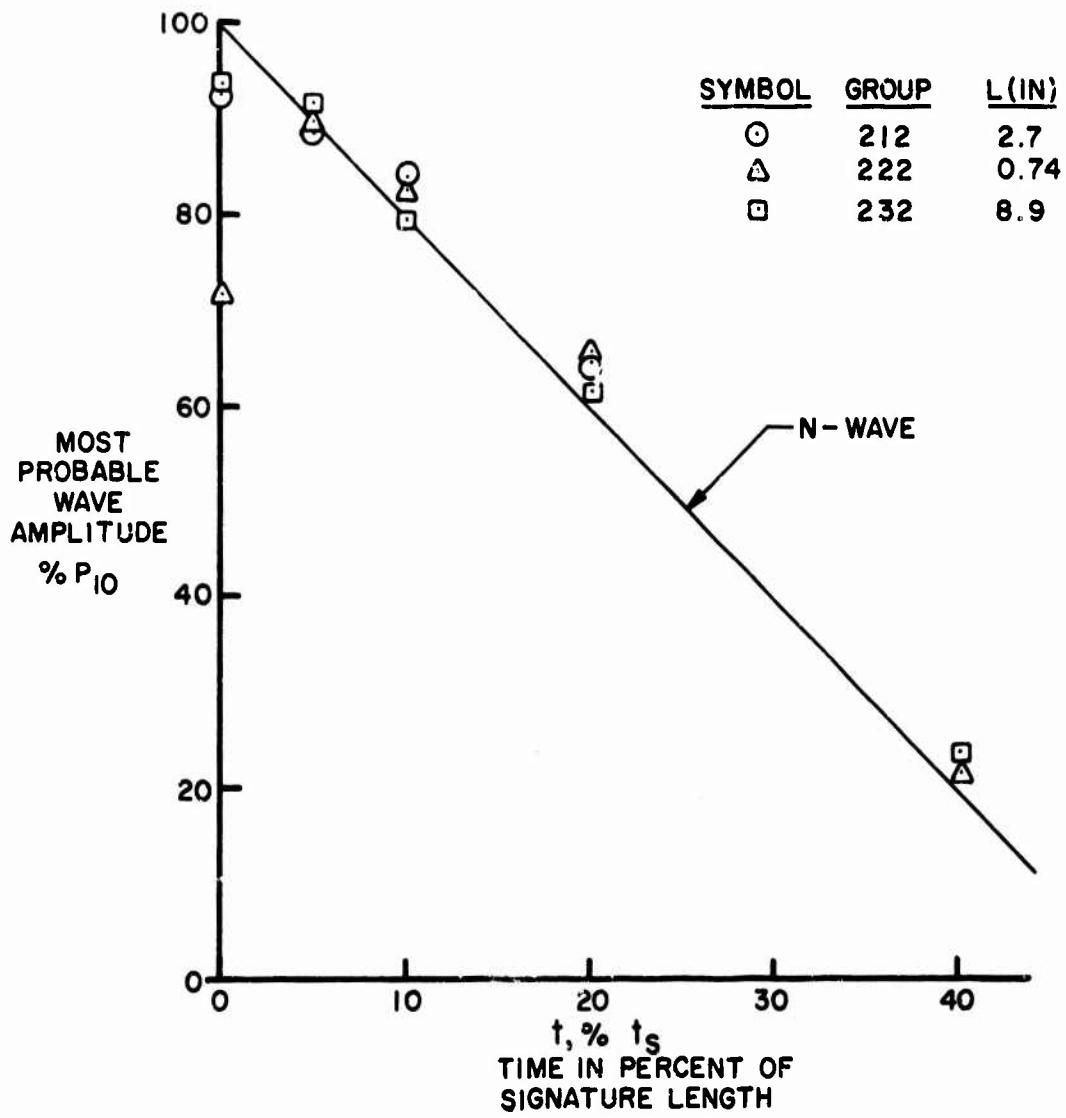
Figure 26 Comparison between an N-wave and the most probable wave amplitude. M = 2.55, E projectile, blower inlet diameter = 16 inches.

For the turbulent jets of figures 8, 9, and 10, we can take a jet thickness of 2.5 ft. and a mean turbulent intensity of 7 ft/sec. Then we can roughly approximate the above integral by

$$I = 1.33 \int_0^{2.5 \text{ ft.}} \frac{(7 \text{ ft/sec})^2 (2.5 \text{ ft})^{1/6}}{(1100 \text{ ft/sec})^2} \, dy \tag{15}$$

so that

$$t_c = 0.50 \left[\frac{M}{(M^2 - 1)^{1/2}} \right]^{11/7} \times 10^{-6} \text{ sec.} \tag{16}$$

Figures 27, 28, and 29 show experimental values of $\langle \psi^2(t) \rangle$ compared with calculations of $(t_c/t)^{1/6}$ based on the above t_c. The results on figures 27 and 28 show rough agreement for t/t_s equal to 0.05 and 0.10. Agreement is best for the 4-inch nozzle where the ensemble average was done for a greater number of shots. Of course, the above calculation of I is quite rough so that good agreement is not really expected. The calculation of I does not apply to the high-speed nozzle, so that agreement for groups 241 and 341 is not expected.

In figure 29 the agreement is not good probably because the small values of $\bar{U}$ and u' lead to large errors in the calculation of factors u_1 through H_5.

G. Correlation of Turbulence Spectra Data and Boom Signatures

As shown by Reference 6, the turbulence spectral function $E_1(n)$ and the correlation function $f(x)$ are Fourier transforms. This fact is useful because it infers that the correlation function is equivalent to the spectral function and vice versa. For the present purposes it is more convenient to use the correlation functions as shown in figure 16.

Figures 30 and 31 show the two-point correlation coefficient for various portions of the boom signatures as computed from equation (11). These f_{ij} may be compared to figure 16. For example, in figure 16 for the 6-inch nozzle at $x = 1$ inch, f is 0.30; for the 4-inch nozzle $f = 0.52$, and for the 24-inch nozzle $f = 0.79$. In figure 30 for i at 5 percent L_s, f_{ij} is equal to 0.38, 0.50, and 0.63 for the three above nozzles at $j = 9$ percent L_s.

73
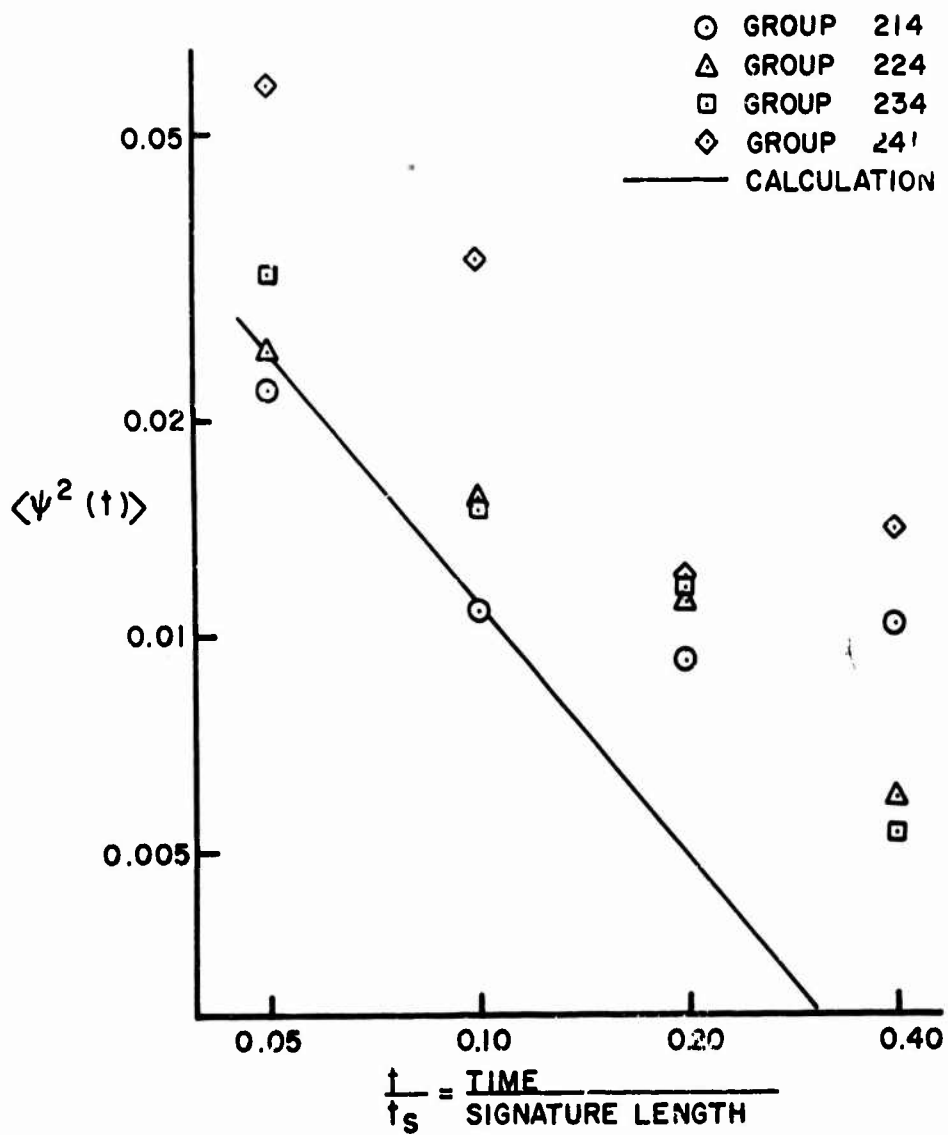
Figure 27 Comparison between $\langle \psi^2(t) \rangle$ measured in the present experiments and that calculated on the basis of theory of Crow. M = 2.55, B projectile.

74
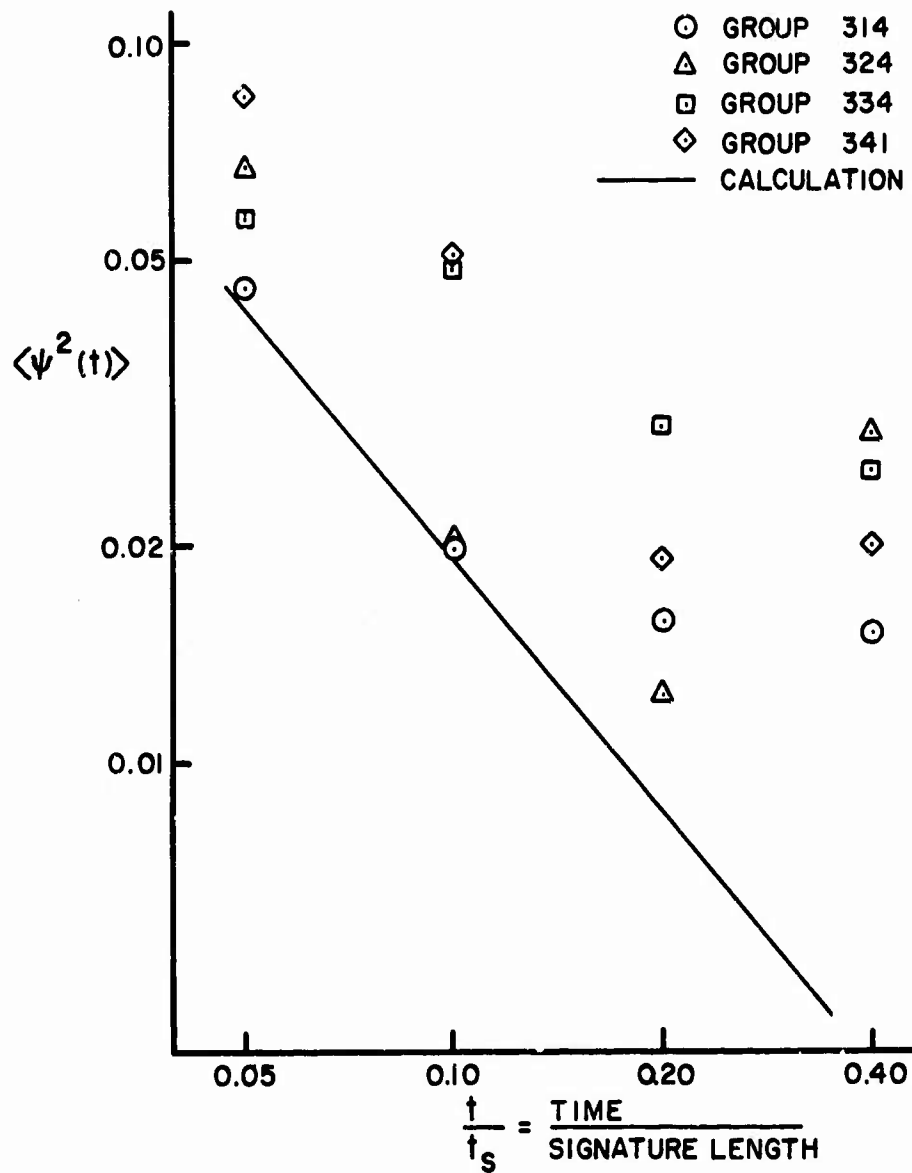
Figure 28 Comparison between $\langle \psi^2(t) \rangle$ measured in the present experiments and that calculated on the basis of the theory of Crow. M = 3.0, 0.22 caliber bullet.
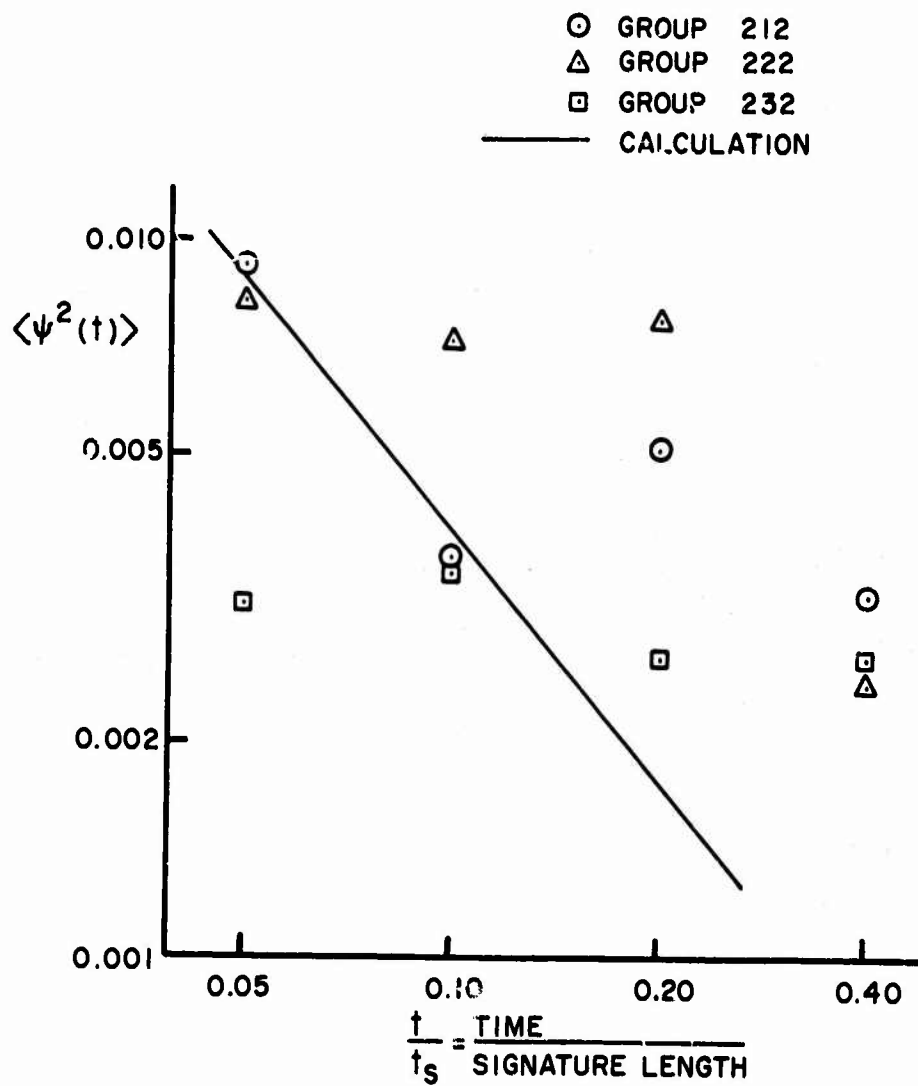
Figure 29 Comparison between $\langle \psi^2(t) \rangle$ measured in the present experiments and that calculated on the basis of the theory of Crow. M = 2.55, B projectile, blower inlet diameter = 16 inches.
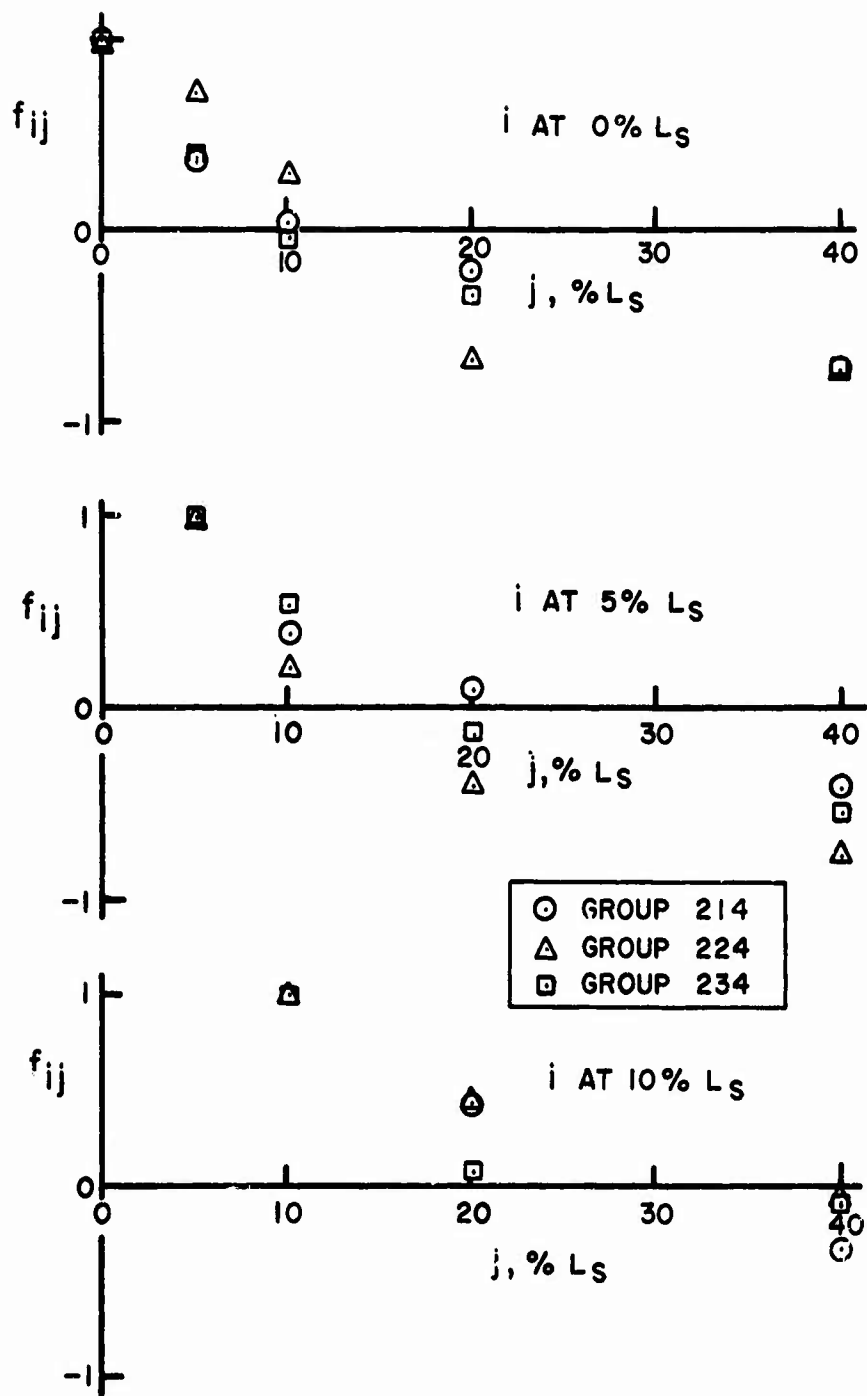
Figure 30 Experimental values of boom signature two-point correlation coefficients. M = 2.55, B projectile, L_s = 9.01 inches, blower inlet diameter = 24 inches.
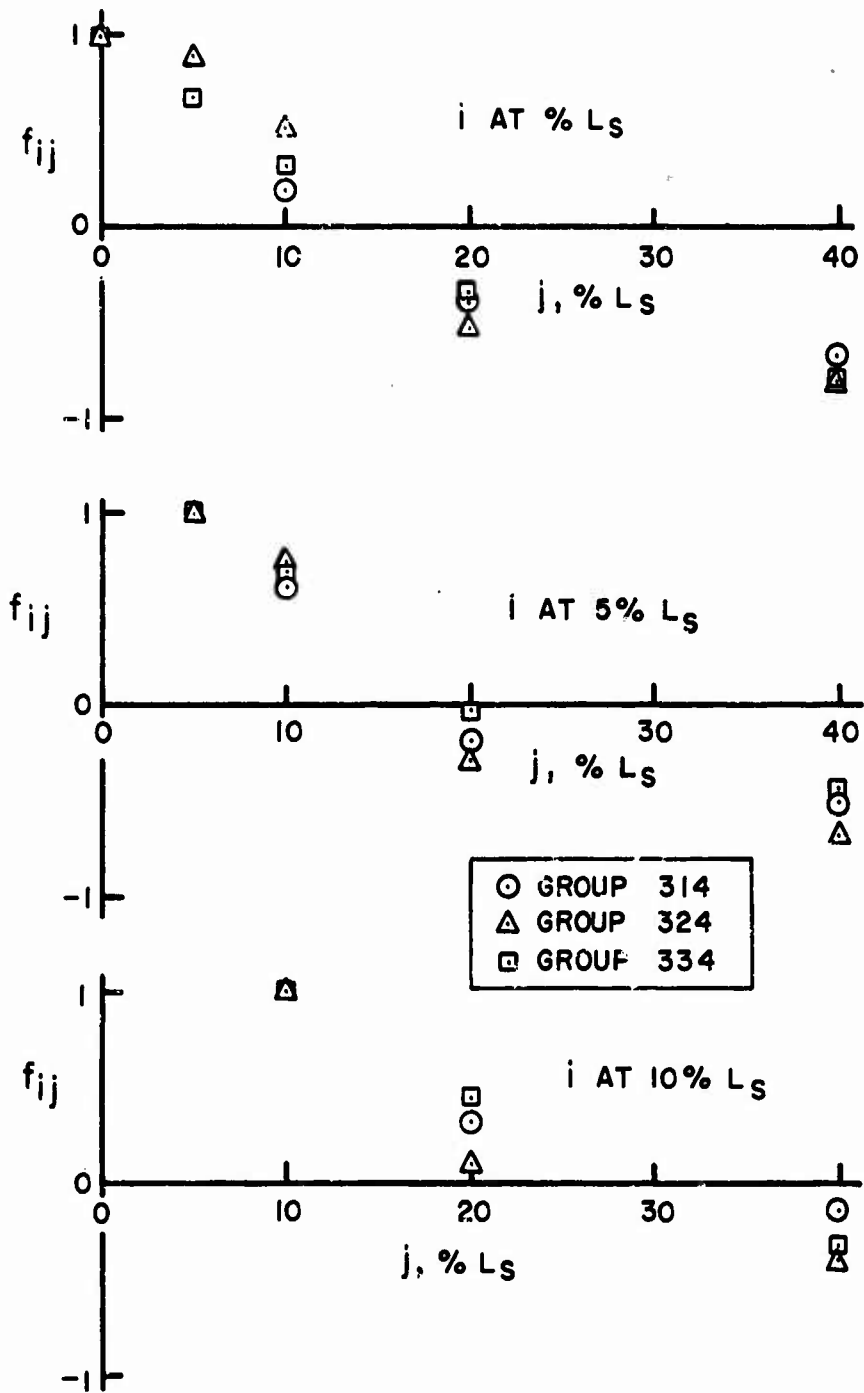
Figure 31 Experimental values of boom signature two-point correlation coefficients. M = 3.0, L_S = 6.41 inches, 0.22 caliber bullet, blower inlet diameter = 24 inches.

These three f_{ij}'s correspond roughly to the above three f's for the same three nozzles. These f_{ij}'s correspond to 4 percent L_s in distance from i; 4 percent L_s is 0.36 inches. Hence, a length of 0.36 inch on the f_{ij} curves corresponds roughly to 1 inch on the f curves. The corresponding length of time is 10.7 microseconds. In this length of time Crow's paraboloid of dependence changes radius R between values R_i and R_j, where R_j minus R_i is given approximately by

$$R_j - R_i = (2cx_n)^{1/2}(t_j^{1/2} - t_i^{1/2}) \tag{17}$$

where t_j and t_i are 24.1 and 13.4 microseconds, respectively. Hence

$$R_j - R_i = 0.200x_n^{1/2} \tag{18}$$

so that at a location x_n = 16 in. along the axis of the paraboloid from the microphone we would have $R_j - R_i$ = 0.80 in. This says that for such a change in the paraboloid of dependence for the three nozzles the three correlation coefficients have been determined from the ensemble of experimental signatures to be 0.38, 0.50, and 0.63. Corresponding lengths x in figure 16 are approximately one inch. These lengths should correspond, if we are to accept the Crow theory, to some average value of $R_j - R_i$. Since $R_j - R_i$ is just one inch at x_n = 25 in., the measurements all seem to fit the paraboloid of dependence idea. Actually x_n varies from 0 to about 33 inches before leaving the turbulent jet field, and the greatest turbulent intensities are near x_n = 28 in.

The above argument takes into account the fact that f is defined (Reference 6) as the longitudinal correlation coefficient. The lateral coefficient g would be inappropriate, since according to the Crow theory only the radial component of the gradient of u' or $(\partial u'/\partial R)$ contributes to the scattering.

The above arguments imply that the f_{ij}'s in figures 30 and 31 should be largest for the nozzle with the largest integral scale L and vice versa, at least for i and j close together so that the correlations are positive. This ordering appears only for the middle portion of figure 31. The upper portions of figures 30 and 31 can probably be excused on the basis that the correlation of data at any point with that at i = 0 depends on conditions

79

where the paraboloid is only a straight line and the Crow theory breaks down.

Another question is the reason for the negative values of the f_{ij}'s at sufficiently large distances between i and j. This is unlike $f(x)$, which is always positive. However, we have already seen in figures 24 and 25 that the turbulent fluctuations near 0 percent L_s and 40 percent L_s tend to be negatively correlated.

H.   Discussion of Interaction Models

It is possible to synthesize the mechanisms put forth by various authors into a model for the sequence of events that occurs after an undisturbed N-wave enters a turbulent boundary layer:

(1)   Wave fronts wrinkle due to refraction (Pierce, Reference 3), and scattered waves are emitted into the regions behind the shocks (Crow, Reference 1).

(2)   Focusing and defocusing of the wave fronts leads to formation of caustics and multiple fronts (Pierce, Reference 3). The shock wave decays due to scattering and formation of multiple fronts.

(3)   The shock wave decays to zero strength, while the subsequent system of compression waves steepens or disperses depending on unbalance between nonlinearity and dispersion:

(a)   Nonlinear steepening. The compressive front steepens in a distance

$$\ell \approx \frac{\delta_o}{\Delta p/p} \tag{19}$$

where δ_o = initial thickness of compression wave and $\Delta p/p$ is its strength.

(b)   Dispersion. If a wave front refracts through a typical angle ϵ with a typical free path λ between refractions, then the extra propagation distance $\Delta \ell = \delta_o$, i.e., the thickness, will be

$$\delta_o = \epsilon \lambda \sqrt{\frac{\ell}{\lambda}} = \epsilon \sqrt{\ell \lambda} \tag{20}$$

80

The transients discussed in (1) through (3) die out.

(4) The disturbance propagates with an equilibrium thickness (George, Reference 2) given by a balance between equations (19) and (20),

$$\delta_o = \epsilon^2 \lambda p / \Delta p \tag{21}$$

Scattered waves in the regions behind the fronts (Crow, Reference 1) do not pile up to infinite amplitude because of the thickness of the front (George, Reference 2).

The time scales of these processes determine at what stage the sonic boom is when it reaches the ground. For example, the path length required for stage (3) is given by equations (19) and (21).

$$\ell = \epsilon^2 \lambda / (\Delta p / p)^2 \tag{22}$$

The "accepted values" for the full-scale atmosphere are

Full scale:

$$\epsilon \sim \frac{\Delta u}{c} \sim 0.01$$

$$\lambda \sim 100 \text{ ft.}$$

$$\Delta p / p \sim 10^{-3}$$

so $\ell \sim 10^4$ ft. Thus, it is unlikely that any sort of equilibrium structure, as discussed by George, is achieved in the full-scale case. Furthermore, for experiments,

Experiments:

$$\epsilon \sim 0.1$$

$$\lambda \sim 1 \text{ ft.}$$

$$\Delta p / p \sim 10^{-2}$$

so $\ell \sim 100$ ft., and it is seen that the experiments are even further from equilibrium. If ℓ is scaled with the boundary-layer thickness δ, then (ℓ/δ) full scale = 3, while (ℓ/δ) exp. = 50. In this sense the experiments do not scale, but this is somewhat academic since equilibrium is not reached either on the full or on the model scales. More work needs to be done to really understand these interactions.

81

I.   Scaling Parameters

The above results lead to the tentative conclusion that the linear Crow theory is for the most part correct, but that a better explanation is needed for the phenomena in the neighborhood of the leading shock.

The significant parameter in the Crow formulation is the critical time t_c. This time is given approximately by

$$t_c \doteq \frac{\delta}{c} \left(\frac{u'}{c}\right)^{12/7} \tag{23}$$

where δ is the thickness of the turbulent layer and u' is a representative value of the turbulent intensity. Then

$$\langle \psi^2(t) \rangle \doteq \left(\frac{u'}{c}\right)^2 \left(\frac{\delta}{ct}\right)^{7/6} \tag{24}$$

Since the theory is a linear one, we should not worry much about how u', δ, or t compare individually between the model scale and the full scale experiments; only the product $u'^2(\delta/t)^{7/6}$ is important since the speed of sound c is essentially the same in both cases. Also, since we are free to choose any length of time t that is convenient, the product $u'^2\delta^{7/6}$ is not too important except for experimental convenience. Of course, these products should be limited so that interesting values of $\langle \psi^2 \rangle$ will appear in times t greater than h_T/c, where h_T is the Taylor shock thickness, and less than t_s. Hence the signature length L_s is of importance only insofar as the second N-wave shock will interfere with the observation of the fluctuation caused by the first N-wave shock.

For the model signatures to appear geometrically similar to the full-scale results, it is necessary that the ratio t_s/t_c be preserved. Crow estimates that t_c is on the order of 1 millisecond whereas t_s is about 250 milliseconds, so that a ratio of 250 may be typical of an average SST on an average day. For the present experiments with the 24-inch blower inlet and the 4-inch, 6-inch, or 24-inch nozzles, t_c is about 0.6 microseconds. Therefore, for the 200 groups t_s/t_c is 450, and for the 300 groups t_s/t_c is 270. Hence the model scale should give a signature that is geometrically like the full-scale results.

In the discussion of the peak pressure parameters in figures 20 and 21 it was noticed that the pressure peaks increased with an increase in L_s. This may have been only the result of a nonlinearity in the results. This nonlinearity is illustrated in figures 24 and 25 as a difference between the most probable shape of a turbulent signature and the shape of the basic N-wave signature. This phenomenon is not understood; if it is a true nonlinearity it would seem that it should appear with greater strength on figure 24 where the basic N-wave amplitude is about 50-percent larger than on figure 25. Instead, the reverse is true.

The turbulence integral scale L has been shown to affect the spectrum of the boom signature; the frequency of the signature fluctuations is increased with decreasing L and vice versa.

J.   Implications for Full-Scale Boom Phenomena

From the above scaling parameter discussion it is clear that two parameters of importance are δ and u'. These are both natural atmospheric parameters over which man has little control. About all that can be done is to design aircraft so that the basic N-wave is as small in amplitude as possible. Then the atmospheric turbulence effects will also be reduced in amplitude.

The shock wave breakup at the front of the boom is not yet understood and hence deserves more attention.

7. DISCUSSION OF ALTERNATE FACILITIES

The present study was limited by the microphone frequency response being limited to 140 kilohertz or less. In any future work one would like to overcome this problem so that sharper spikes might be recorded with the boom signatures.

Equation (24) shows that

$$\langle \psi^2(t) \rangle \doteq \left(\frac{u'}{c}\right)^2 \left(\frac{\delta}{ct}\right)^{7/6}$$

This means that the product $u'^2 \delta^{7/6}$ must be increased in future experiments so that a longer time t is available in which to measure a given amplitude of $\langle \psi^2(t) \rangle$. The unfortunate problem here is that increasing either u' or δ means an increased power input into the turbulent jet.

For a longer measurement time t a longer signature length L_s is also required to preserve the factor t_s/t_c and to enable the measurements to be made well before the arrival of the trailing shock. Since many shots are required to obtain meaningful data, the gun or other mechanism used to produce the long L_s must be economical to operate.

Hence, the problems in alternate methods of performing the Task II work on a scale more nearly full scale are two-fold:

(1) The turbulence generator must be greatly enlarged with a resulting increase in cost.

(2) A larger gun or other mechanism must be used to generate the booms.

The logical extension of this line of reasoning is to use the natural turbulence in the atmosphere, but this then requires a rather large supersonic projectile or airplane. Also, the atmospheric variability is not conducive to this approach. Therefore, a suitable facility compromise between size and cost is discussed below.

A. Alternate Facility for Obtaining Data for Task II and IV Problem Areas

The facility layout is sketched in figure 32. This would give a four-fold or better increase available in the product $u'^2\delta^{7/6}$; the boom signature length would be a factor of 2 larger than with the present B projectiles. The increase in $u'^2\delta^{7/6}$ would mean approximately a four-fold increase in microphone resolution. The facility could also be used for topographical model experiments.

The greater microphone resolution available with the above facility would enable the spiky structure of the turbulent booms to be recorded with better fidelity. The apparently nonlinear mechanism illustrated in figures 24 and 25 would also be studied.

B. Suggestions for Other Types of Sonic Boom Generation Facilities

Two novel techniques for sonic boom generation have recently been suggested and are illustrated in figure 33. These techniques are so new that a thorough study of their feasibility has not yet been made. They are added here for completeness. The first of these techniques, the vented shock tube, had its origin from a Douglas Aircraft Company sponsored study on means of simulating the sonic boom generated by maneuvering aircraft. The second technique, the hammer-driven shock tube, originated from the present contract study on alternate facilities.

1. Vented Shock Tube Facility

The vented shock tube is composed of a long tube containing a driver section and a vented section as shown in figure 33a. The vented section contains a long slit open to the atmosphere. As the shock passes the vented section, gas is ejected through the slit. This gas acts as a finite-length line source which is effectively a body moving at supersonic speed so that the usual bow shock is formed. This facility has the advantages of economical operation and an effective body diameter that can easily be much larger than the projectiles used to date. These advantages are combined with the lack of danger from flying projectiles; this means that such a facility may be constructured on as large a scale as desired without the disadvantages of a location remote from population centers.
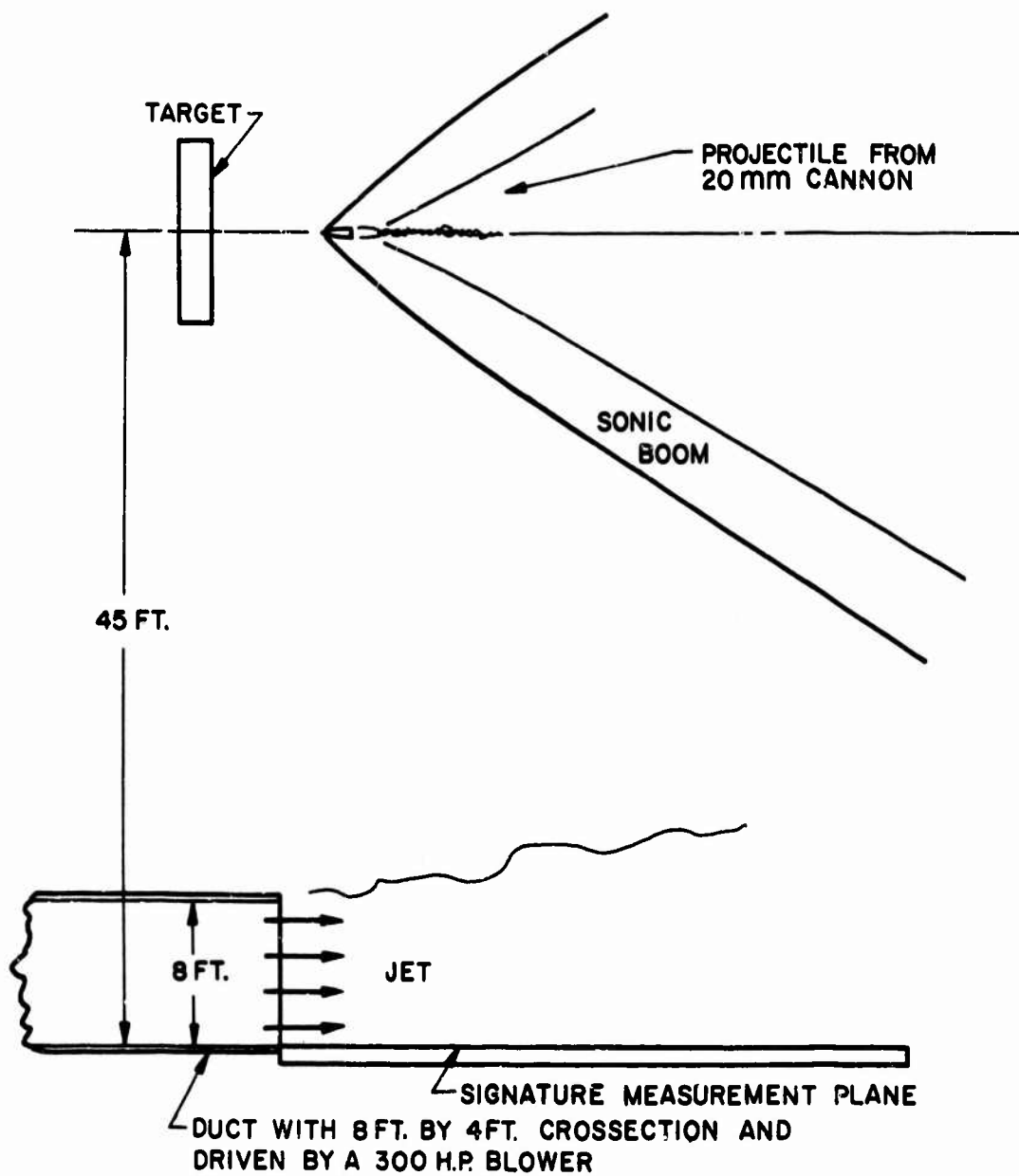
Figure 32 Plan view of an alternate facility for sonic boom testing on a larger scale for improved high-frequency fidelity.
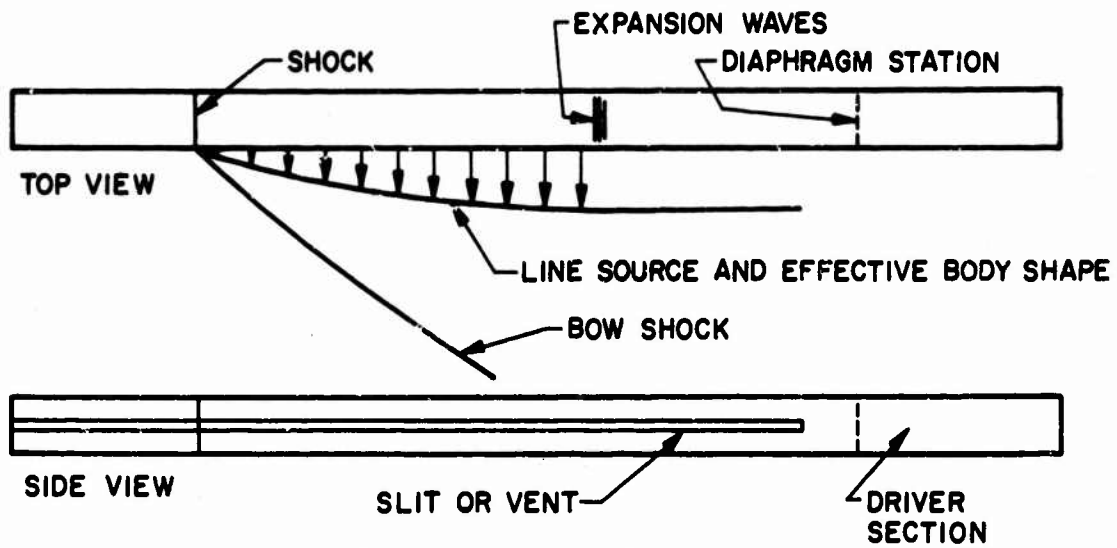
(a) VENTED SHOCK TUBE
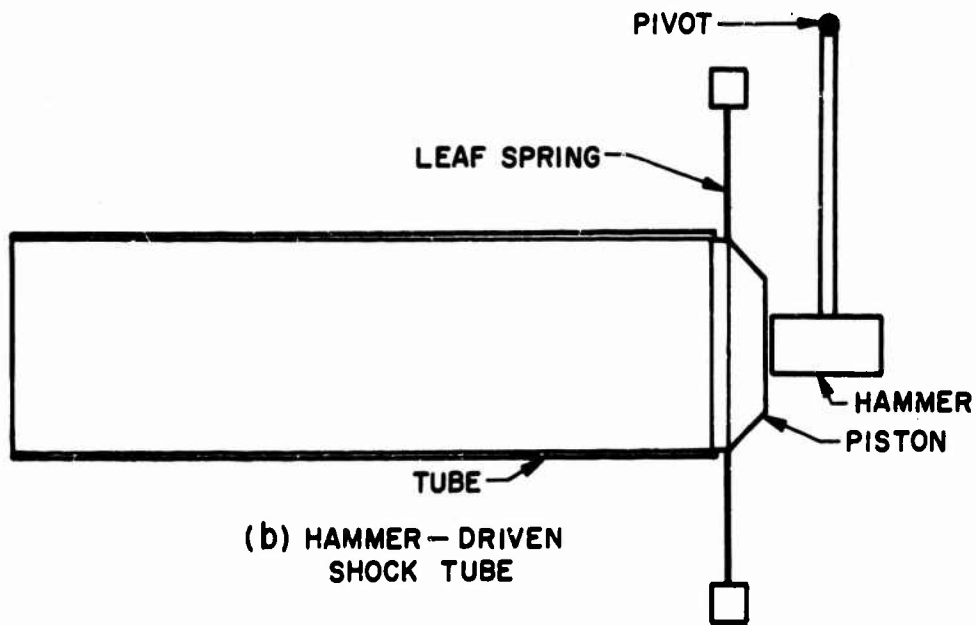
(b) HAMMER — DRIVEN
SHOCK TUBE

Figure 33 Novel techniques for sonic boom generation.

2. Hammer-Driven Shock Tube

The flow inside a conventional shock tube may be used for boom research, but the chief problem in this technique is the difficulty of generation of the required low-amplitude N-waves. The facility envisioned in figure 33b is intended to overcome this problem through the use of a large piston driven by a hammer. The hammer is released from an elevated position and gravity is utilized to accelerate the hammer into the piston so as to make the piston motion as impulsive as possible. This impulse would generate the leading compression wave. The spring then gradually decelerates the piston and returns it to the stop. This motion generates the expansion portion of the N-wave. The stop is probably in the form of a heavy mass designed to impulsively decelerate the piston and to produce the trailing compression wave.

Such a facility could be constructed on a fairly large scale, say a cross-section of 8 feet by 8 feet. Since the overpressures would be low, conventional building methods might be used to build the tube walls. The facility could be designed to produce N-waves having the same amplitude and length as full-scale sonic booms.

8. CONCLUSIONS

A sonic boom modeling investigation of topographical and atmospheric effects has been carried out and the following conclusions have been reached:

(1) Boom focusing will usually occur in structural shapes having interior corners, but almost any sort of shielding of the corners will reduce the focusing effect.

(2) Boom focusing effects depend on the direction of the incident wave with respect to the structure or topographical shape.

(3) Large canyons and similar shapes can cause strong focusing of booms, but large focusing effects will occur only for rather specialized shapes and particular directions of the booms.

(4) The theory of Crow explains the essentials of boom signature fluctuations in a turbulent atmosphere, but the mechanisms of the shock front breakup and of certain nonlinear features are not yet understood.

(5) The boom signature fluctuations depend primarily on the height δ of the atmospheric boundary layer, the distribution of turbulence intensities u', and the turbulent spectral energy distribution and related integral scale L. Mean velocity and temperature gradients will also affect the fluctuations.

(6) Atmospheric shear layers cannot be studied alone for their affect on boom signatures because such shear layers always generate turbulence which affects the signatures.

(7) The boom signature fluctuations can be better understood by obtaining a larger number of data shots and by a more detailed study of the statistical data. The fine scale spiky structure can be studied on a larger scale by increasing the turbulence intensities u' and by increasing the turbulent layer thickness δ. This larger scale is needed so that no fine structure might be overlooked because of limitations in microphone response to high frequencies.

(8) The experiments clearly show that the signature perturbations observed
     near the leading N-wave shock are repeated near the trailing N-wave
     shock: this result agrees with full-scale observations and is
     explained in the Crow theory by the "freezing" of the turbulence
     during the short passage time of the N-wave.

9. REFERENCES

1. Crow, S.C.: Distortion of Sonic Bangs by Atmospheric Turbulence. J. Fluid Mech., Vol. 37, p. 529, 1969. (Also see NPL Aero Report 1260, 1968.)

2. George, A.R., and Plotkin, K.E.: Weak Shock Waves in Turbulent Media. AIAA Paper No. 70-54, Jan. 1970.

3. Pierce, A.D.: Statistical Theory of Atmospheric Turbulence Effects on Sonic Boom Rise Times. MIT Dept. of Mech. Eng. Preprint No. 1059, Oct. 1969.

4. Pierce, A.D.: Spikes on Sonic-Boom Pressure Waveforms. J. Acoust. Soc. Amer. 44, pp. 1052, 1968.

5. Ting, L.; and Pan, Y.S.: Incidence of N-Waves on Structures. NASA SP-180, p. 89, May 1968.

6. Hinze, J.O.: Turbulence. McGraw-Hill, 1959.

7. Crow, S.C.: Proposals for Exercise Checkerboard. NPL Aero Note 1068, A.R.C. 30, 159, Apr. 1968.

8. Maglieri, D.J.; Huckel, V.; and Henderson, H.R.: Variability in Sonic-Boom Signatures Measured Along an 8000-Foot Linear Array. NASA TN D-5040, Feb. 1969.

9. Anon.: Sonic Boom Modeling Investigation of Topographical and Atmospheric Effects. McDonnell Douglas Report 3968T, Oct. 1968.

10. Freymuth, P.: Noise in Hot-Wire Anemometers. Rev. Sci. Instruments, Vol. 39, p. 550, 1968.

11. Freymuth, P.: Feedback Control Theory for Constant-Temperature Hot-Wire Anemometers. Rev. Sci. Instruments, Vol. 38, p. 677, 1967.

12. Collis, D.C.; and Williams, M.J.: Two-Dimensional Convection from Heated Wires at Low Reynolds Number. J. of Fluid Mech., Vol. 6, p. 359, 1959.

APPENDIX A
BOOM SIGNATURE TRACES

Presented here are the boom overpressure time histories as recorded by photographing the microphone outputs displayed on an oscilloscope screen. On each picture the abscissa is the time scale and the ordinate is the pressure scale. The time scale in microseconds per division is given below each picture or group of pictures. The pressure scale in pounds per square inch per division is shown to the right or left of each picture; when two pictures are side by side and have the same pressure scale, it is shown to the left of the two pictures. The number in the lower left-hand corner of each picture is the shot number. Since it is sometimes of interest to distinguish the sensitivity factors and the high frequency response characteristics of the various microphones, the microphones have been labeled A, B, C, or D and one of these is specified next to each signature trace. The microphone location is also called out for each trace by Roman numeral. The group numbers are explained in the title of the figures; see section 5C for a fuller discussion of the group numbers.

Figures A1 through A5 are "basic" signatures in the sense that no turbulence or topographical interactions are contained in the figures. Figures A6 and A7 show signatures with turbulent interactions obtained in the course of Task I. Figures A8 and A9 are the topographical results obtained during Task III; figures A10 through A58 are the turbulence results obtained during Task II; and figures A59 through A65 are topographical results obtained during Task IV.
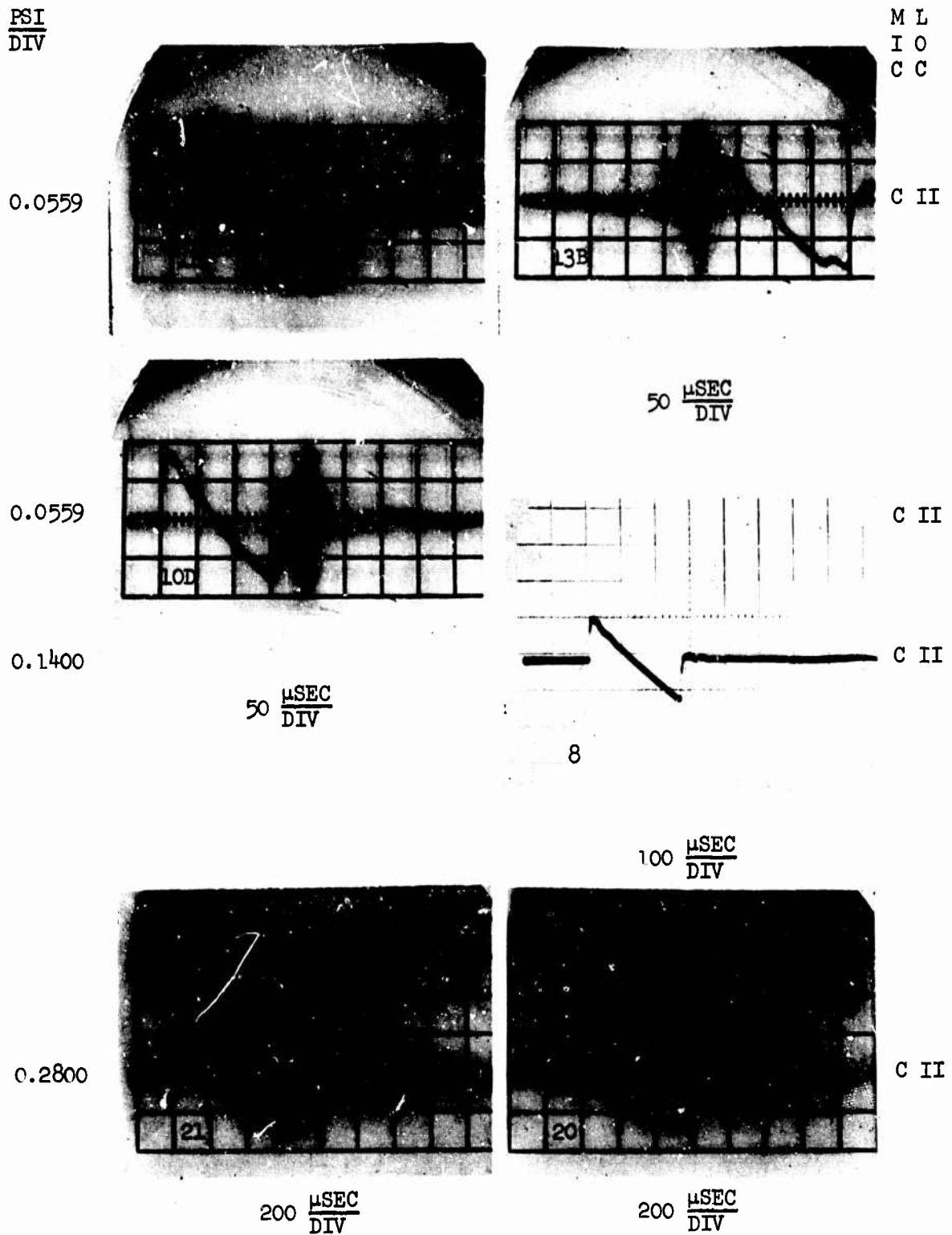
Figure A1 Basic signatures recorded during tasks I and III using projectile sizes A, B, C, and D. Upper two signatures are D shots at M = 2.5 and 1.4, reading from right to left. Middle two signatures are C and B shots at M = 1.8 and 2.6, respectively. Lower two signatures are A shots at M = 1.95 and 1.55.
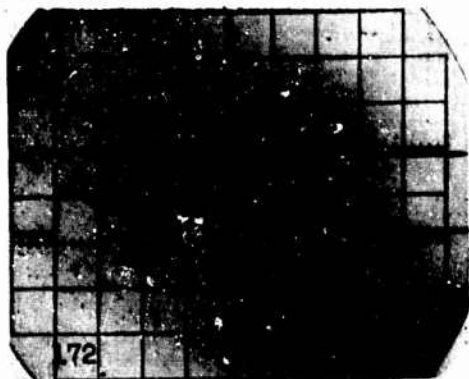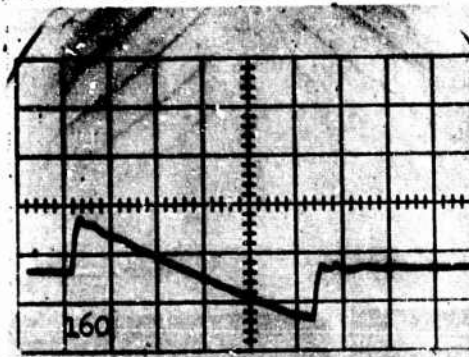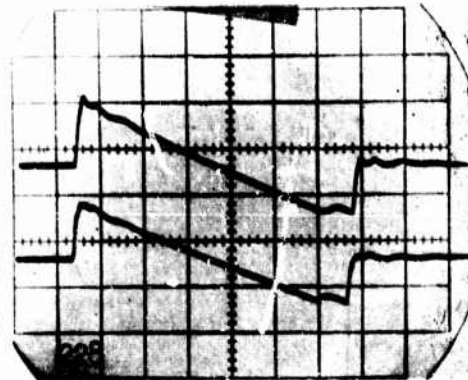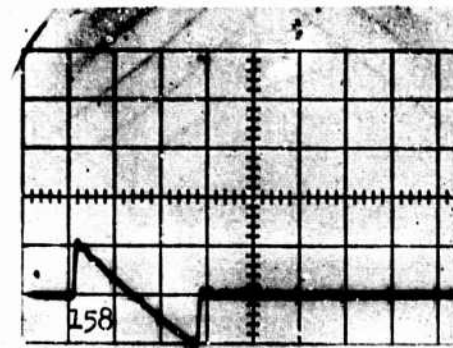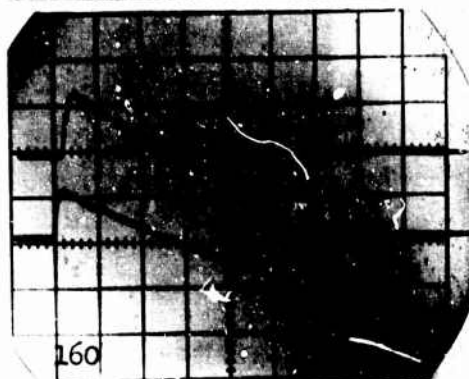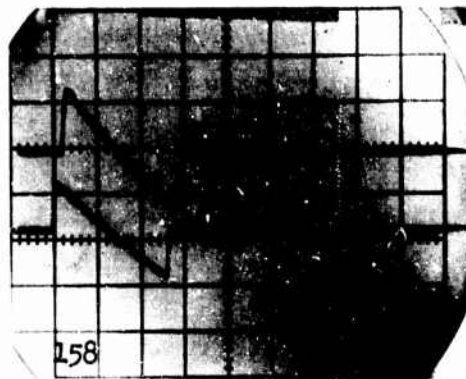
Figure A2 Basic signatures recorded during tasks II and IV. Upper two pictures are 0.46 caliber bullet shots at M = 2.16. Other pictures are B shots at M = 2.56.
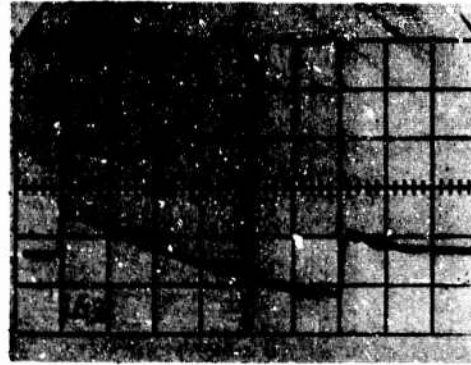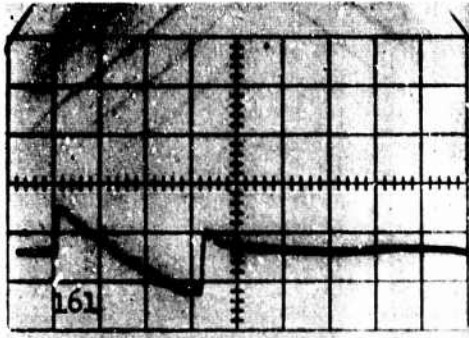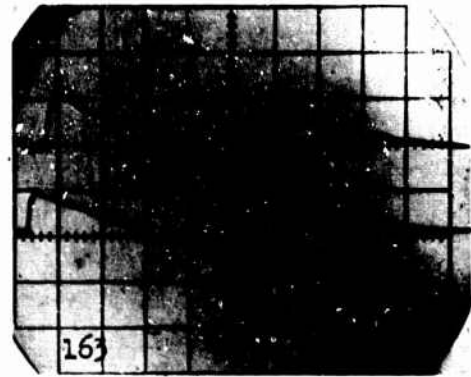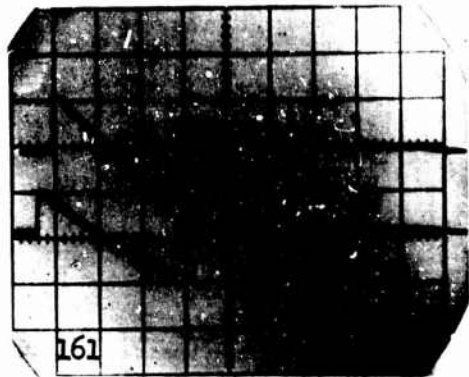
94
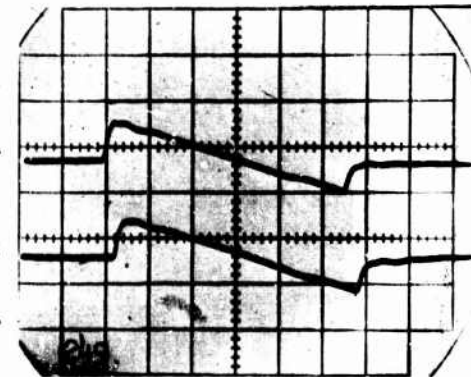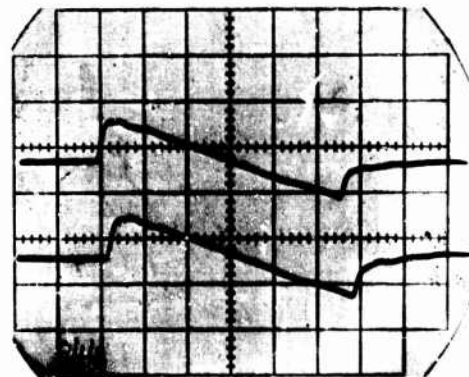
Figure A3 Basic signatures recorded during tasks II and IV using B projectiles. The first four pictures are at M = 1.40; and the last two are at M = 1.26 and M = 1.24 respectively.

95

Figure A4 Basic signatures recorded during tasks II and IV using 0.22 caliber projectiles at M = 3.0.
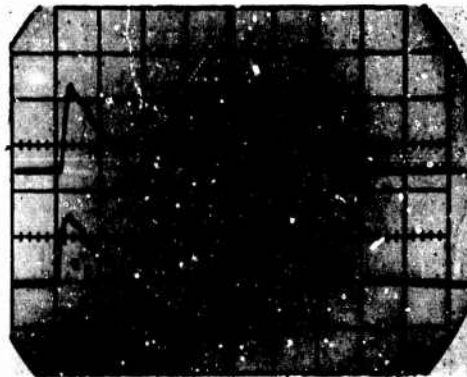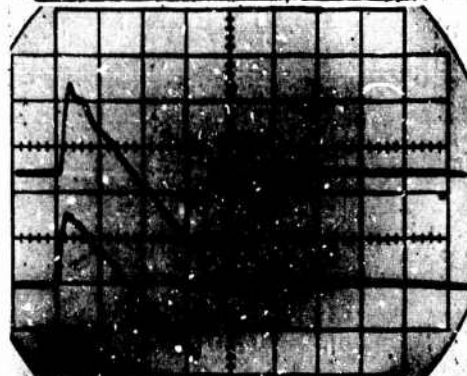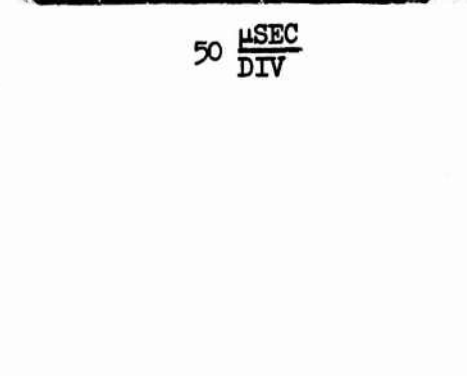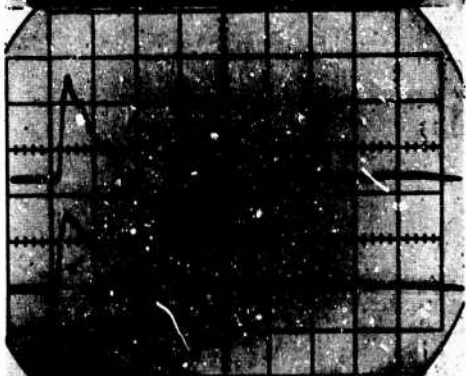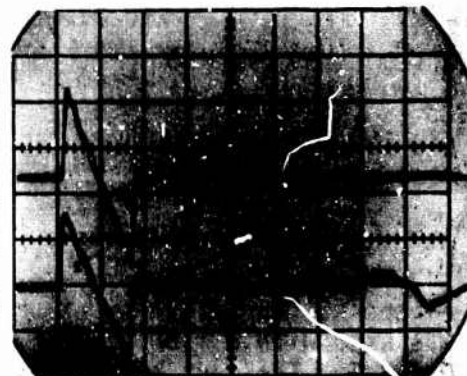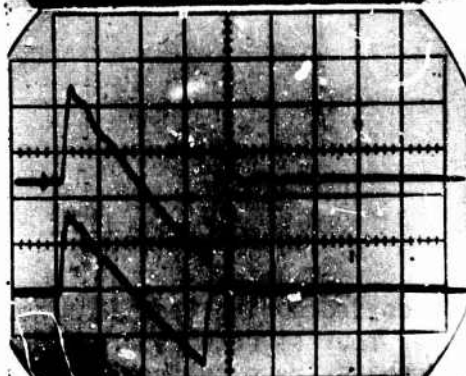
Figure A5 Basic signatures recorded during tasks II and IV using 0.22 caliber projectiles at M = 3.0.
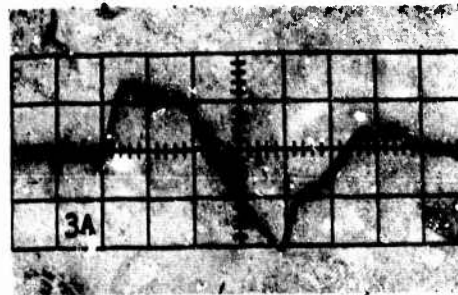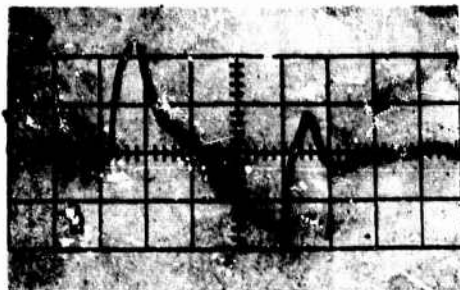
Figure A6 Turbulent signatures recorded during task I. The 24 inch nozzle was used with U = 80 ft/sec. Upper four signatures are with D projectile at M = 2.5. The next three signatures are, reading from right to left, C, B, and A projectiles at M = 1.8, 2.6, and 2.2, respectively.

$$\frac{PSI}{DIV}$$

M L
I O
C C

0.0559   C II

0.0559   C II

$$50 \, \frac{\mu SEC}{DIV}$$

0.0559   C II
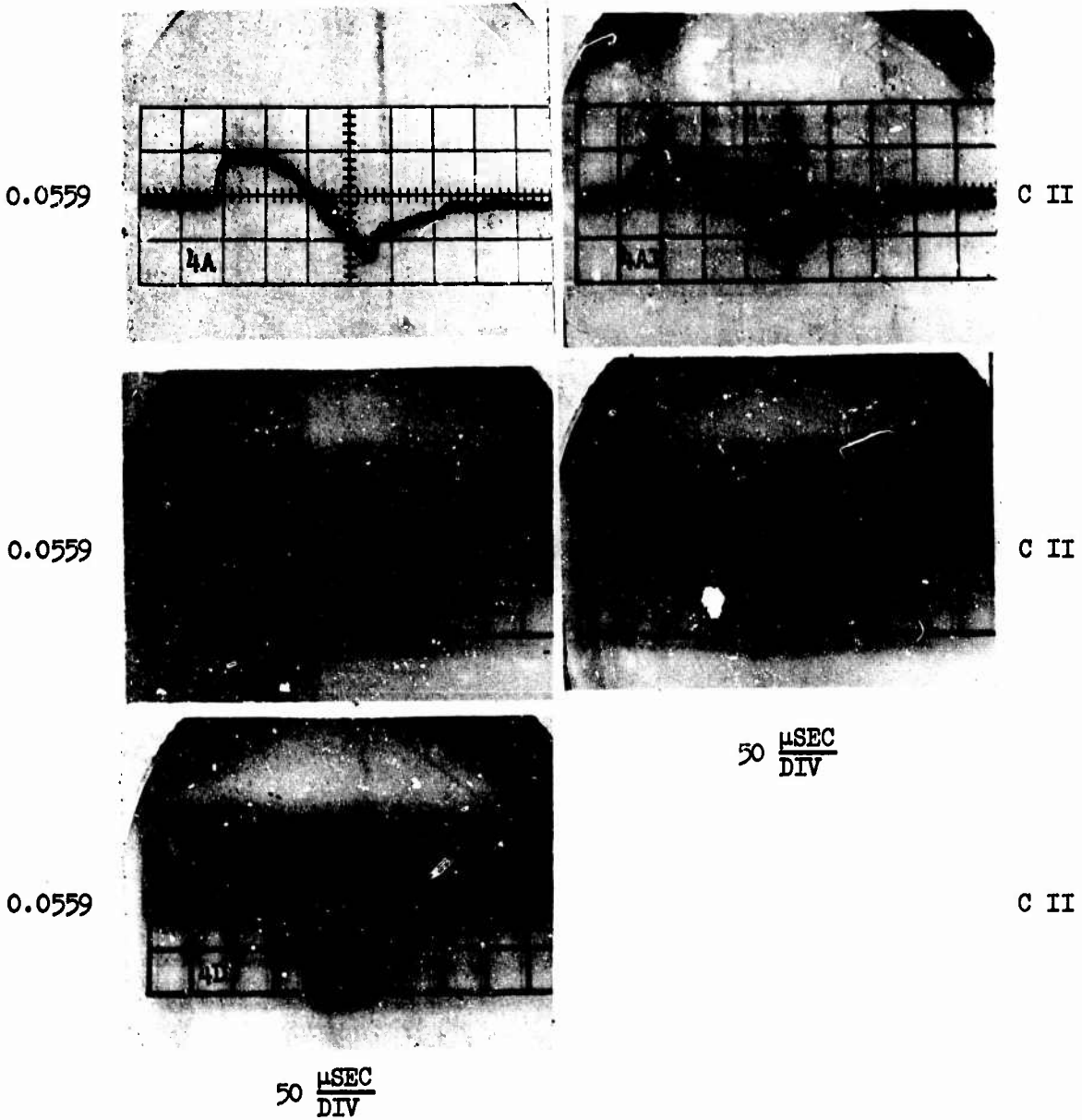
$$50 \, \frac{\mu SEC}{DIV}$$

Figure A7 Signatures recorded during task I using thermal generators positioned as shown by table 5 and figure 18. The projectiles were B types at M = 2.5.

99
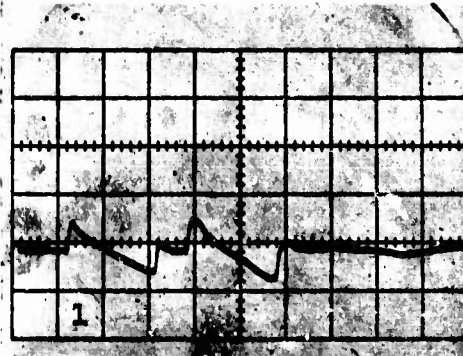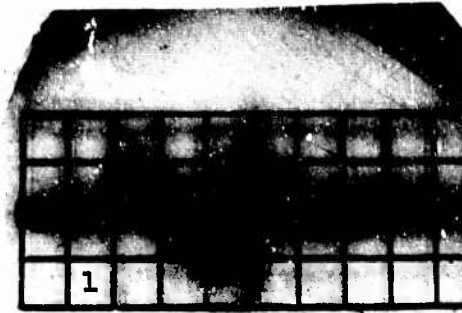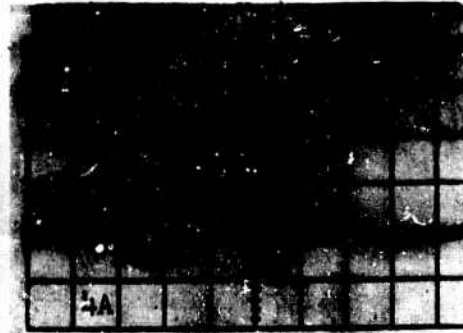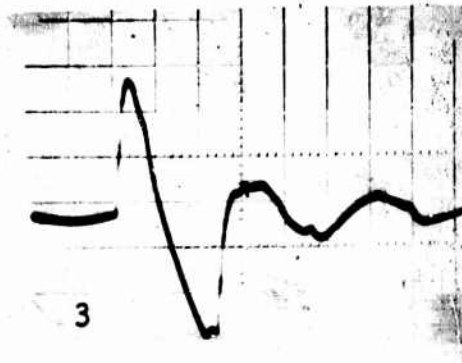
Figure A8 Signatures recorded during task III at locations V and VI on topographical models using D projectiles. Upper two pictures are on the step model at M = 2.5. Middle two pictures are on the 90° corner model at M = 2.5. Bottom two pictures are on the step model at M = 1.4.
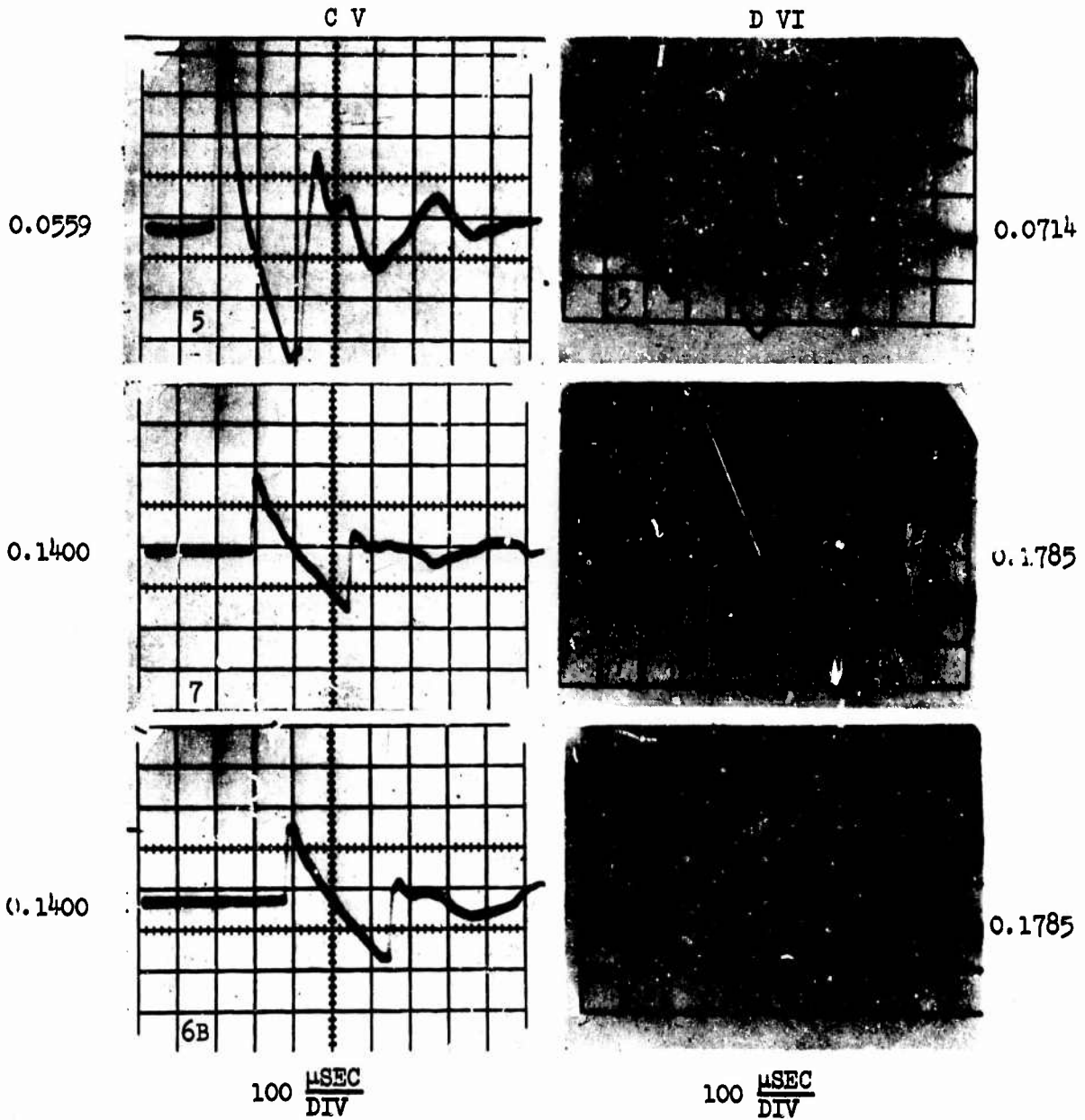
Figure A9 Signatures recorded during task III at locations V and VI on topographical models. Upper two pictures are for the 90° corner model, D projectiles, and M - 1.4. Middle two pictures are for the step model, B projectiles, and M = 2.6. Bottom two pictures are for the 90° corner model, B projectiles, and M = 2.6.

Figure A10 Boom signatures for group 114 -- B projectiles, M as noted, 4 in. nozzle, and 24 in. inlet.
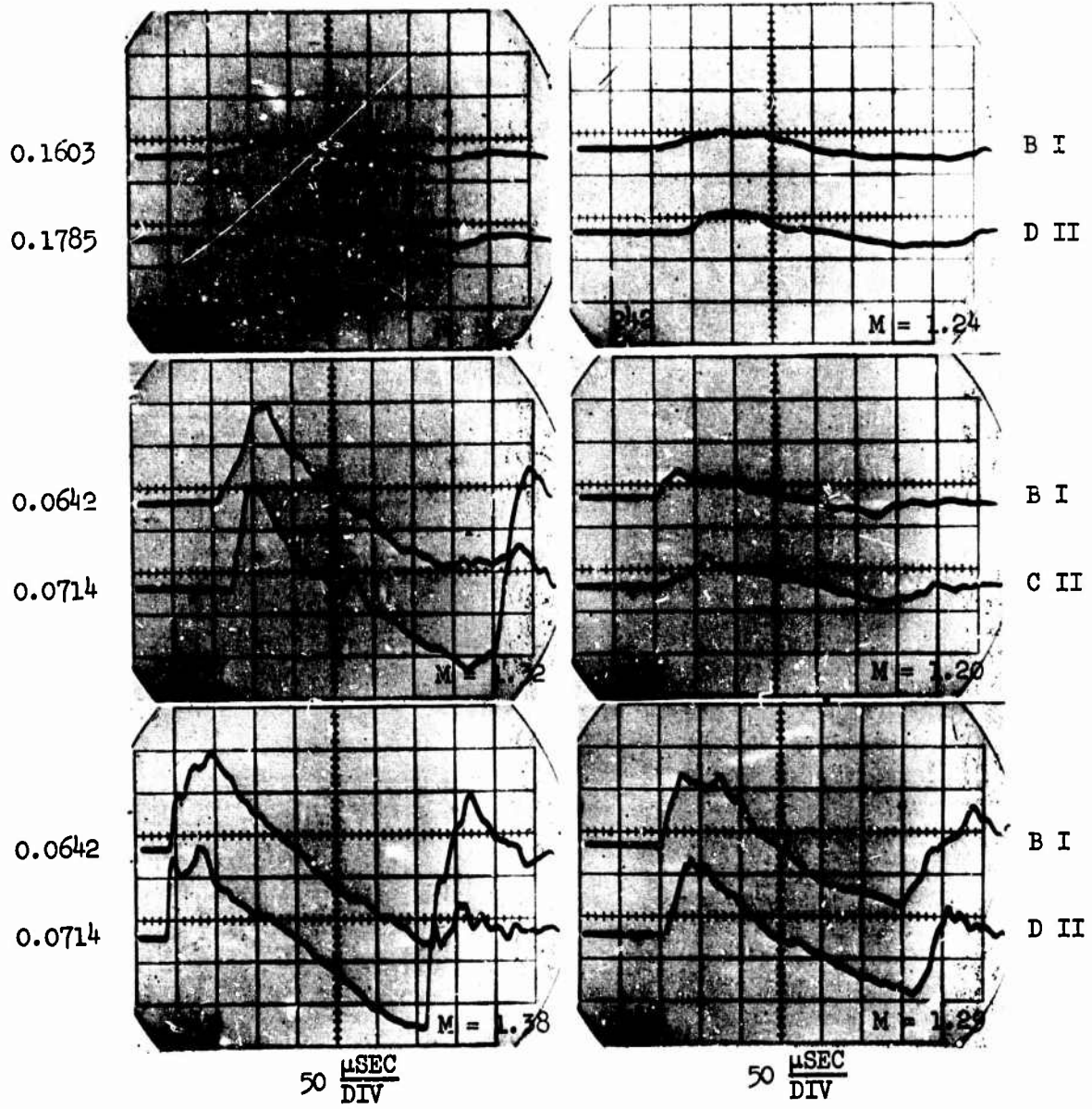
Figure A11 Boom signatures for group 124 -- B projectiles, M as noted, 6 in. nozzle, and 24 in. inlet.

103

$\frac{PSI}{DIV}$

M L
I O
C C

0.1603
0.1785

B I

D II

0.1603

0.1785

B I

D II

0.1603

0.1785

E I

D II

$50\frac{\mu SEC}{DIV}$ $50\ \frac{\mu SEC}{DIV}$
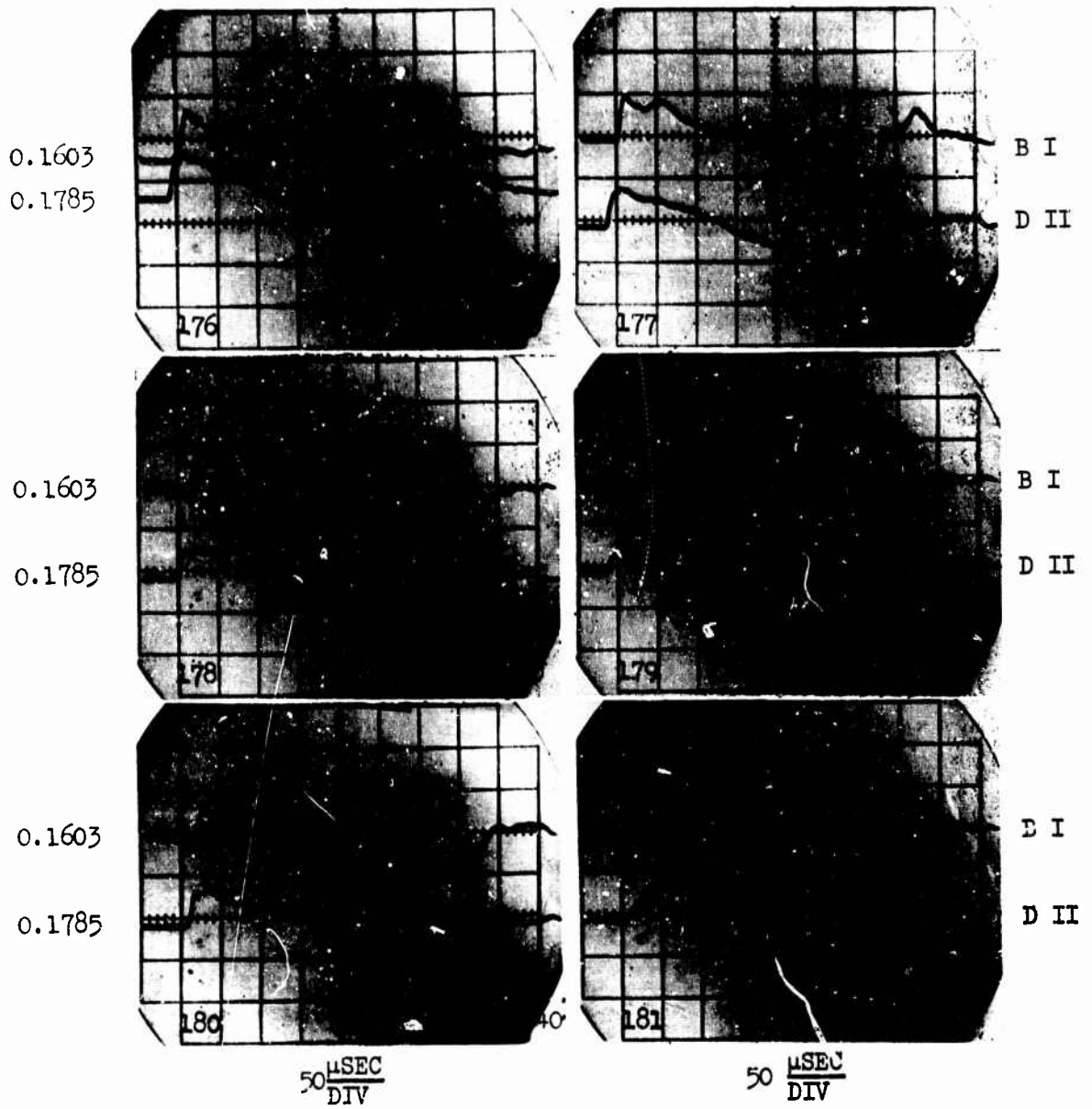
Figure A12 Boom signatures for group 134 -- B projectiles, M = 1.4, 24 in. nozzle, and 24 in. inlet.

104
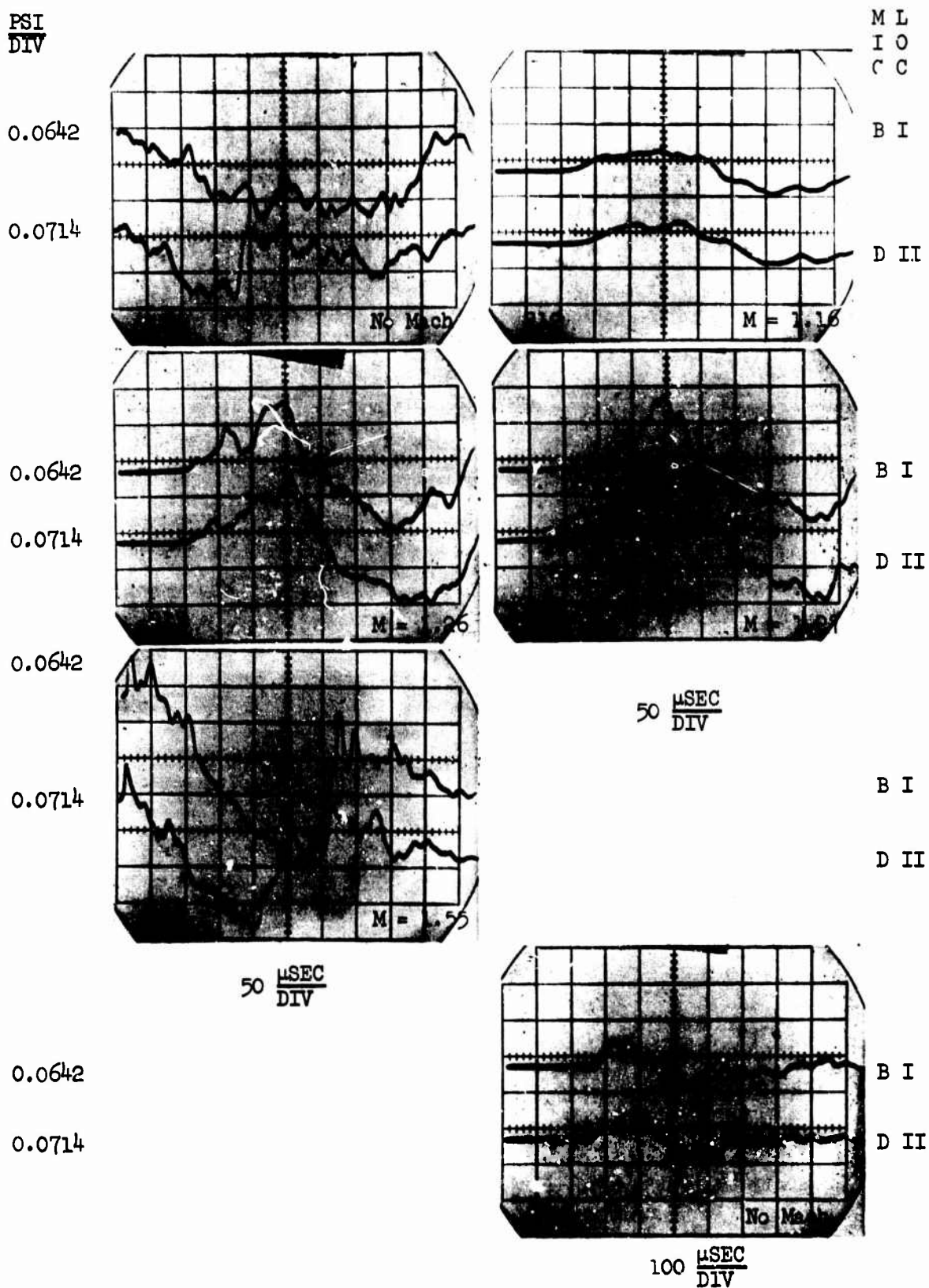
Figure A13 Boom signatures for group 144 -- B projectiles, M as noted, high-speed nozzle no. 1, and 24 in. inlet.
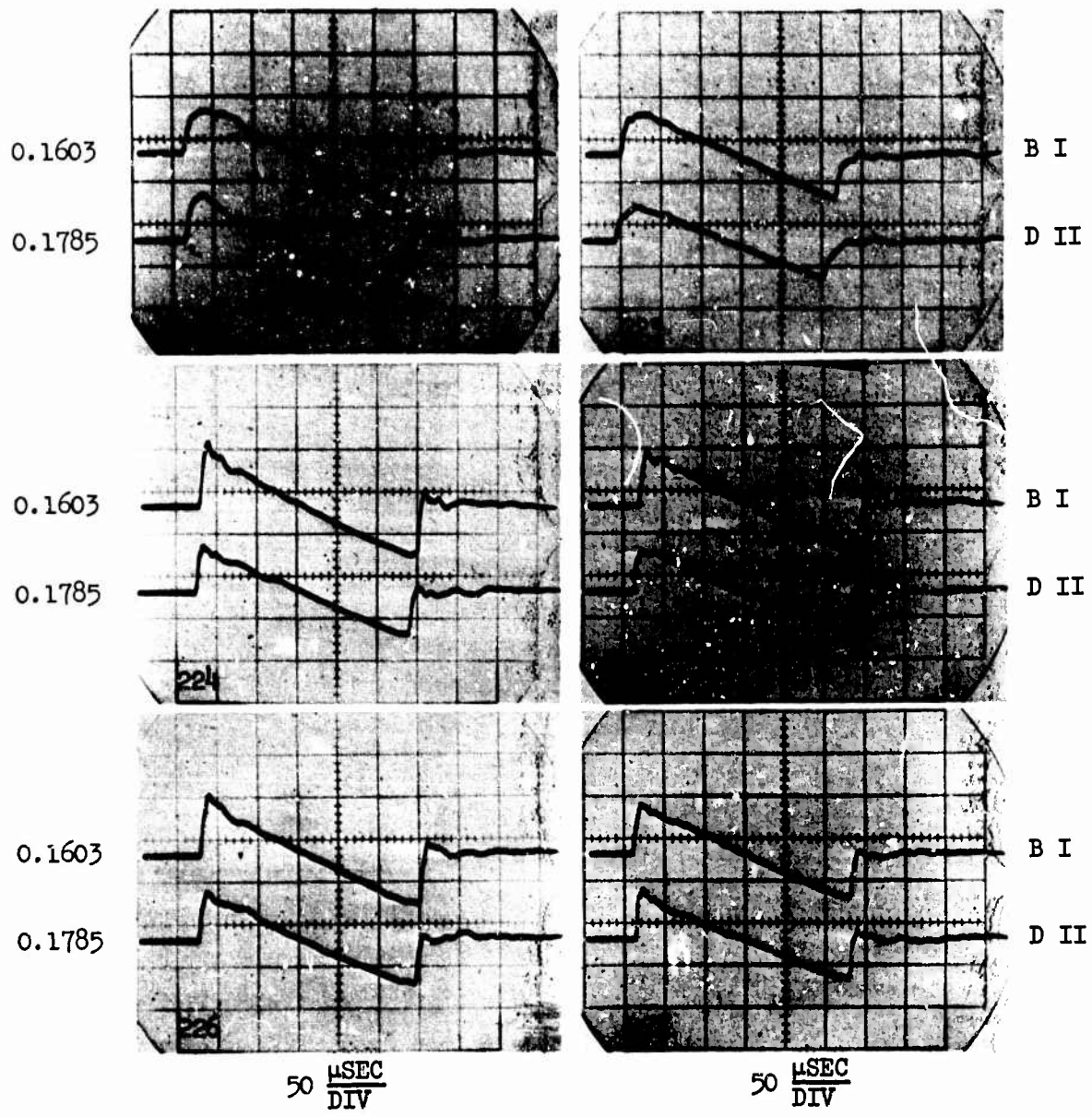
Figure A14   Boom signatures for group 212 -- B projectiles, M = 2.56, 4 in.
nozzle, and 16 in. inlet.
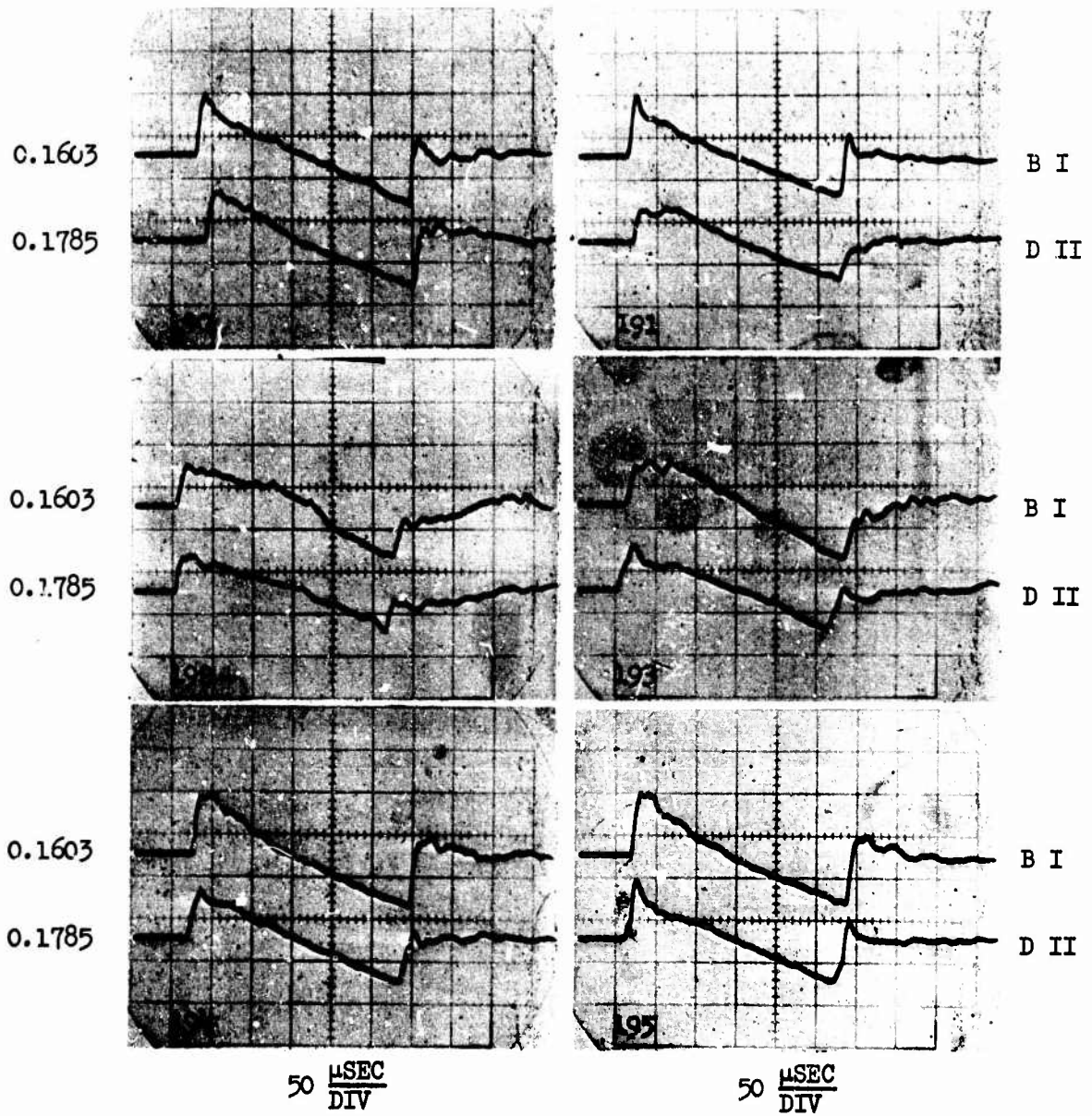
Figure A15 Boom signatures for group 214 -- B projectiles, M = 2.56, 4 in. nozzle, and 24 in. inlet.

0.1603

0.1785

0.1603

.0.1785

0.1603

0.1785

B I

D II

B I

D II

B I

D II

50 $\frac{\mu SEC}{DIV}$

50 $\frac{\mu SEC}{DIV}$
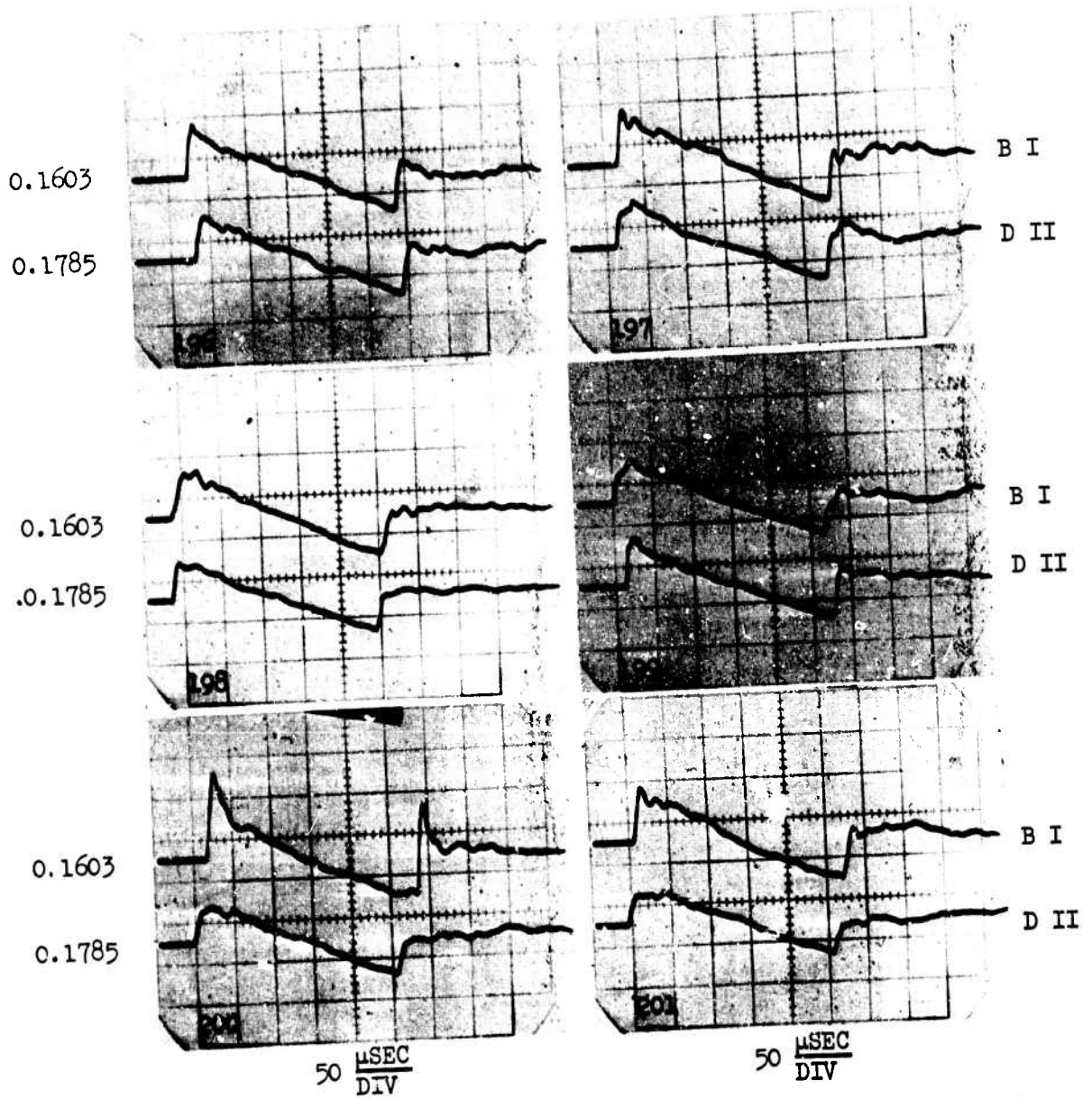
Figure A16 Boom signatures for group 214 -- B projectiles, M = 2.56, 4 in.
nozzle, and 24 in. inlet.
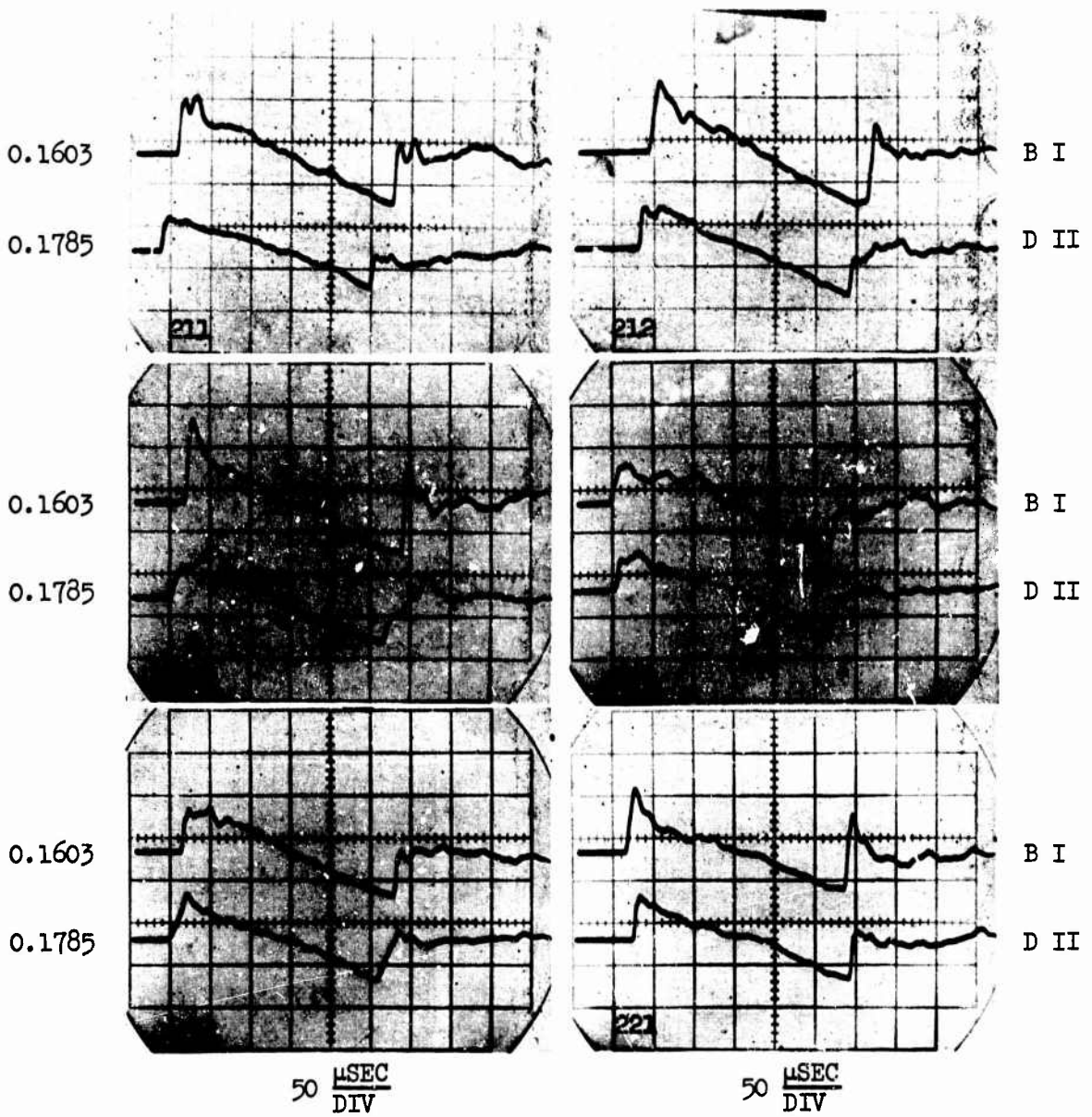
Figure A17 Boom signatures for group 215 -- B projectiles, M = 2.56, 4 inch nozzle, and open inlet.

$\dfrac{\text{PSI}}{\text{DIV}}$

0.1603

0.1785

B I

D II

0.1603

0.1785

B I

D II

0.1603

0.1785

B I

D II

$50\ \dfrac{\mu\text{SEC}}{\text{DIV}}$ $50\ \dfrac{\mu\text{SEC}}{\text{DIV}}$
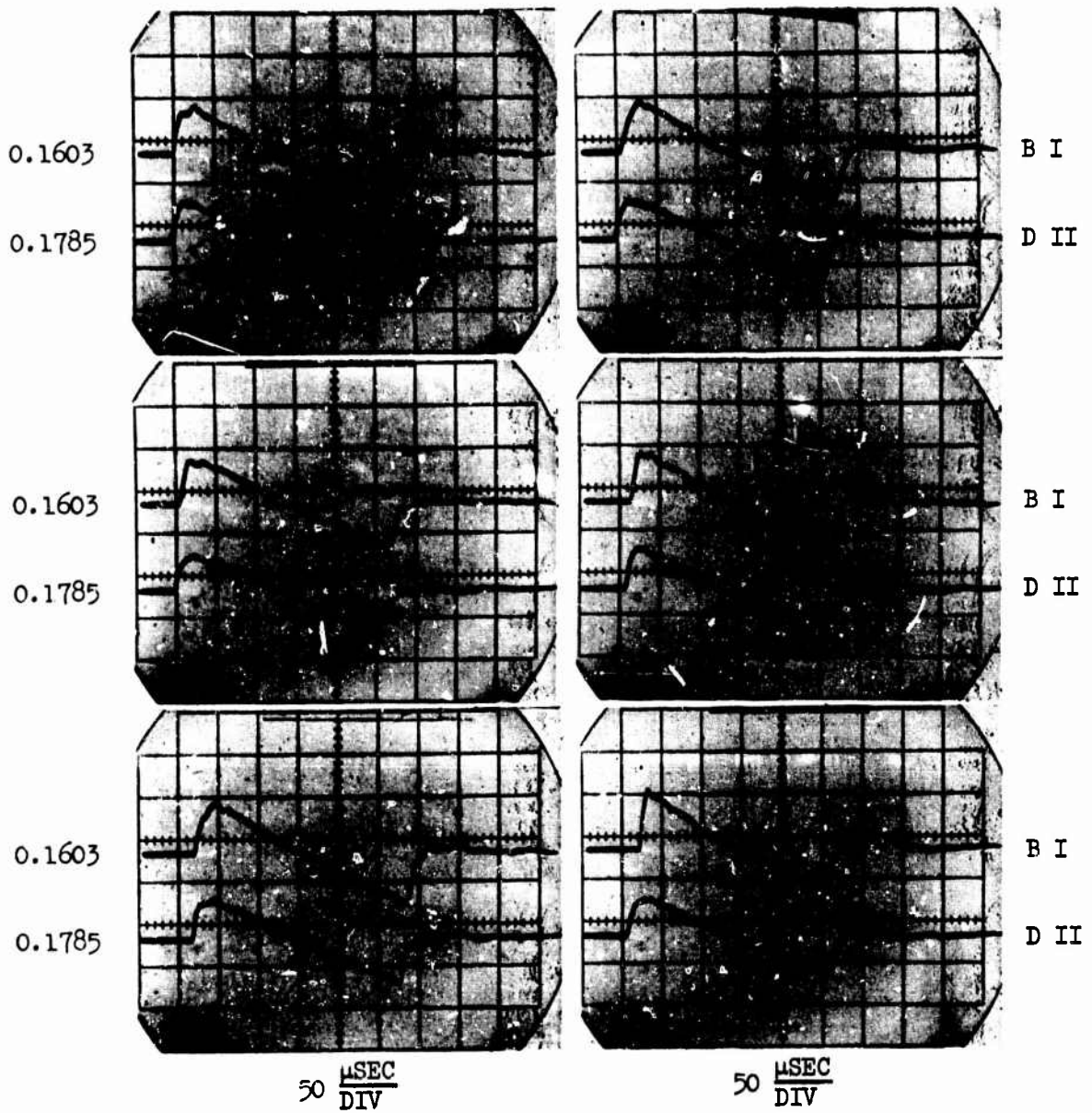
Figure A18 Boom signatures for group 222 -- B projectiles, M = 2.56, 6 inch nozzle, and 16 inch inlet.

110

0.1603

0.1785

B I

D II

0.1603

0.1785

B I

D II

0.1603

0.1785

B I

D II

$50 \ \dfrac{\mu\text{SEC}}{\text{DIV}}$

$50 \ \dfrac{\mu\text{SEC}}{\text{DIV}}$
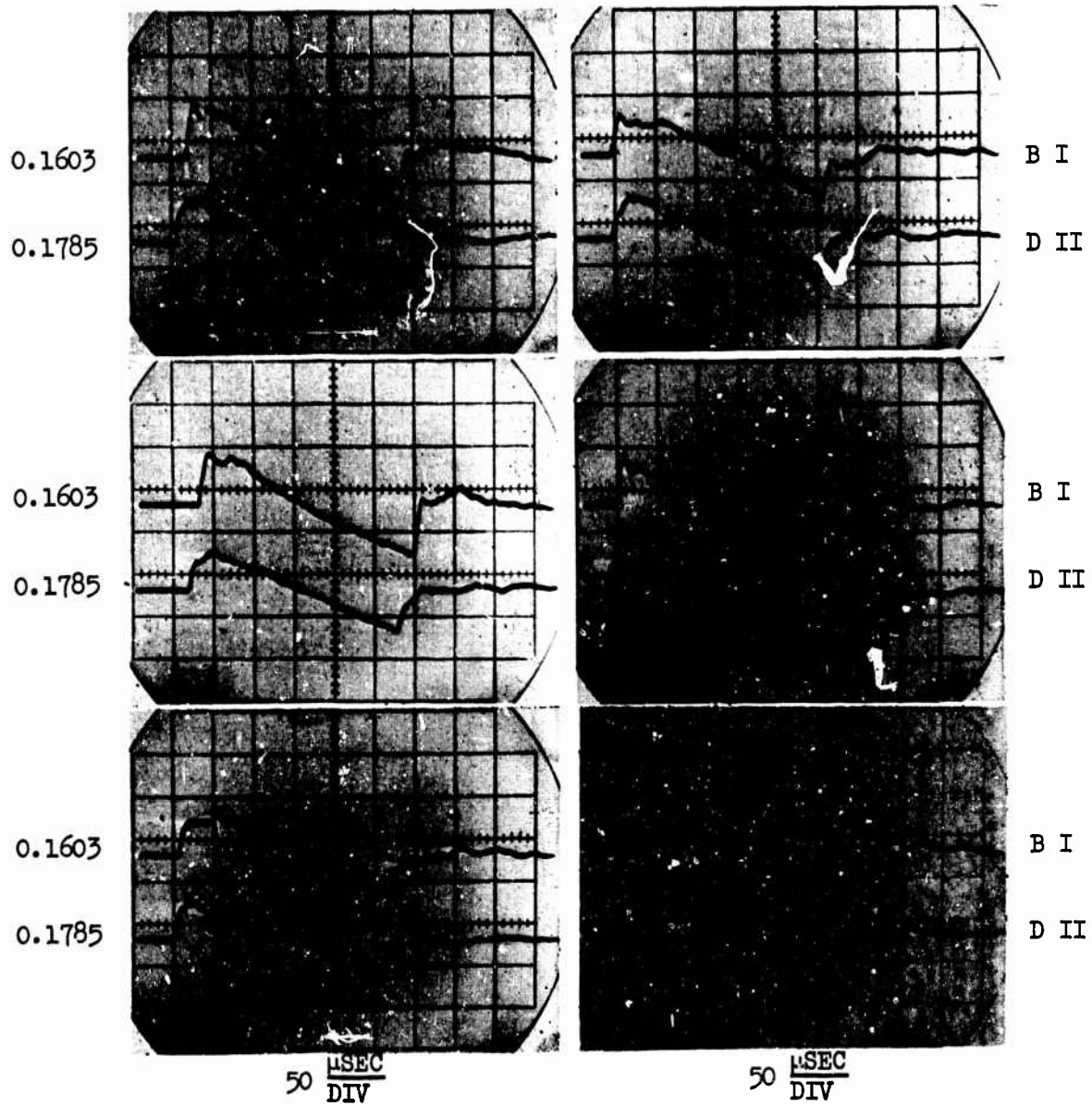
Figure A19   Boom signatures for group 224 -- B projectiles, M = 2.25, 6 inch
nozzle, and 24 inch inlet.

111

$\frac{PSI}{DIV}$

0.1603

0.1785

B I

D II

0.1603

0.1785

B I

D II

0.1603

0.1785

B I

D II

$50 \frac{\mu SEC}{DIV}$

$50 \frac{\mu SEC}{DIV}$
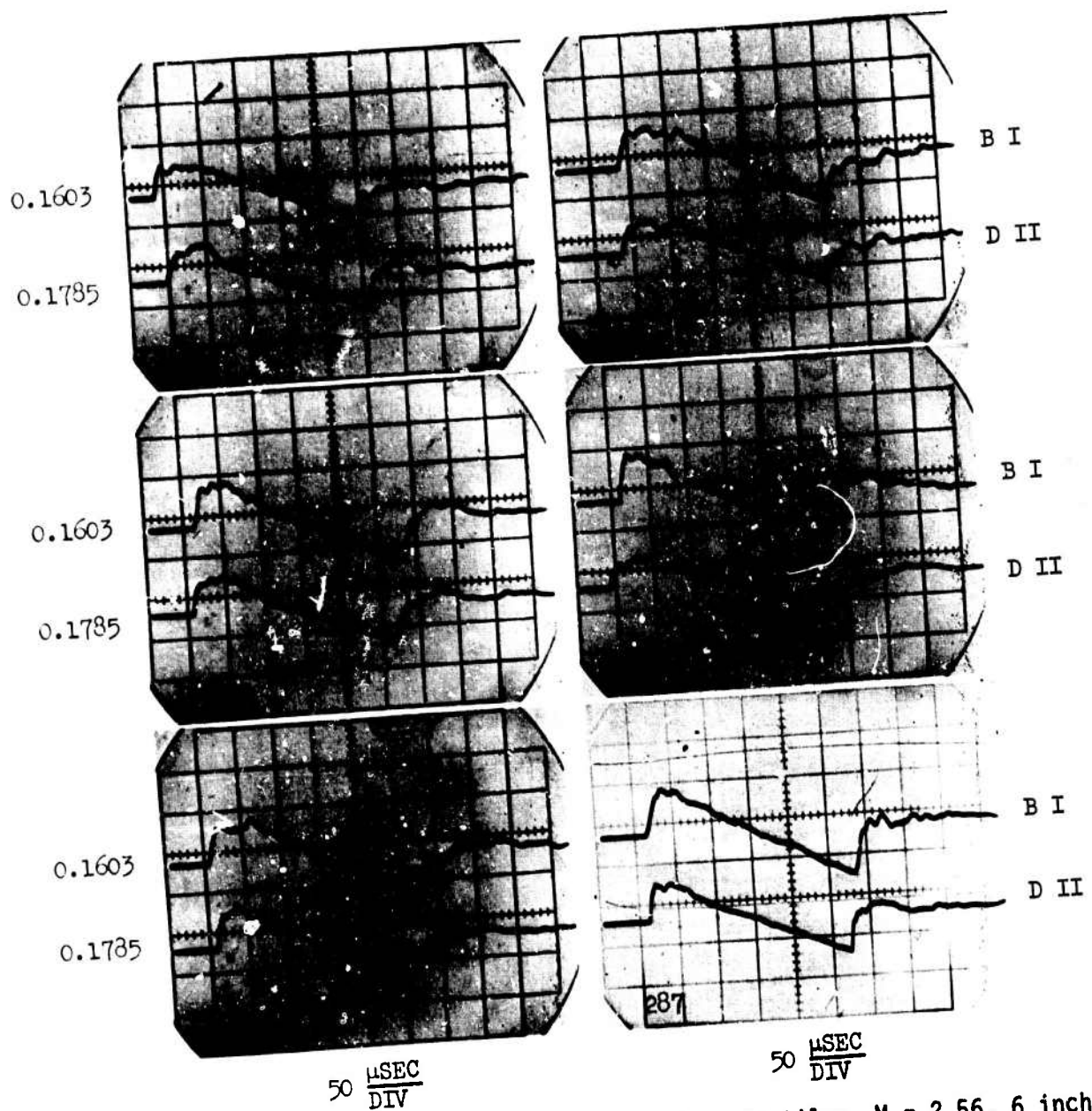
Figure A20   Boom signatures for group 224 -- B projectiles, M = 2.56, 6 inch nozzle, and 24 inch inlet.
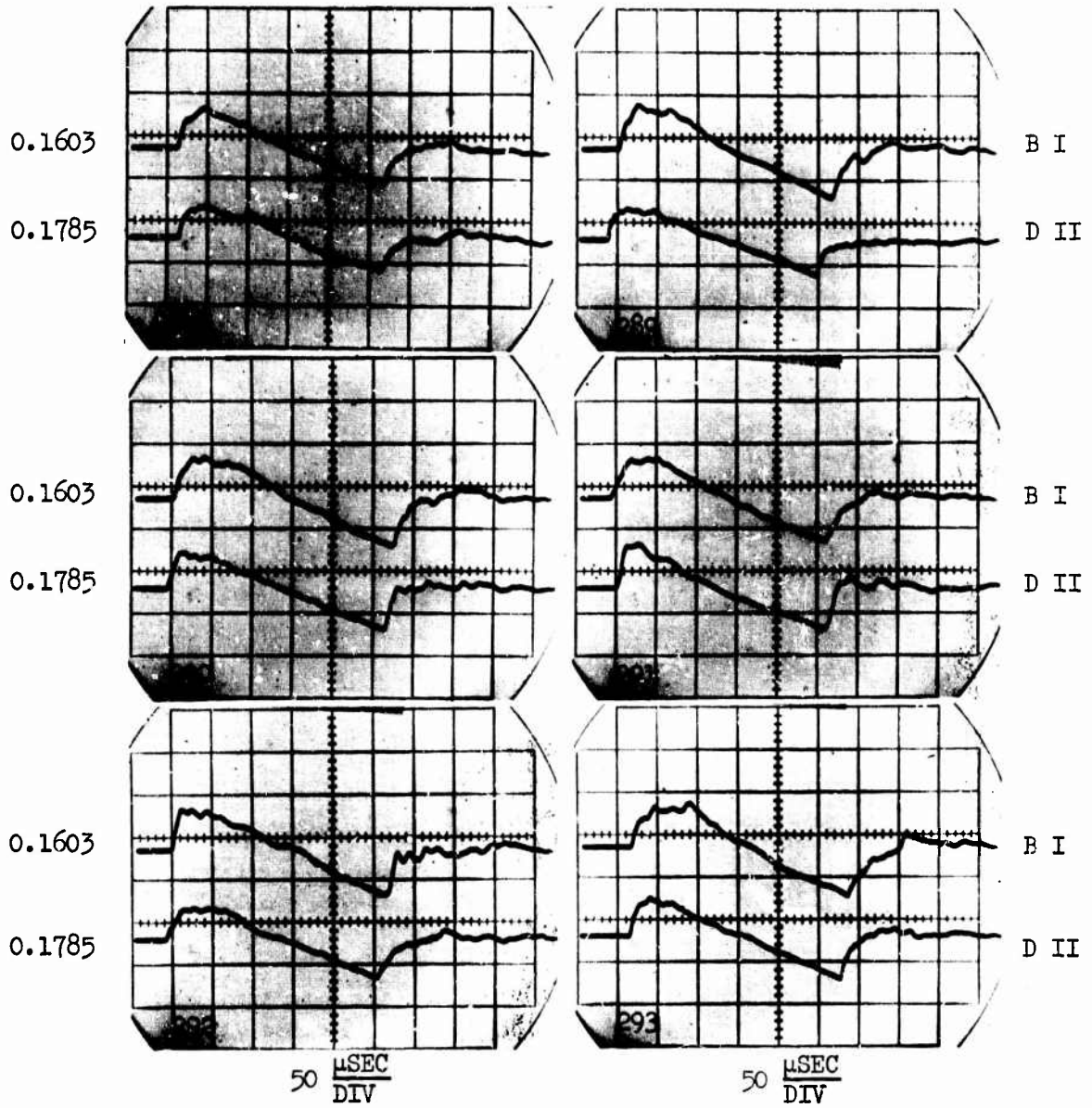
Figure A21   Boom signatures for group 225 -- B projectiles, M = 2.56, 6 inch nozzle, and open inlet.

0.1603

0.1785

B I

D II

0.1605

0.1785

B I

D II

0.1603

0.1785

B I

D II

$50 \dfrac{\mu\text{SEC}}{\text{DIV}}$ $50 \dfrac{\mu\text{SEC}}{\text{DIV}}$
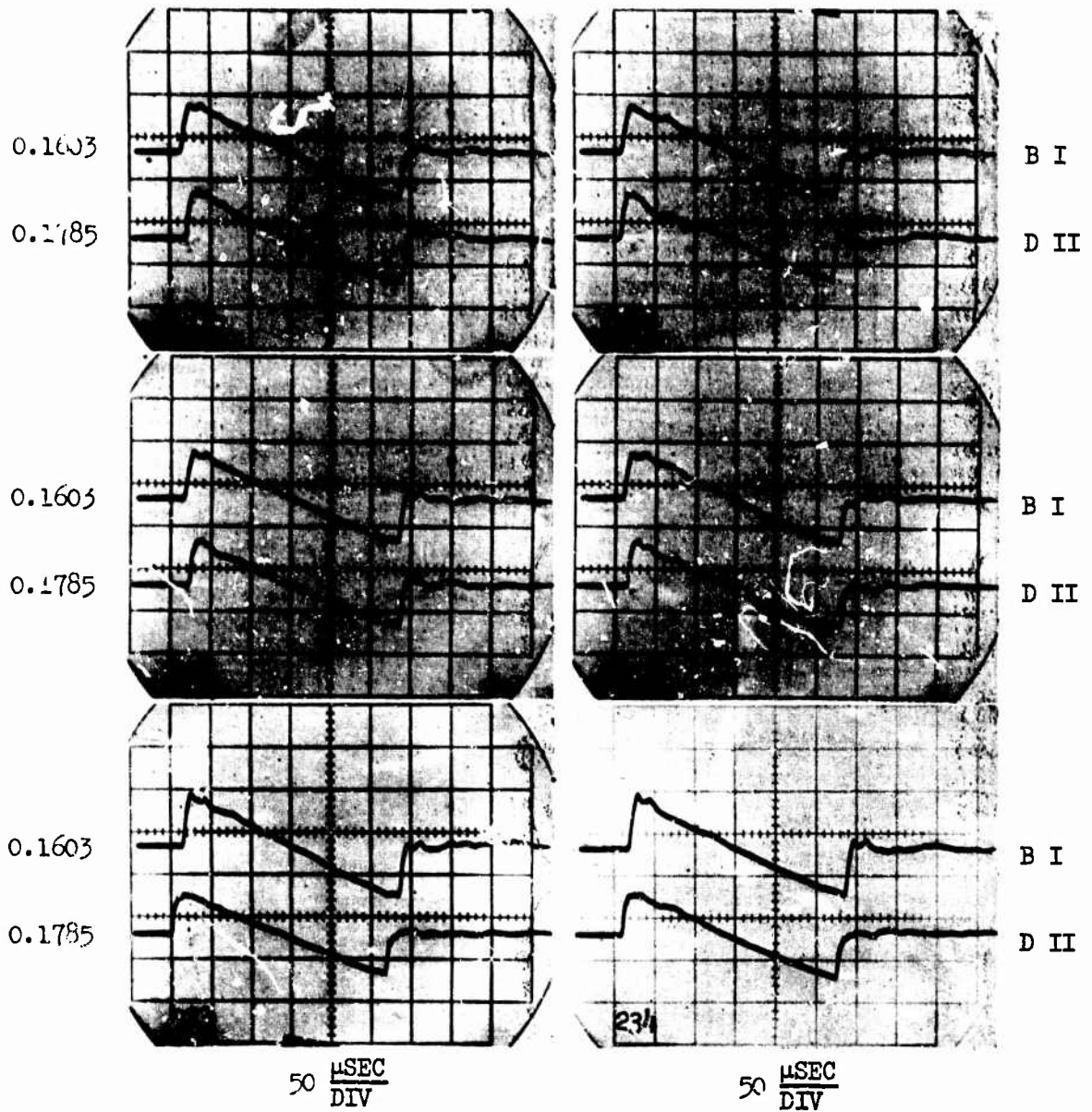
Figure A22 Boom signatures for group 232 -- B projectiles, M = 2.56, 24 inch nozzle, and 16 inch inlet.

114

$\dfrac{\text{PSI}}{\text{DIV}}$

M L
I O
C C

0.1603   B I

0.1785   D II

0.1603   B I

0.1785   D II

0.1603   B I

0.1785   D II

$50 \dfrac{\mu \text{SEC}}{\text{DIV}}$ $50 \dfrac{\mu \text{SEC}}{\text{DIV}}$
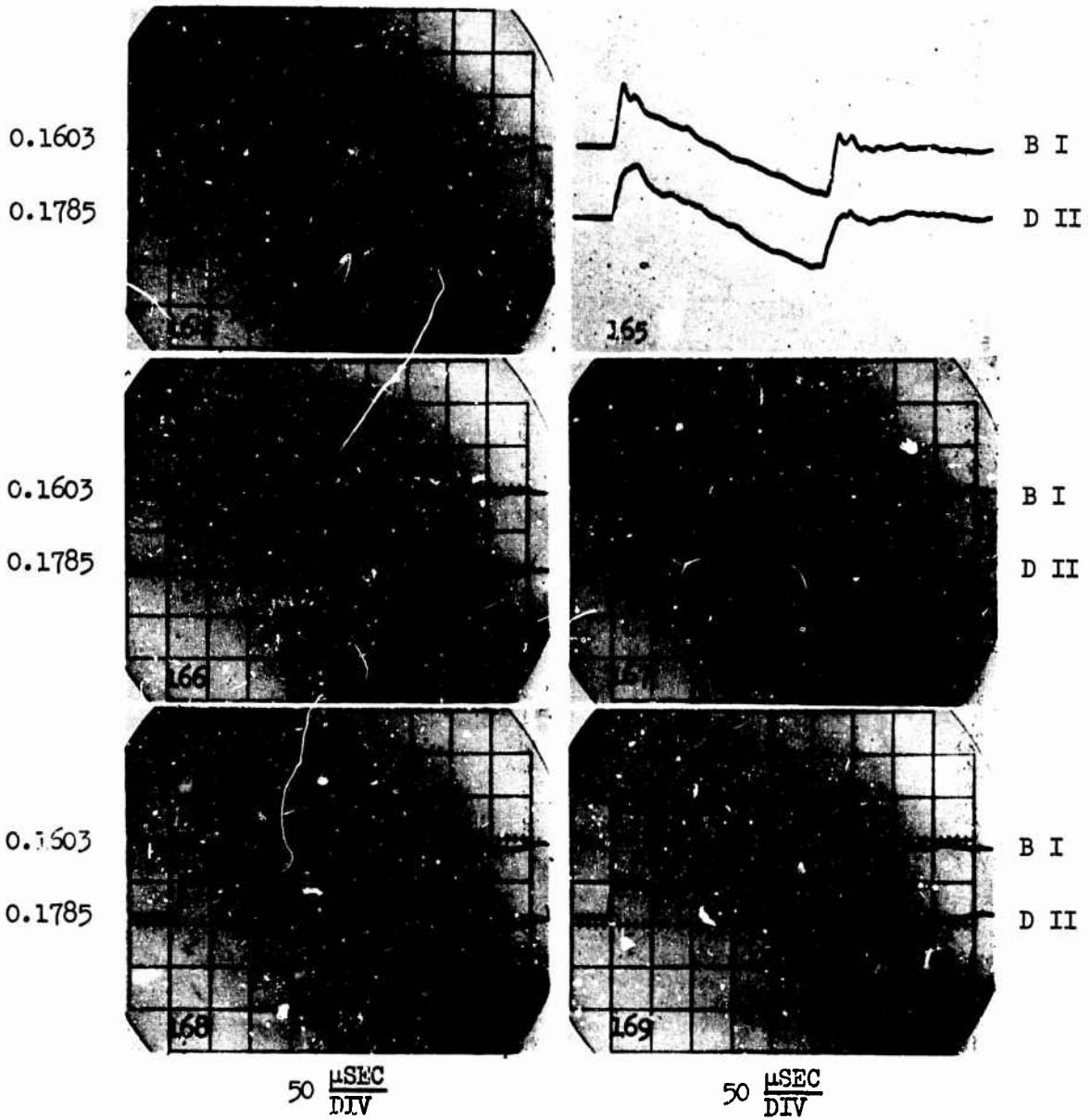
Figure A23 Boom signatures for group 234 -- B projectiles, M = 2.56, 24 inch nozzle, and 24 inch inlet.

115

M L
I O
C C

0.1603

0.1785

B I

D II

0.1603

0.1785

B I

D II

$50 \frac{\mu SEC}{DIV}$

0.1603

0.1785

B I

D II

$50 \frac{\mu SEC}{DIV}$
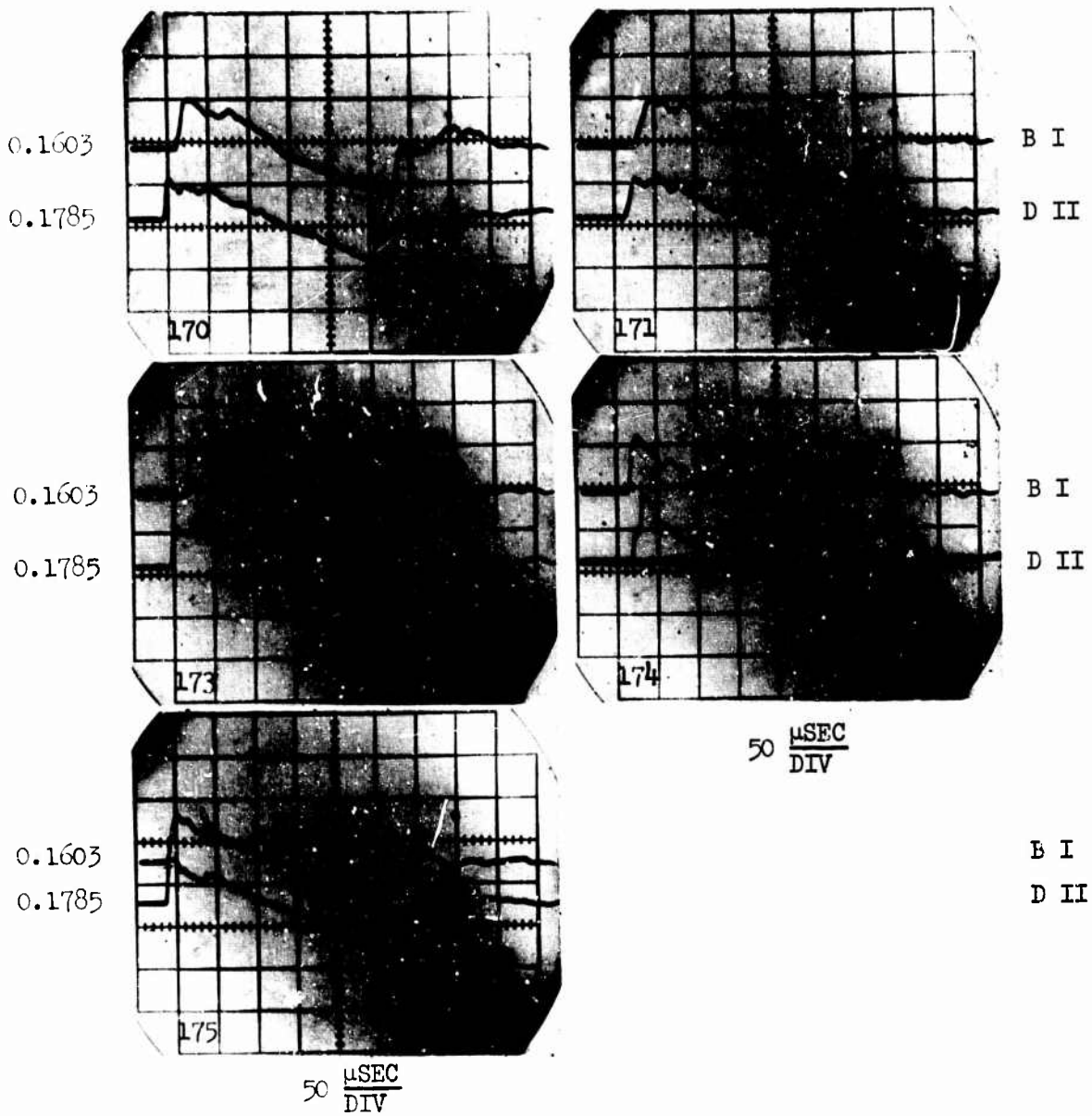
Figure A24   Boom signatures for group 234 -- B projectiles, M = 2.56, 24 inch nozzle, and 24 inch inlet.
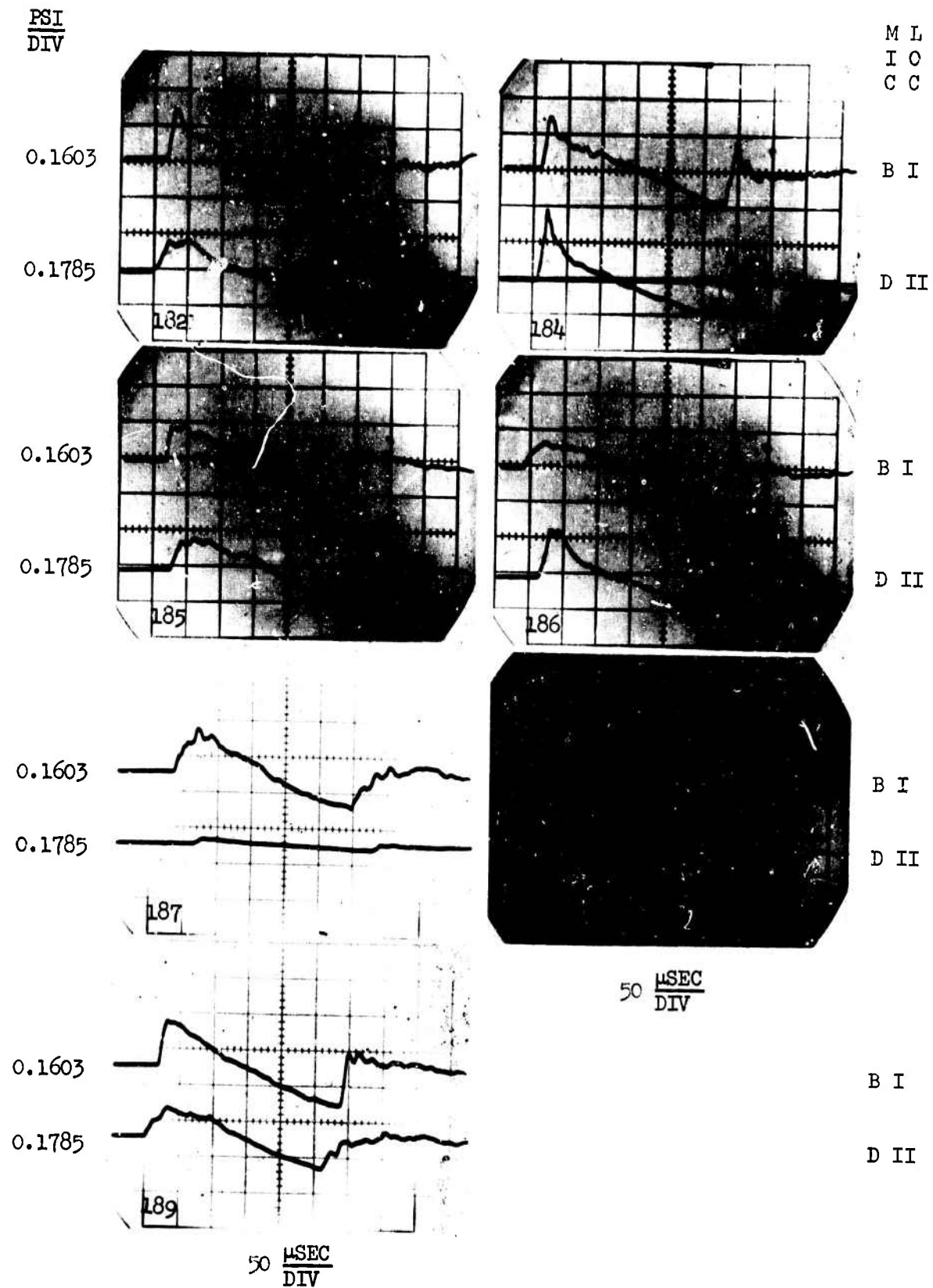
Figure A25 Boom signatures for group 235 -- B projectiles, M = 2.56, 24 inch nozzle, and open inlet.

117

$$\frac{PSI}{DIV}$$

0.1603

0.1785

B I

D II

0.1603

0.1785

B I

D II

0.1603

0.1785

B I

D II

$$50 \frac{\mu SEC}{DIV}$$

$$50 \frac{\mu SEC}{DIV}$$

Figure A26 Boom signatures for group 241 -- B projectiles, M = 2.56, high-speed nozzle no. 1, and 12 inch inlet.

118

0.1603

0.1785

B I

D II

0.1603

0.1785

B I

D II

0.1603

0.1785

B I

D II

$50 \frac{\mu SEC}{DIV}$

$50 \frac{\mu SEC}{DIV}$
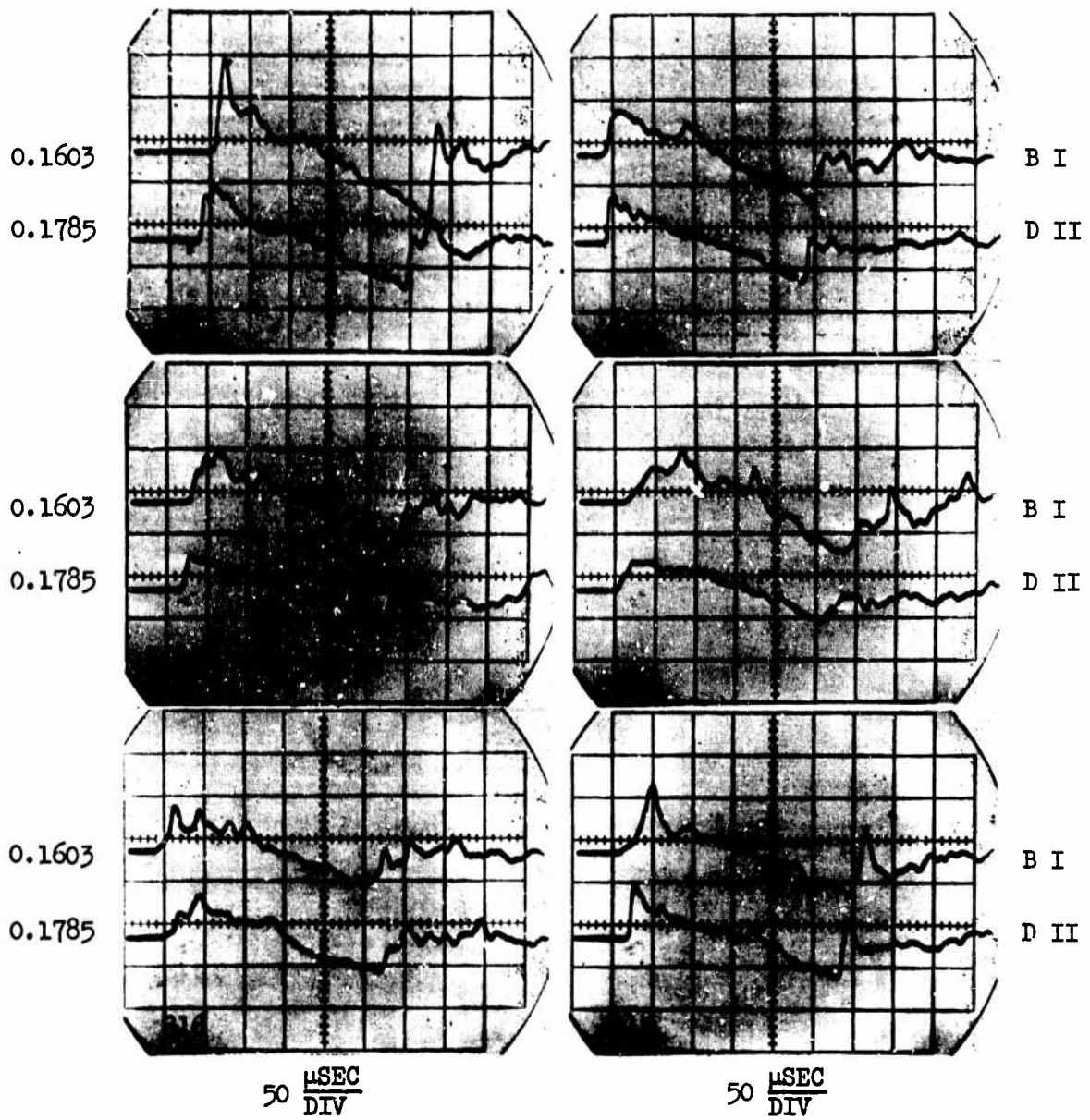
Figure A27 Boom signatures for group 244 -- B projectiles, M = 2.56, high-speed nozzle no. 1, and 24 inch inlet.

Figure A28 Boom signatures for group 314 -- 0.22 caliber projectiles,
M = 3.0, 4 inch nozzle, and 24 inch inlet.

120
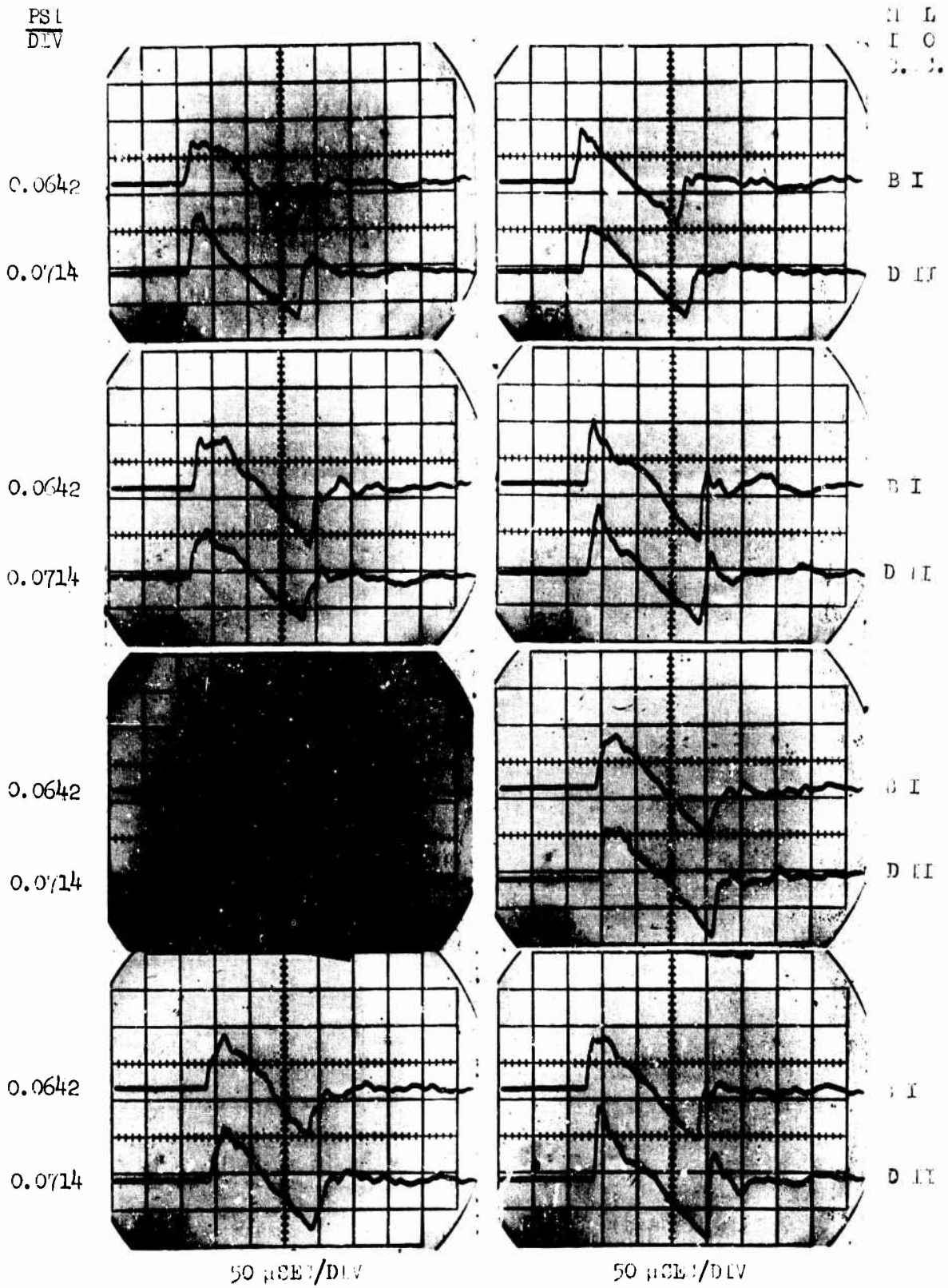
Figure A29 Boom signatures for group 314 -- 0.22 caliber projectiles, M = 3.0, 4 inch nozzle, and 24 inch inlet.
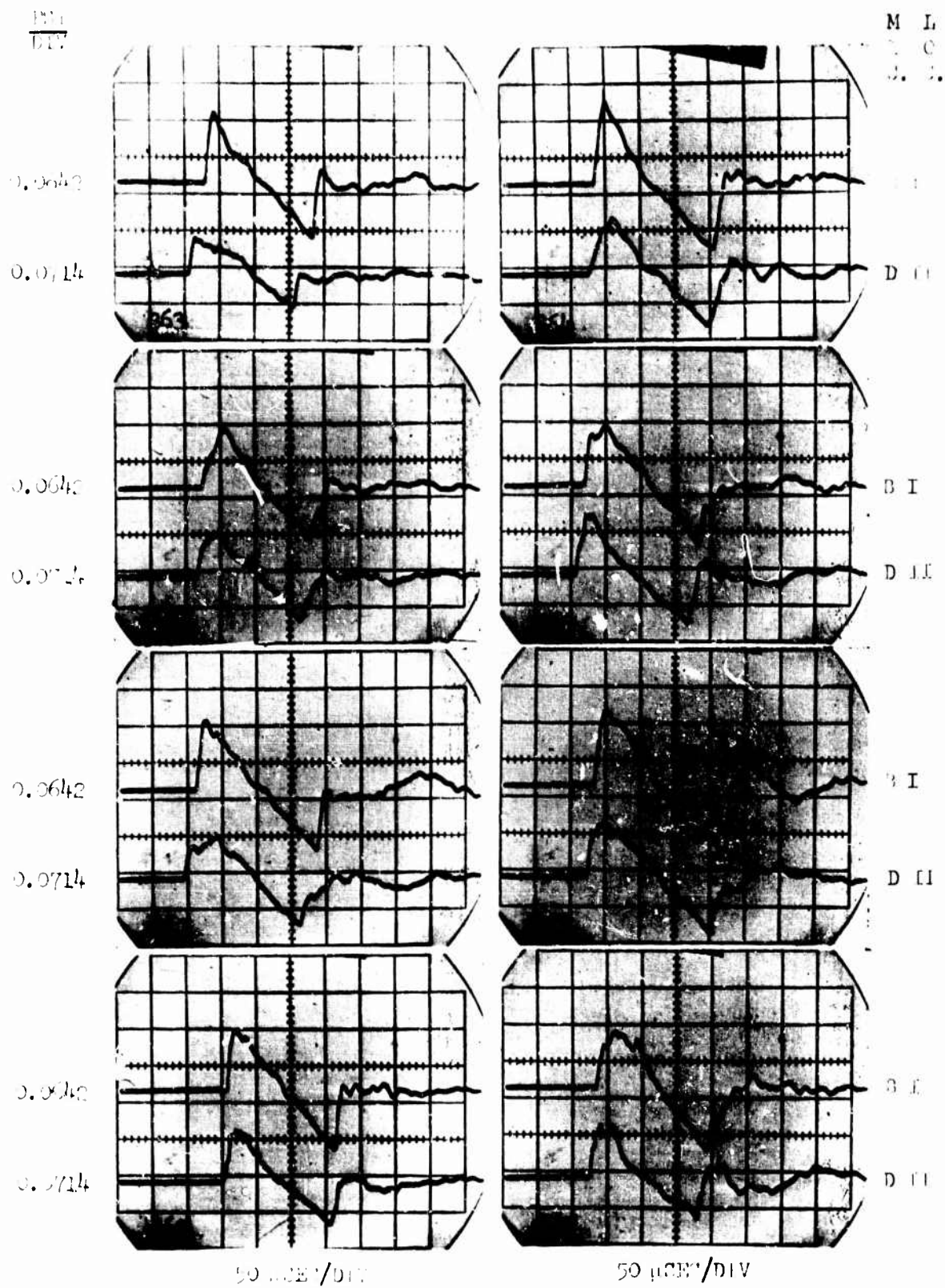
Figure A30 Boom signatures for group 314 -- 0.22 caliber projectiles,
M = 3.0, 4 inch nozzle, and 24 inch inlet.

122

Figure A31 Boom signatures for group 314 -- 0.22 caliber projectiles, M = 3.0, 4 inch nozzle, and 24 inch inlet.
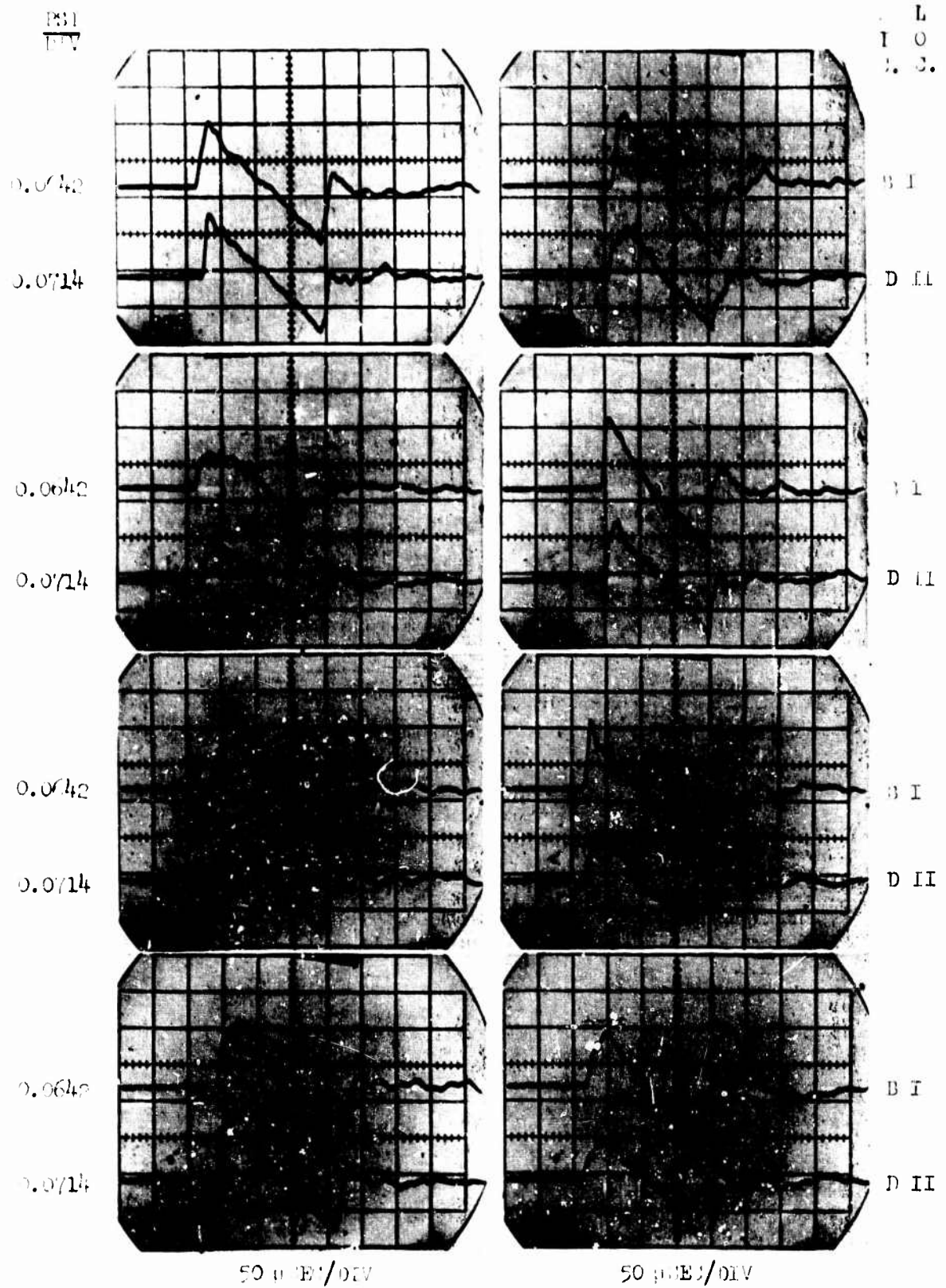
Figure A32 Boom signatures for group 314 -- 0.22 caliber projectiles,
M = 3.0, 4-inch nozzle, and 24-inch inlet.

Figure A33 Boom signatures for group 314 -- 0.22 caliber projectiles, M = 3.0, 4-inch nozzle, and 24-inch inlet.
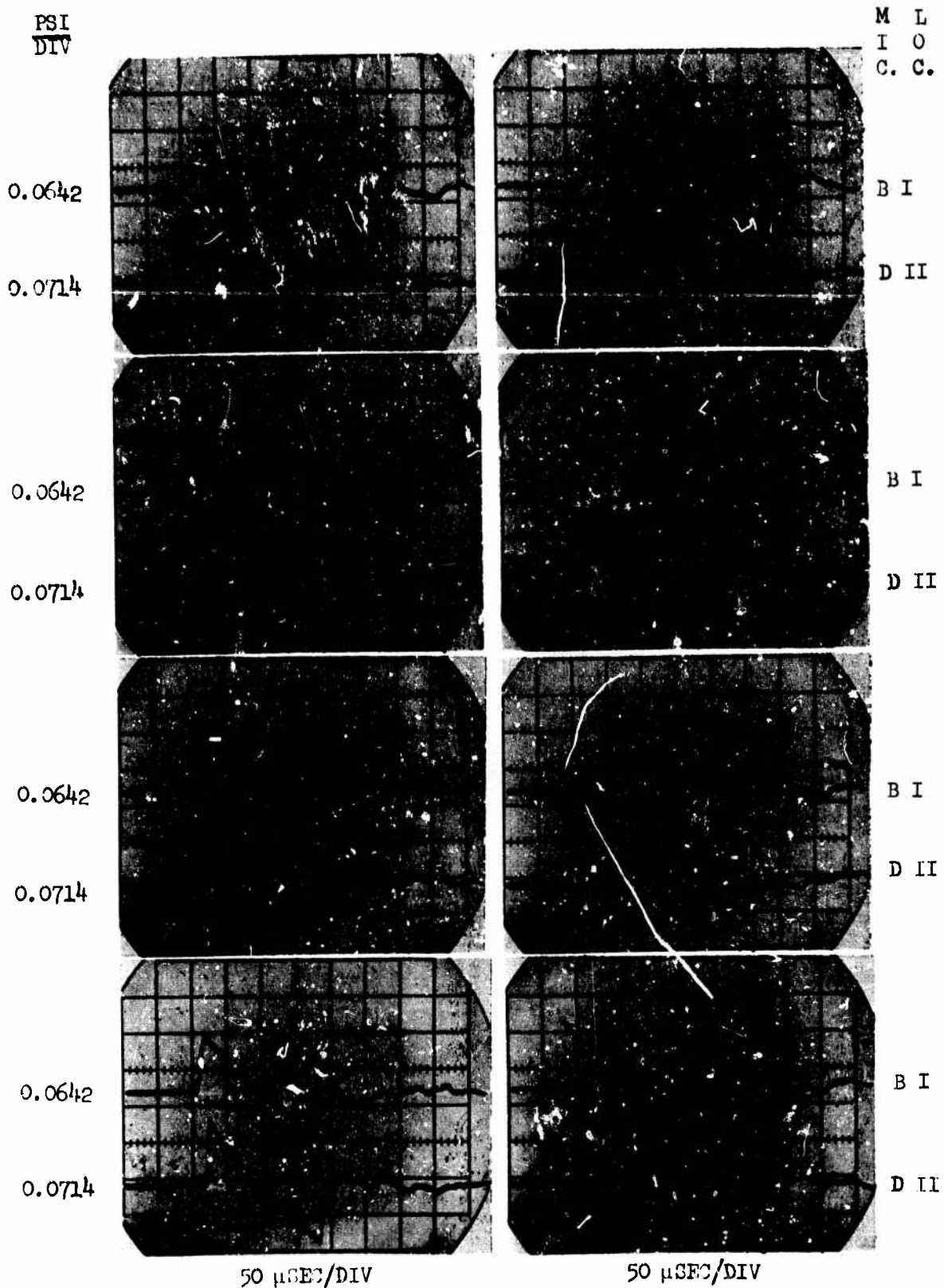
Figure A34 Boom signatures for group 314 -- 0.22 caliber projectiles,
M = 3.0, 4-inch nozzle, and 24-inch inlet.

126
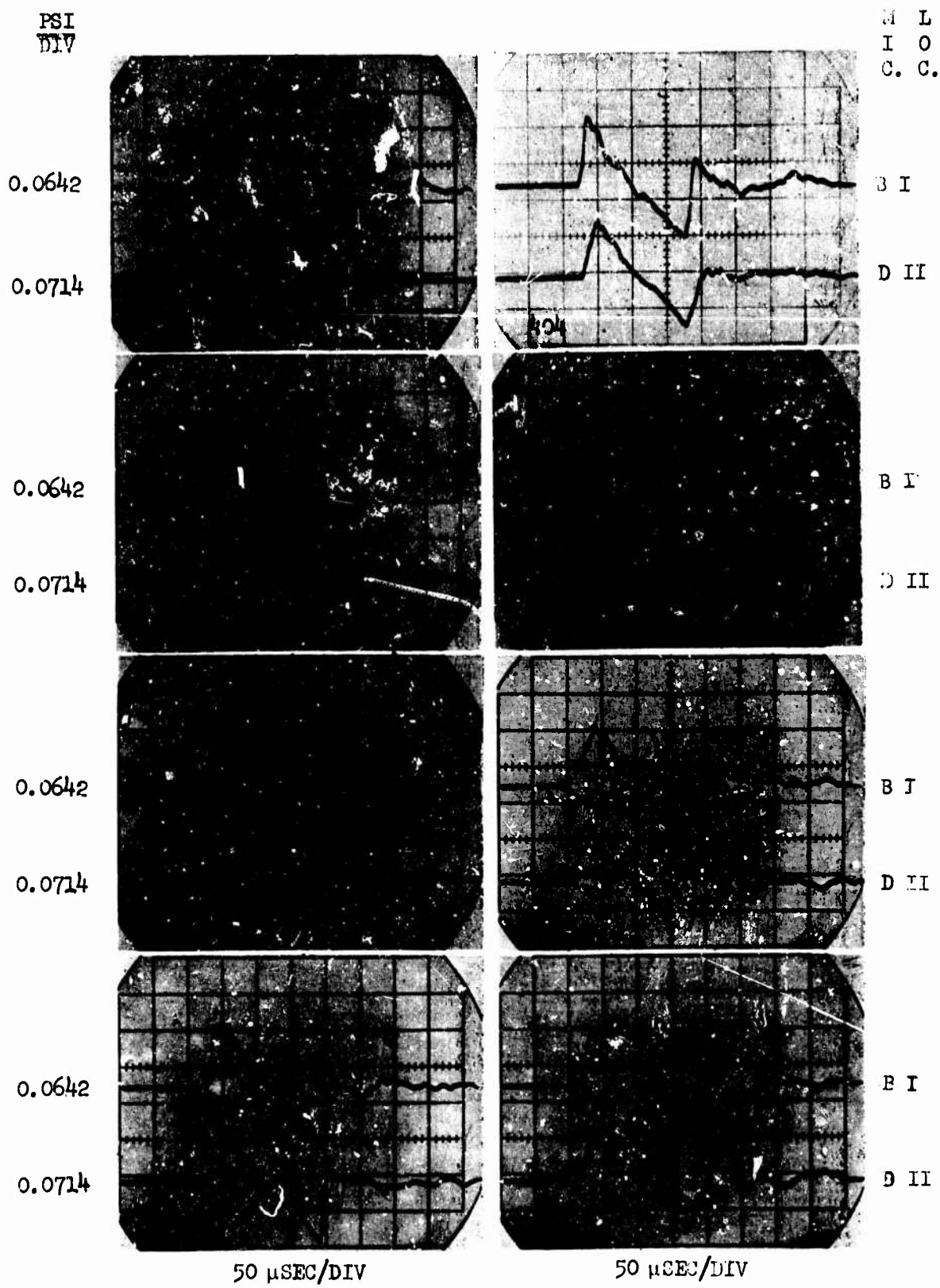
Figure A35 Boom signatures for group 314 -- 0.22 caliber projectiles,
M ≈ 3.0, 4-inch nozzle, and 24-inch inlet.

Figure A36 Boom signatures for group 314 -- 0.22 caliber projectiles,
M = 3.0, 4 inch nozzle, and 24 inch inlet.

128

Figure A37   Boom signatures for group 314 -- 0.22 caliber projectiles,
M = 3.0, 4 inch nozzle, and 24 inch inlet.
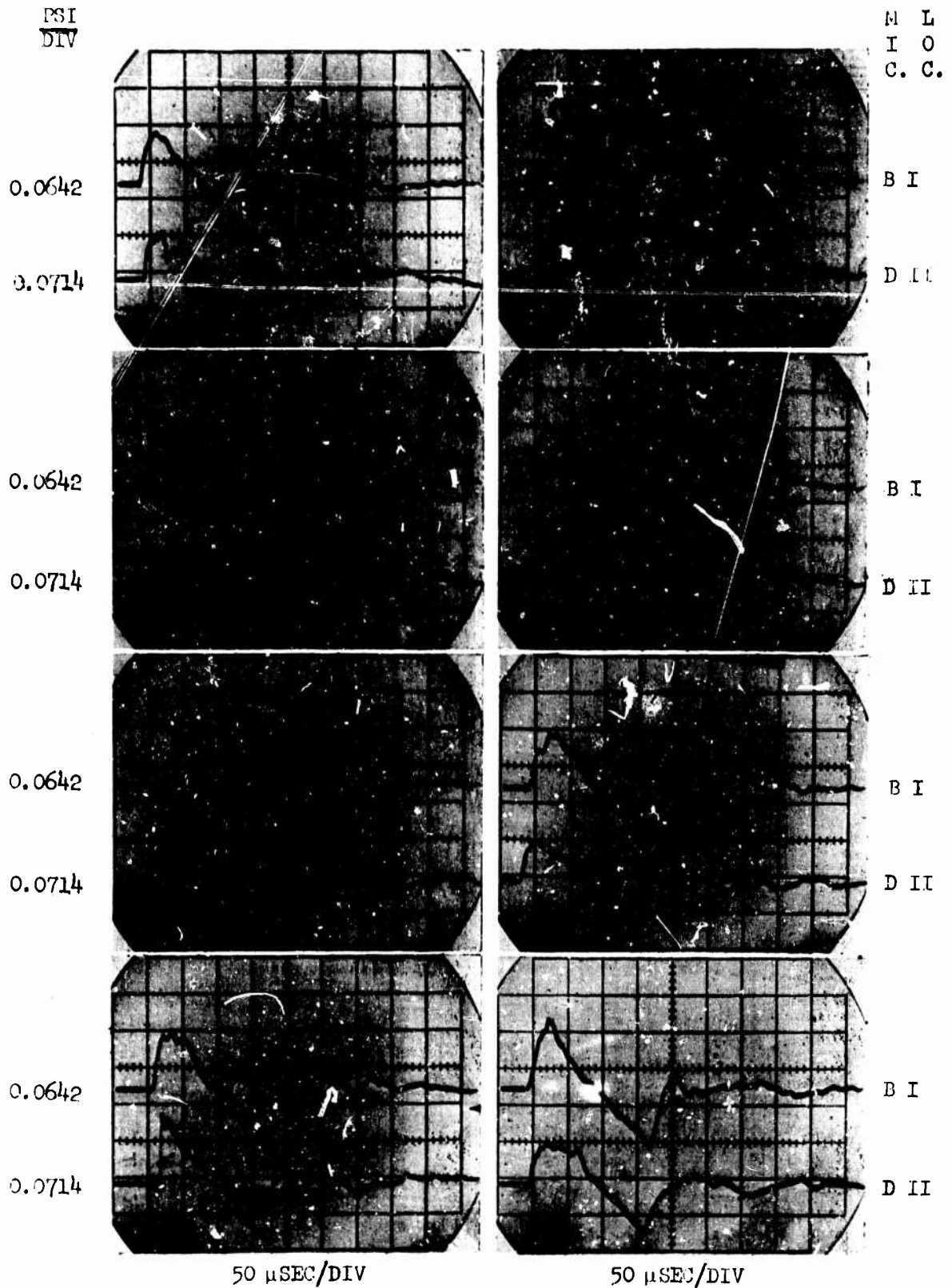
Figure A38 Boom signatures for group 314 -- 0.22 caliber projectiles,
M = 3.0, 4 inch nozzle, and 24 inch inlet.

130
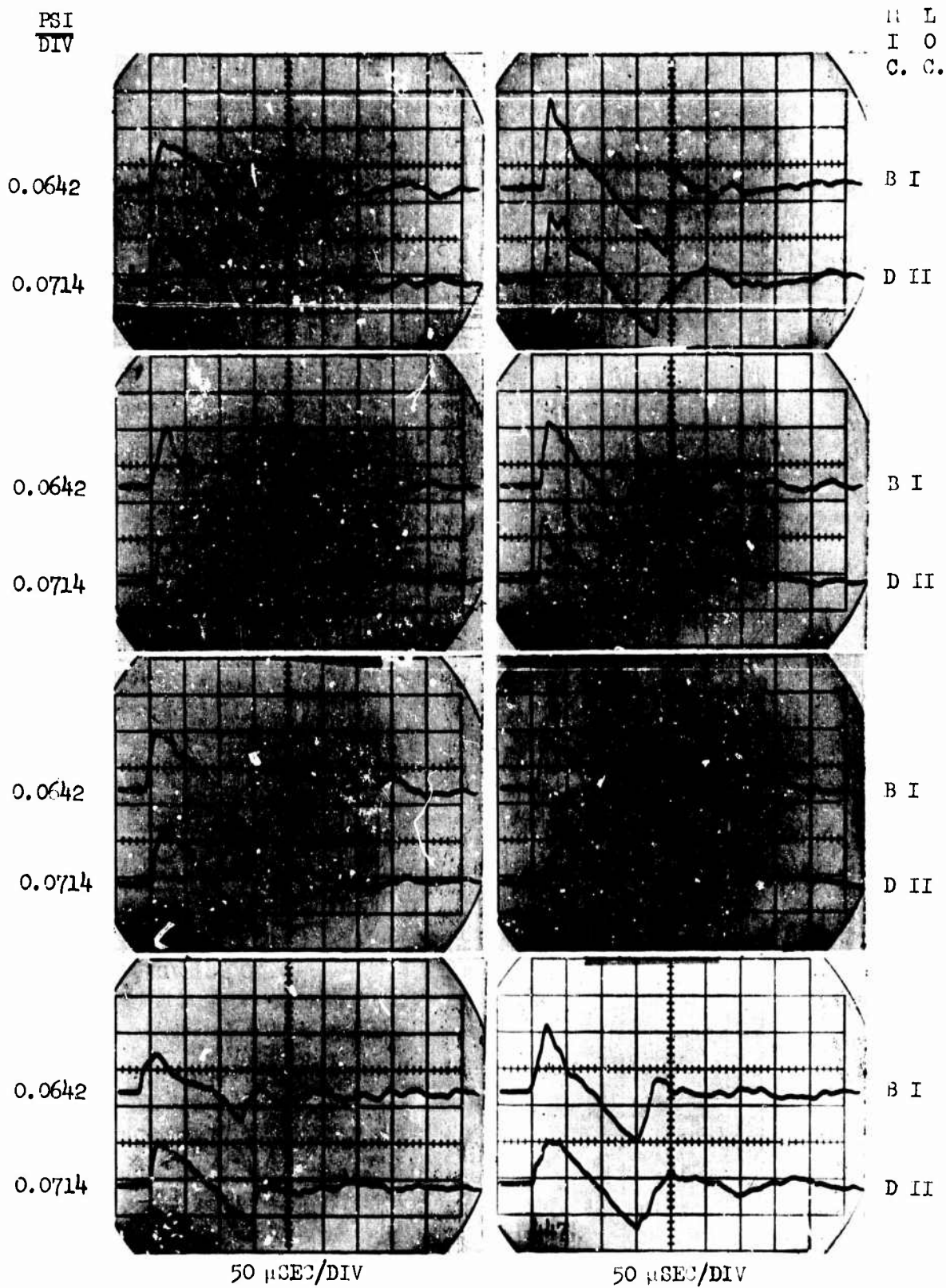
Figure A39 Boom signatures for group 314 -- 0.22 caliber projectiles, M = 3.0, 4 inch nozzle, and 24 inch inlet.

131
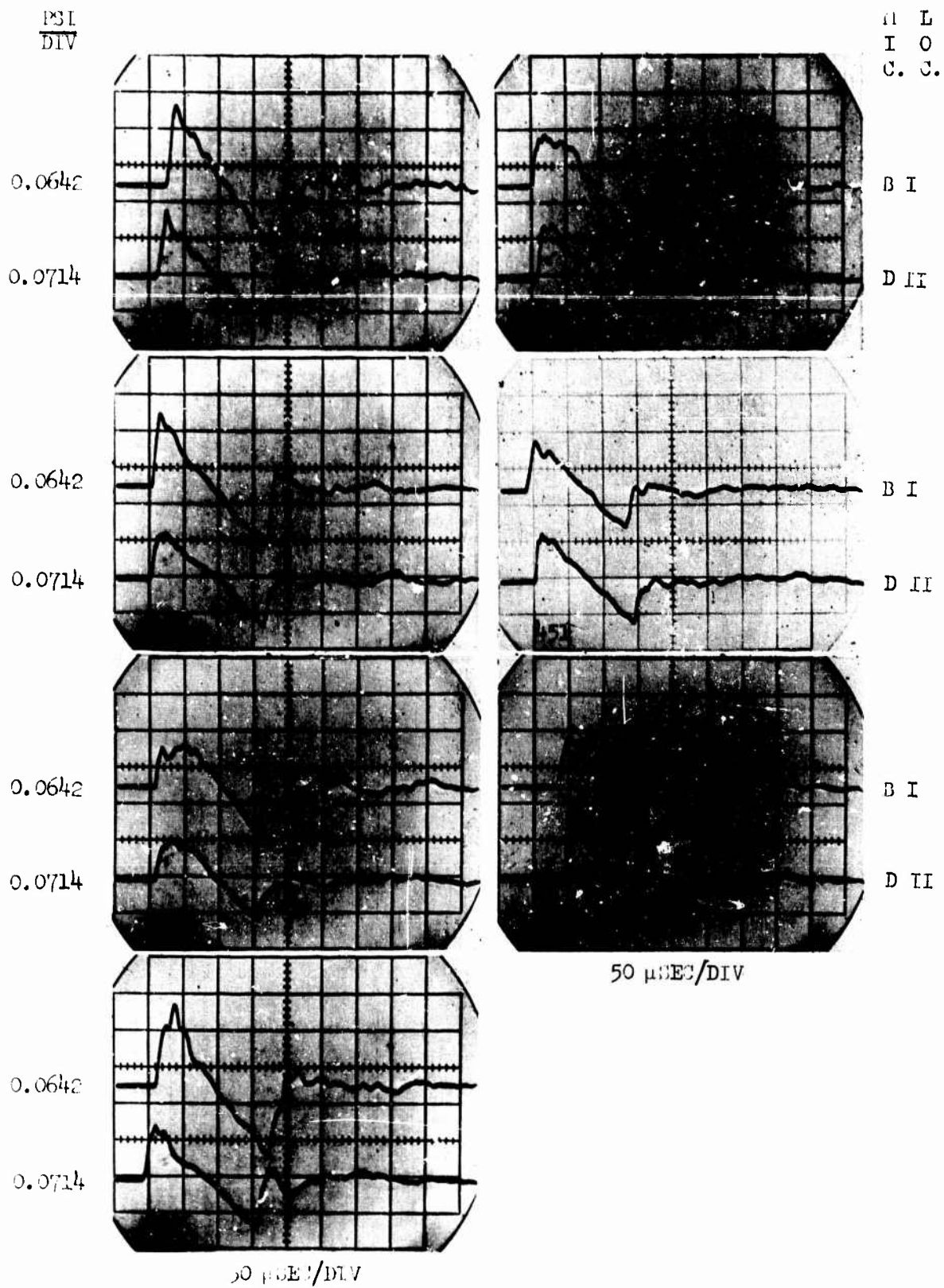
Figure A40 Boom signatures for group 314 -- 0.22 caliber projectiles, M = 3.0, 4 inch nozzle, and 24 inch inlet.

Figure A41 Boom signatures for group 324 -- 0.22 caliber projectiles, M = 3.0, 6 inch nozzle, and 24 inch inlet.

Figure A42 Boom signatures for group 324 -- 0.22 caliber projectiles,
M = 3.0, 6 inch nozzle, and 24 inch inlet.

134

Figure A43 Boom signatures for group 324 -- 0.22 caliber projectiles, M = 3.0, 6 inch nozzle, and 24 inch inlet.

135
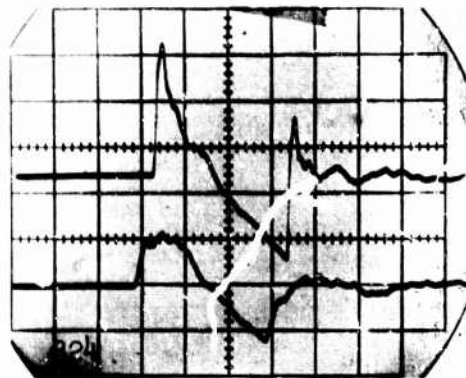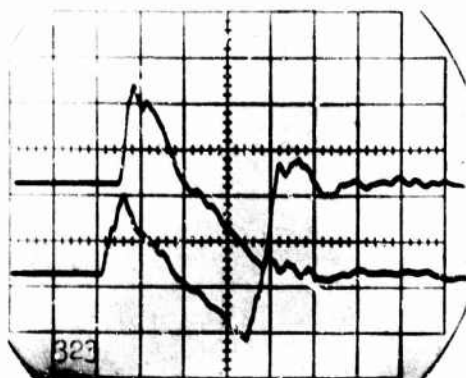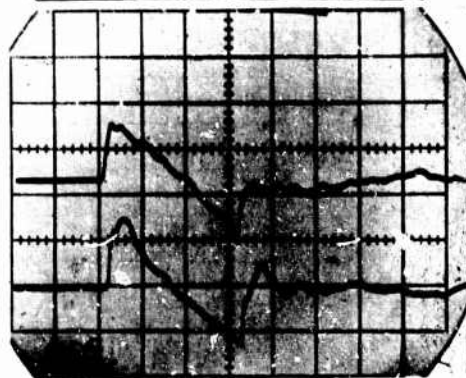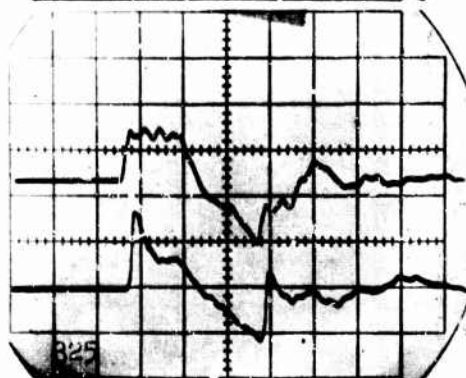
Figure A44   Boom signatures for group 334 -- 0.22 caliber projectiles, M = 3.0, 24 inch nozzle, and 24 inch inlet.

Figure A45 Boom signatures for group 334 -- 0.22 caliber projectiles, M = 3.0, 24 inch nozzle, and 24 inch inlet.

Figure A46 Boom signatures for group 334 -- 0.22 caliber projectiles,
M = 3.0, 24 inch nozzle, and 24 inch inlet.

138

Figure A47 Boom signatures for group 341 -- 0.22 caliber projectiles, M = 3.0, high-speed nozzle no. 1, and 12 inch inlet.

Figure A48 Boom signatures for group 341 -- 0.22 caliber projectiles, M = 3.0, high-speed nozzle no. 1, and 12 inch inlet.

Figure A49 Boom signatures for group 344 -- 0.22 caliber projectiles, M = 3.0, high-speed nozzle no. 1, and 24 inch inlet.

Figure A50 Boom signatures for group 344 -- 0.22 caliber projectiles;
M = 3.0, high-speed nozzle no. 1, and 24 inch inlet.

142

Figure A51 Boom signatures for group 351 -- 0.22 caliber projectiles, M = 3.0, high-speed nozzle no. 2, and 12 inch inlet.

0.0642 — B I

0.0714 — D II

497   498

0.0642 — B I

0.0714 — D II

499   500

0.0642 — B I

0.0714 — D II

501   502

50 µSEC/DIV   50 µSEC/DIV

Figure A52 Boom signatures for group 351 -- 0.22 caliber projectiles,
M = 3.0, high-speed nozzle no. 2, and 12 inch inlet.

$\dfrac{\text{PSI}}{\text{DIV}}$

M L
I O
C C

0.0642
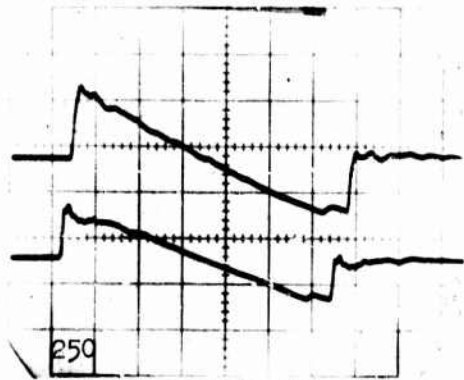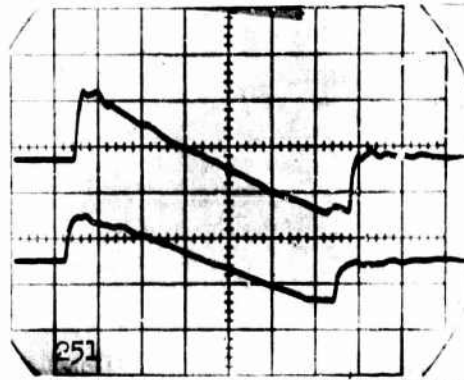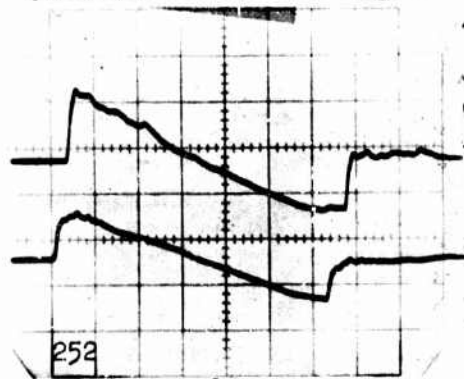
0.0714

503 504 B I

D II

0.0642

0.0714

505 506 B I

D II

0.0642

0.0714

507 508 B I

D II

50 µSEC/DIV   50 µSEC/DIV

Figure A53 Boom signatures for group 354 -- 0.22 caliber projectiles,
M = 3.0, high-speed nozzle no. 2, and 24 inch inlet.

M L
I O
C C

0.0642   B I

0.0714   D II

0.0642   B I

0.0714   D II

0.0642   B I

0.0714   D II

50 μSEC/DIV   50 μSEC/DIV

Figure A54   Boom signatures for group 354 -- 0.22 caliber projectiles, M = 3.0, high-speed nozzle no. 2, and 24 inch inlet.

146
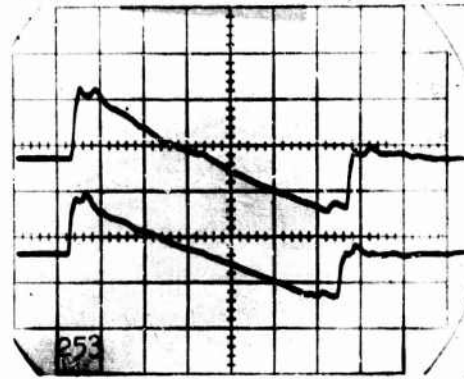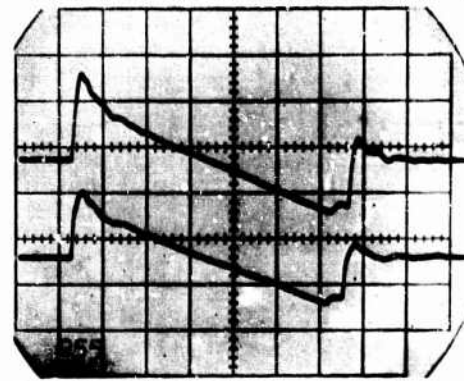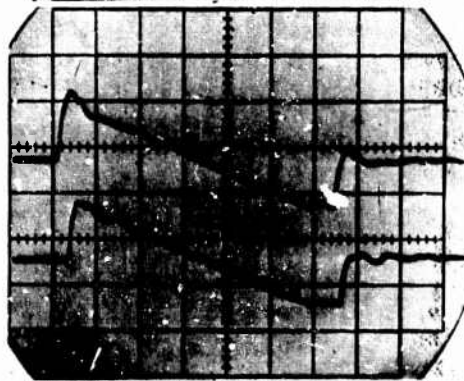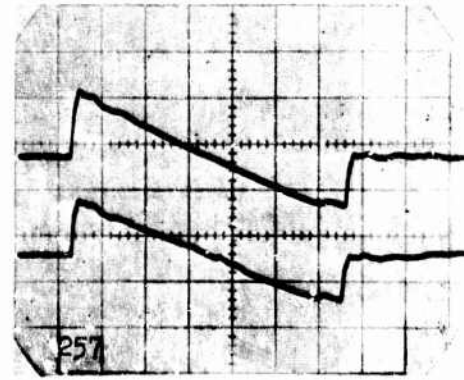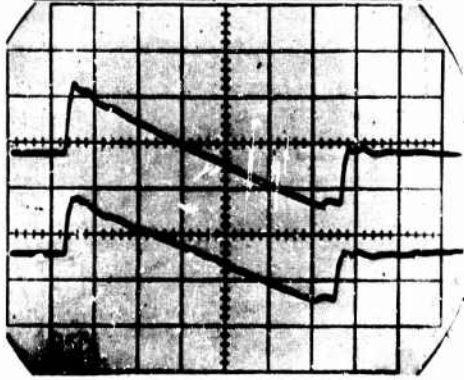
Figure A55 Boom signatures with thermal generators operating. See table 5 and figure 18 for generator locations.

147
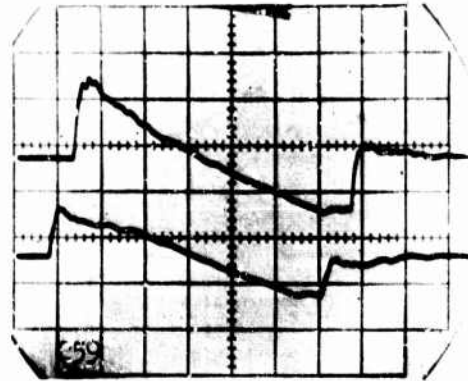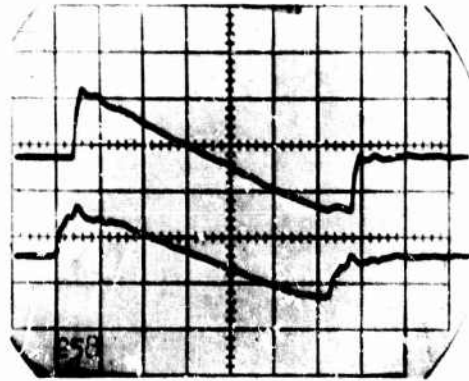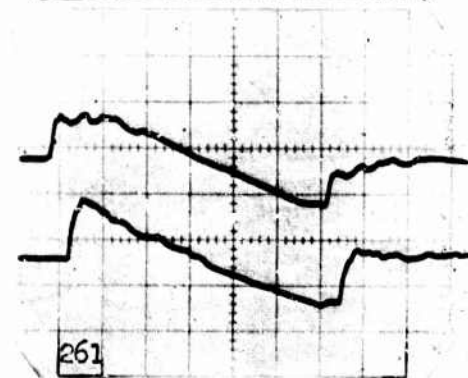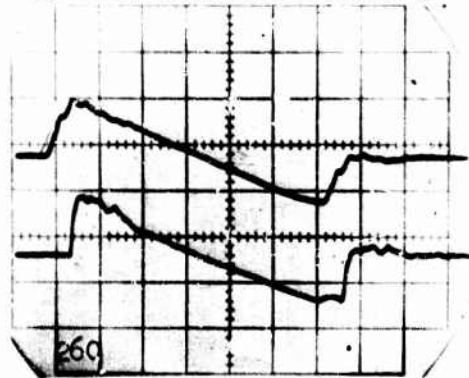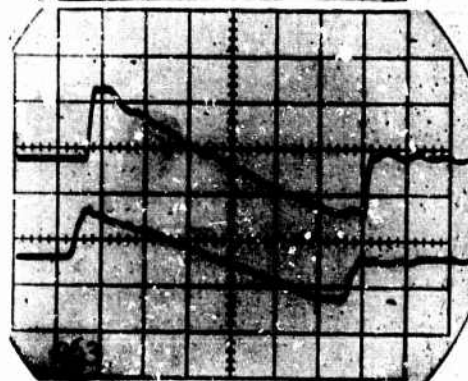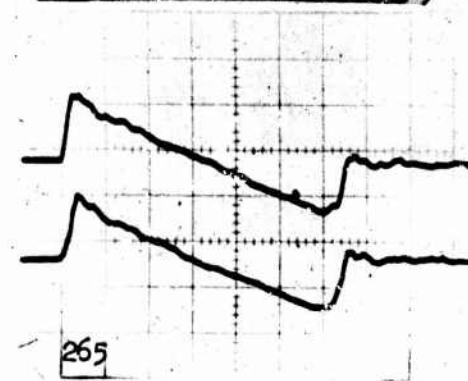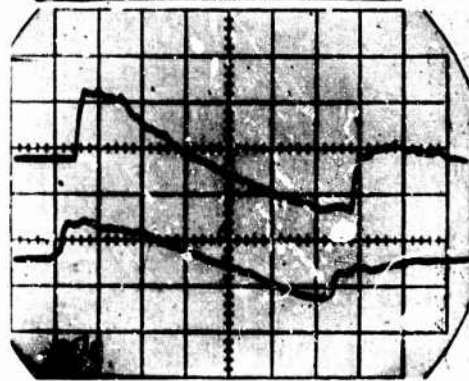
Figure A56 Boom signatures with thermal generators operating. See table 5 and figure 18 for generator locations.

148
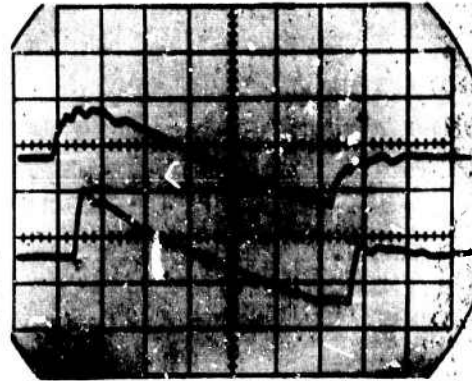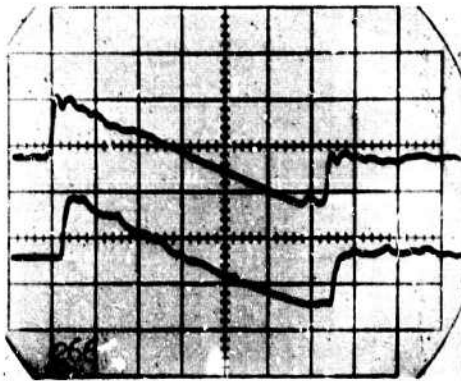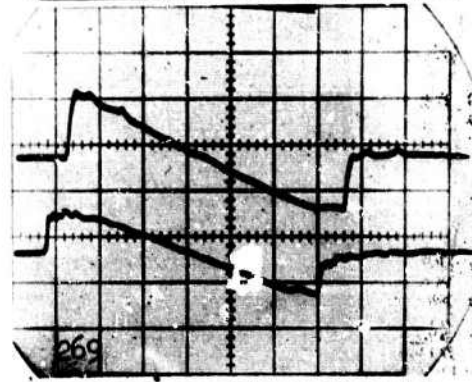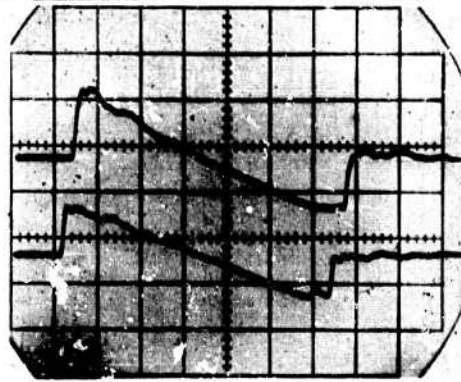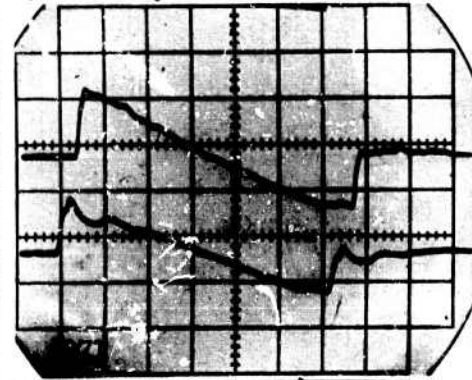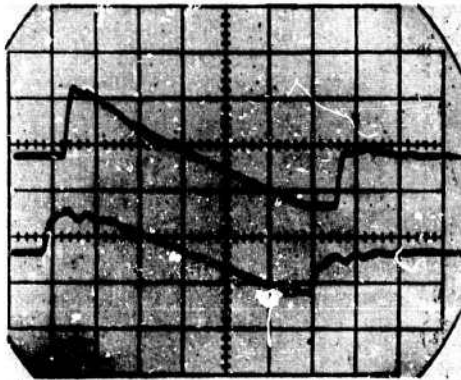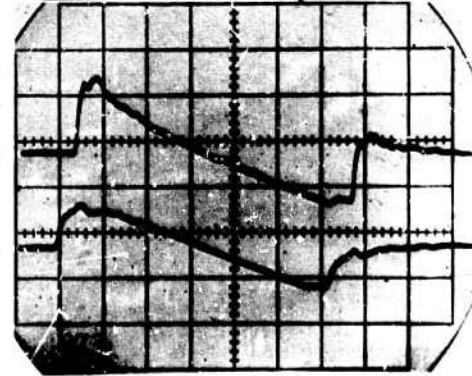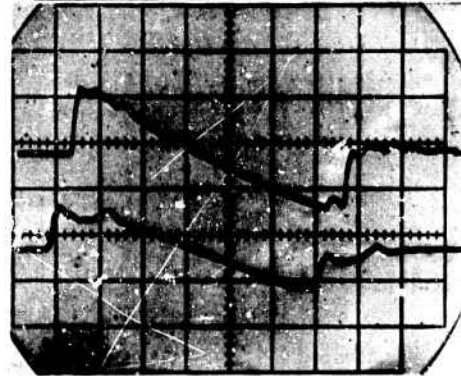
Figure A57 Boom signatures with thermal generators operating. See table 5
and figure 18 for generator locations.
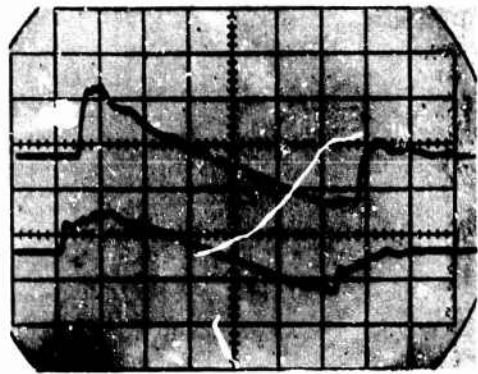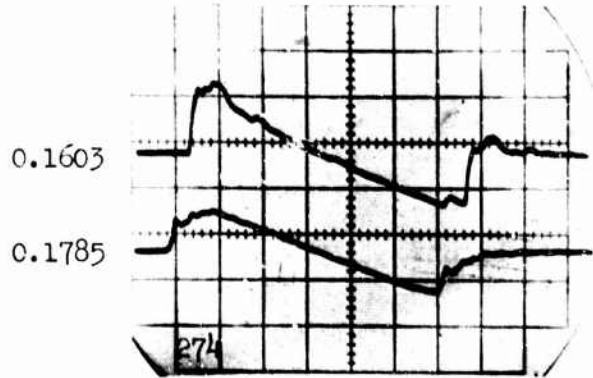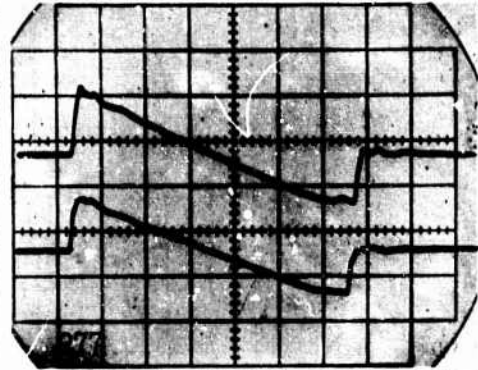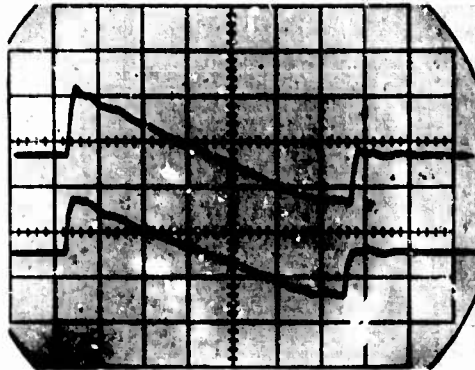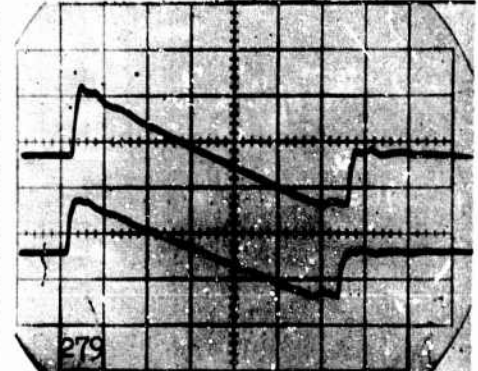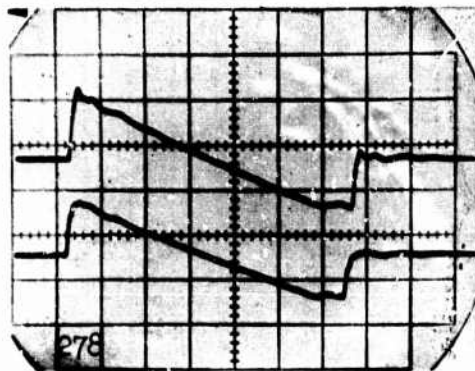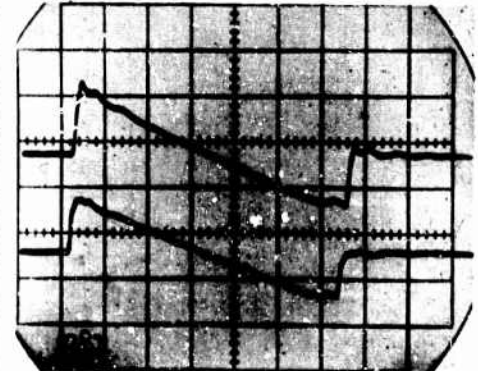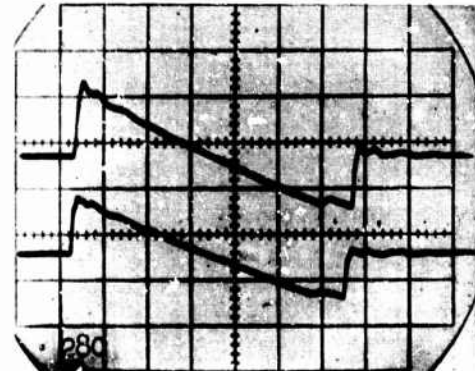
Figure A58 Boom signatures with one thermal generator operating in top two pictures and with helium injection in bottom six pictures. See table 5 and figure 18 for generator and helium nozzle locations.
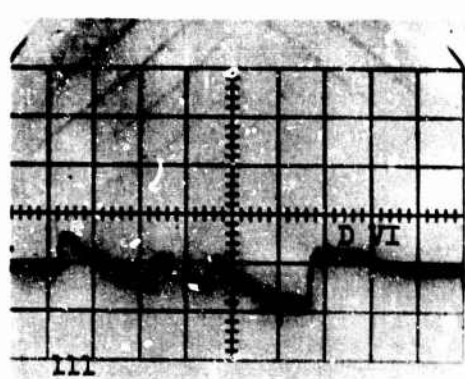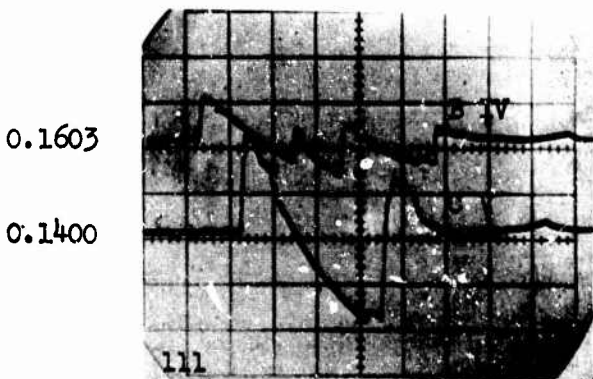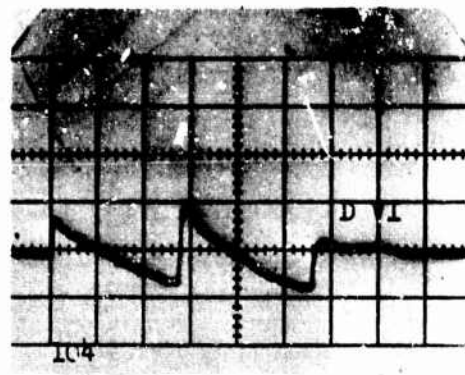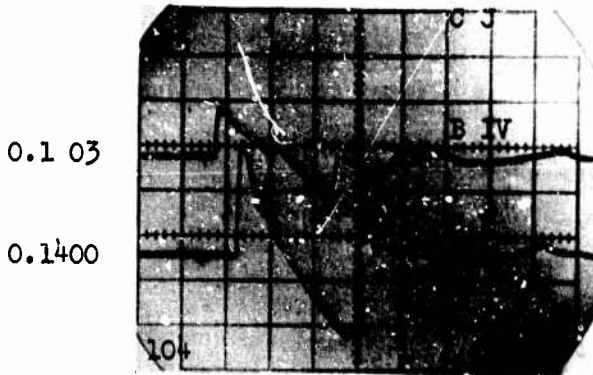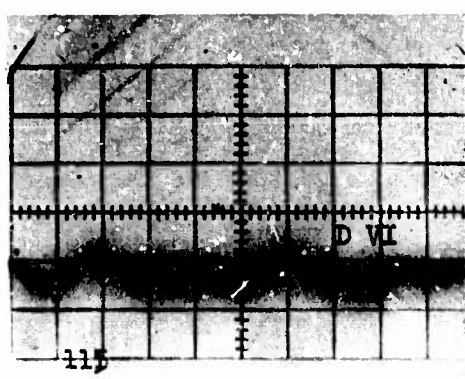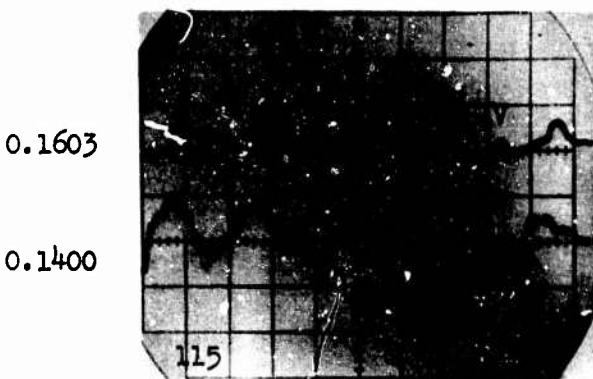
Figure A59 Signatures at locations IV, V, and VI from B projectiles and topographical models. Upper two pictures are for the step model and M = 1.40. Center two pictures are for the step model and M = 2.56. Bottom two pictures are for the 2 inch overhang model and M = 1.40; compare this with similar signatures on figure A60.

151
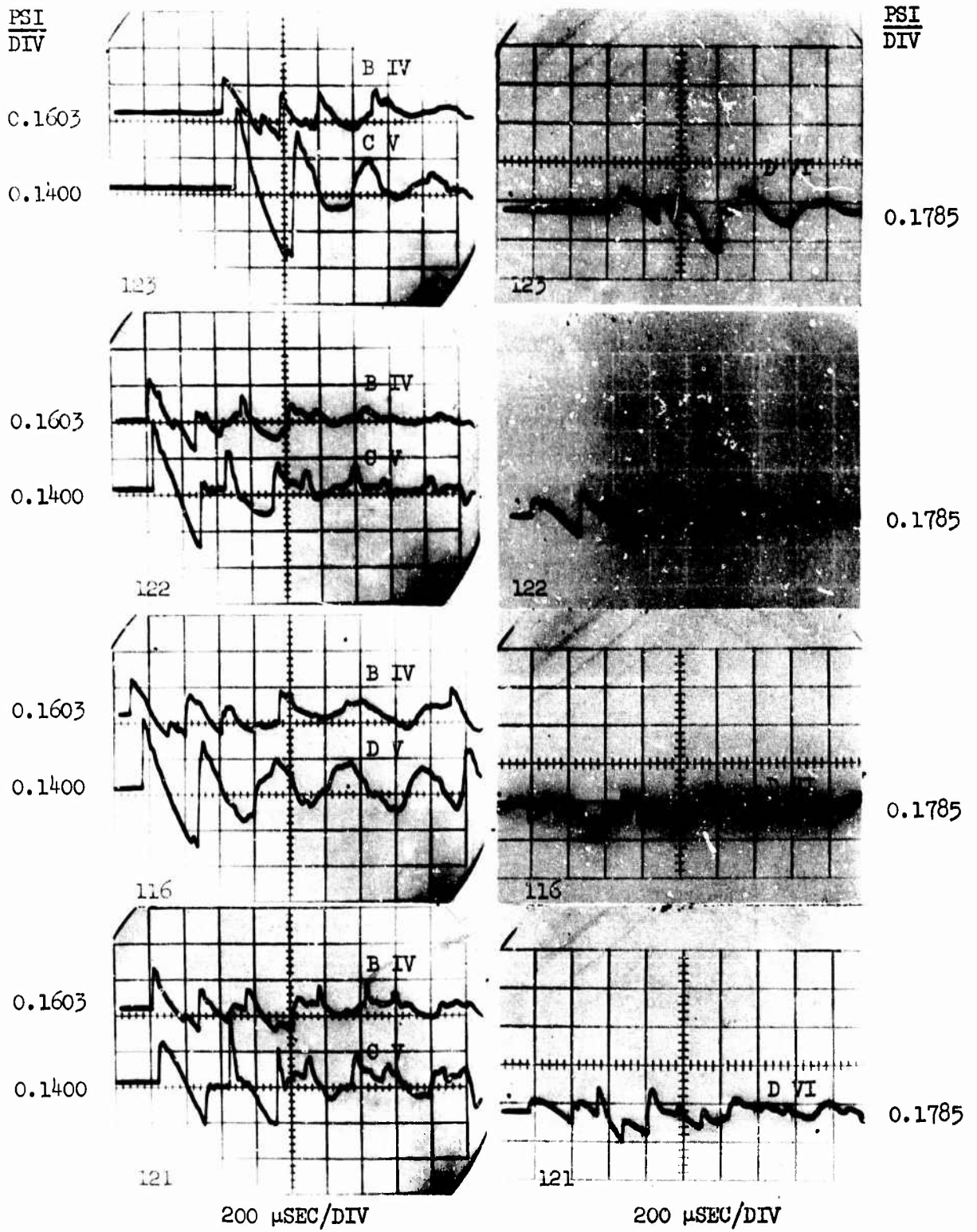
Figure A60 Signatures at locations IV, V, and VI from B projectiles and overhang models. First two pictures, M = 1.39, 1-inch overhang. Second two pictures, M = 2.56, 1-inch overhang. Third two pictures, M = 1.4C, 2-inch overhang. Last two pictures, M = 2.56, 2-inch overhang.

152
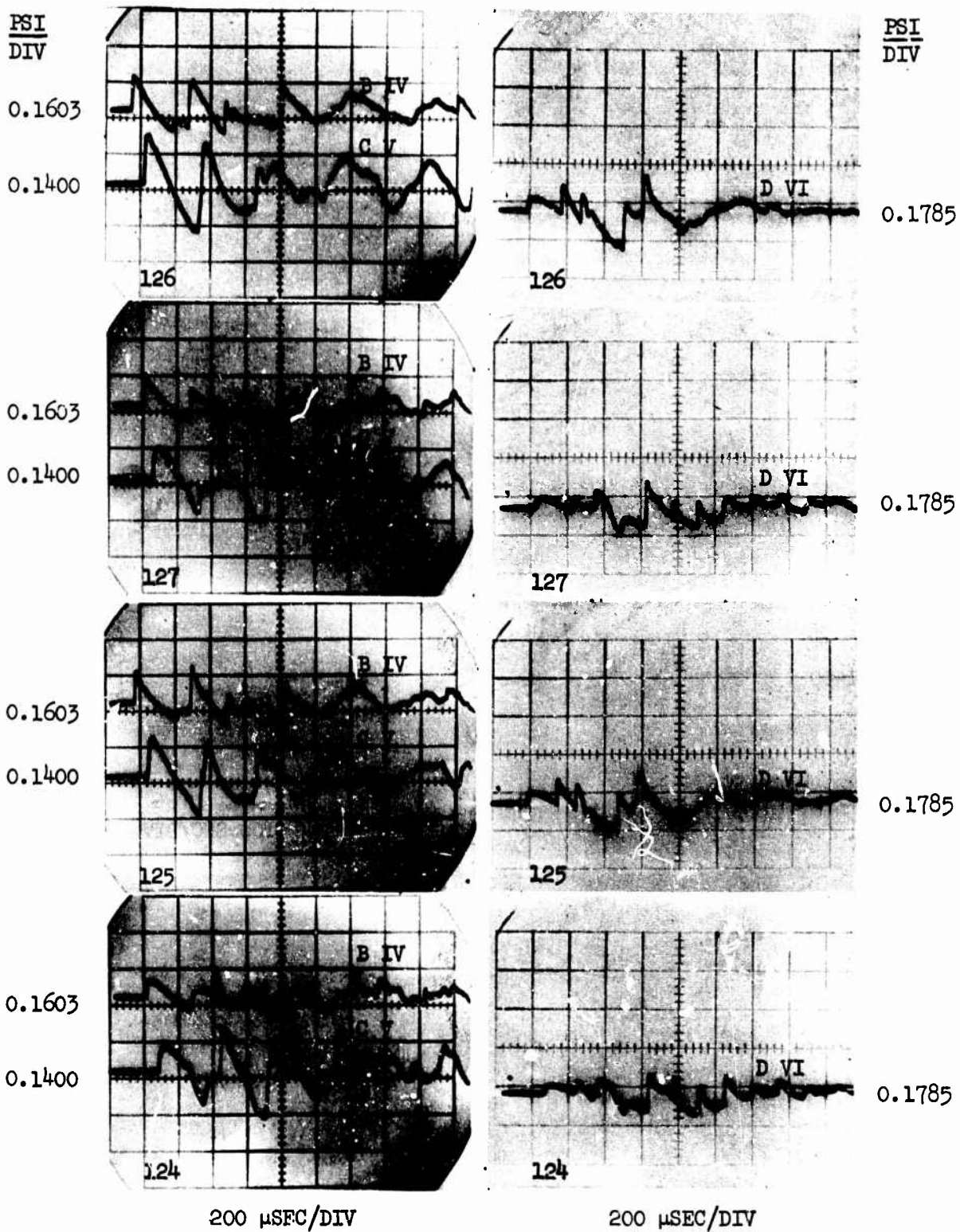
Figure A61 Signatures at locations IV, V, and VI from B projectiles and overhang models. First two pictures, M = 1.40, 3 inch overhang. Second two pictures, M = 2.56, 3 inch overhang. Third two picutres, M = 1.36, 4 inch overhang. Last two pictures, M = 2.57, 4 inch overhang.
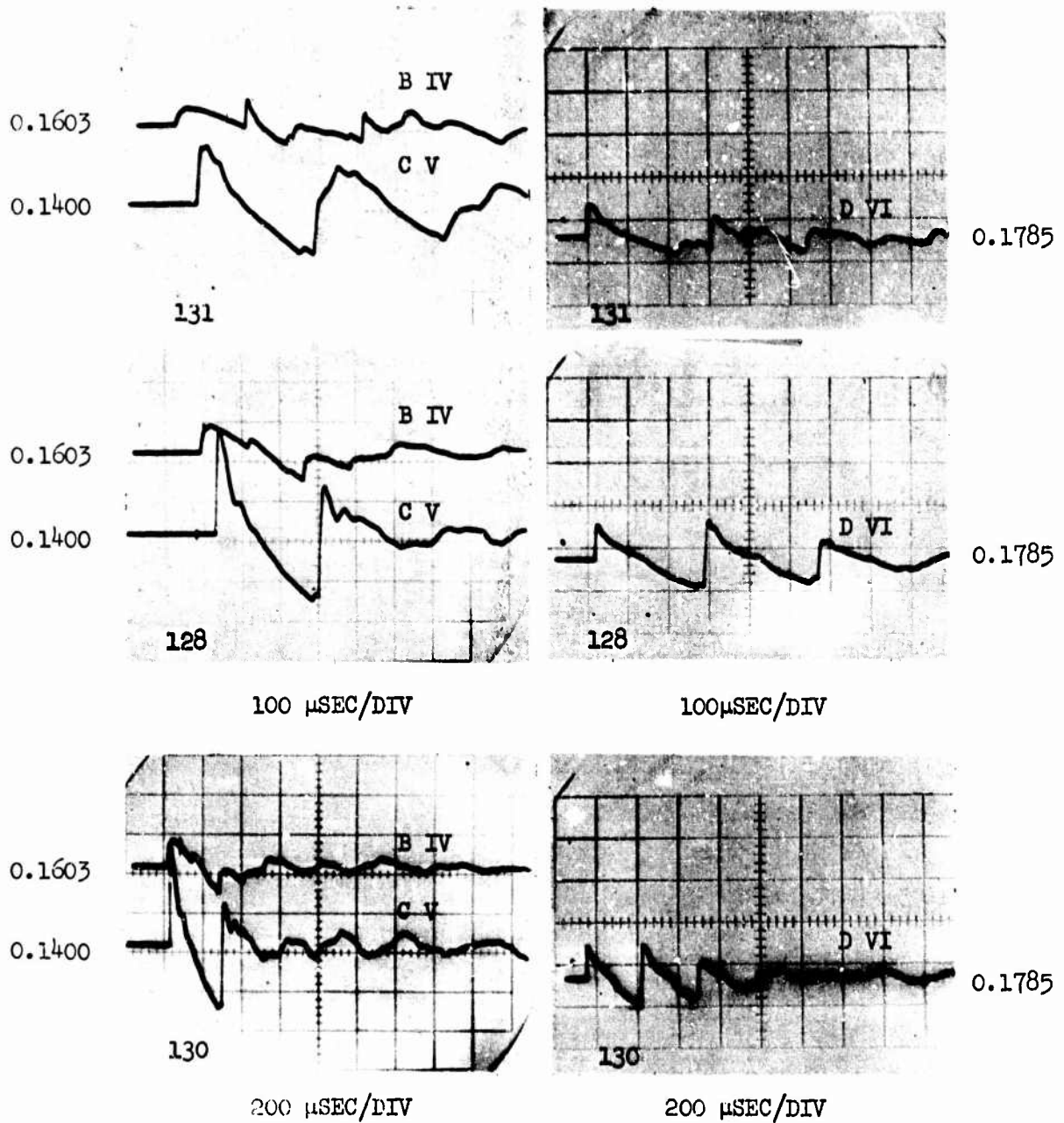
Figure A62 Signatures at locations IV, V, and VI from B projectiles and parallel wall models. First two pictures are for M = 1.47. Last four pictures pictures are for M = 2.56.
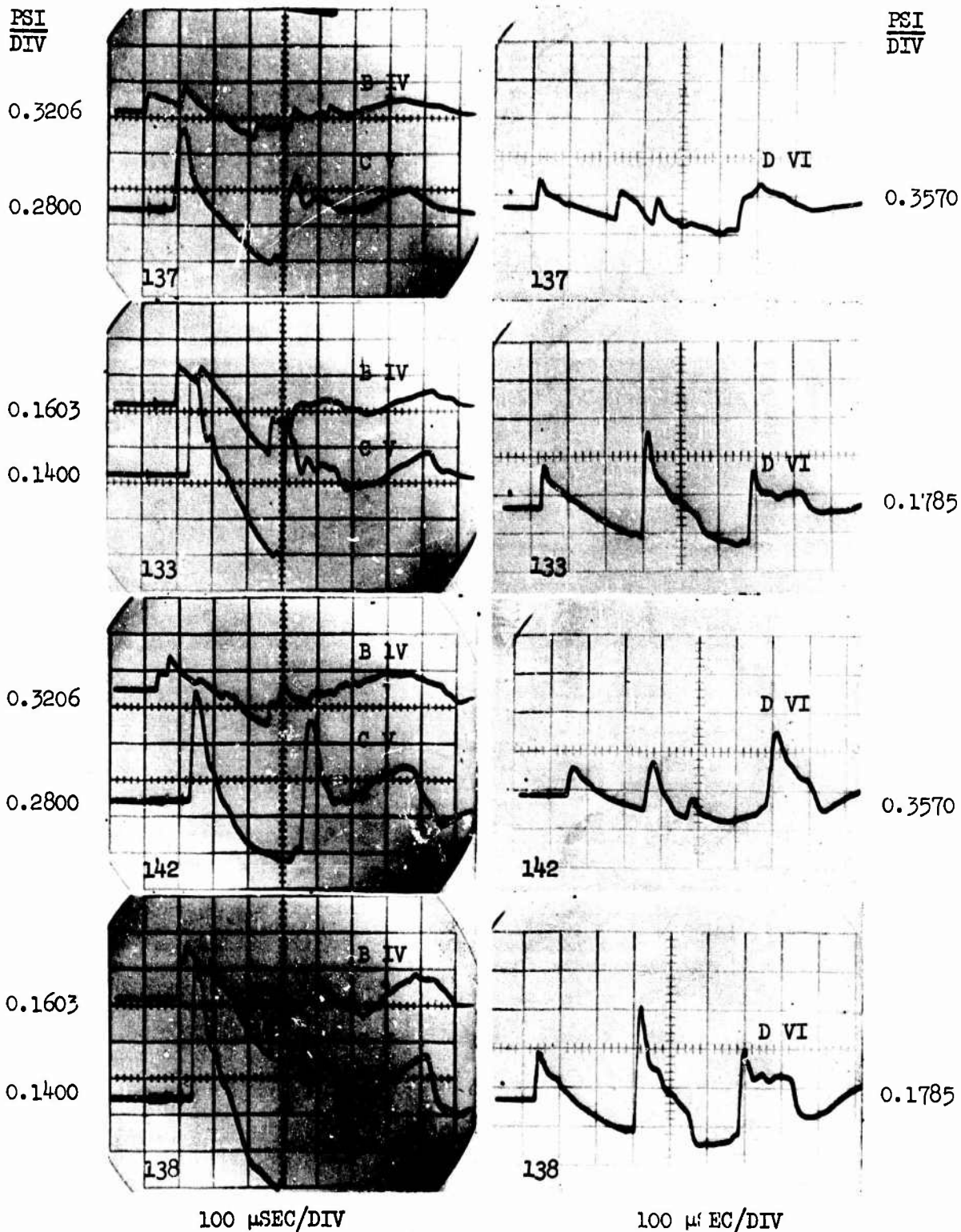
Figure A63 Signatures at locations IV, V, and VI from B projectiles and
corner models. First two pictures, M = 1.46 and θ_c = 90°. Second two
pictures, M = 2.57 and θ_c = 90°. Third two pictures, M = 1.40 and θ_c = 45°.
Last two pictures, M = 2.57 and θ_c = 45°.
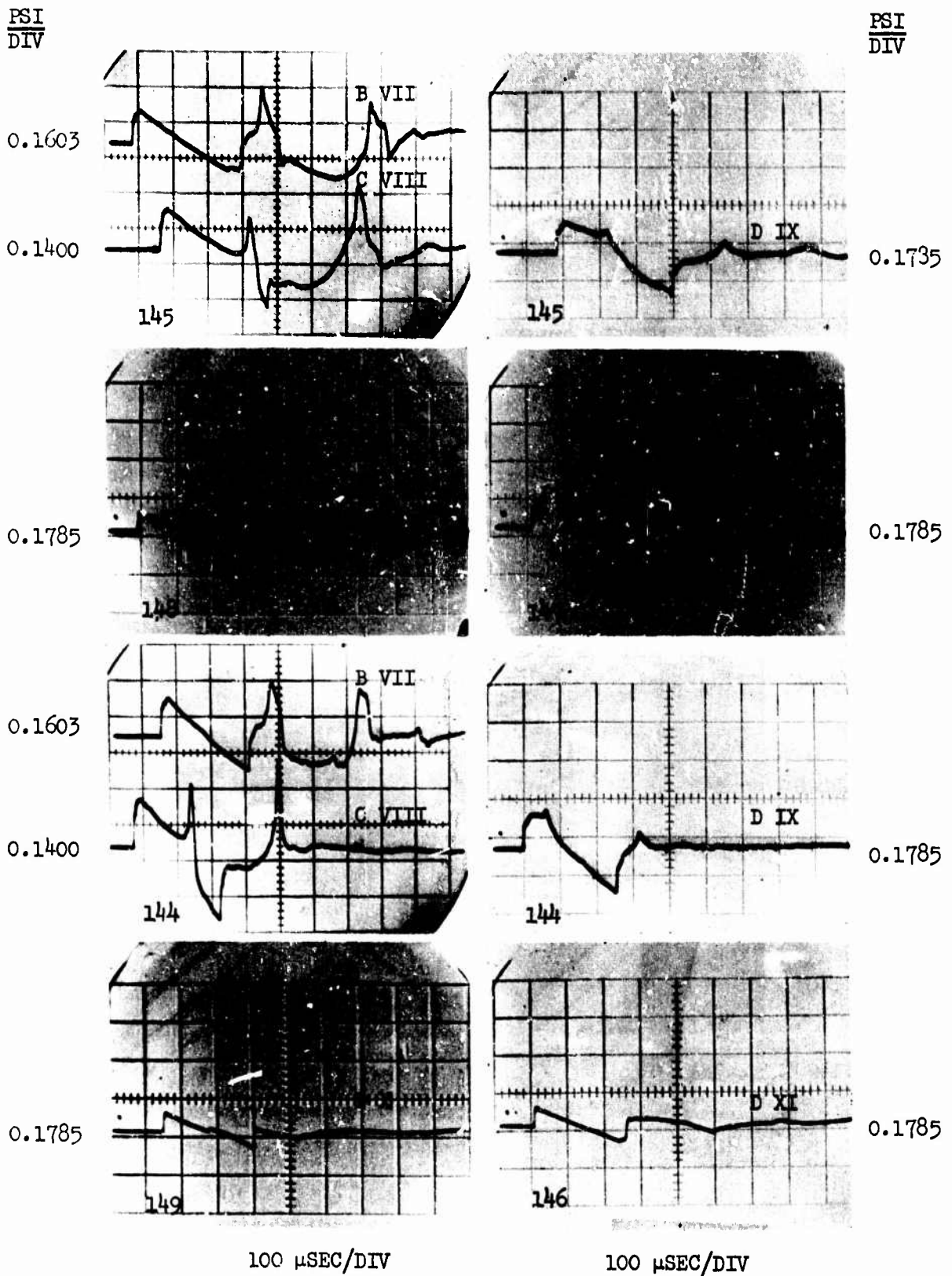
Figure A64 Signatures at locations VII, VIII, IX, X, and XI from B projectiles and paraboloidal canyon model at $\alpha_c = 0°$. First four pictures are for M = 1.40. Last four pictures are for $M = 2.57$.
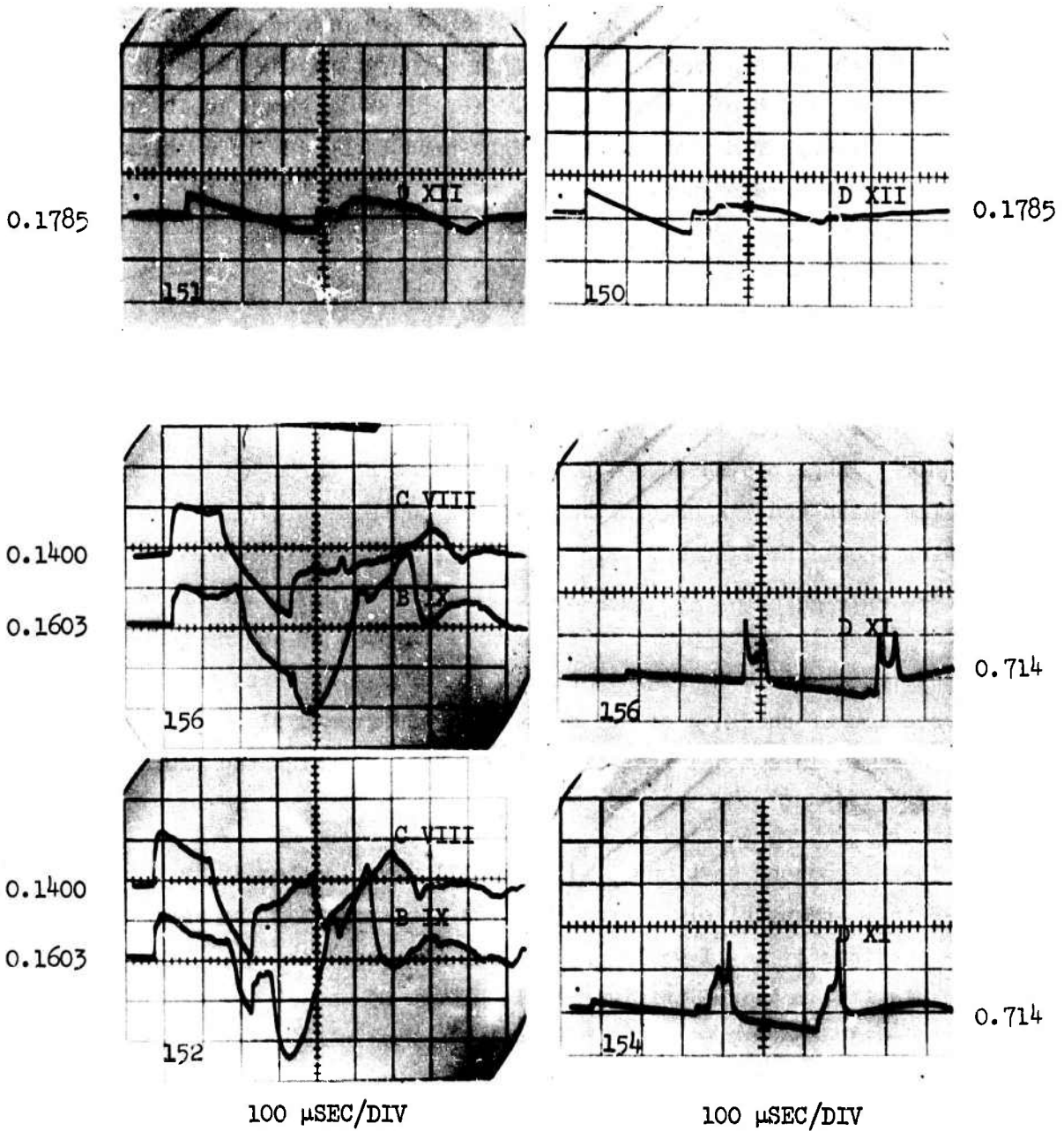
Figure A65 Signatures at locations VII, VIII, IX, and XII from B projectiles and paraboloidal canyon model. First two pictures are for $\alpha_c = 0°$ and M = 1.39 and 2.58, respectively. Second two pictures are for $\alpha_c = 45°$ and M = 1.40. Last two pictures are for $\alpha_c = 66°$ and M = 2.56.

APPENDIX B
SHADOWGRAPH PICTURES

The sketch below illustrates the geometry used to obtain the shadowgraph pictures. The image of the leading and trailing shocks and their reflections from the ground plane are shown on the film plate of the perspective sketch below. In the prints made from the film or negative the image is reversed as shown on the sketch of a print below. The print is shown as it appears in Figure B1 through B19; that is, the right-hand edge AB is vertical and shows the ground plane edge in all pictures.

The spark was located along the line $y = 0$ and $z = 72$ in. The microphones and the topographical models (when used) were centered in the plane $z = 0$, which also contained the projectile path at $y = 180$ in. The film plane was at $z = -26$ in. Two pins were located at $x = 7$ in. and at $x = 0$ in. along the line $y = 0$, $z = -24$ in. and appeared as shadows on the film. These pin shadows appear in figures B1 through B3 and B5 through B7. The third and larger pin that appears on these figures above the other two pins should be ignored. Pin 2 only was used in figures B4 and B8 through B10, and no pins were used in figures B11 through B19. The spark source was located directly above pin 1 in figures B1 through B3 and B5 through B7, directly above pin 2 in figures B4 and B8 through B10, and in line with the intersection of one face of the model with the ground plane in figures B11 through B19. This model face is the one which contains the microphones, as shown in figure 3.

The microphone stations I, II, and III were located at $x = 6$ in., 0 in., and -2 in., respectively. From this one can show that the rays past microphone stations I and II would appear 0.59 in. and 4.14 in., respectively, above pin 1 as measured in figures B1 through B3 and B5 through B7. Stations I and II would appear 0.59 in. and 4.14 in. above pin 2 in figures B4 and B8. In figures B9 and B10 stations I and II would appear 3.55 in. and 0 in. below pin 2. This information enables one to correlate the boom pressure signatures at the microphone stations with the shadowgraphs of the turbulence-shock interactions.

SPARK

SKETCH OF SHADOWGRAPH
SYSTEM GEOMETRY

GROUND
PLANE

z

x

y

STEP MODEL

PIN 1   PIN 2

A   B

LEADING SHOCK

D   C

FILM   TRAILING SHOCK

PROJECTILE DIRECTION———→

C   B

LEADING SHOCK

TRAILING SHOCK

SKETCH OF PRINT
FROM THE ABOVE
FILM.

PIN 2   NOTE IMAGE
REVERSAL.

PIN 1

PROJECTILE
DIRECTION

D   A
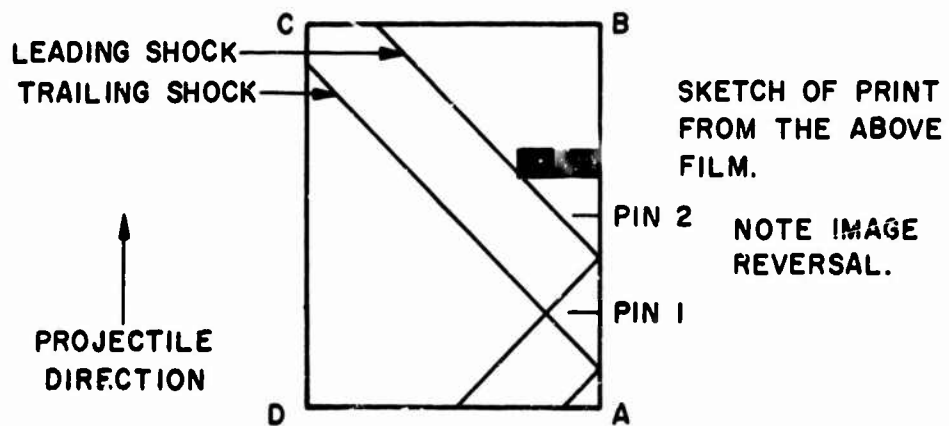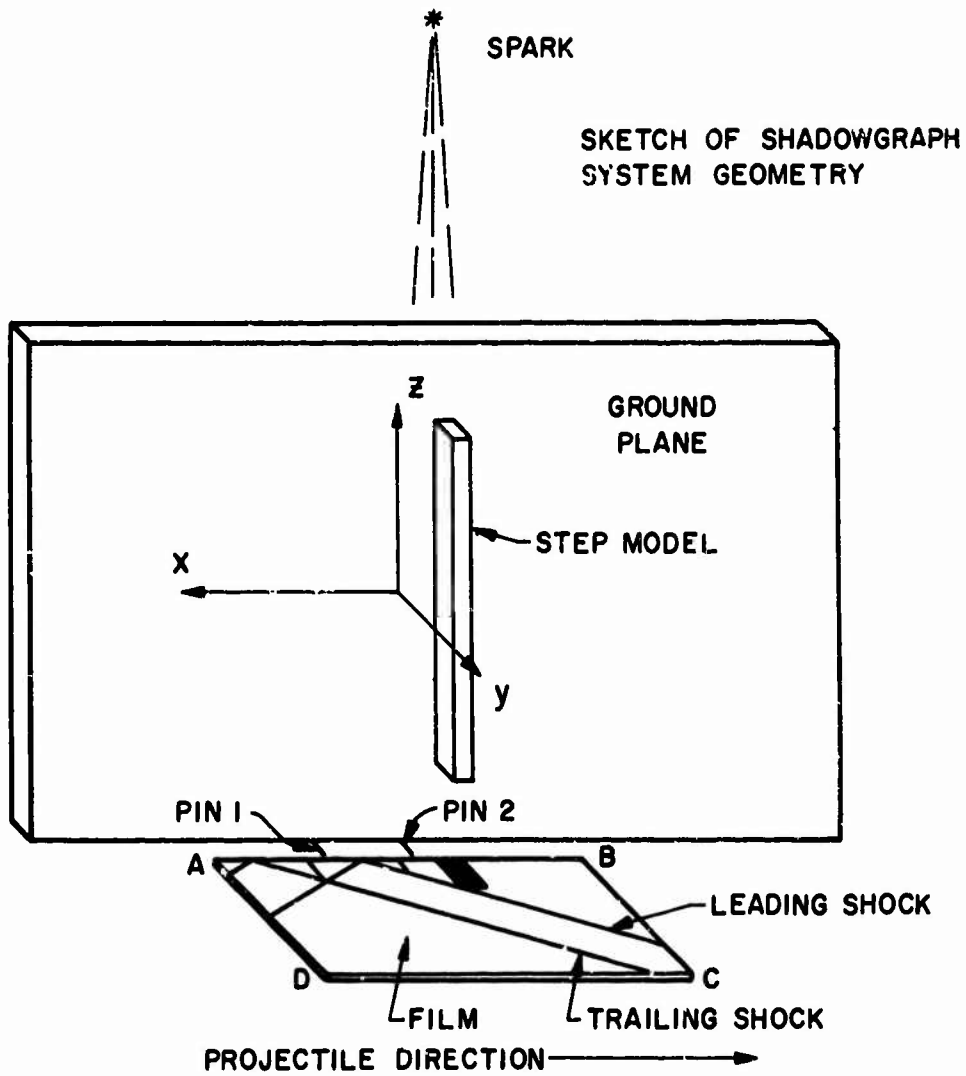
For the topographical models in figures B11 through B19, the shadowgraph ray divergence causes model shadows to be distorted from the two-dimensional form shown in figure 3. This can be seen clearly in figure B18 wherein one end of the two walls is amplified by a factor of $9/7$ in comparison with the opposite end. The same factors appear in figures B11 through B17, but are not as obvious.

The group numbers are explained in the title of the figures; see section 5C for a fuller discussion of the group numbers.
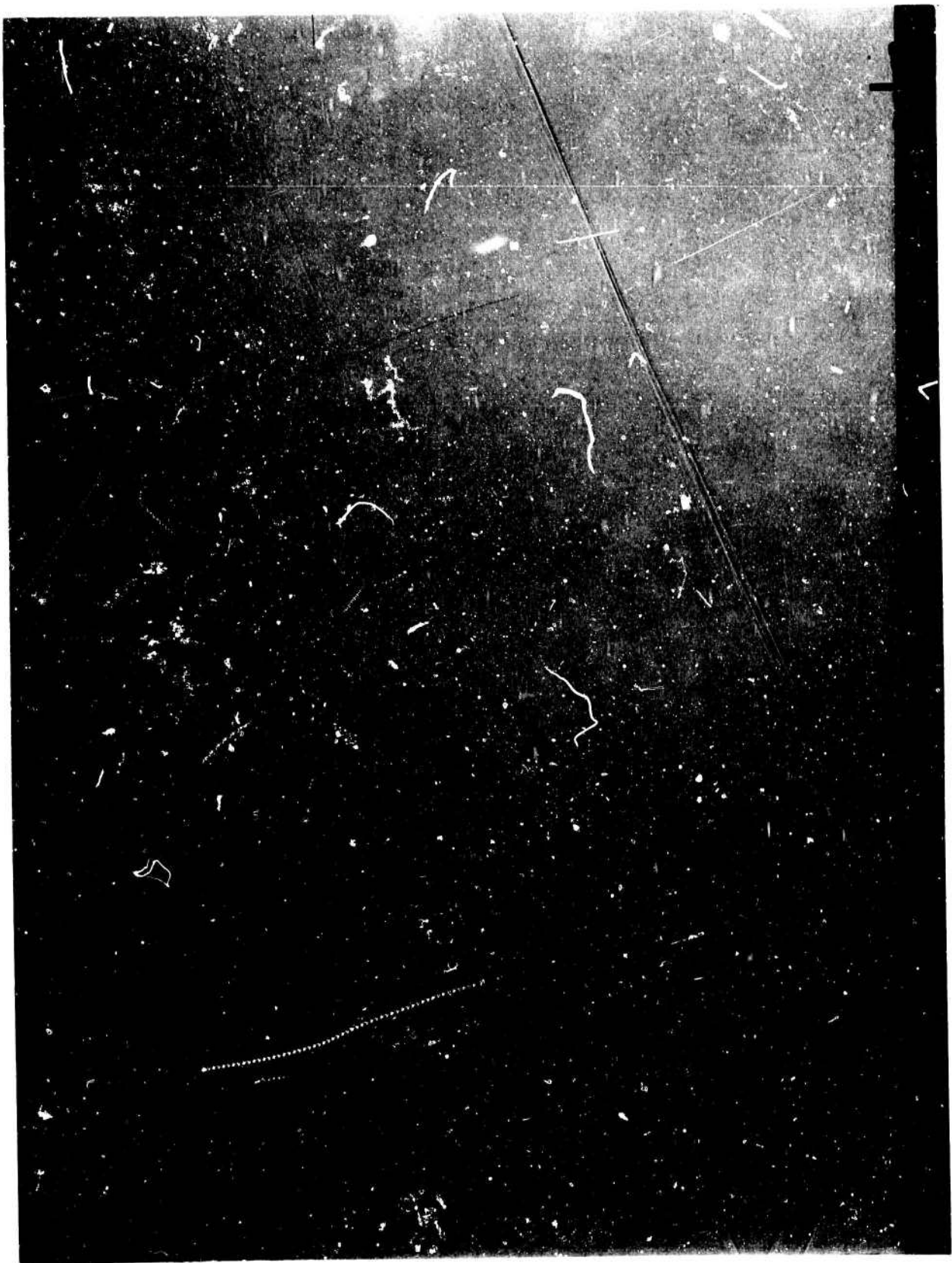
Figure B1 Shot 226 of group 212 -- B projectile, M = 2.52, 4 inch nozzle, and 16 inch inlet.
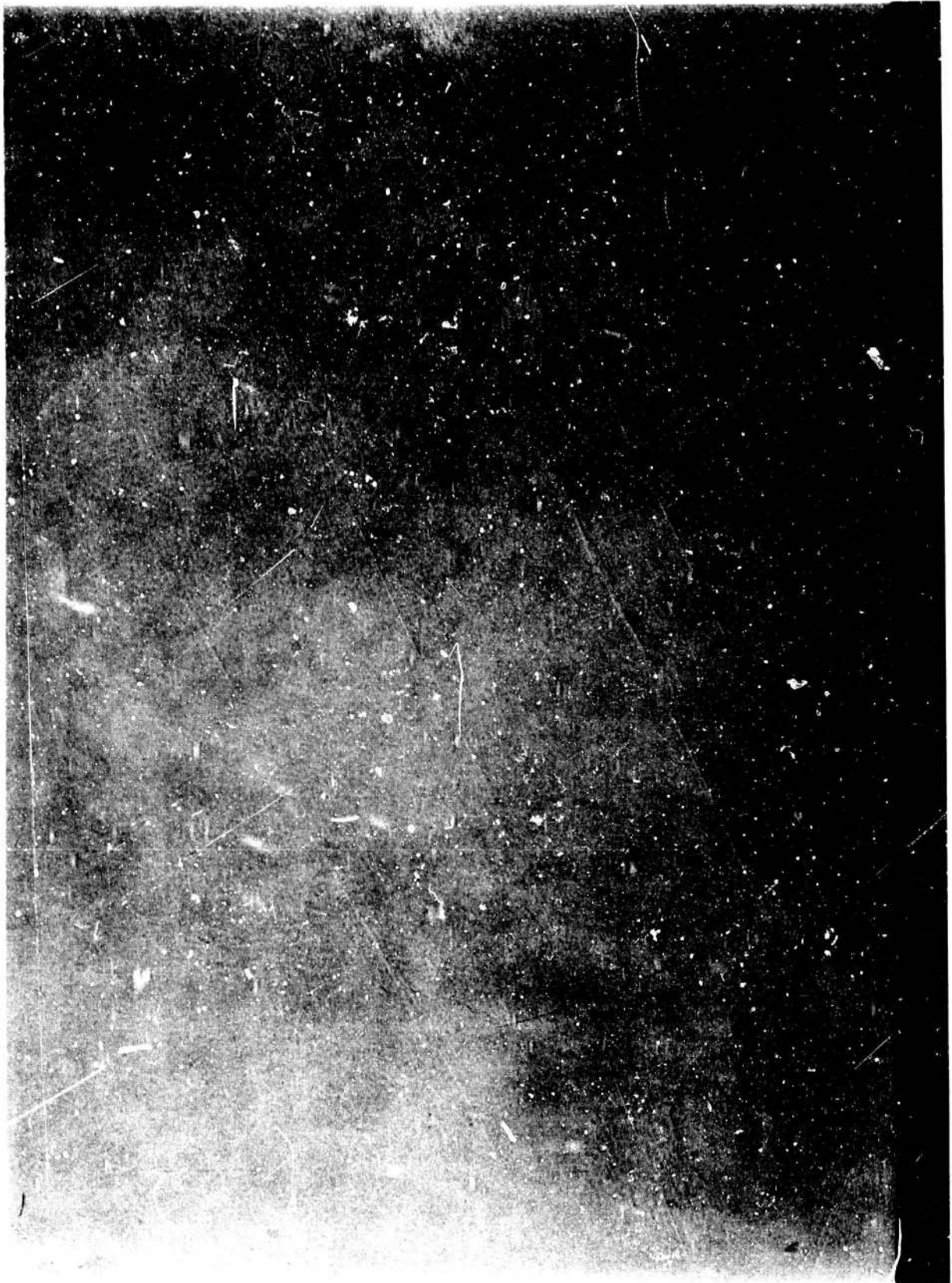
Figure B2 Shot 199 of group 214 -- B projectile, M = 2.55, 4 inch nozzle, and 24 inch inlet.

162
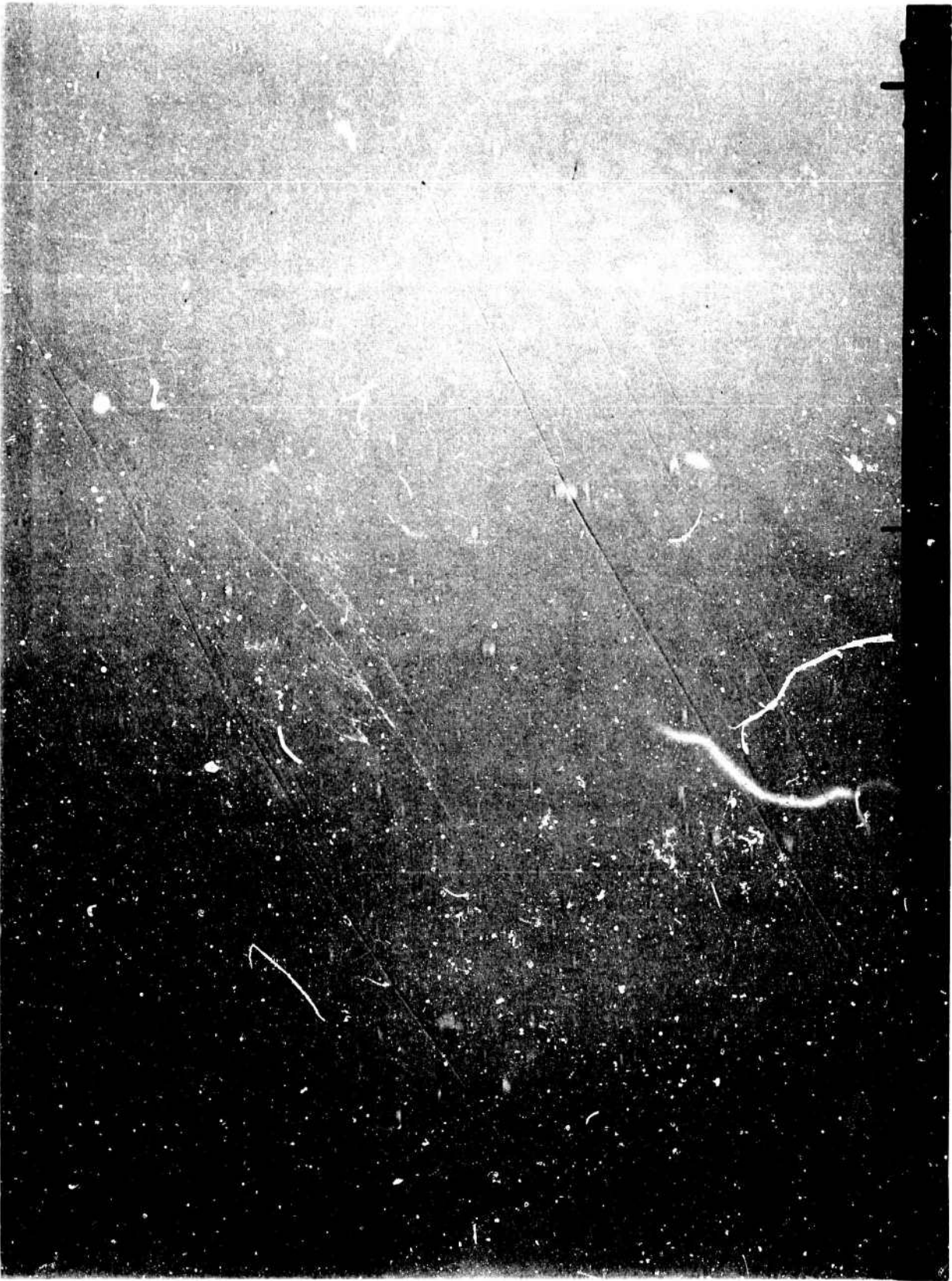
Figure B3 Shot 218 of group 415 -- 0.46 caliber bullet, M = 2.17, 4 inch nozzle, and open inlet.
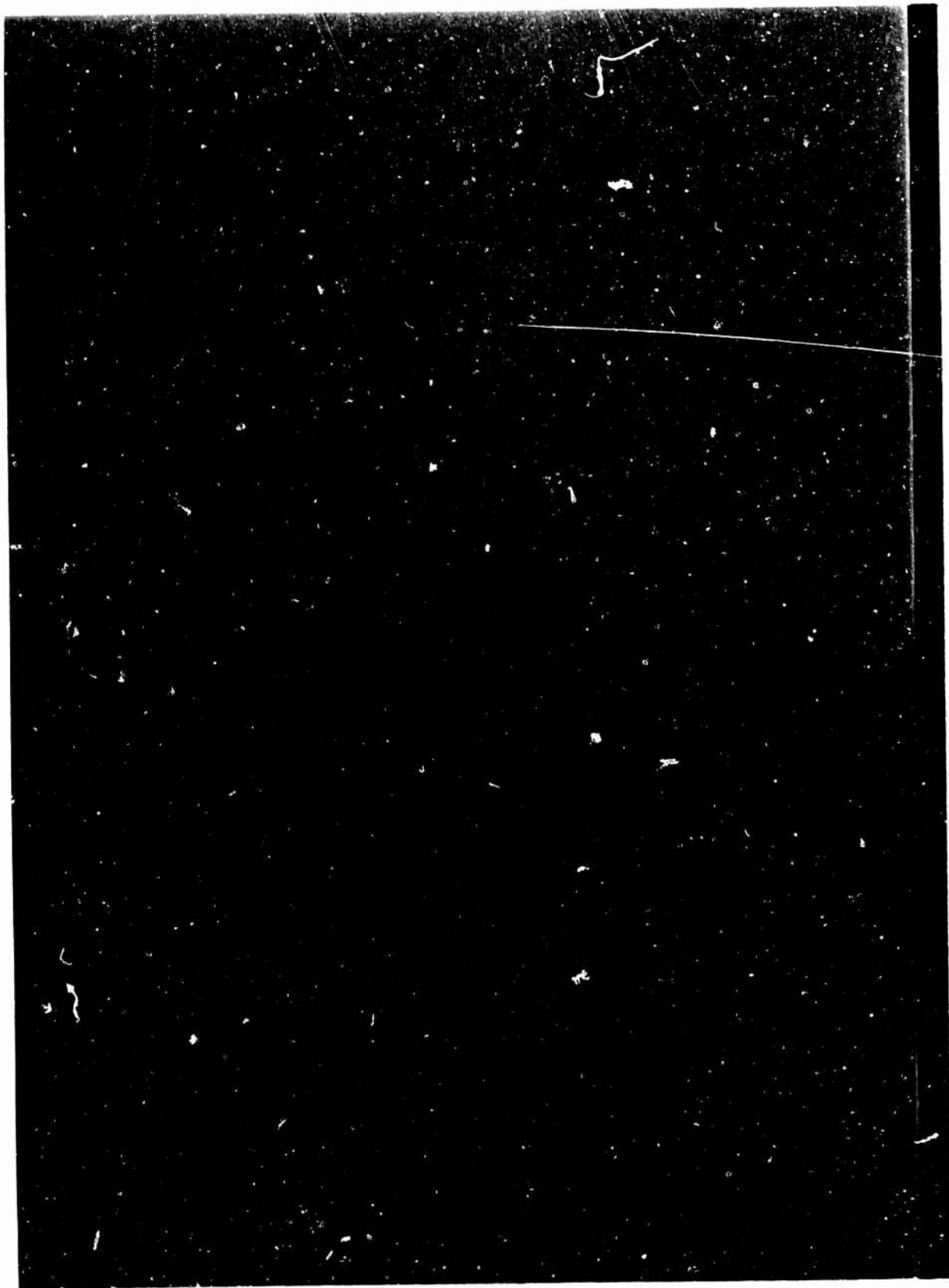
Figure 84   Shot 294 of group 222 -- B projectile, M = 2.56, 6 inch nozzle, and 16 inch inlet.

164
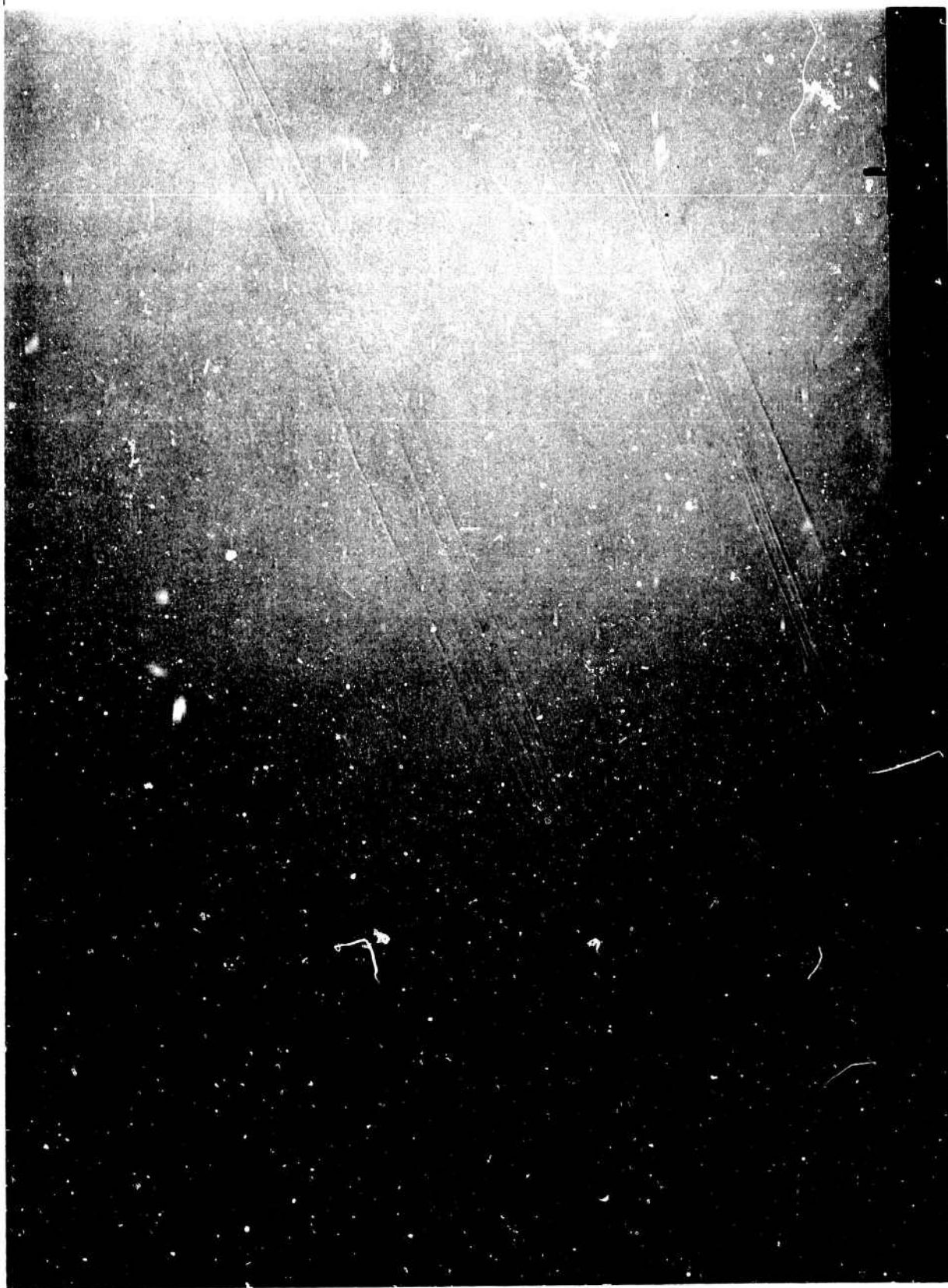
Figure B5 Shot 239 of group 224 -- B projectile, M = 2.55, 6 inch nozzle,
and 24 inch inlet.
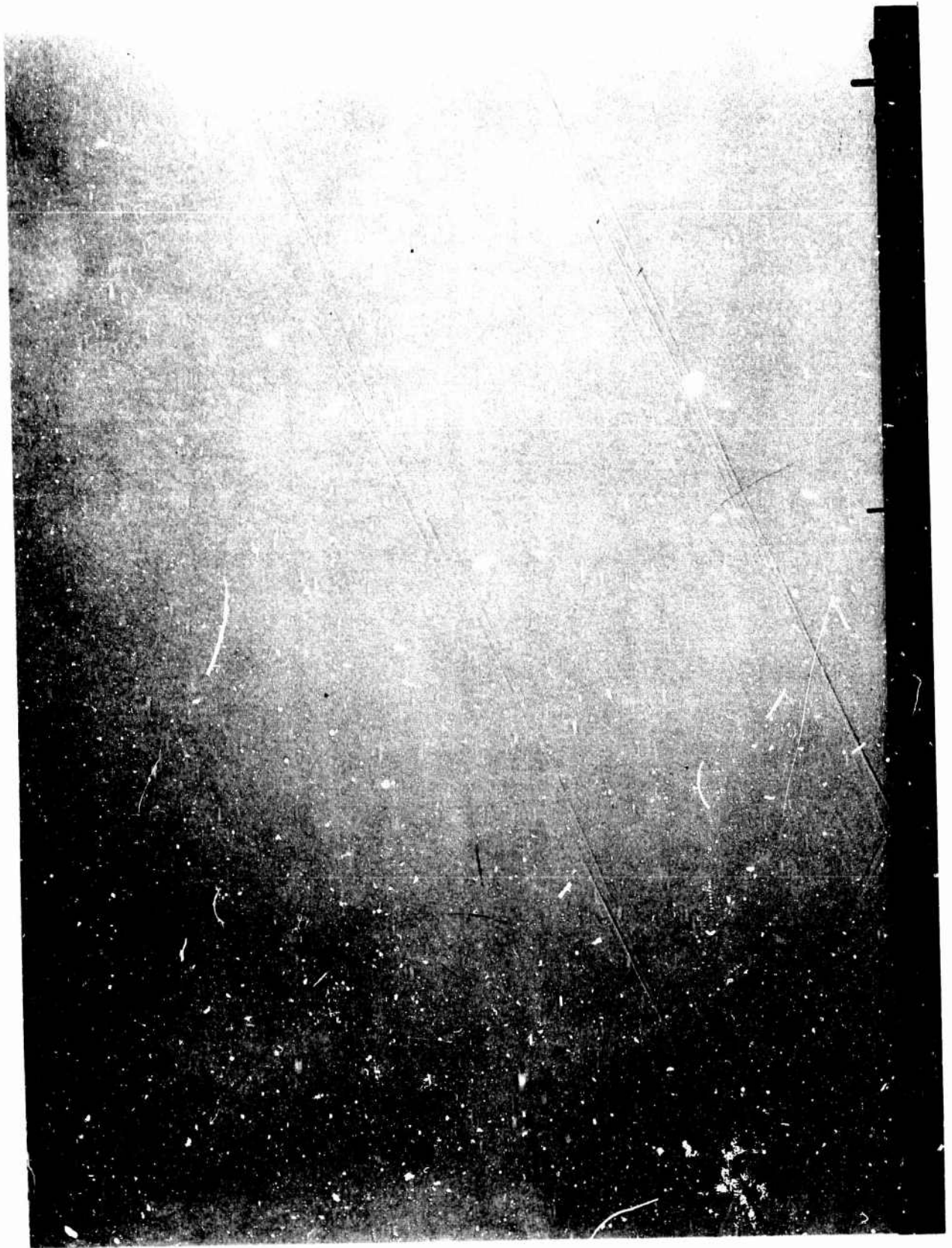
Figure B6   Shot 229 of group 232 -- B projectile, M = 2.54, 24 inch
nozzle, and 16 inch inlet.
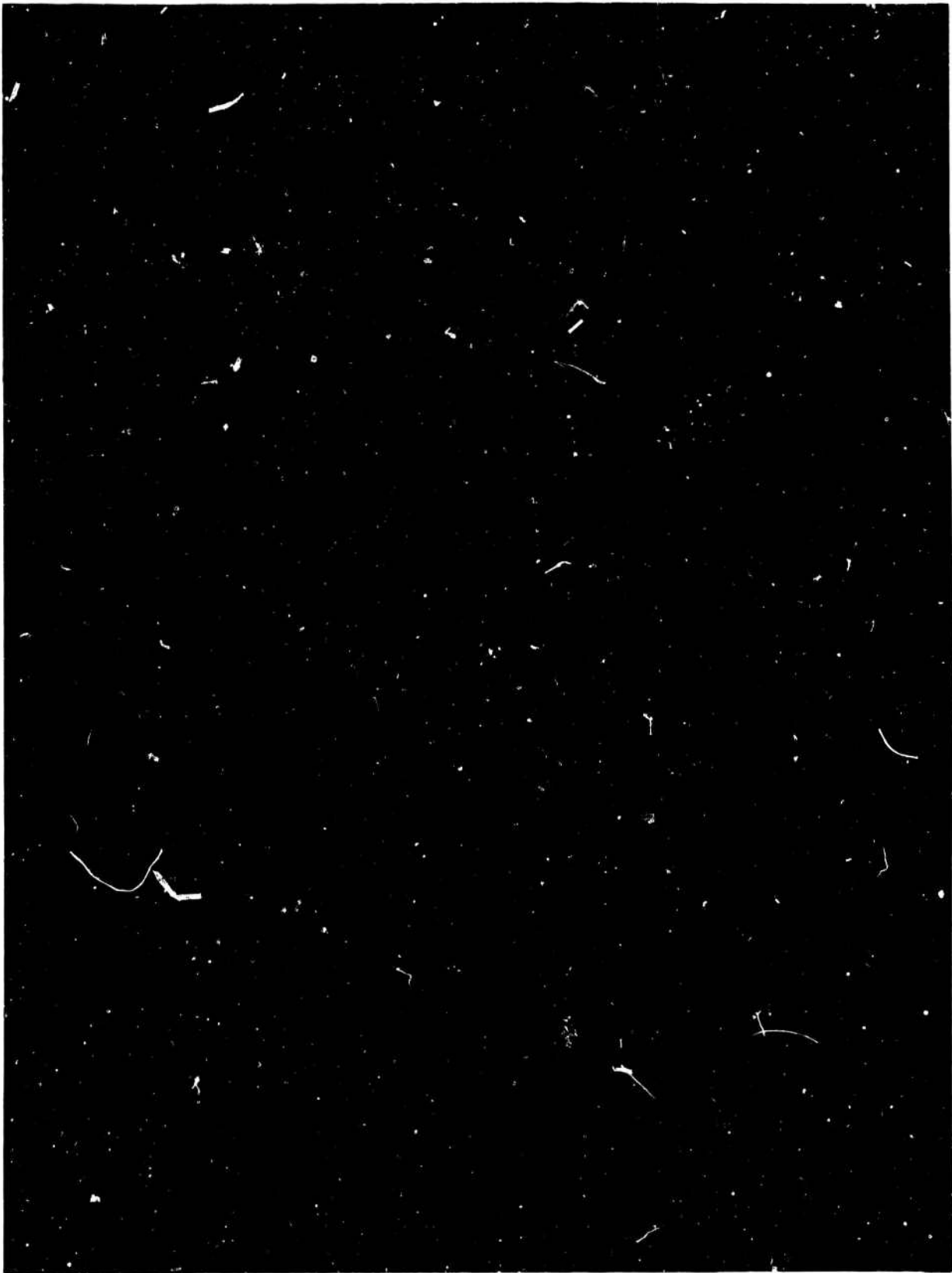
Figure B7   Shot 174 of group 234 -- B projectile, M = 2.55, 24 inch
nozzle, and 24 inch inlet.
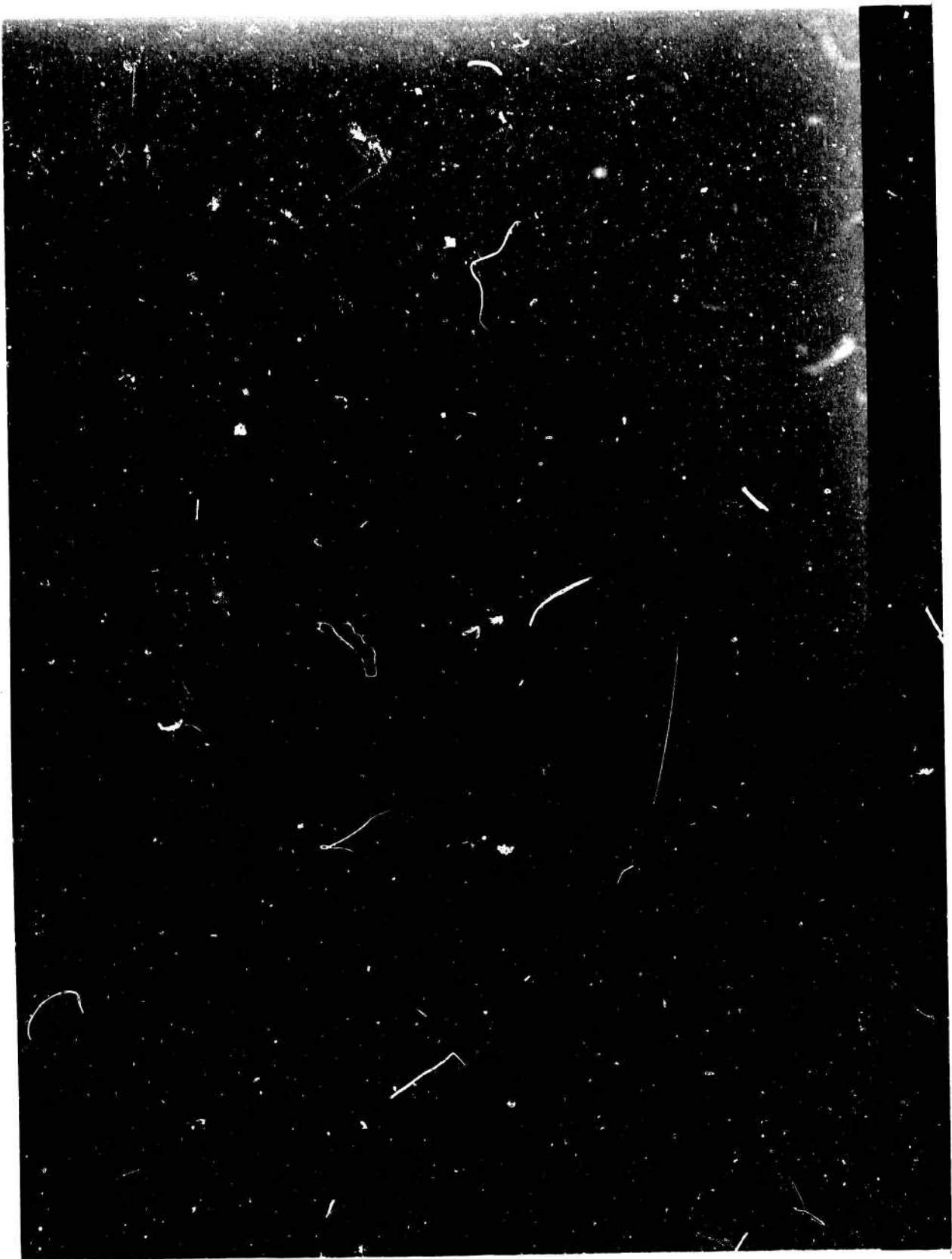
Figure B8   Shot 347 of group 314 -- 0.22 caliber bullet, M = 2.99, 4 inch
nozzle, and 24 inch inlet.
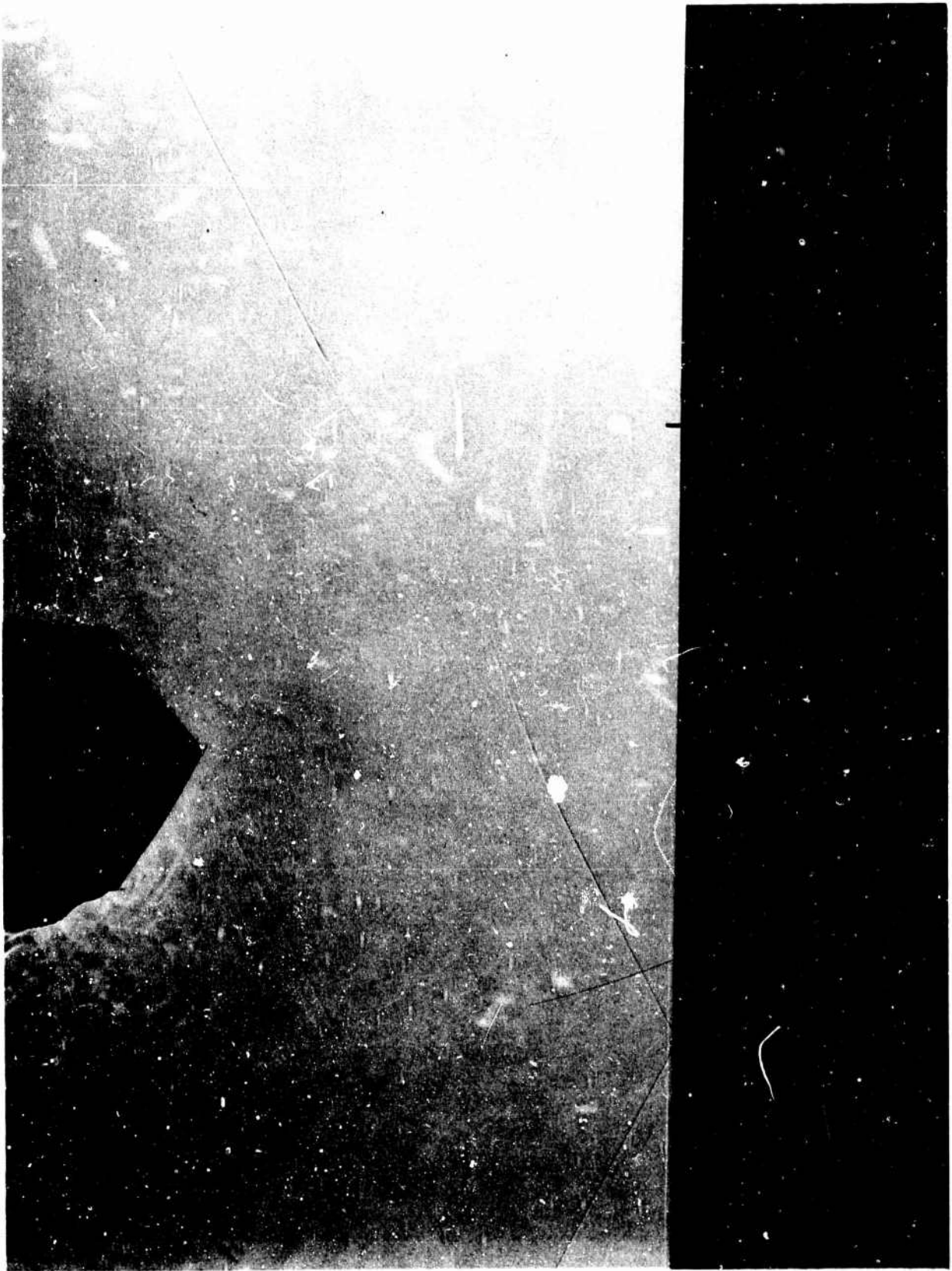
Figure B9   Shot 270 taken with a 0.46 caliber bullet and a thermal
generator located at x = 5.3 inches, y = 10.2 inches, and z = -20 inches.
M = 2.16.
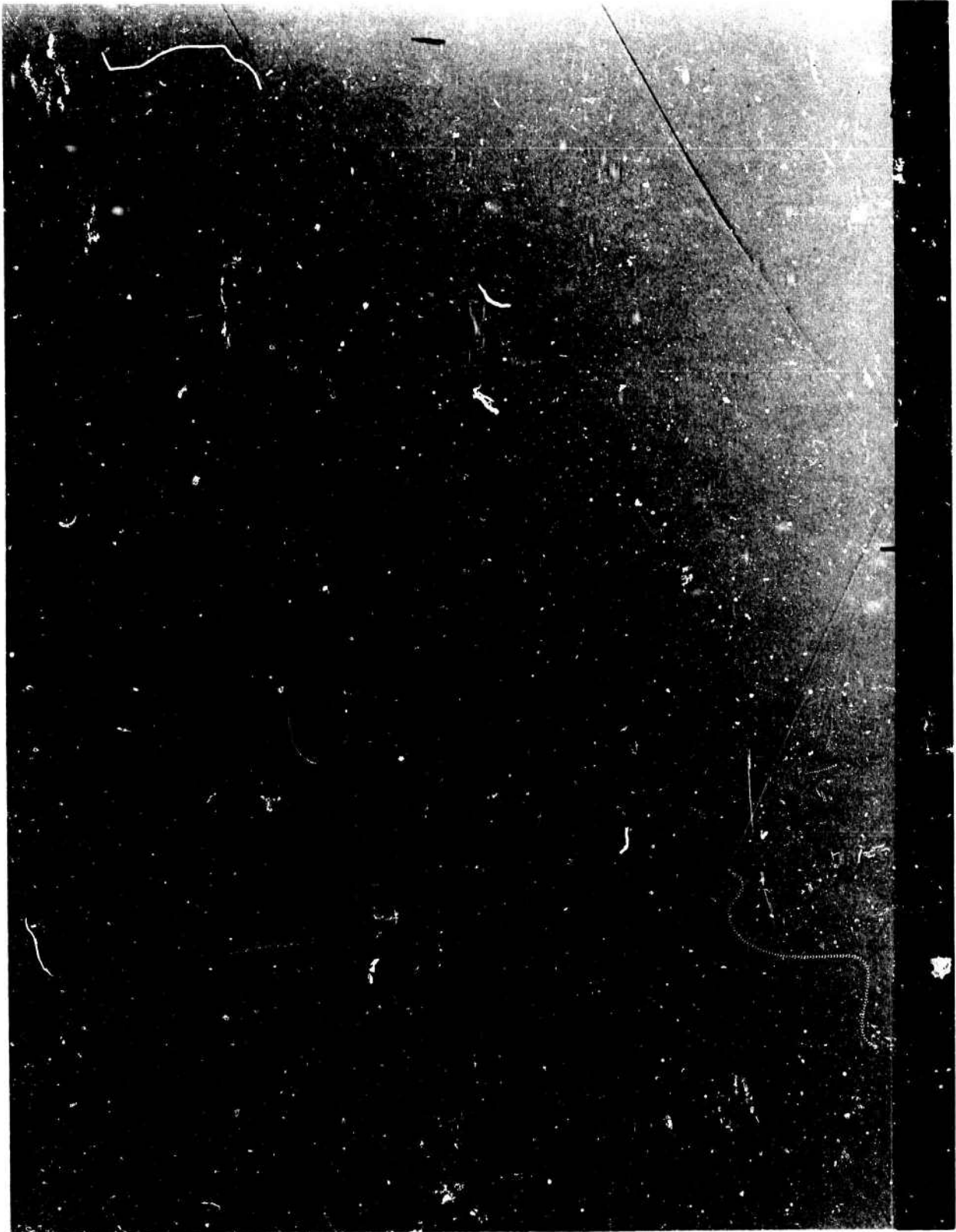
Figure B10 Shot 275 taken with a 0.46 caliber bullet and a thermal generator located at x = 9.05 inches, y = 17.3 inches, and z = -20 inches. M = 2.16.
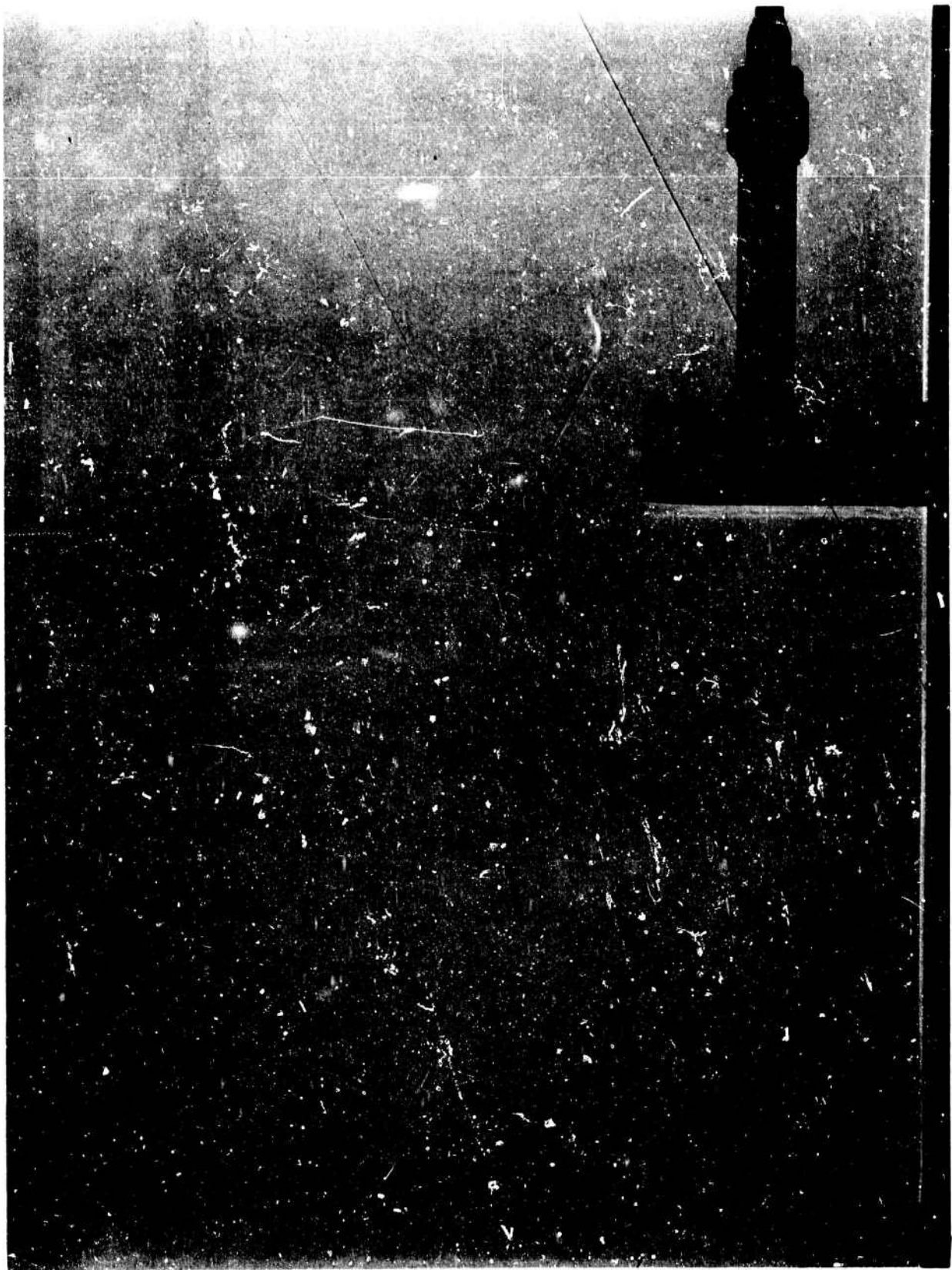
Figure B11 Step model and N waves from B projectile. M = 2.55.
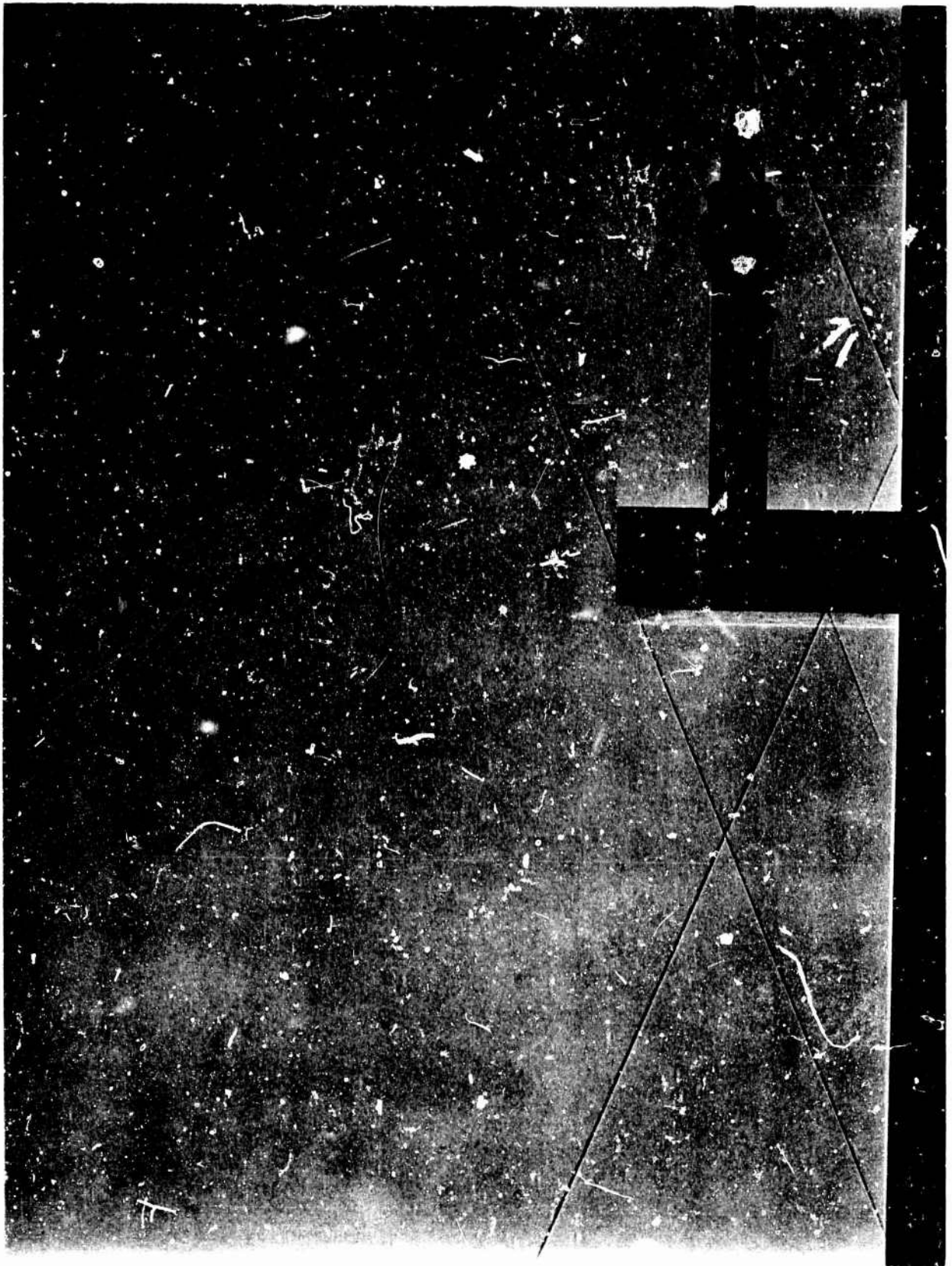
Figure B12   Step model and N waves from B projectile.   M = 2.55.
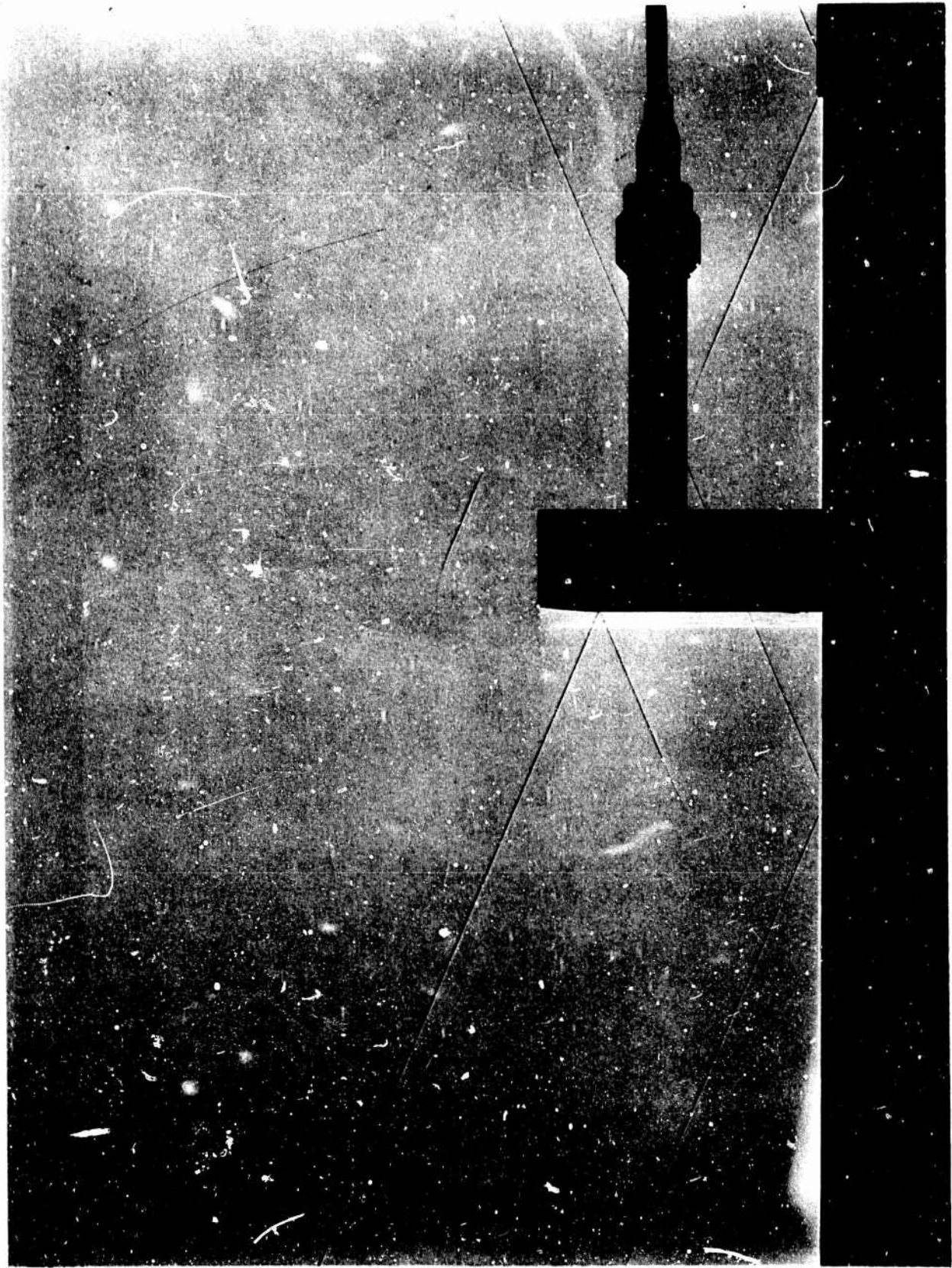
Figure B13 Step model and N waves from B projectile. M = 2.55.
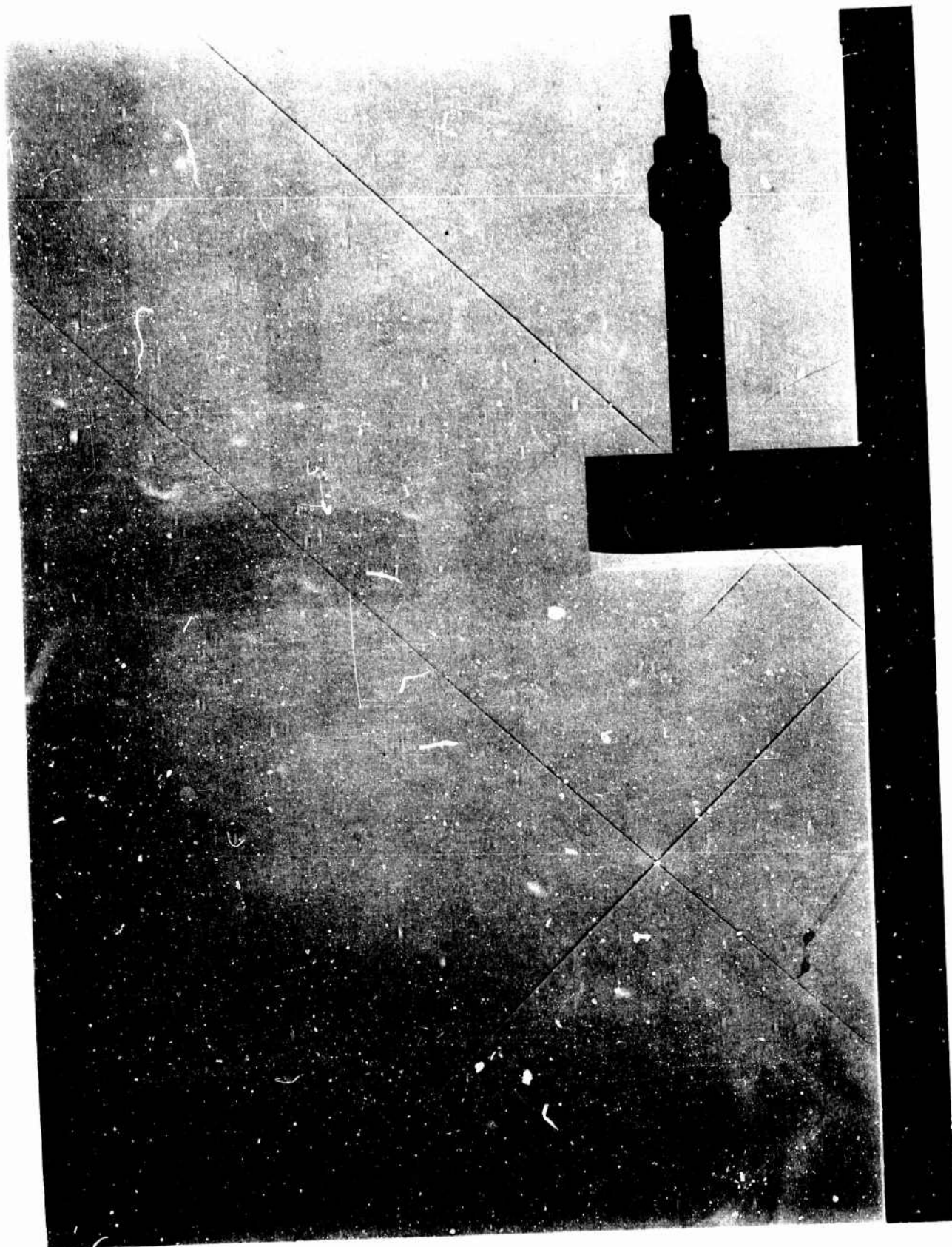
Figure B14 Step model and N waves from B projectile. M = 1.4.
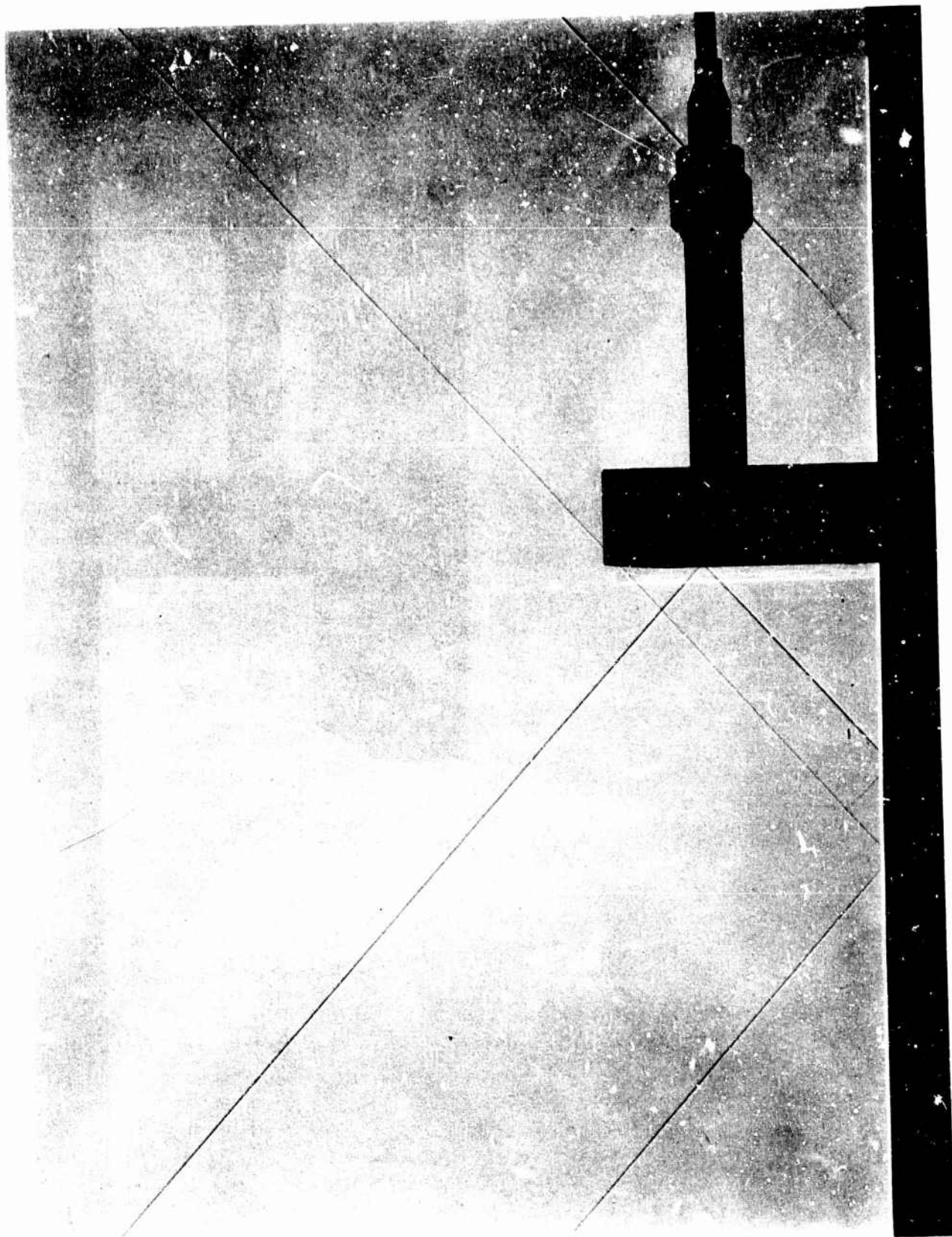
Figure B15 Step model and N waves from B projectile. M = 1.4.

175
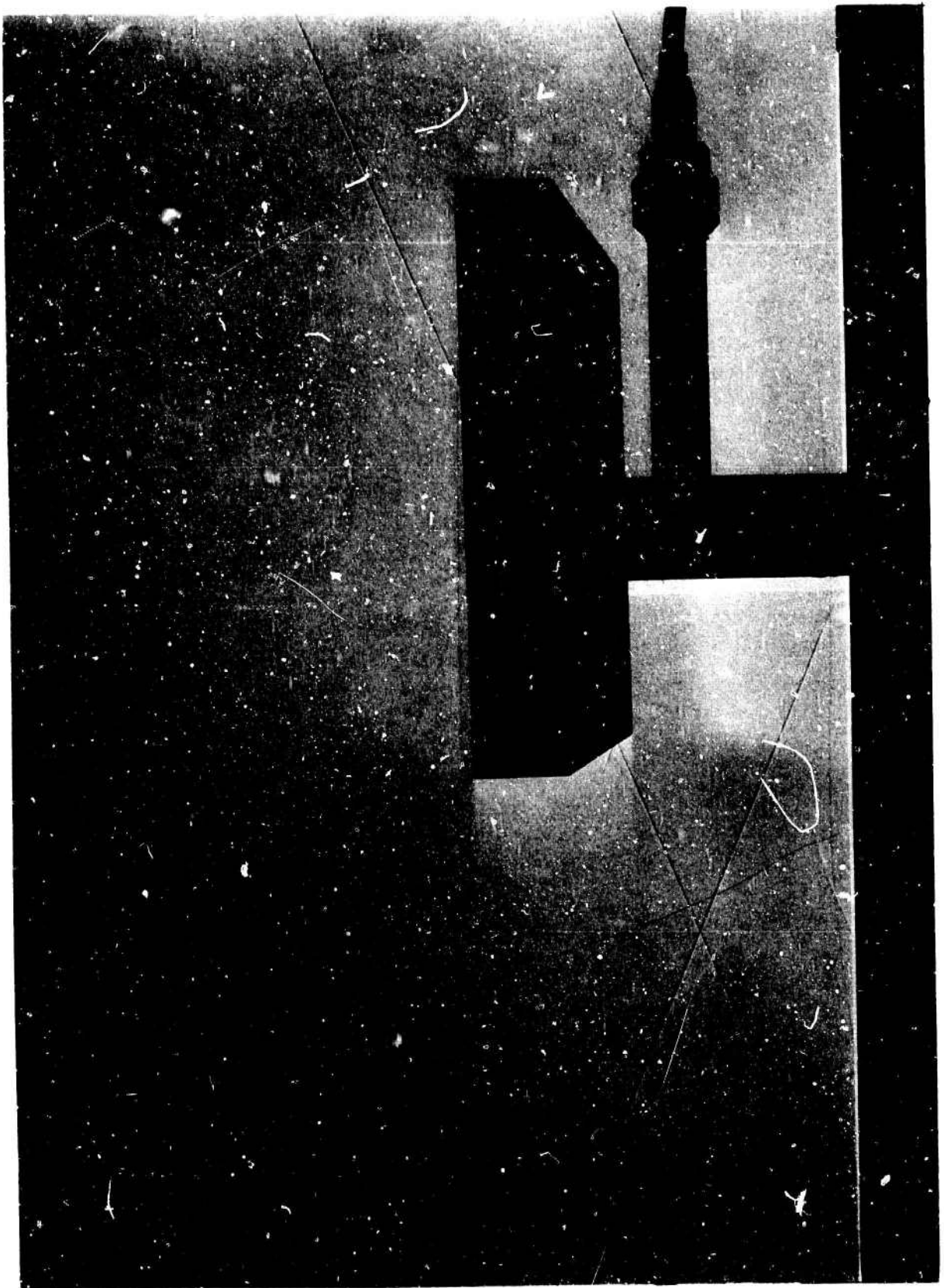
Figure B16   Two inch overhang model and N waves from B projectile.   M = 2.55

Figure B17 Two inch overhang model and N waves from B projectile. M = 2.55

Figure B18   Parallel wall model and N waves from B projectile.   M = 2.55.

178
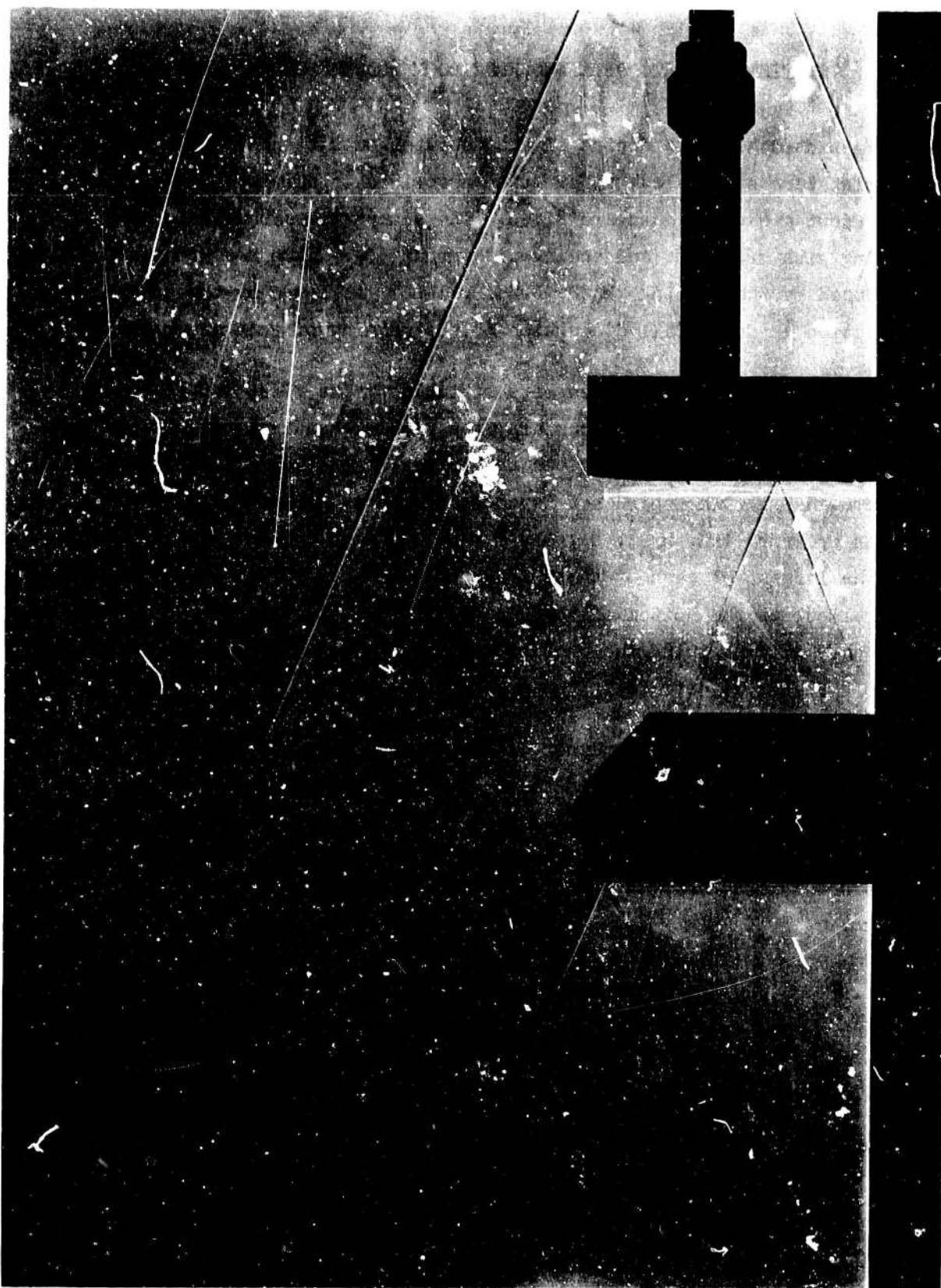
Figure B19 Parallel wall model and N waves from B projectile. M = 2.55

179

APPENDIX C

STATISTICAL DATA OBTAINED FROM BOOM AND TURBULENCE INTERACTIONS

Presented here are copies of the computer output sheets tabulating the boom signature statistical information described in section 6C. Nineteen independent groups of data are given. The groups are arranged in order starting with group 134 and ending with group 354. Each new group of data is introduced by the heading "MACH, NOZZLE, INLET" followed by the group number. See section 5C for a full discussion of the meaning of each group number.

Under each group are three sets of tables. The first set is arranged in the order of the listed shot numbers; the tabular headings are explained in section 6C. The second set gives the values of the correlation coefficients F_{12} through F_{45}. The third set is comprised of 14 columns. Seven of these columns are for TPK, H_{MAX}, H_1, H_2, H_3, H_4, and H_5 arranged in order running from the largest of each of these observed variables descending in order to the smallest at the bottom of the table. Next to each of these seven columns is another column giving the probability of exceeding each particular value of the variable as defined by equation (12) in section 6C.

In certain groups the number of shots was so large that several pages are required for the tabulation; in these cases the tabulation headings are given only at the beginning of the group tabulation; data on subsequent pages fall directly below the same headings.

MACH, NOZZLE, INLET =134

SHOT	T	TPK	PMAX	P1	P2	P3	P4	P5		HMAX	H1	H2	H3	H4	H5
176	1	3.0	1.19	0.40	0.95	0.76	0.58	0.15		1.253	-0.579	0.105	0.084	0.158	0.179
176	2	2.8	1.11	0.85	0.94	0.88	0.71	-0.08		1.261	-0.034	0.148	0.261	0.295	-0.136
177	1	0.5	1.08	1.06	0.83	0.84	0.67	0.10		1.137	0.116	-0.021	0.168	0.253	0.126
177	2	2.8	0.90	0.74	0.88	0.68	0.58	0.18		1.023	-0.159	0.080	0.034	0.148	0.159
178	1	1.0	0.87	0.80	0.76	0.52	0.51	0.21		0.916	-0.158	-0.095	-0.168	0.084	0.242
178	2	20.0	0.70	0.65	0.66	0.64	0.70	0.07		0.795	-0.261	-0.170	-0.011	0.284	0.034
179	1	1.0	0.96	0.90	0.69	0.63	0.55	0.16		1.011	-0.053	-0.168	-0.053	0.126	0.189
179	2	17.5	0.90	0.40	0.61	0.70	0.82	0.08		1.023	-0.545	-0.227	0.057	0.420	0.045
180	1	17.0	0.68	0.65	0.65	0.52	0.60	0.16		0.716	-0.316	-0.211	-0.168	0.179	0.189
180	2	6.0	0.91	0.75	0.89	0.69	0.46	0.16		1.034	-0.148	0.091	0.045	0.011	0.136
181	1	5.0	1.49	0.43	1.49	1.07	0.69	0.08		1.568	-0.547	0.674	0.411	0.274	0.105
181	2	8.5	0.96	0.32	0.65	0.95	0.75	0.04		1.091	-0.636	-0.182	0.341	0.341	0.0

HRMS = 1.090 0.365 0.241 0.195 0.242 0.146

F12	F13	F14	F15	F23	F24	F25	F34	F35	F45
-0.0841	-0.5137	-0.7961	-0.5159	0.5589	-0.0297	-0.0448	0.5965	-0.0732	0.4272

TPK	P(TPK)	HMAX	P(HMAX)	H1	P(H1)	H2	P(H2)	H3	P(H3)	H4	P(H4)	H5	P(H5)
20.0	0.042	1.568	0.042	0.116	0.042	0.674	0.042	0.411	0.042	0.420	0.042	0.242	0.042
17.5	0.125	1.261	0.125	-0.034	0.125	0.148	0.125	0.341	0.125	0.341	0.125	0.189	0.167
17.0	0.208	1.253	0.208	-0.053	0.208	0.105	0.208	0.261	0.208	0.295	0.208	0.189	0.167
8.5	0.292	1.137	0.292	-0.148	0.292	0.091	0.292	0.168	0.292	0.284	0.292	0.179	0.292
6.0	0.375	1.091	0.375	-0.158	0.375	0.080	0.375	0.084	0.375	0.274	0.375	0.159	0.375
5.0	0.458	1.034	0.458	-0.159	0.458	-0.021	0.458	0.057	0.458	0.253	0.458	0.136	0.458
3.0	0.542	1.023	0.583	-0.261	0.542	-0.095	0.542	0.045	0.542	0.179	0.542	0.126	0.542
2.8	0.667	1.023	0.583	-0.316	0.625	-0.168	0.625	0.034	0.625	0.158	0.625	0.105	0.625
2.8	0.667	1.011	0.708	-0.545	0.708	-0.170	0.708	-0.011	0.708	0.148	0.708	0.045	0.708
1.0	0.833	0.916	0.792	-0.547	0.792	-0.182	0.792	-0.053	0.792	0.126	0.792	0.034	0.792
1.0	0.833	0.795	0.875	-0.579	0.875	-0.211	0.875	-0.168	0.917	0.084	0.875	0.0	0.875
0.5	0.958	0.716	0.958	-0.636	0.958	-0.227	0.958	-0.168	0.917	0.011	0.958	-0.136	0.958

MACH, NOZZLE, INLET =212

SHOT	T	TPK	PMAX	P1	P2	P3	P4	P5		HMAX	H1	H2	H3	H4	H5
222	1	7.5	1.00	0.70	0.96	0.94	0.82	0.23		0.877	-0.386	-0.035	0.070	0.158	0.070
222	2	6.0	1.05	0.86	1.04	0.90	0.54	0.14		1.029	-0.157	0.118	0.108	-0.039	0.049
223	1	8.5	0.94	0.81	0.93	0.93	0.67	0.23		0.825	-0.289	-0.06	0.061	0.026	0.070
223	2	7.0	0.81	0.59	0.75	0.76	0.63	0.20		0.794	-0.422	-0.16	-0.029	0.049	0.108
224	1	0.0	1.52	1.52	1.17	0.84	0.71	0.12		1.333	0.333	0.149	-0.018	0.061	-0.026
224	2	0.0	1.09	1.09	0.90	0.77	0.63	0.19		1.069	0.069	-0.020	-0.020	0.049	0.098
225	1	0.5	1.23	1.20	1.04	0.97	0.70	0.20		1.079	0.053	0.035	0.096	0.053	0.044
225	2	0.0	0.93	0.93	0.88	0.80	0.52	0.08		0.912	-0.088	-0.039	0.010	-0.059	-0.010
226	1	1.2	1.44	1.20	1.22	0.92	0.70	0.18		1.263	0.053	0.193	0.053	0.073	0.026
226	2	0.0	1.13	1.13	0.92	0.85	0.71	0.11		1.108	0.108	0.0	0.059	0.127	0.020
227	1	1.0	1.14	1.00	0.98	0.87	0.68	0.20		1.000	-0.123	-0.018	0.009	0.035	0.044
227	2	0.0	1.15	1.15	0.92	0.72	0.56	0.08		1.127	0.127	0.0	-0.069	-0.020	-0.010

HRMS = 1.047 0.225 0.096 0.059 0.072 0.057

F12	F13	F14	F15	F23	F24	F25	F34	F35	F45
0.5781	-0.3311	-0.2132	-0.6639	0.3250	0.0236	-0.2833	0.4160	0.4321	0.5641

TPK	P(TPK)	HMAX	P(HMAX)	H1	P(H1)	H2	P(H2)	H3	P(H3)	H4	P(H4)	H5	P(H5)
8.5	0.042	1.333	0.042	0.333	0.042	0.193	0.042	0.108	0.042	0.158	0.042	0.108	0.042
7.5	0.125	1.263	0.125	0.127	0.125	0.149	0.125	0.096	0.125	0.127	0.125	0.098	0.125
7.0	0.208	1.127	0.208	0.108	0.208	0.118	0.208	0.070	0.208	0.061	0.208	0.070	0.250
6.0	0.292	1.108	0.292	0.069	0.292	0.035	0.292	0.061	0.292	0.053	0.333	0.070	0.250
1.2	0.375	1.079	0.375	0.053	0.417	0.0	0.417	0.059	0.375	0.053	0.333	0.049	0.375
1.0	0.458	1.069	0.458	0.053	0.417	0.0	0.417	0.053	0.458	0.049	0.500	0.044	0.500
0.5	0.542	1.029	0.542	-0.088	0.542	-0.018	0.542	0.010	0.542	0.049	0.500	0.044	0.500
0.0	0.792	1.000	0.625	-0.123	0.625	-0.020	0.625	0.009	0.525	0.035	0.625	0.026	0.625
0.0	0.792	0.912	0.708	-0.157	0.708	-0.035	0.708	-0.018	0.708	0.026	0.708	0.020	0.708
0.0	0.792	0.877	0.792	-0.289	0.792	-0.039	0.792	-0.020	0.792	-0.020	0.792	-0.010	0.833
0.0	0.792	0.825	0.875	-0.386	0.875	-0.061	0.875	-0.029	0.875	-0.039	0.875	-0.010	0.833
0.0	0.792	0.794	0.958	-0.422	0.958	-0.167	0.958	-0.069	0.958	-0.059	0.958	-0.026	0.958

181

MACH. NOZZLE. INLET =214

SHOT	T	TPK	FMAX	P1	P2	P3	P4	P5		HMAX	H1	H2	H3	H4	H5
190	1	1.2	1.41	1.24	1.14	0.80	0.61	0.12		1.237	0.088	0.123	-0.053	-0.026	-0.026
190	2	3.0	1.16	1.00	1.04	0.92	0.62	-0.01		1.137	-0.020	0.118	0.127	0.039	-0.098
191	1	1.2	1.42	1.20	0.94	0.84	0.55	0.09		1.246	0.053	-0.053	-0.018	-0.079	-0.053
191	2	12.0	0.80	0.74	0.68	0.72	0.71	0.16		0.784	-0.275	-0.235	-0.069	0.127	0.069
192	1	2.0	0.92	0.40	0.84	0.80	0.67	0.47		0.807	-0.298	-0.140	-0.053	0.026	0.281
192	2	5.0	0.83	0.80	0.82	0.57	0.53	0.24		0.814	-0.216	-0.098	-0.216	-0.049	0.147
193	1	7.0	1.02	0.76	0.90	0.90	0.92	0.30		0.895	-0.333	-0.088	0.035	0.246	0.132
193	2	3.5	1.04	0.38	0.97	0.60	0.56	0.21		1.020	-0.627	0.049	-0.186	-0.029	0.118
194	1	0.5	1.41	1.49	1.37	1.06	0.80	0.04		1.237	0.219	0.325	0.175	0.140	-0.096
194	2	3.0	1.17	0.73	0.96	0.81	0.68	0.21		1.147	-0.084	0.039	0.020	0.098	0.118
195	1	1.0	1.45	1.37	1.40	0.99	0.75	0.09		1.272	0.202	0.351	0.114	0.096	-0.053
195	2	2.0	1.35	0.60	1.07	0.75	0.52	0.20		1.324	-0.412	0.147	-0.039	-0.059	0.108
196	1	0.5	1.26	1.23	0.97	0.80	0.55	0.16		1.105	0.079	-0.026	-0.053	-0.079	0.009
196	2	2.0	1.02	0.91	0.93	0.72	0.62	0.20		1.000	-0.108	0.010	-0.069	0.039	0.108
197	1	0.0	1.30	1.30	1.03	0.80	0.70	0.26		1.140	0.140	0.026	-0.053	0.053	0.096
197	2	6.0	1.10	0.83	1.00	0.93	0.63	0.08		1.078	-0.186	0.078	0.137	0.049	-0.010
198	1	9.5	1.14	0.40	1.05	1.13	0.70	0.21		1.000	-0.649	0.044	0.237	0.053	0.053
198	2	0.0	0.89	0.89	0.80	0.78	0.56	0.09		0.873	-0.127	-0.118	-0.010	-0.020	0.0
199	1	6.5	1.02	0.71	0.99	0.85	0.65	0.25		0.895	-0.377	-0.009	-0.009	0.009	0.088
199	2	0.0	1.14	1.14	0.87	0.70	0.53	0.04		1.118	0.118	-0.049	-0.088	-0.049	-0.049
200	1	1.0	2.03	1.87	1.38	0.80	0.65	0.0		1.781	0.640	0.333	-0.053	0.009	-0.132
200	2	5.5	0.86	0.68	0.85	0.76	0.63	0.14		0.843	-0.333	-0.069	-0.029	0.049	0.049
201	1	1.0	1.30	1.21	0.91	0.90	0.78	0.12		1.140	0.061	-0.079	0.035	0.123	-0.026
201	2	14.0	0.98	0.90	0.92	0.86	0.82	0.22		0.961	-0.118	0.0	0.069	0.235	0.127

HRMS = 1.098   0.308   0.148   0.104   0.096   0.104

F12	F13	F14	F15	F23	F24	F25	F34	F35	F45
0.3693	0.0407	-0.2060	-0.7200	0.3847	0.0973	-0.4229	0.4231	-0.3435	0.2868

TPK	P(TPK)	HMAX	P(HMAX)	H1	P(H1)	H2	P(H2)	H3	P(H3)	H4	P(H4)	H5	P(H5)
14.0	0.021	1.781	0.021	0.640	0.021	0.351	0.021	0.237	0.021	0.246	0.021	0.281	0.021
12.0	0.063	1.324	0.063	0.219	0.063	0.333	0.063	0.175	0.063	0.235	0.063	0.147	0.063
9.5	0.104	1.272	0.104	0.202	0.104	0.325	0.104	0.137	0.104	0.140	0.104	0.132	0.104
7.0	0.146	1.246	0.146	0.140	0.146	0.147	0.146	0.127	0.146	0.127	0.146	0.127	0.146
6.5	0.188	1.237	0.208	0.118	0.188	0.123	0.188	0.114	0.188	0.123	0.188	0.118	0.208
6.0	0.229	1.237	0.208	0.088	0.229	0.119	0.229	0.069	0.229	0.098	0.229	0.118	0.208
5.5	0.271	1.147	0.271	0.071	0.271	0.078	0.271	0.035	0.292	0.096	0.271	0.108	0.292
5.0	0.313	1.140	0.333	0.061	0.313	0.049	0.313	0.035	0.292	0.053	0.333	0.108	0.292
3.5	0.354	1.140	0.333	0.053	0.354	0.044	0.354	0.020	0.354	0.053	0.333	0.096	0.354
3.0	0.417	1.137	0.396	-0.020	0.396	0.039	0.396	-0.009	0.396	0.049	0.417	0.088	0.396
3.0	0.417	1.118	0.438	-0.108	0.438	0.026	0.438	-0.010	0.438	0.049	0.417	0.069	0.438
2.0	0.521	1.105	0.479	-0.118	0.479	0.010	0.479	-0.018	0.479	0.039	0.500	0.053	0.479
2.0	0.521	1.078	0.521	-0.127	0.521	0.0	0.521	-0.029	0.521	0.039	0.500	0.049	0.521
2.0	0.521	1.020	0.563	-0.186	0.563	-0.009	0.563	-0.039	0.563	0.026	0.563	0.009	0.563
1.2	0.625	1.000	0.625	-0.216	0.604	-0.026	0.604	-0.053	0.688	0.009	0.625	0.0	0.604
1.2	0.625	1.000	0.625	-0.275	0.646	-0.049	0.646	-0.053	0.688	0.009	0.625	-0.010	0.646
1.0	0.729	0.961	0.688	-0.284	0.688	-0.053	0.688	-0.053	0.688	-0.020	0.708	-0.026	0.708
1.0	0.729	0.895	0.750	-0.298	0.729	-0.069	0.729	-0.053	0.688	-0.020	0.708	-0.026	0.708
1.0	0.729	0.895	0.750	-0.333	0.771	-0.079	0.771	-0.053	0.688	-0.026	0.771	-0.049	0.771
0.5	0.833	0.873	0.813	-0.333	0.813	-0.088	0.813	-0.069	0.853	-0.049	0.833	-0.053	0.833
0.5	0.833	0.843	0.854	-0.377	0.854	-0.098	0.854	-0.069	0.833	-0.049	0.833	-0.053	0.833
0.0	0.938	0.914	0.896	-0.412	0.896	-0.118	0.896	-0.088	0.896	-0.059	0.896	-0.096	0.896
0.0	0.938	0.807	0.938	-0.627	0.938	-0.140	0.938	-0.186	0.938	-0.079	0.958	-0.098	0.938
0.0	0.938	0.784	0.979	-0.649	0.979	-0.235	0.979	-0.216	0.979	-0.079	0.958	-0.132	0.979

MACH, NOZZLE, INLET =215

SHOT	T	TPK	PMAX	P1	P2	P3	P4	P5	HMAX	H1	H2	H3	H4	H5
211	1	6.0	1.35	1.25	1.34	0.74	0.67	0.25	1.184	0.176	0.298	-0.105	0.026	0.088
211	2	0.0	0.76	0.76	0.68	0.66	0.47	0.25	0.745	-0.255	-0.235	-0.127	-0.108	0.157
212	1	1.6	1.67	1.20	1.38	0.90	0.71	0.20	1.465	0.053	0.333	0.035	0.051	0.044
212	2	0.0	0.94	0.94	0.82	0.90	0.65	0.15	0.922	-0.078	-0.098	0.108	5.069	0.059
213	1	1.0	1.95	1.90	1.31	0.91	0.70	0.04	1.711	0.667	0.272	0.044	0.053	-0.096
213	2	17.5	1.19	0.61	0.71	0.91	1.00	0.20	1.167	-0.402	-0.206	0.118	0.412	0.108
219	1	4.5	0.92	0.63	0.91	0.63	0.68	0.60	0.807	-0.447	-0.079	-0.202	0.035	0.395
219	2	6.5	0.86	0.73	0.79	0.80	0.53	0.23	0.843	-0.284	-0.127	0.010	-0.049	0.137
220	1	0.5	1.00	0.97	0.90	1.00	0.70	0.22	0.877	-0.149	-0.088	0.123	0.053	0.061
220	2	5.5	1.05	0.34	1.04	0.77	0.49	0.17	1.029	-0.667	0.118	-0.020	-0.088	0.078
221	1	1.2	1.48	1.30	1.00	0.70	0.46	0.23	1.298	0.140	0.0	-0.140	-0.158	0.070
221	2	0.5	1.02	1.00	0.83	0.67	0.49	0.11	1.000	-0.020	-0.088	-0.118	-0.088	0.020

HRMS = 1.122 0.348 0.190 0.110 0.141 0.144

F12	F13	F14	F15	F23	F24	F25	F34	F35	F45
0.4858	0.1356	-0.1247	-0.6799	-0.0024	-0.0845	-0.2953	0.5585	-0.5114	0.0904

TPK	P(TPK)	HMAX	P(HMAX)	H1	P(H1)	H2	P(H2)	H3	P(H3)	H4	P(H4)	H5	P(H5)
17.5	0.042	1.711	0.042	0.667	0.042	0.333	0.042	0.123	0.042	0.412	0.042	0.395	0.042
6.5	0.125	1.465	0.125	0.140	0.125	0.298	0.125	0.118	0.125	0.069	0.125	0.157	0.125
6.0	0.208	1.298	0.208	0.096	0.208	0.272	0.208	0.108	0.208	0.061	0.208	0.137	0.208
5.5	0.292	1.184	0.292	0.053	0.292	0.118	0.292	0.044	0.292	0.053	0.333	0.108	0.292
4.5	0.375	1.167	0.375	-0.020	0.375	0.0	0.375	0.035	0.375	0.053	0.333	0.088	0.375
1.6	0.458	1.029	0.45	-0.078	0.458	-0.079	0.458	0.010	0.458	0.035	0.458	0.078	0.458
1.2	0.542	1.000	0.542	-0.149	0.542	-0.088	0.542	-0.020	0.542	0.026	0.542	0.070	0.542
1.0	0.625	0.922	0.625	-0.255	0.625	-0.088	0.625	-0.105	0.625	-0.049	0.625	0.061	0.625
0.5	0.750	0.877	0.708	-0.284	0.708	-0.098	0.708	-0.118	0.708	-0.088	0.750	0.059	0.708
0.5	0.750	0.843	0.792	-0.402	0.792	-0.127	0.792	-0.127	0.792	-0.088	0.750	0.044	0.792
0.0	0.917	0.807	0.875	-0.447	0.875	-0.206	0.875	-0.140	0.875	-0.108	0.875	0.020	0.875
0.0	0.917	0.745	0.958	-0.667	0.958	-0.235	0.958	-0.202	0.958	-0.158	0.958	-0.096	0.958

MACH, NOZZLE, INLET =222

SHOT	T	TPK	PMAX	P1	P2	P3	P4	P5	HMAX	H1	H2	H3	H4	H5
294	1	7.0	1.11	0.90	1.02	0.97	0.66	0.22	0.974	-0.211	0.018	0.096	0.018	0.061
294	2	3.2	0.90	0.55	0.86	0.82	0.66	0.09	0.882	-0.461	-0.059	0.029	0.078	0.0
295	1	6.5	1.16	0.60	1.14	1.07	0.79	0.18	1.018	-0.474	0.123	0.184	0.132	0.026
295	2	2.5	0.88	0.68	0.87	0.81	0.62	0.14	0.863	-0.333	-0.049	0.020	0.039	0.049
296	1	2.5	1.00	0.88	0.95	0.94	0.72	0.20	0.877	-0.228	-0.044	0.070	0.070	0.044
296	2	6.5	0.82	0.58	0.80	0.74	0.62	0.16	0.804	-0.431	-0.118	-0.049	0.039	0.069
297	1	1.0	1.15	1.00	1.10	0.89	0.70	0.11	1.009	-0.123	0.088	0.026	0.053	-0.035
297	2	2.5	0.95	0.80	0.94	0.79	0.73	0.03	0.931	-0.216	-0.020	0.0	0.147	-0.059
298	1	6.5	1.19	0.72	1.10	1.01	0.83	0.20	1.044	-0.368	0.088	0.132	0.167	0.044
298	2	6.0	0.92	0.82	0.90	0.82	0.66	0.11	0.902	-0.196	-0.020	0.029	0.078	0.020
299	1	0.7	1.40	1.30	1.23	1.00	0.70	0.06	1.228	0.140	0.202	0.123	0.053	-0.079
299	2	7.0	0.86	0.54	0.85	0.80	0.58	0.13	0.843	-0.471	-0.069	0.010	0.0	0.039

HRMS = 0.954 0.330 0.091 0.085 0.088 0.049

F12	F13	F14	F15	F23	F24	F25	F34	F35	F45
0.1657	-0.4996	-0.7340	-0.5924	0.6705	0.3495	-0.5205	0.7177	0.1535	0.1254

TPK	P(TPK)	HMAX	P(HMAX)	H1	P(H1)	H2	P(H2)	H3	P(H3)	H4	P(H4)	H5	P(H5)
7.0	0.083	1.228	0.042	0.140	0.042	0.202	0.042	0.184	0.042	0.167	0.042	0.069	0.042
7.0	0.083	1.044	0.125	-0.123	0.125	0.123	0.125	0.132	0.125	0.147	0.125	0.061	0.125
6.5	0.292	1.018	0.208	-0.196	0.208	0.088	0.250	0.123	0.208	0.132	0.208	0.049	0.208
6.5	0.292	1.009	0.292	-0.211	0.292	0.088	0.250	0.096	0.292	0.078	0.333	0.044	0.333
6.5	0.292	0.974	0.375	-0.216	0.375	0.020	0.375	0.070	0.375	0.078	0.333	0.044	0.333
6.0	0.458	0.931	0.458	-0.228	0.458	0.018	0.458	0.029	0.500	0.070	0.458	0.039	0.458
3.2	0.542	0.902	0.542	-0.333	0.542	-0.020	0.542	0.029	0.500	0.053	0.583	0.026	0.542
2.5	0.708	0.882	0.625	-0.368	0.625	-0.044	0.625	0.026	0.625	0.053	0.583	0.020	0.625
2.5	0.708	0.877	0.708	-0.431	0.708	-0.049	0.708	0.020	0.708	0.039	0.750	0.0	0.708
2.5	0.708	0.863	0.792	-0.461	0.792	-0.059	0.792	0.010	0.792	0.059	0.750	-0.035	0.792
1.0	0.875	0.843	0.875	-0.471	0.875	-0.069	0.875	0.0	0.875	0.018	0.875	-0.059	0.875
0.7	0.958	0.804	0.958	-0.474	0.958	-0.118	0.958	-0.049	0.958	0.0	0.958	-0.079	0.958

MACH, NOZZLE, INLET =224

SHOT	T	TPK	PMAX	P1	P2	P3	P4	P5	HMAX	H1	H2	H3	H4	H5
235	1	0.5	1.25	1.19	0.99	1.05	0.79	0.19	1.096	0.044	-0.009	0.167	0.132	0.035
235	2	3.0	0.95	0.78	0.89	0.93	0.57	0.08	0.931	-0.235	-0.029	0.137	-0.010	-0.010
236	1	1.2	0.93	0.80	0.74	0.75	0.75	0.31	0.816	-0.298	-0.278	-0.096	0.096	0.140
236	2	5.0	0.95	0.57	0.95	0.92	0.51	0.06	0.931	-0.441	0.029	0.127	0.029	-0.029
237	1	1.9	1.16	1.05	1.00	1.05	0.31	0.12	1.016	-0.079	0.0	0.167	0.149	-0.026
237	2	7.5	0.86	0.65	0.78	0.82	0.59	0.17	0.843	-0.363	-0.137	0.029	0.010	0.078
238	1	0.0	1.15	1.15	0.61	0.75	0.70	0.16	1.009	0.009	-0.167	-0.096	0.053	0.009
238	2	0.5	0.74	0.72	0.67	0.63	0.54	0.20	0.725	-0.294	-0.245	-0.157	-0.039	0.108
239	1	13.5	0.92	0.75	.77	0.80	0.75	0.23	0.807	-0.342	-0.202	-0.053	0.096	0.070
239	2	6.0	0.86	0.72	0.85	0.71	0.59	0.15	0.843	-0.294	-0.069	-0.078	0.010	0.059
240	1	11.5	1.28	0.90	0.86	1.25	0.84	0.25	1.123	-0.649	-0.123	0.342	0.175	0.088
240	2	6.5	0.86	0.84	0.84	0.74	0.69	0.11	0.843	-0.176	-0.078	-0.049	0.108	0.020
282	1	1.0	0.75	0.71	0.64	0.72	0.68	0.24	0.658	-0.377	-0.316	-0.123	0.035	0.079
282	2	12.0	0.86	0.52	0.71	0.84	0.65	0.11	0.843	-0.490	-0.206	0.049	0.069	0.020
283	1	10.0	0.94	0.64	0.80	0.94	0.76	0.36	0.825	-0.439	-0.175	0.070	0.105	0.184
283	2	6.0	0.78	0.56	0.75	0.75	0.66	0.19	0.765	-0.451	-0.167	-0.039	0.078	0.098
284	1	12.0	1.09	0.80	0.92	1.00	0.81	0.17	0.956	-0.298	-0.070	0.123	0.149	0.018
284	2	11.5	0.86	0.70	0.79	0.84	0.69	0.06	0.843	-0.314	-0.127	0.049	0.108	-0.029
285	1	1.1	1.12	1.00	1.04	0.95	0.84	0.18	0.982	-0.123	0.061	0.079	0.175	0.026
285	2	13.0	0.70	0.54	0.59	0.68	0.60	0.22	0.686	-0.471	-0.324	-0.108	.020	0.127
286	1	17.5	1.04	0.70	0.88	0.82	0.93	0.31	0.912	-0.386	-0.105	-0.035	0.254	0.140
286	2	6.5	1.02	0.80	0.90	0.93	0.64	0.08	1.000	-0.216	-0.020	0.137	0.059	-0.010
287	1	5.0	1.13	0.60	1.13	1.06	0.74	0.21	0.991	-0.474	0.114	0.175	0.088	0.053
287	2	0.7	0.91	0.87	0.78	0.85	0.54	0.10	0.892	-0.147	-0.137	0.059	-0.039	0.010

HRMS = 0.897 0.345 0.158 0.125 0.106 0.078

F12	F13	F14	F15	F23	F24	F25	F34	F35	F45
0.7268	-0.3012	-0.6687	-0.7480	0.2298	-0.4004	-0.7607	0.4409	-0.0803	0.5610

TPK	P(TPK)	HMAX	P(HMAX)	H1	P(H1)	H2	P(H2)	H3	P(H3)	H4	P(H4)	H5	P(H5)
17.5	0.021	1.123	0.021	0.044	0.021	0.114	0.021	0.342	0.021	0.254	0.021	0.184	0.021
13.5	0.063	1.096	0.063	0.009	0.063	0.061	0.063	0.175	0.063	0.175	0.083	0.140	0.083
13.0	0.104	1.018	0.104	-0.079	0.104	0.029	0.104	0.167	0.125	0.175	0.083	0.140	0.083
12.0	0.146	1.009	0.146	-0.123	0.145	0.0	0.146	0.167	0.125	0.149	0.167	0.127	0.146
12.0	0.167	1.000	0.188	-0.147	0.188	-0.009	0.188	0.137	0.208	0.149	0.167	0.108	0.188
11.5	0.250	0.991	0.229	-0.176	0.229	-0.020	0.229	0.137	0.208	0.132	0.229	0.098	0.229
11.5	0.250	0.982	0.271	-0.216	0.271	-0.029	0.271	0.127	0.271	0.108	0.292	0.086	0.271
10.0	0.313	0.956	0.313	-0.235	0.313	-0.069	0.313	0.123	0.313	0.108	0.292	0.079	0.313
7.5	0.354	0.931	0.375	-0.294	0.375	-0.070	0.354	0.079	0.354	0.105	0.354	0.078	0.354
6.5	0.417	0.931	0.375	-0.294	0.375	-0.078	0.396	0.070	0.396	0.096	0.417	0.070	0.396
6.5	0.417	0.912	0.438	-0.293	0.458	-0.105	0.438	0.059	0.438	0.096	0.417	0.059	0.438
6.0	0.500	0.892	0.479	-0.298	0.458	-0.123	0.479	0.049	0.500	0.088	0.479	0.053	0.479
6.0	0.500	0.843	0.604	-0.314	0.521	-0.127	0.521	0.049	0.500	0.078	0.521	0.035	0.521
5.0	0.583	0.843	0.604	-0.342	0.563	-0.137	0.583	0.029	0.563	0.069	0.563	0.026	0.563
5.0	0.583	0.843	0.604	-0.363	0.604	-0.137	0.583	-0.035	0.604	0.059	0.604	0.020	0.625
3.0	0.646	0.843	0.604	-0.377	0.646	-0.157	0.646	-0.039	0.646	0.053	0.646	0.020	0.625
1.9	0.688	0.843	0.688	-0.386	0.688	-0.177	0.688	-0.049	0.688	0.035	0.688	0.018	0.688
1.2	0.729	0.825	0.729	-0.439	0.729	-0.205	0.729	-0.053	0.729	0.029	0.729	0.010	0.729
1.1	0.771	0.816	0.771	-0.441	0.771	-0.202	0.771	-0.078	0.771	0.020	0.771	0.009	0.771
1.0	0.813	0.807	0.813	-0.451	0.813	-0.206	0.813	-0.096	0.833	0.010	0.833	-0.010	0.833
0.7	0.854	0.765	0.854	-0.471	0.854	-0.228	0.854	-0.096	0.833	0.010	0.833	-0.010	0.833
0.5	0.917	0.725	0.896	-0.474	0.896	-0.245	0.896	-0.108	0.896	-0.010	0.896	-0.026	0.876
0.5	0.917	0.686	0.938	-0.490	0.938	-0.316	0.938	-0.123	0.938	-0.039	0.958	-0.029	0.958
0.0	0.979	0.658	0.979	-0.549	0.979	-0.324	0.979	-0.157	0.979	-0.039	0.958	-0.029	0.958

184

MACH, NOZZLE, INLET =225

SHOT	T	TPK	PMAX	P1	P2	P3	P4	P5	HMAX	H1	H2	H3	H4	H5
288	1	9.5	0.94	0.60	0.74	0.93	0.66	0.20	0.825	-0.474	-0.228	0.061	0.018	0.044
288	2	6.7	0.73	0.51	0.66	0.70	0.54	0.22	0.716	-0.500	-0.255	-0.088	-0.039	0.127
289	1	6.0	1.04	0.59	0.99	0.90	0.91	0.26	0.912	-0.482	-0.009	0.035	0.237	0.096
289	2	6.5	0.73	0.59	0.69	0.68	0.62	0.15	0.716	-0.422	-0.225	-0.108	0.039	0.059
290	1	11.5	0.94	0.56	0.89	0.92	0.82	0.36	0.825	-0.509	-0.096	0.053	0.158	0.184
290	2	3.0	0.85	0.45	0.84	0.77	0.67	0.25	0.833	-0.559	-0.078	-0.020	0.088	0.157
291	1	15.0	0.92	0.34	0.84	0.85	0.88	0.30	0.807	-0.702	-0.140	-0.009	0.211	0.132
291	2	6.5	1.02	0.78	0.99	0.90	0.68	0.09	1.000	-0.235	0.069	0.108	0.098	0.0
292	1	1.5	0.95	0.79	0.92	0.81	0.78	0.30	0.833	-0.307	-0.070	-0.044	0.123	0.132
292	2	9.5	0.75	0.29	0.73	0.74	0.70	0.18	0.735	-0.716	-0.186	-0.049	0.118	0.088
293	1	23.5	1.02	0.55	0.68	0.85	0.85	0.31	0.895	-0.518	-0.281	-0.009	0.184	0.140
293	2	6.5	0.88	0.60	0.80	0.81	0.67	0.16	0.863	-0.412	-0.118	0.020	0.088	0.069

HRMS = 0.834 0.504 0.168 0.061 0.134 0.114

F12	F13	F14	F15	F23	F24	F25	F34	F35	F45
0.8434	0.1461	-0.8286	-0.9186	0.4081	-0.5250	-0.7734	0.1318	-0.1931	0.8150

TPK	P(TPK)	HMAX	P(HMAX)	H1	P(H1)	H2	P(H2)	H3	P(H3)	H4	P(H4)	H5	P(H5)
23.5	0.042	1.000	0.042	-0.235	0.042	0.069	0.042	0.108	0.042	0.237	0.042	0.184	0.042
15.0	0.125	0.912	0.125	-0.307	0.125	-0.009	0.125	0.061	0.125	0.211	0.125	0.157	0.125
11.5	0.208	0.895	0.208	-0.412	0.208	-0.070	0.208	0.053	0.208	0.184	0.208	0.140	0.208
9.5	0.333	0.863	0.292	-0.422	0.292	-0.078	0.292	0.035	0.292	0.158	0.292	0.132	0.333
9.5	0.333	0.833	0.375	-0.474	0.375	-0.096	0.375	0.020	0.375	0.123	0.375	0.132	0.353
6.7	0.458	0.833	0.458	-0.482	0.458	-0.118	0.458	-0.009	0.500	0.118	0.458	0.127	0.458
6.5	0.625	0.825	0.583	-0.500	0.542	-0.140	0.542	-0.009	0.500	0.098	0.542	0.096	0.542
6.5	0.625	0.825	0.583	-0.509	0.625	-0.186	0.625	-0.020	0.625	0.088	0.667	0.088	0.625
6.5	0.625	0.807	0.708	-0.518	0.708	-0.225	0.708	-0.044	0.708	0.088	0.667	0.069	0.708
6.0	0.792	0.735	0.792	-0.559	0.792	-0.228	0.792	-0.049	0.792	0.039	0.792	0.059	0.792
3.0	0.875	0.716	0.917	-0.702	0.875	-0.255	0.875	-0.088	0.875	0.018	0.875	0.044	0.875
1.5	0.958	0.716	0.917	-0.716	0.958	-0.281	0.958	-0.108	0.958	-0.039	0.958	0.0	0.958

MACH, NOZZLE, INLET =232

SHOT	T	TPK	PMAX	P1	P2	P3	P4	P5	HMAX	H1	H2	H3	H4	H5
229	1	1.5	1.09	0.94	1.05	0.96	0.67	0.20	0.956	-0.175	0.044	0.088	0.026	0.044
229	2	2.3	1.10	1.03	1.03	0.90	0.59	0.06	1.078	0.010	0.108	0.108	0.010	-0.029
230	1	1.3	1.06	0.92	0.98	0.84	0.74	0.23	0.930	-0.193	-0.018	-0.018	0.088	0.070
230	2	0.5	1.04	1.03	0.98	0.70	0.52	0.20	1.020	0.010	0.059	-0.088	-0.059	0.108
231	1	0.8	1.09	1.00	1.00	0.86	0.64	0.20	0.956	-0.123	0.0	0.0	0.0	0.044
231	2	2.8	1.05	1.00	0.95	0.71	0.59	0.06	1.029	-0.020	0.029	-0.078	0.010	-0.029
232	1	0.7	1.02	0.97	0.97	0.91	0.71	0.19	0.895	-0.149	-0.026	0.044	0.061	0.035
232	2	2.5	1.04	1.00	0.93	0.74	0.64	0.13	1.020	-0.020	0.010	-0.049	0.059	0.039
233	1	0.7	1.20	1.13	1.06	0.88	0.73	0.21	1.053	-0.009	0.053	0.018	0.079	0.053
233	2	2.5	0.91	0.85	0.90	0.79	0.56	0.12	0.892	-0.167	-0.020	0.0	-0.020	0.029
234	1	1.0	1.29	1.18	1.14	0.93	0.65	0.20	1.132	0.035	0.123	0.061	0.009	0.044
234	2	5.5	0.95	0.92	0.94	0.80	0.65	0.11	0.931	-0.098	0.020	0.010	0.069	0.020

HRMS = 0.994 0.110 0.056 0.059 0.051 0.051

F12	F13	F14	F15	F23	F24	F25	F34	F35	F45
0.0768	-0.1897	-0.5454	-0.5537	0.3850	0.1008	0.3061	0.2409	-0.1205	0.3303

TPK	P(TPK)	HMAX	P(HMAX)	H1	P(H1)	H2	P(H2)	H3	P(H3)	H4	P(H4)	H5	P(H5)
5.5	0.042	1.132	0.042	0.035	0.042	0.123	0.042	0.108	0.042	0.088	0.042	0.108	0.042
2.8	0.125	1.078	0.125	0.010	0.167	0.108	0.125	0.088	0.125	0.079	0.125	0.070	0.125
2.5	0.250	1.053	0.208	0.010	0.167	0.059	0.208	0.061	0.208	0.069	0.208	0.053	0.208
2.5	0.250	1.029	0.292	-0.009	0.292	0.053	0.292	0.044	0.292	0.061	0.292	0.044	0.375
2.3	0.375	1.020	0.417	-0.020	0.417	0.044	0.375	0.018	0.375	0.059	0.375	0.044	0.375
1.5	0.458	1.020	0.417	-0.020	0.417	0.029	0.458	0.010	0.458	0.026	0.458	0.044	0.375
1.3	0.542	0.956	0.583	-0.098	0.542	0.020	0.542	0.0	0.583	0.010	0.583	0.039	0.542
1.0	0.625	0.956	0.583	-0.123	0.625	0.010	0.625	0.0	0.583	0.010	0.583	0.035	0.625
0.8	0.708	0.931	0.708	-0.149	0.708	0.0	0.708	-0.018	0.708	0.009	0.708	0.029	0.708
0.7	0.833	0.930	0.792	-0.167	0.792	-0.018	0.792	-0.049	0.792	0.0	0.792	0.020	0.792
0.7	0.833	0.895	0.875	-0.175	0.875	-0.020	0.875	-0.078	0.875	-0.020	0.875	-0.029	0.917
0.5	0.958	0.892	0.958	-0.193	0.958	-0.026	0.958	-0.088	0.958	-0.059	0.958	-0.029	0.917

MACH, NOZZLE, INLET =234

SHOT	T	TPK	PMAX	P1	P2	P3	P4	P5		HMAX	H1	H2	H3	H4	H5
164	1	3.3	0.90	0.59	0.80	0.77	0.63	0.19		0.789	-0.482	-0.175	-0.079	-0.009	0.035
164	2	10.5	0.90	0.40	0.80	0.89	0.60	0.21		0.882	-0.608	-0.118	0.098	0.020	0.118
165	1	1.5	1.46	1.00	1.13	0.99	0.64	0.11		1.281	-0.123	0.114	0.114	0.0	-0.035
165	2	7.5	1.24	0.92	1.20	1.00	0.55	0.13		1.216	-0.098	0.275	0.206	-0.029	0.039
166	1	14.0	1.00	0.58	0.75	0.80	0.76	0.27		0.877	-0.491	-0.219	-0.053	0.105	0.105
166	2	0.5	1.20	1.05	0.90	0.80	0.77	0.13		1.176	0.029	-0.020	0.010	0.186	0.039
167	1	8.0	1.15	0.80	1.09	1.08	0.71	0.15		1.009	-0.298	0.079	0.193	0.061	0.0
167	2	0.0	1.94	1.94	1.25	0.86	0.62	-0.05		1.902	0.902	0.324	0.069	0.039	-0.137
168	1	1.2	1.57	1.45	1.11	1.04	0.66	0.04		1.377	0.272	0.096	0.158	0.018	-0.096
168	2	0.0	1.00	1.00	1.00	0.80	0.63	0.19		0.980	-0.020	0.078	0.010	0.049	0.098
169	1	6.0	0.86	0.32	0.85	0.77	0.66	0.20		0.754	-0.719	-0.132	-0.079	0.018	0.044
169	2	6.5	0.99	0.91	0.90	0.89	0.81	0.21		0.971	-0.108	-0.020	0.098	0.225	0.118
170	1	2.0	1.14	1.00	1.10	0.82	0.84	0.20		1.000	-0.123	0.088	-0.035	0.175	0.044
170	2	0.0	0.90	0.90	0.69	0.70	0.65	0.14		0.882	-0.118	-0.225	-0.088	0.069	0.049
171	1	4.5	1.11	0.56	1.10	1.02	0.97	0.26		0.974	-0.509	0.088	0.140	0.289	0.096
171	2	11.0	0.94	0.56	0.80	0.90	0.67	0.18		0.922	-0.451	-0.118	0.108	0.088	0.088
173	1	1.2	1.65	1.30	1.11	1.19	0.54	0.10		1.447	0.140	0.096	0.289	-0.088	-0.044
173	2	0.0	0.95	0.95	0.90	0.80	0.54	0.14		0.931	-0.069	-0.118	0.010	-0.039	0.049
174	1	1.0	1.33	1.25	1.12	0.80	0.60	0.13		1.167	0.096	0.105	-0.053	-0.035	-0.018
174	2	1.9	1.55	0.79	1.42	0.91	0.51	0.0		1.520	-0.225	0.490	0.118	-0.069	-0.088
175	1	1.0	1.11	1.10	0.98	0.75	0.69	0.16		0.974	-0.035	-0.018	-0.096	0.044	0.009
175	2	0.0	1.02	1.02	0.79	0.64	0.67	0.11		1.000	0.0	-0.127	-0.147	0.088	0.020

HRMS = 1.125   0.366   0.178   0.122   0.108   0.073

F12	F13	F14	F15	F23	F24	F25	F34	F35	F45
0.3892	-0.0303	-0.3240	-0.7216	0.5452	-0.1356	-0.5506	0.0689	-0.0819	0.5827

TPK	P(TPK)	HMAX	P(HMAX)	H1	P(H1)	H2	P(H2)	H3	P(H3)	H4	P(H4)	H5	P(H5)
14.0	0.023	1.902	0.023	0.902	0.023	0.490	0.023	0.289	0.023	0.289	0.023	0.118	0.045
11.0	0.068	1.520	0.068	0.272	0.068	0.324	0.068	0.206	0.068	0.225	0.068	0.118	0.045
10.5	0.114	1.447	0.114	0.140	0.114	0.275	0.114	0.193	0.114	0.186	0.114	0.105	0.114
8.0	0.159	1.377	0.159	0.096	0.159	0.114	0.159	0.158	0.159	0.175	0.159	0.098	0.159
7.5	0.205	1.281	0.205	0.029	0.205	0.105	0.205	0.140	0.205	0.105	0.205	0.096	0.205
6.5	0.250	1.216	0.250	0.0	0.250	0.096	0.273	0.118	0.250	0.088	0.273	0.088	0.250
6.0	0.295	1.176	0.295	-0.020	0.295	0.096	0.273	0.114	0.295	0.088	0.273	0.049	0.318
4.5	0.341	1.167	0.341	-0.035	0.341	0.088	0.364	0.108	0.341	0.069	0.341	0.049	0.318
3.3	0.386	1.009	0.386	-0.069	0.386	0.088	0.364	0.058	0.409	0.061	0.386	0.044	0.409
2.0	0.432	1.000	0.455	-0.098	0.432	0.098	0.432	0.098	0.409	0.049	0.432	0.044	0.409
1.9	0.477	1.000	0.455	-0.106	0.477	0.078	0.477	0.069	0.477	0.044	0.477	0.039	0.500
1.5	0.523	0.980	0.523	-0.118	0.523	-0.018	0.523	0.010	0.568	0.039	0.523	0.039	0.500
1.2	0.591	0.974	0.591	-0.123	0.591	-0.020	0.591	0.010	0.568	0.020	0.568	0.035	0.568
1.2	0.591	0.974	0.591	-0.123	0.591	-0.020	0.591	0.010	0.568	0.018	0.636	0.020	0.614
1.0	0.682	0.971	0.659	-0.225	0.659	-0.118	0.705	-0.035	0.659	0.018	0.636	0.009	0.659
1.0	0.682	0.931	0.705	-0.298	0.705	-0.118	0.705	-0.053	0.727	0.0	0.705	0.0	0.705
0.5	0.750	0.922	0.750	-0.451	0.750	-0.118	0.705	-0.053	0.727	-0.009	0.750	-0.018	0.750
0.0	0.886	0.882	0.818	-0.482	0.795	-0.127	0.795	-0.079	0.818	-0.029	0.795	-0.035	0.795
0.0	0.886	0.882	0.818	-0.491	0.841	-0.152	0.841	-0.079	0.818	-0.035	0.841	-0.044	0.841
0.0	0.886	0.877	0.886	-0.509	0.886	-0.175	0.886	-0.088	0.886	-0.039	0.886	-0.088	0.886
0.0	0.886	0.789	0.932	-0.608	0.932	-0.219	0.932	-0.096	0.932	-0.069	0.932	-0.096	0.932
0.0	0.886	0.754	0.977	-0.719	0.977	-0.225	0.977	-0.147	0.977	-0.088	0.977	-0.137	0.977

MACH, NOZZLE, INLET =235

SHOT	T	TPK	PMAX	P1	P2	P3	P4	P5	HMAX	H1	H2	H3	H4	H5
182	1	2.0	1.35	1.00	1.00	0.70	0.61	0.14	1.184	-0.123	0.0	-0.140	-0.026	-0.009
182	2	15.0	0.88	0.20	0.82	0.80	0.78	0.14	0.863	-0.804	-0.098	0.010	0.196	0.049
184	1	1.5	1.42	1.20	0.97	0.80	0.57	0.24	1.246	0.053	-0.026	-0.053	-0.061	0.074
184	2	1.5	1.92	1.15	1.35	0.90	0.44	0.0	1.882	0.127	0.422	0.108	-0.137	-0.088
185	1	7.5	0.96	0.89	0.89	0.85	0.66	0.20	0.842	-0.219	-0.096	-0.009	0.018	0.044
185	2	10.0	0.85	0.49	0.73	0.85	0.74	0.21	0.833	-0.520	-0.186	0.059	0.157	0.118
186	1	8.2	0.71	0.36	0.60	0.66	0.60	0.45	0.623	-0.684	-0.351	-0.175	-0.035	0.263
186	2	3.5	1.32	0.48	1.26	1.15	0.44	0.02	1.294	-0.529	0.333	0.353	-0.137	-0.069
187	1	9.5	1.20	0.44	0.80	1.19	0.81	0.29	1.053	-0.614	-0.175	0.289	0.149	0.123
188	1	.5	1.17	1.16	0.71	0.65	0.54	0.46	1.026	0.018	-0.254	-0.184	-0.088	0.272
188	2	6.5	0.83	0.66	0.66	0.68	0.54	0.18	0.814	-0.353	-0.255	-0.108	-0.039	0.088
189	1	1.4	1.25	1.09	1.20	1.06	0.72	0.10	1.096	-0.044	0.175	0.175	0.070	-0.044
189	2	9.0	0.79	0.31	0.48	0.79	0.60	0.29	0.775	-0.696	-0.431	0.0	0.020	0.196

HRMS = 1.086 0.459 0.255 0.165 0.105 0.137

F12	F13	F14	F15	F23	F24	F25	F34	F35	F45
0.5257	-0.2297	-0.4147	-0.6082	0.4934	-0.3731	-0.8627	0.1630	-0.3668	0.1513

TPK	P(TPK)	HMAX	P(HMAX)	H1	P(H1)	H2	P(H2)	H3	P(H3)	H4	P(H4)	H5	P(H5)
15.0	0.038	1.882	0.038	0.127	0.038	0.422	0.038	0.353	0.038	0.195	0.038	0.272	0.038
10.0	0.115	1.294	0.115	0.053	0.115	0.333	0.115	0.289	0.115	0.157	0.115	0.263	0.115
9.5	0.192	1.246	0.192	0.018	0.192	0.175	0.192	0.175	0.192	0.149	0.192	0.196	0.192
9.0	0.269	1.184	0.269	-0.044	0.269	0.0	0.269	0.108	0.269	0.070	0.269	0.123	0.269
8.2	0.346	1.096	0.346	-0.123	0.346	-0.026	0.346	0.059	0.346	0.020	0.346	0.118	0.346
7.5	0.423	1.053	0.423	-0.219	0.423	-0.096	0.423	0.010	0.423	0.018	0.423	0.088	0.423
6.5	0.500	1.026	0.500	-0.353	0.500	-0.098	0.500	0.0	0.500	-0.026	0.500	0.079	0.500
3.5	0.577	0.863	0.577	-0.520	0.577	-0.175	0.577	-0.009	0.577	-0.035	0.577	0.049	0.577
2.0	0.654	0.842	0.654	-0.529	0.654	-0.186	0.654	-0.053	0.654	-0.039	0.654	0.044	0.654
1.5	0.769	0.833	0.731	-0.614	0.731	-0.254	0.731	-0.108	0.731	-0.061	0.731	-0.009	0.731
1.5	0.769	0.814	0.808	-0.684	0.808	-0.255	0.808	-0.140	0.808	-0.088	0.808	-0.044	0.808
1.4	0.885	0.775	0.885	-0.696	0.885	-0.351	0.885	-0.175	0.885	-0.137	0.923	-0.069	0.885
0.5	0.962	0.623	0.962	-0.804	0.962	-0.431	0.962	-0.184	0.962	-0.137	0.923	-0.088	0.962

MACH, NOZZLE, INLET =241

SHOT	T	TPK	PMAX	P1	P2	P3	P4	P5	HMAX	H1	H2	H3	H4	H5
304	1	0.6	1.86	1.80	1.53	1.34	0.81	-0.01	1.632	0.579	0.465	0.421	0.149	-0.140
304	2	1.5	1.35	1.10	1.14	0.74	0.47	0.19	1.324	0.078	0.215	-0.049	-0.108	0.098
305	1	3.0	1.47	0.98	1.25	1.18	0.68	0.20	1.289	-0.140	0.219	0.281	0.035	0.044
305	2	1.5	0.86	0.83	0.78	0.62	0.54	0.18	0.843	-0.186	-0.137	-0.167	-0.039	0.088
306	1	2.8	1.52	1.13	1.38	1.10	0.75	0.10	1.333	-0.009	0.333	0.211	0.096	-0.044
306	2	10.0	0.78	0.19	0.64	0.78	0.75	0.30	0.765	-0.814	-0.275	-0.010	0.167	0.206
307	1	12.0	1.12	0.34	0.95	1.03	0.77	0.32	0.982	-0.702	-0.044	0.149	0.114	0.149
307	2	2.8	1.19	0.65	1.16	0.88	0.75	0.21	1.167	-0.363	0.235	0.088	0.167	0.118
308	1	1.8	1.55	1.10	1.18	0.78	0.55	0.19	1.360	-0.035	0.158	-0.070	-0.079	0.035
308	2	0.0	1.60	1.60	1.07	0.82	0.52	-0.10	1.569	0.569	0.147	0.029	-0.059	-0.186
309	1	8.7	1.13	0.50	0.73	1.05	0.65	0.32	0.991	-0.561	-0.237	0.167	0.009	0.149
309	2	0.0	1.68	1.68	1.07	0.71	0.48	0.0	1.647	0.647	0.147	-0.078	-0.098	-0.088

HRMS = 1.274 0.478 0.241 0.183 0.106 0.124

F12	F13	F14	F15	F23	F24	F25	F34	F35	F45
0.5446	-0.0230	-0.4882	-0.9241	0.5656	0.1380	-0.4637	0.6384	-0.0774	0.3264

TPK	P(TPK)	HMAX	P(HMAX)	H1	P(H1)	H2	P(H2)	H3	P(H3)	H4	P(H4)	H5	P(H5)
12.0	0.042	1.647	0.042	0.647	0.042	0.465	0.042	0.421	0.042	0.167	0.083	0.206	0.042
10.0	0.125	1.632	0.125	0.579	0.125	0.333	0.125	0.281	0.125	0.167	0.083	0.149	0.167
8.7	0.208	1.569	0.208	0.569	0.208	0.235	0.208	0.211	0.208	0.149	0.208	0.149	0.167
3.0	0.292	1.360	0.292	0.078	0.292	0.219	0.292	0.167	0.292	0.114	0.292	0.118	0.292
2.8	0.417	1.333	0.375	-0.009	0.375	0.216	0.375	0.149	0.375	0.096	0.375	0.098	0.375
2.8	0.417	1.324	0.458	-0.035	0.458	0.158	0.458	0.086	0.458	0.035	0.458	0.088	0.458
1.8	0.542	1.289	0.542	-0.140	0.542	0.147	0.583	0.029	0.542	0.009	0.542	0.044	0.542
1.5	0.667	1.167	0.625	-0.186	0.625	0.147	0.583	-0.010	0.625	-0.039	0.625	0.035	0.625
1.5	0.667	0.991	0.708	-0.363	0.708	-0.044	0.708	-0.049	0.708	-0.059	0.708	-0.044	0.708
0.6	0.792	0.982	0.792	-0.561	0.792	-0.137	0.792	-0.070	0.792	-0.079	0.792	-0.088	0.792
0.0	0.917	0.843	0.875	-0.702	0.875	-0.237	0.875	-0.078	0.875	-0.098	0.875	-0.140	0.875
0.0	0.917	0.765	0.958	-0.814	0.958	-0.275	0.958	-0.167	0.958	-0.108	0.958	-0.186	0.958

MACH, NOZZLE, INLET =244

SHOT	T	TPK	PMAX	P1	P2	P3	P4	P5		HMAX	H1	H2	H3	H4	H5
300	1	1.5	2.20	0.75	1.95	0.92	0.56	0.27		1.930	-0.342	0.833	0.053	0.018	0.105
300	2	5.0	1.25	1.00	1.25	1.05	0.43	0.25		1.225	-0.020	0.324	0.255	-0.147	0.157
301	1	6.0	1.05	0.33	1.04	0.92	0.56	0.60		0.921	-0.711	0.035	0.053	-0.070	0.395
301	2	1.5	1.14	1.00	0.81	0.65	0.55	0.12		1.118	-0.020	-0.108	-0.137	-0.029	0.029
302	1	11.2	1.14	0.32	1.00	1.12	0.51	0.33		1.000	-0.719	0.0	0.228	-0.114	0.158
302	2	7.2	0.82	0.48	0.70	0.61	0.45	0.08		0.804	-0.529	-0.216	-0.176	-0.127	-0.010
303	1	23.0	1.24	0.15	0.44	0.79	0.90	0.49		1.088	-0.868	-0.491	-0.061	0.228	0.298
303	2	4.5	0.66	0.31	0.65	0.65	0.53	0.45		0.647	-0.696	-0.265	-0.137	-0.049	0.353
316	1	6.0	1.03	0.13	1.00	0.51	0.65	0.64		0.904	-0.886	0.0	-0.307	0.009	0.430
316	2	12.5	0.95	0.10	0.53	0.68	0.57	0.31		0.931	-0.902	-0.382	-0.108	-0.010	0.216
317	1	12.5	1.57	0.11	0.38	1.35	0.50	0.32		1.377	-0.904	-0.544	0.439	-0.123	0.149
317	2	0.7	1.24	1.15	0.87	0.63	0.45	0.08		1.216	0.137	-0.049	-0.157	-0.127	-0.010

HRMS = 1.141   0.651   0.367   0.208   0.109   0.239

F12	F13	F14	F15	F23	F24	F25	F34	F35	F45
0.4326	-0.0172	0.1494	-0.8809	0.0633	-0.0563	-0.2395	-0.3033	-0.0924	-0.0999

TPK	P(TPK)	HMAX	P(HMAX)	H1	P(H1)	H2	P(H2)	H3	P(H3)	H4	P(H4)	H5	P(H5)
23.0	0.042	1.930	0.042	0.137	0.042	0.833	0.042	0.439	0.042	0.228	0.042	0.430	0.042
12.5	0.167	1.377	0.125	-0.020	0.167	0.324	0.125	0.255	0.125	0.018	0.125	0.395	0.125
12.5	0.167	1.225	0.208	-0.020	0.167	0.035	0.208	0.228	0.208	0.009	0.208	0.353	0.208
11.2	0.292	1.216	0.292	-0.342	0.292	0.0	0.333	0.053	0.333	-0.010	0.292	0.298	0.292
6.0	0.417	1.118	0.375	-0.529	0.375	0.0	0.333	0.053	0.333	-0.029	0.375	0.216	0.375
6.0	0.417	1.088	0.458	-0.696	0.458	-0.049	0.458	-0.061	0.458	-0.049	0.458	0.158	0.458
5.0	0.542	1.000	0.542	-0.711	0.542	-0.108	0.542	-0.108	0.542	-0.070	0.542	0.157	0.542
4.5	0.625	0.931	0.625	-0.719	0.625	-0.216	0.625	-0.137	0.667	-0.114	0.625	0.149	0.625
3.5	0.708	0.921	0.708	-0.868	0.708	-0.265	0.708	-0.137	0.667	-0.123	0.708	0.105	0.708
2.2	0.792	0.904	0.792	-0.886	0.792	-0.382	0.792	-0.157	0.792	-0.127	0.833	0.029	0.792
1.5	0.875	0.804	0.875	-0.902	0.875	-0.491	0.875	-0.176	0.875	-0.127	0.833	-0.010	0.917
0.7	0.958	0.647	0.958	-0.904	0.958	-0.544	0.958	-0.307	0.958	-0.147	0.958	-0.010	0.917

MACH, NOZZLE, INLET =314

SHOT	T	TPK	PMAX	P1	P2	P3	P4	P5		HMAX	H1	H2	H3	H4	H5
347	1	1.0	2.47	2.40	1.88	1.25	0.62	0.0		1.335	0.297	0.141	-0.081	-0.184	-0.124
347	2	12.0	1.01	0.65	0.85	0.94	0.85	0.41		0.673	-0.567	-0.333	-0.173	0.047	0.193
348	1	6.5	1.99	1.30	1.85	1.76	0.94	0.24		1.076	-0.297	0.124	0.195	-0.011	0.005
348	2	17.0	1.32	0.55	0.75	1.24	1.15	0.30		0.780	-0.633	-0.400	0.027	0.247	0.120
349	1	16.5	1.24	0.80	0.86	1.13	1.02	0.43		0.670	-0.568	-0.411	-0.146	0.032	0.108
349	2	1.0	1.05	1.03	0.94	0.95	0.78	0.10		0.700	-0.313	-0.273	-0.167	0.0	-0.013
350	1	5.0	1.60	1.00	1.60	1.50	1.09	0.29		0.865	-0.459	-0.011	0.054	0.070	0.032
350	2	8.0	1.30	0.98	1.20	1.22	0.68	0.33		0.867	-0.413	-0.100	0.013	-0.067	0.140
351	1	1.0	1.62	1.40	1.40	1.28	0.80	0.36		0.876	-0.243	-0.119	-0.065	-0.086	0.070
351	2	12.5	1.09	0.89	0.93	1.05	0.80	0.10		0.727	-0.407	-0.280	-0.100	0.013	0.013
352	1	8.0	1.80	1.47	1.70	1.77	1.12	-0.02		0.973	-0.205	0.043	0.200	0.086	-0.135
352	2	5.0	1.49	1.24	1.49	1.18	0.83	0.25		0.993	-0.173	0.093	-0.013	0.033	0.037
353	1	7.5	1.15	1.05	1.04	1.12	0.94	0.71		0.622	-0.432	-0.314	-0.151	-0.011	0.259
353	2	2.5	1.66	1.56	1.57	1.29	0.65	0.18		1.107	0.040	0.147	0.060	-0.087	0.040
354	1	12.0	1.10	0.92	0.93	1.07	0.87	0.45		0.595	-0.503	-0.373	-0.178	-0.049	0.119
354	2	0.0	1.75	1.75	1.28	1.13	0.47	0.0		1.167	0.167	-0.047	-0.047	-0.207	-0.080
355	1	1.8	1.09	0.89	1.01	1.04	0.95	0.55		0.589	-0.519	-0.330	-0.195	-0.005	0.173
355	2	6.0	1.55	1.42	1.47	1.20	0.84	0.07		1.033	-0.053	0.080	0.0	0.040	-0.033
356	1	1.5	1.37	1.17	1.25	1.13	0.71	0.11		0.741	-0.368	-0.200	-0.146	-0.135	-0.065
356	2	2.5	1.13	1.10	1.11	1.04	0.80	0.07		0.753	-0.267	-0.160	-0.107	0.013	-0.033
357	1	1.4	1.30	1.27	1.14	1.22	1.24	0.33		0.703	-0.314	-0.259	-0.097	0.151	0.054
357	2	10.0	1.25	0.94	1.07	1.25	0.80	0.42		0.833	-0.373	-0.187	0.033	0.013	0.200
358	1	0.0	1.69	1.69	1.23	1.12	0.62	0.24		0.914	-0.086	-0.211	-0.151	-0.184	0.005
358	2	3.5	1.70	1.27	1.72	1.17	0.68	0.26		1.193	-0.153	0.247	-0.020	-0.067	0.093
359	1	5.0	1.32	1.15	1.32	1.31	0.99	0.60		0.714	-0.378	-0.162	-0.049	0.016	0.200
359	2	1.0	1.22	1.13	1.07	1.15	0.55	0.27		0.813	-0.247	-0.187	-0.033	-0.153	0.100
360	1	12.5	1.36	0.92	1.24	1.34	1.01	0.45		0.735	-0.503	-0.205	-0.032	0.027	0.119
360	2	11.0	1.33	1.28	1.29	1.30	0.72	0.26		0.887	-0.147	-0.040	0.067	-0.040	0.093
361	1	10.0	1.38	0.81	1.06	1.38	0.96	0.42		0.746	-0.562	-0.303	-0.011	0.0	0.103
361	2	7.0	1.36	0.69	1.14	1.31	0.91	0.20		0.907	-0.540	-0.140	0.073	0.087	0.053
362	1	10.0	1.32	1.25	1.28	1.32	0.98	0.31		0.714	-0.324	-0.184	-0.043	0.011	0.043
362	2	0.0	1.90	1.90	1.63	1.24	0.68	0.24		1.267	0.267	0.187	0.027	-0.067	0.080

188

```
363  1   2.5  1.87  1.67  1.73  1.35  0.77  0.05      1.011 -0.097  0.059 -0.027 -0.103 -0.097
363  2   0.0  0.92  0.92  0.86  0.75  0.68  0.42      0.613 -0.387 -0.327 -0.300 -0.067  0.200
364  1   5.0  2.20  1.65  2.20  1.80  1.29  0.07      1.189 -0.168  0.314  0.216  0.178 -0.086
364  2  13.0  1.48  0.55  1.05  1.24  1.30  0.31      0.987 -0.633 -0.200  0.027  0.347  0.127
365  1  15.0  1.53  0.67  0.95  1.45  1.33  0.24      0.827 -0.638 -0.362  0.027  0.200  0.005
365  2  12.0  1.25  0.84  1.06  1.08  0.80  0.38      0.833 -0.440 -0.193 -0.080  0.013  0.173
366  1  13.0  1.62  1.31  1.27  1.48  1.23  0.48      0.876 -0.292 -0.189  0.043  0.146  0.135
366  2   3.5  1.68  1.07  1.58  1.54  0.85  0.16      1.120 -0.287  0.153  0.227  0.047  0.027
367  1   3.5  1.86  1.74  1.75  1.48  1.23  0.30      1.005 -0.059  0.070  0.043  0.146  0.038
367  2  23.0  1.14  0.85  0.78  0.91  1.12  0.64      0.760 -0.433 -0.380 -0.193  0.227  0.347
368  1   3.5  1.95  1.65  1.93  1.69  1.47  0.63      1.054 -0.108  0.168  0.157  0.276  0.216
368  2   3.5  1.35  1.19  1.33  1.27  1.13  0.53      0.900 -0.207 -0.013  0.047  0.233  0.273
369  1   1.0  1.60  1.50  1.48  1.37  0.90  0.27      0.865 -0.189 -0.076 -0.016 -0.032  0.022
369  2   8.0  1.34  0.80  1.31  1.32  0.86  0.09      0.893 -0.467 -0.027  0.080  0.053 -0.020
370  1  10.5  1.49  1.10  1.20  1.48  1.22  0.44      0.805 -0.405 -0.227  0.043  0.141  0.114
370  2   3.0  1.39  1.17  1.19  1.18  0.80  0.03      0.927 -0.220 -0.113 -0.013  0.013 -0.060
371  1  13.0  1.12  0.67  0.74  1.02  0.97  0.60      0.605 -0.638 -0.476 -0.205  0.005  0.200
371  2   4.0  1.56  1.45  1.52  1.30  0.71  0.22      1.040 -0.033  0.113  0.067 -0.047  0.067
372  1   1.5  2.21  1.87  1.88  1.76  1.10 -0.06      1.195  0.011  0.141  0.195  0.076 -0.157
372  2  12.5  1.15  0.80  1.08  1.13  0.98  0.27      0.767 -0.467 -0.180 -0.047  0.133  0.100
373  1   1.0  1.85  1.83  1.50  1.55  0.91  0.12      1.000 -0.011 -0.065  0.081 -0.027 -0.059
373  2  12.0  1.15  0.64  1.03  1.29  1.09  0.50      0.767 -0.573 -0.213  0.060  0.207  0.253
374  1  10.5  1.59  0.85  1.35  1.58  1.44  0.84      0.859 -0.541 -0.146  0.097  0.259  0.330
374  2   5.5  1.71  1.10  1.71  1.57  1.28  0.40      1.140 -0.267  0.240  0.247  0.333  0.187
375  1  10.0  2.06  1.90  1.98  2.06  1.06  0.70      1.114  0.027  0.195  0.357  0.054  0.254
375  2  12.5  1.53  0.32  0.93  1.12  1.05  0.40      1.020 -0.787 -0.280 -0.053  0.180  0.187
376  1   5.0  1.09  0.75  1.09  0.94  1.00  0.49      0.589 -0.595 -0.286 -0.249  0.022  0.141
376  2   0.0  1.31  1.31  1.18  0.97  0.69  0.09      0.873 -0.127 -0.113 -0.153 -0.060 -0.020
377  1   2.5  1.71  1.35  1.64  1.32  1.35  0.72      0.924 -0.270  0.011 -0.043  0.211  0.265
377  2   0.0  1.63  1.63  1.30  1.63  0.92  0.25      1.087  0.087 -0.033  0.287  0.093  0.087
378  1   4.5  1.15  0.89  1.14  0.99  0.72  0.50      0.622 -0.519 -0.259 -0.222 -0.130  0.146
378  2   9.0  1.36  1.20  1.16  1.32  0.85  0.06      0.907 -0.200 -0.127  0.080  0.047 -0.040
379  1   5.0  1.73  1.11  1.73  1.51  0.99  0.44      0.935 -0.400  0.059  0.059  0.016  0.114
379  2   0.0  1.66  1.66  1.38  1.29  0.89  0.33      1.107  0.107  0.020  0.060  0.073  0.140
380  1   5.5  1.89  1.54  1.88  1.67  1.11  0.27      1.022 -0.168  0.141  0.146  0.081  0.022
380  2   8.5  1.30  0.98  1.04  1.29  1.11  0.07      0.867 -0.347 -0.207  0.060  0.220 -0.033
381  1   7.0  0.91  0.74  0.90  0.87  0.80  0.40      0.492 -0.600 -0.389 -0.286 -0.086  0.092
381  2   0.0  1.03  1.03  0.95  0.97  0.68  0.17      0.687 -0.313 -0.267 -0.153 -0.067  0.033
382  1   1.4  1.86  1.80  1.74  1.45  0.87 -0.13      1.005 -0.027  0.065  0.027 -0.049 -0.195
382  2   5.0  1.60  1.30  1.60  1.05  0.67  0.24      1.067 -0.133  0.167 -0.100 -0.073  0.080
383  1  10.0  1.16  0.90  1.16  1.16  1.05  0.38      0.627 -0.514 -0.276 -0.130  0.049  0.081
383  2   4.0  1.14  1.13  1.13  1.08  0.70  0.20      0.760 -0.247 -0.147 -0.080 -0.053  0.053
384  1   1.5  1.82  1.40  1.53  1.12  0.65  0.09      0.984 -0.243 -0.049 -0.151 -0.168 -0.076
384  2   2.0  1.24  1.10  1.11  1.03  0.78  0.17      0.827 -0.267 -0.160 -0.113  0.0    0.033
385  1  12.0  1.79  1.30  1.48  1.65  1.33  0.39      0.968 -0.297 -0.076  0.135  0.200  0.086
385  2   5.0  1.66  0.97  1.66  1.32  1.00  0.30      1.107 -0.353  0.207  0.030  0.147  0.120
386  1  12.5  1.54  0.85  1.14  1.40  1.09  0.42      0.832 -0.541 -0.259  0.0    0.070  0.103
386  2  17.0  1.11  0.64  0.84  1.10  1.00  0.23      0.740 -0.573 -0.340 -0.067  0.147  0.073
387  1   2.5  2.03  1.60  1.82  1.60  0.85  0.11      1.097 -0.135  0.108  0.108 -0.059 -0.065
387  2   0.0  1.82  1.82  1.29  1.04  0.64  0.05      1.213  0.213 -0.040 -0.107 -0.093 -0.047
388  1  17.0  1.50  0.63  1.05  1.26  1.31  0.60      0.811 -0.632 -0.308 -0.076  0.189  0.200
388  2   0.0  1.61  1.61  1.50  1.26  0.77  0.27      1.073  0.073  0.100  0.040 -0.007  0.100
389  1   0.0  2.05  2.05  1.40  1.52  0.98  0.32      1.108  0.108 -0.119  0.065  0.011  0.049
389  2   0.0  1.30  1.30  1.22  1.18  0.83  0.37      0.867 -0.133 -0.087 -0.013  0.033  0.167
390  1   5.0  1.27  0.89  1.27  1.10  0.83  0.42      0.686 -0.519 -0.189 -0.162 -0.070  0.103
390  2   9.5  1.42  0.54  0.87  1.40  0.87  0.34      0.947 -0.640 -0.320  0.133  0.060  0.147
391  1   0.5  1.43  1.40  1.09  1.19  0.79  0.35      0.773 -0.243 -0.286 -0.114 -0.092  0.065
391  2  13.5  1.15  0.68  0.91  1.06  0.95  0.35      0.767 -0.547 -0.293 -0.093  0.113  0.153
392  1   1.0  1.55  1.53  1.29  1.24  1.26  0.03      0.838 -0.173 -0.178 -0.086  0.162 -0.108
392  2   0.0  1.57  1.57  1.46  1.34  0.85  0.0       1.047  0.047  0.073  0.093  0.047 -0.080
393  1   5.0  1.68  1.21  1.68  1.62  1.03  0.31      0.908 -0.346  0.032  0.119  0.038  0.043
393  2  15.0  1.22  0.98  1.00  1.20  1.08  0.42      0.813 -0.347 -0.233  0.0    0.200  0.200
394  1   5.0  1.75  1.14  1.75  1.51  1.00  0.25      0.946 -0.384  0.070  0.059  0.022  0.011
394  2  12.5  1.19  1.04  1.12  1.17  0.95  0.22      0.793 -0.307 -0.153 -0.020  0.113  0.067
395  1  10.5  1.07  0.44  0.66  1.04  0.95  0.47      0.578 -0.762 -0.519 -0.195 -0.005  0.103
395  2   8.0  0.90  0.81  0.85  0.88  0.71  0.33      0.600 -0.460 -0.333 -0.213 -0.047  0.140
396  1   4.0  1.03  0.91  1.02  0.94  0.64  0.22      0.557 -0.508 -0.324 -0.249 -0.173  0.049
396  2   0.0  1.20  1.20  0.91  0.91  0.72  0.16      0.800 -0.200 -0.293 -0.193 -0.040  0.027
397  1   1.5  1.59  1.50  1.52  1.58  0.94  0.15      0.859 -0.189 -0.054  0.097 -0.011 -0.043
397  2   0.0  1.50  1.50  1.31  1.07  0.71  0.09      1.000  0.0   -0.027 -0.087 -0.047 -0.020
398  1   6.0  1.84  1.09  1.80  1.28  0.65  0.30      0.995 -0.411  0.097 -0.065 -0.168  0.038
398  2   3.0  1.09  0.88  1.02  0.92  0.68  0.30      0.727 -0.413 -0.220 -0.187 -0.067  0.120
399  1  11.0  1.34  0.76  1.18  1.33  1.10  0.50      0.724 -0.589 -0.238 -0.038  0.076  0.146
399  2   0.0  1.90  1.90  1.40  1.20  0.54  0.30      1.267  0.267  0.033  0.0   -0.160  0.120
400  1  28.0  1.46  0.95  0.96  1.16  1.36  0.69      0.789 -0.486 -0.357 -0.130  0.216  0.249
400  2   4.0  1.70  1.20  1.66  1.39  1.02  0.03      1.133 -0.200  0.207  0.127  0.160 -0.060
401  1   0.5  1.46  1.40  1.36  1.23  0.94  0.10      0.789 -0.243 -0.141 -0.092 -0.011 -0.070
401  2   0.0  1.80  1.80  1.46  1.24  0.78  0.05      1.200  0.200  0.073  0.027  0.0   -0.047
402  1   7.0  1.66  1.05  1.54  1.45  1.05  0.52      0.897 -0.432 -0.043  0.027  0.049  0.157
402  2   6.0  0.94  0.93  0.93  0.92  0.75  0.39      0.627 -0.380 -0.280 -0.187 -0.020  0.180
```

189

```
403   1   12.0   1.50   1.17   1.24   1.49   1.01   0.63      0.811 -0.368 -0.205   0.049   0.027   0.216
404   1    2.0   1.80   1.50   1.70   1.54   0.73   0.02      0.973 -0.189   0.043   0.076 -0.124 -0.114
404   2    6.2   1.44   0.84   1.42   1.34   0.95   0.08      0.960 -0.440   0.047   0.093   0.113 -0.027
405   1    4.5   1.90   1.31   1.89   1.46   0.80   0.24      1.027 -0.292   0.146   0.032 -0.086   0.005
405   2    0.0   1.15   1.15   0.86   1.15   0.98   0.13      0.767 -0.233 -0.327 -0.033   0.133   0.007
406   1    6.5   1.75   0.53   1.74   1.73   1.09   0.31      0.946 -0.714   0.065   0.178   0.070   0.043
406   2    4.0   1.20   0.95   1.17   1.15   1.00   0.33      0.800 -0.367 -0.120 -0.033   0.147   0.140
407   1    1.2   1.55   1.40   1.45   1.34   0.82   0.35      0.838 -0.243 -0.092 -0.032 -0.076   0.065
407   2    0.0   1.87   1.87   1.30   1.40   0.79 -0.05      1.247   0.247 -0.033   0.133   0.007 -0.113
413   1   17.0   1.64   0.38   0.76   1.07   1.48   0.53      0.886 -0.795 -0.465 -0.178   0.281   0.162
413   2    6.0   1.65   1.25   1.55   1.47   0.77   0.24      1.100 -0.167   0.133   0.180 -0.007   0.080
414   1    4.5   1.54   1.27   1.53   1.29   1.12   0.30      0.832 -0.314 -0.049 -0.059   0.086   0.038
414   2    4.0   1.76   1.57   1.70   1.31   0.89   0.19      1.173   0.047   0.233   0.073   0.073   0.047
415   1    1.2   1.32   1.20   1.29   1.18   1.01   0.36      0.714 -0.351 -0.178 -0.119   0.027   0.070
415   2    2.0   1.06   1.03   1.04   0.99   0.94   0.39      0.707 -0.313 -0.207 -0.140   0.107   0.180
416   1    4.5   2.45   1.30   2.43   1.64   0.71   0.29      1.324 -0.297   0.438   0.130 -0.135   0.032
416   2   11.0   1.16   0.87   1.07   1.15   0.75   0.29      0.773 -0.420 -0.187 -0.033 -0.020   0.113
417   1    9.0   1.07   0.55   0.93   1.06   0.92   0.46      0.578 -0.703 -0.373 -0.184 -0.022   0.124
417   2    8.5   1.55   0.56   1.18   1.45   1.04   0.52      1.033 -0.627 -0.113   0.167   0.173   0.267
418   1    8.5   2.44   0.90   1.92   2.30   0.98   0.27      1.319 -0.514   0.162   0.486   0.011   0.022
418   2    0.0   1.58   1.58   1.09   0.99   0.65   0.10      1.053   0.053 -0.173 -0.140 -0.087 -0.013
419   1   10.0   1.80   1.38   1.40   1.80   1.17   0.39      0.973 -0.254 -0.119   0.216   0.114   0.086
419   2    7.0   1.09   0.48   0.97   1.03   0.87   0.44      0.727 -0.680 -0.253 -0.113   0.060   0.213
420   1    0.0   1.20   1.20   0.96   1.08   1.20   0.49      0.649 -0.351 -0.357 -0.173   0.130   0.141
420   2    1.0   1.93   1.30   1.72   1.25   0.85   0.34      1.287 -0.133   0.247   0.033   0.047   0.147
421   1    0.0   1.45   1.45   1.43   1.30   0.83   0.34      0.784 -0.216 -0.103 -0.054 -0.070   0.059
421   2    3.0   1.08   1.02   0.88   0.92   0.92   0.24      0.720 -0.320 -0.313 -0.187   0.093   0.080
422   1    0.8   1.54   1.49   1.49   1.30   0.53   0.10      0.832 -0.195 -0.070 -0.108 -0.232 -0.070
422   2    3.0   1.24   1.15   1.10   0.96   0.67   0.30      0.827 -0.233 -0.167 -0.160 -0.073   0.120
423   1    8.5   1.35   0.73   1.22   1.30   0.94   0.64      0.730 -0.605 -0.216 -0.054 -0.011   0.222
423   2    0.0   1.37   1.37   0.98   1.09   0.82   0.17      0.913 -0.087 -0.247 -0.073   0.027   0.033
424   1    0.5   1.89   1.87   1.75   1.45   0.69   0.09      1.022   0.011   0.070   0.027 -0.038 -0.076
424   2   13.0   1.30   1.15   1.23   1.27   0.73   0.26      0.867 -0.233 -0.080   0.047 -0.033   0.093
425   1    6.5   1.50   0.88   1.38   1.32   1.15   0.27      0.811 -0.524 -0.130 -0.043   0.103   0.022
425   2   10.0   1.41   0.96   1.18   1.41   0.84   0.20      0.940 -0.360 -0.113   0.140   0.040   0.053
426   1    3.5   1.55   1.33   1.46   1.30   1.15   0.30      0.838 -0.281 -0.066 -0.054   0.103   0.038
426   2    4.5   1.78   1.31   1.76   1.29   0.75   0.0       1.187 -0.127   0.273   0.060 -0.020 -0.080
427   1    1.8   2.30   2.08   1.78   1.73   1.08   0.26      1.243   0.124   0.086   0.178   0.065   0.016
427   2    1.0   1.53   1.42   1.32   1.04   0.65   0.38      1.020 -0.053 -0.020 -0.107 -0.087   0.173
428   1    6.3   1.19   0.86   1.15   1.09   0.88   0.21      0.643 -0.535 -0.254 -0.168 -0.043 -0.011
428   2    3.0   1.31   1.16   1.22   1.07   0.77   0.07      0.873 -0.227 -0.087 -0.087 -0.007 -0.033
429   1   20.0   2.15   0.98   1.70   1.92   2.15   0.07      1.162 -0.470   0.043   0.281   0.643 -0.086
429   2   13.0   1.60   1.06   1.41   1.54   1.10   0.34      1.067 -0.293   0.040   0.227   0.213   0.147
430   1    2.5   1.67   1.16   1.51   1.08   0.67   0.32      0.903 -0.373 -0.059 -0.173 -0.157   0.049
430   2    8.0   1.07   0.94   1.03   1.02   1.00   0.33      0.713 -0.373 -0.213 -0.120   0.147   0.140
431   1    1.5   2.13   1.90   1.95   1.50   1.04   0.22      1.151   0.027   0.178   0.054   0.043 -0.005
431   2    8.5   1.33   0.95   1.32   1.30   0.97   0.23      0.887 -0.367 -0.020   0.067   0.127   0.073
432   1    8.7   1.34   0.92   1.26   1.33   1.00   0.34      0.724 -0.503 -0.195 -0.038   0.022   0.059
432   2    8.5   1.25   1.01   1.10   1.20   0.76   0.54      0.833 -0.327 -0.167   0.0   -0.013   0.280
433   1    7.5   2.24   1.78   2.10   2.12   1.18   0.32      1.211 -0.038   0.259   0.389   0.119   0.049
433   2   10.0   1.55   0.86   0.96   1.55   1.26   0.50      1.033 -0.427 -0.260   0.233   0.320   0.253
434   1    3.0   1.34   1.08   1.32   1.09   0.85   0.26      0.724 -0.416 -0.162 -0.168 -0.059   0.016
434   2   11.5   1.31   0.76   1.02   1.30   0.91   0.28      0.873 -0.493 -0.220   0.067   0.087   0.107
435   1   12.0   1.51   0.72   1.27   1.50   1.13   0.36      0.816 -0.611 -0.189   0.054   0.092   0.070
435   2    5.5   1.45   0.89   1.44   1.24   0.80   0.29      0.967 -0.407   0.060   0.027   0.013   0.113
436   1    8.7   1.52   1.12   1.40   1.48   0.81   0.39      0.822 -0.395 -0.119   0.043 -0.081   0.086
436   2    4.0   3.00   0.84   2.74   1.84   0.66   0.13      2.000 -0.440   0.927   0.477 -0.080   0.007
437   1   12.0   1.46   0.94   0.99   1.36   1.33   0.47      0.789 -0.492 -0.341 -0.022   0.200   0.130
437   2    9.0   1.05   0.72   1.01   1.04   0.84   0.39      0.700 -0.520 -0.227 -0.107   0.040   0.180
438   1   10.0   1.49   1.08   1.39   1.49   1.33   0.21      0.805 -0.416 -0.124   0.049   0.200 -0.011
438   2    0.0   1.85   1.85   1.58   1.35   0.85   0.07      1.233   0.233   0.153   0.100   0.047 -0.033
439   1   14.0   1.85   0.65   1.32   1.56   1.37   0.40      1.005 -0.649 -0.162   0.086   0.222   0.092
439   2    8.7   1.09   0.76   0.96   1.06   0.97   0.68      0.727 -0.493 -0.260 -0.093   0.127   0.373
440   1    6.0   1.23   0.70   1.21   1.13   1.00   0.50      0.665 -0.622 -0.222 -0.146   0.022   0.146
440   2    4.0   1.16   1.05   1.14   1.01   0.61   0.26      0.773 -0.300 -0.140 -0.127 -0.113   0.107
441   1    1.8   2.36   2.08   2.00   1.70   1.12   0.31      1.276   0.124   0.205   0.162   0.086   0.043
441   2    0.0   1.79   1.79   1.45   1.66   0.84   0.45      1.193   0.193   0.067   0.307   0.040   0.220
442   1   10.0   1.53   0.68   1.30   1.53   0.72   0.30      0.827 -0.632 -0.173   0.070 -0.124   0.135
442   2    5.5   1.24   1.09   1.19   1.04   0.72   0.30      0.800 -0.273 -0.107 -0.107 -0.040   0.120
443   1    1.6   1.71   1.47   1.64   1.55   1.20   0.20      0.924 -0.205   0.011   0.081   0.130 -0.016
443   2    0.0   1.58   1.68   1.19   0.85   0.58   0.20      1.120   0.120 -0.107 -0.233 -0.133   0.053
444   1    6.0   1.53   1.25   1.51   1.51   1.03   0.58      0.827 -0.324 -0.059   0.059   0.038   0.189
444   2    4.5   1.51   1.10   1.50   1.30   1.05   0.32      1.007 -0.267   0.100   0.067   0.180   0.133
445   1    1.7   1.42   1.27   1.32   1.20   0.84   0.39      0.768 -0.314 -0.162 -0.108 -0.065   0.086
445   2    4.0   1.58   1.20   1.55   1.55   0.85   0.31      1.053 -0.200   0.133   0.233   0.047   0.127
446   1    8.5   1.00   0.71   0.88   0.99   0.62   0.24      0.541 -0.616 -0.400 -0.222 -0.184   0.005
446   2    1.0   1.10   1.09   1.08   0.98   0.71   0.17      0.733 -0.273 -0.180 -0.147 -0.047   0.033
447   1    8.7   1.76   0.69   1.40   1.73   1.11   0.24      0.951 -0.627 -0.119   0.178   0.081   0.005
447   2    8.5   1.14   0.66   1.05   1.12   1.00   0.27      0.760 -0.560 -0.200 -0.053   0.147   0.100
```

```
448   1    2.5   2.13   1.90   1.91   1.35   1.25   0.23          1.151   0.027   0.157   0.081   0.157   0.0
448   2    1.2   1.75   1.40   1.43   1.12   0.92   0.20          1.167  -0.067   0.053  -0.053   0.093   0.053
449   1    5.0   1.35   1.25   1.35   1.27   1.00   0.28          0.730  -0.324  -0.146  -0.070   0.022   0.027
449   2    6.5   1.46   1.42   1.38   1.34   0.83   0.32          0.973  -0.053   0.020   0.093   0.033   0.133
450   1    0.8   1.93   1.86   1.66   1.54   0.91   0.24          1.043   0.005   0.022   0.076  -0.027   0.005
450   2    7.0   1.22   1.07   1.20   1.15   0.84   0.32          0.813  -0.287  -0.100  -0.033   0.040   0.133
451   1    2.0   1.30   1.11   1.16   0.95   0.84   0.20          0.703  -0.400  -0.249  -0.243  -0.065  -0.016
451   2    0.0   1.25   1.25   1.08   1.10   0.64   0.07          0.833  -0.167  -0.180  -0.067  -0.093  -0.033
452   1   18.5   1.11   1.02   0.76   0.96   1.06   0.50          0.600  -0.449  -0.465  -0.238   0.054   0.146
452   2    8.0   1.10   0.85   0.94   1.03   0.90   0.32          0.733  -0.433  -0.273  -0.113   0.080   0.133
453   1    4.0   1.24   1.00   1.23   1.07   1.13   0.32          0.570  -0.459  -0.211  -0.178   0.092   0.049
453   2    0.0   2.00   2.00   1.46   1.15   0.66  -0.08          1.333   0.333   0.073  -0.033  -0.080  -0.133
454   1   11.7   2.16   1.26   1.58   2.10   1.46   0.28          1.168  -0.319  -0.022   0.378   0.270   0.027
454   2    5.0   1.42   1.10   1.42   1.26   0.76   0.29          0.947  -0.267   0.047   0.040  -0.013   0.113
455   1   13.0   1.66   0.80   1.32   1.55   1.26   0.20          0.897  -0.568  -0.162   0.081   0.162  -0.016
455   2    1.0   1.65   1.62   1.50   1.64   0.76   0.02          1.100   0.080   0.100   0.293  -0.013  -0.067
456   1    2.5   1.74   1.50   1.72   1.16   0.72   0.27          0.941  -0.189   0.054  -0.130  -0.130   0.022
456   2    5.0   1.05   0.86   1.05   1.02   0.98   0.27          0.700  -0.427  -0.200  -0.120   0.133   0.100

                                                        HRMS =   0.925   0.380   0.214   0.141   0.125   0.123
```

```
 F12      F13      F14      F15      F23      F24      F25      F34      F35      F45
0.6656   0.1940  -0.3931  -0.6721   0.6129  -0.1886  -0.5095   0.3362  -0.1352   0.3916
```

TPK	P(TPK)	HMAX	P(HMAX)	H1	P(H1)	H2	P(H2)	H3	P(H3)	H4	P(H4)	H5	P(H5)
28.0	0.002	2.000	0.002	0.333	0.002	0.927	0.002	0.486	0.002	0.643	0.002	0.373	0.002
23.0	0.007	1.335	0.007	0.297	0.007	0.438	0.007	0.427	0.007	0.347	0.007	0.347	0.007
20.0	0.012	1.333	0.012	0.267	0.014	0.314	0.012	0.389	0.012	0.333	0.012	0.330	0.012
18.5	0.017	1.324	0.017	0.267	0.014	0.273	0.017	0.378	0.017	0.320	0.017	0.280	0.017
17.0	0.029	1.319	0.022	0.247	0.022	0.259	0.022	0.357	0.022	0.281	0.022	0.273	0.022
17.0	0.029	1.287	0.026	0.233	0.026	0.247	0.029	0.307	0.026	0.276	0.026	0.267	0.026
17.0	0.029	1.276	0.031	0.213	0.031	0.247	0.029	0.293	0.031	0.270	0.031	0.265	0.031
17.0	0.029	1.267	0.038	0.200	0.036	0.240	0.036	0.287	0.036	0.259	0.036	0.259	0.036
16.5	0.041	1.267	0.038	0.193	0.041	0.233	0.041	0.281	0.041	0.247	0.041	0.254	0.041
15.0	0.048	1.247	0.045	0.167	0.045	0.207	0.048	0.247	0.045	0.233	0.045	0.253	0.048
15.0	0.048	1.243	0.050	0.124	0.053	0.207	0.048	0.233	0.053	0.227	0.050	0.253	0.048
14.0	0.055	1.233	0.055	0.124	0.053	0.205	0.055	0.233	0.053	0.222	0.055	0.249	0.055
13.5	0.060	1.213	0.060	0.120	0.060	0.195	0.060	0.227	0.062	0.220	0.060	0.222	0.060
13.0	0.077	1.211	0.065	0.108	0.065	0.187	0.065	0.227	0.062	0.216	0.065	0.220	0.065
13.0	0.077	1.200	0.069	0.107	0.069	0.178	0.069	0.216	0.072	0.213	0.069	0.216	0.072
13.0	0.077	1.195	0.074	0.087	0.074	0.168	0.074	0.216	0.072	0.211	0.074	0.216	0.072
13.0	0.077	1.193	0.081	0.080	0.079	0.167	0.079	0.200	0.079	0.207	0.079	0.213	0.079
13.0	0.077	1.193	0.081	0.073	0.084	0.162	0.084	0.195	0.086	0.200	0.091	0.200	0.089
13.0	0.077	1.189	0.089	0.053	0.089	0.157	0.089	0.195	0.086	0.200	0.091	0.200	0.089
12.5	0.105	1.187	0.093	0.047	0.096	0.153	0.096	0.180	0.093	0.200	0.091	0.200	0.089
12.5	0.105	1.173	0.098	0.047	0.096	0.153	0.096	0.178	0.103	0.200	0.091	0.200	0.103
12.5	0.105	1.168	0.103	0.040	0.103	0.147	0.103	0.178	0.103	0.200	0.103	0.200	0.103
12.5	0.103	1.167	0.110	0.027	0.112	0.146	0.108	0.178	0.103	0.189	0.108	0.200	0.103
12.5	0.105	1.167	0.110	0.027	0.112	0.141	0.117	0.167	0.112	0.180	0.115	0.193	0.112
12.5	0.105	1.162	0.117	0.027	0.112	0.141	0.117	0.162	0.117	0.180	0.115	0.189	0.117
12.0	0.139	1.151	0.124	0.011	0.124	0.141	0.117	0.157	0.122	0.178	0.122	0.187	0.124
12.0	0.139	1.151	0.124	0.011	0.124	0.133	0.129	0.146	0.127	0.173	0.127	0.187	0.124
12.0	0.139	1.140	0.132	0.005	0.132	0.133	0.129	0.140	0.132	0.162	0.134	0.180	0.136
12.0	0.139	1.133	0.136	0.0	0.136	0.124	0.136	0.135	0.136	0.162	0.134	0.180	0.136
12.0	0.139	1.120	0.144	-0.011	0.141	0.113	0.141	0.133	0.144	0.160	0.141	0.180	0.136
12.0	0.139	1.120	0.144	-0.027	0.146	0.108	0.146	0.133	0.144	0.157	0.146	0.173	0.148
12.0	0.139	1.114	0.151	-0.033	0.151	0.100	0.156	0.130	0.151	0.151	0.151	0.173	0.148
12.0	0.139	1.108	0.156	-0.038	0.156	0.100	0.156	0.127	0.156	0.147	0.165	0.173	0.156
11.7	0.160	1.107	0.165	-0.053	0.165	0.100	0.156	0.119	0.160	0.147	0.165	0.167	0.160
11.5	0.165	1.107	0.165	-0.053	0.165	0.097	0.165	0.108	0.165	0.147	0.165	0.162	0.165
11.0	0.175	1.107	0.165	-0.053	0.165	0.093	0.170	0.100	0.170	0.147	0.165	0.157	0.170
11.0	0.175	1.100	0.175	-0.059	0.175	0.086	0.175	0.097	0.177	0.147	0.165	0.153	0.175
11.0	0.175	1.100	0.177	-0.067	0.179	0.080	0.179	0.097	0.177	0.146	0.182	0.147	0.184
10.5	0.189	1.097	0.184	-0.086	0.184	0.073	0.189	0.093	0.189	0.146	0.182	0.147	0.184
10.5	0.189	1.087	0.189	-0.087	0.189	0.073	0.189	0.093	0.189	0.141	0.189	0.147	0.184
10.5	0.189	1.076	0.194	-0.097	0.194	0.073	0.189	0.093	0.189	0.133	0.199	0.146	0.201
10.0	0.220	1.073	0.199	-0.108	0.201	0.070	0.203	0.086	0.199	0.133	0.199	0.146	0.201
10.0	0.220	1.067	0.206	-0.108	0.201	0.070	0.203	0.081	0.211	0.133	0.199	0.146	0.201
10.0	0.220	1.067	0.206	-0.127	0.211	0.070	0.203	0.081	0.211	0.130	0.211	0.146	0.201
10.0	0.220	1.054	0.213	-0.127	0.211	0.067	0.213	0.081	0.211	0.130	0.211	0.141	0.215
10.0	0.220	1.053	0.220	-0.133	0.222	0.065	0.220	0.081	0.211	0.127	0.220	0.141	0.215
10.0	0.220	1.053	0.220	-0.133	0.222	0.065	0.220	0.080	0.227	0.127	0.220	0.140	0.232
10.0	0.220	1.047	0.227	-0.133	0.222	0.060	0.227	0.080	0.227	0.119	0.227	0.140	0.232
10.0	0.220	1.043	0.232	-0.135	0.232	0.059	0.234	0.080	0.227	0.114	0.232	0.140	0.232
10.0	0.220	1.040	0.237	-0.147	0.237	0.059	0.234	0.076	0.239	0.113	0.242	0.140	0.232
10.0	0.220	1.033	0.246	-0.153	0.242	0.054	0.242	0.076	0.239	0.113	0.242	0.140	0.232
9.5	0.246	1.033	0.246	-0.167	0.249	0.053	0.246	0.073	0.249	0.113	0.242	0.135	0.249
9.0	0.256	1.033	0.246	-0.167	0.249	0.047	0.254	0.073	0.249	0.107	0.251	0.135	0.249
9.0	0.256	1.027	0.256	-0.168	0.256	0.047	0.254	0.070	0.256	0.103	0.258	0.133	0.263

9.0 0.256	1.022 0.263	-0.173 0.261	0.043 0.266	0.067 0.270	0.103 0.258	0.133 0.263
8.7 0.273	1.022 0.263	-0.173 0.266	0.043 0.266	0.067 0.270	0.093 0.270	0.133 0.263
8.7 0.273	1.020 0.273	-0.189 0.278	0.043 0.266	0.067 0.270	0.093 0.270	0.133 0.263
8.7 0.273	1.020 0.273	-0.189 0.278	0.040 0.275	0.067 0.270	0.093 0.270	0.130 0.275
8.7 0.273	1.011 0.280	-0.189 0.278	0.033 0.280	0.067 0.270	0.092 0.282	0.127 0.282
8.5 0.301	1.007 0.285	-0.189 0.278	0.032 0.285	0.065 0.285	0.092 0.282	0.127 0.282
8.5 0.301	1.005 0.294	-0.195 0.289	0.022 0.289	0.060 0.299	0.087 0.292	0.124 0.289
8.5 0.301	1.005 0.294	-0.200 0.301	0.020 0.297	0.060 0.299	0.087 0.292	0.120 0.306
8.5 0.301	1.005 0.294	-0.200 0.301	0.020 0.297	0.060 0.299	0.086 0.304	0.120 0.306
8.5 0.301	1.000 0.306	-0.200 0.301	0.011 0.306	0.060 0.299	0.086 0.304	0.120 0.306
8.5 0.301	1.000 0.306	-0.200 0.301	0.011 0.306	0.060 0.299	0.086 0.304	0.120 0.306
8.5 0.301	0.995 0.313	-0.205 0.316	-0.011 0.313	0.059 0.318	0.081 0.315	0.120 0.306
8.5 0.301	0.993 0.318	-0.205 0.316	-0.013 0.318	0.059 0.318	0.081 0.316	0.120 0.306
8.0 0.335	0.987 0.323	-0.207 0.323	-0.020 0.325	0.059 0.318	0.080 0.323	0.119 0.325
8.0 0.335	0.984 0.328	-0.216 0.328	-0.020 0.325	0.054 0.333	0.076 0.330	0.119 0.325
8.0 0.335	0.973 0.333	-0.220 0.333	-0.022 0.333	0.054 0.333	0.076 0.330	0.114 0.335
8.0 0.335	0.973 0.342	-0.227 0.337	-0.027 0.340	0.054 0.333	0.073 0.340	0.114 0.335
8.0 0.335	0.973 0.342	-0.233 0.347	-0.027 0.340	0.049 0.344	0.073 0.340	0.113 0.347
8.0 0.335	0.973 0.342	-0.233 0.347	-0.033 0.349	0.049 0.344	0.070 0.352	0.113 0.347
7.5 0.354	0.968 0.352	-0.233 0.347	-0.033 0.349	0.047 0.354	0.070 0.352	0.113 0.347
7.5 0.354	0.967 0.356	-0.243 0.366	-0.040 0.359	0.047 0.354	0.070 0.352	0.108 0.356
7.0 0.371	0.960 0.361	-0.243 0.366	-0.040 0.359	0.043 0.368	0.065 0.361	0.107 0.364
7.0 0.371	0.951 0.366	-0.243 0.366	-0.043 0.366	0.043 0.368	0.060 0.368	0.107 0.364
7.0 0.371	0.947 0.373	-0.243 0.366	-0.047 0.371	0.043 0.368	0.060 0.368	0.103 0.378
7.0 0.371	0.947 0.373	-0.243 0.366	-0.049 0.373	0.043 0.368	0.054 0.378	0.103 0.378
7.0 0.371	0.946 0.383	-0.247 0.383	-0.049 0.378	0.040 0.383	0.054 0.378	0.103 0.378
6.5 0.392	0.946 0.383	-0.247 0.383	-0.054 0.385	0.040 0.383	0.053 0.385	0.103 0.378
6.5 0.392	0.941 0.390	-0.254 0.390	-0.059 0.392	0.033 0.392	0.049 0.392	0.100 0.400
6.5 0.392	0.940 0.395	-0.267 0.404	-0.059 0.392	0.033 0.392	0.049 0.392	0.100 0.400
6.5 0.392	0.935 0.400	-0.267 0.404	-0.065 0.400	0.032 0.400	0.047 0.414	0.100 0.400
6.1 0.404	0.927 0.404	-0.267 0.404	-0.070 0.404	0.027 0.411	0.047 0.414	0.100 0.400
6.2 0.409	0.924 0.411	-0.267 0.404	-0.076 0.411	0.027 0.411	0.047 0.414	0.100 0.400
6.0 0.426	0.924 0.411	-0.267 0.404	-0.076 0.411	0.027 0.411	0.047 0.414	0.093 0.419
6.0 0.426	0.914 0.419	-0.270 0.419	-0.080 0.419	0.027 0.411	0.047 0.414	0.093 0.419
6.0 0.426	0.913 0.423	-0.273 0.426	-0.086 0.423	0.027 0.433	0.047 0.414	0.093 0.419
6.0 0.426	0.908 0.428	-0.273 0.426	-0.087 0.431	0.027 0.433	0.047 0.414	0.092 0.431
6.0 0.426	0.907 0.435	-0.281 0.433	-0.087 0.431	0.027 0.433	0.043 0.433	0.092 0.431
6.0 0.426	0.907 0.435	-0.287 0.440	-0.092 0.438	0.027 0.433	0.040 0.447	0.087 0.440
5.5 0.450	0.903 0.443	-0.287 0.440	-0.100 0.445	0.027 0.433	0.040 0.447	0.087 0.440
5.5 0.450	0.900 0.447	-0.292 0.450	-0.100 0.445	0.013 0.447	0.040 0.447	0.086 0.455
5.5 0.450	0.897 0.455	-0.292 0.450	-0.103 0.452	0.0 0.462	0.040 0.447	0.086 0.455
5.5 0.450	0.897 0.455	-0.293 0.457	-0.107 0.459	0.0 0.462	0.040 0.447	0.086 0.455
5.0 0.493	0.893 0.462	-0.297 0.467	-0.107 0.459	0.0 0.462	0.038 0.464	0.086 0.455
5.0 0.493	0.887 0.467	-0.297 0.467	-0.113 0.474	0.0 0.462	0.038 0.464	0.081 0.467
5.0 0.493	0.887 0.469	-0.297 0.467	-0.113 0.474	0.0 0.462	0.033 0.476	0.080 0.478
5.0 0.493	0.886 0.476	-0.300 0.476	-0.113 0.474	-0.011 0.476	0.033 0.476	0.080 0.478
5.0 0.493	0.880 0.481	-0.307 0.481	-0.113 0.474	-0.013 0.486	0.033 0.476	0.080 0.478
5.0 0.493	0.876 0.488	-0.313 0.490	-0.119 0.495	-0.013 0.486	0.032 0.486	0.080 0.478
5.0 0.493	0.876 0.488	-0.313 0.490	-0.119 0.495	-0.013 0.486	0.027 0.495	0.073 0.493
5.0 0.493	0.873 0.500	-0.313 0.490	-0.119 0.495	-0.016 0.495	0.027 0.495	0.073 0.493
5.0 0.493	0.873 0.500	-0.314 0.505	-0.119 0.495	-0.020 0.502	0.027 0.495	0.070 0.505
5.0 0.493	0.873 0.500	-0.314 0.505	-0.119 0.495	-0.020 0.502	0.027 0.505	0.070 0.505
5.0 0.493	0.867 0.517	-0.314 0.505	-0.120 0.510	-0.022 0.510	0.022 0.519	0.070 0.505
5.0 0.493	0.867 0.517	-0.319 0.514	-0.124 0.514	-0.027 0.514	0.022 0.519	0.067 0.517
5.0 0.493	0.867 0.517	-0.320 0.519	-0.127 0.519	-0.032 0.522	0.022 0.519	0.067 0.517
5.0 0.493	0.867 0.517	-0.324 0.529	-0.130 0.524	-0.032 0.522	0.022 0.519	0.065 0.526
4.5 0.541	0.865 0.531	-0.324 0.529	-0.140 0.531	-0.033 0.541	0.022 0.519	0.065 0.526
4.5 0.541	0.865 0.531	-0.324 0.529	-0.140 0.531	-0.033 0.541	0.016 0.536	0.059 0.536
4.5 0.541	0.859 0.541	-0.327 0.538	-0.141 0.538	-0.033 0.541	0.016 0.536	0.059 0.536
4.5 0.541	0.859 0.541	-0.346 0.543	-0.146 0.545	-0.033 0.541	0.013 0.555	0.054 0.543
4.5 0.541	0.828 0.553	-0.347 0.550	-0.146 0.545	-0.033 0.541	0.013 0.555	0.053 0.557
4.5 0.541	0.838 0.553	-0.347 0.550	-0.147 0.553	-0.033 0.541	0.013 0.555	0.053 0.557
4.0 0.579	0.833 0.553	-0.351 0.560	-0.153 0.557	-0.038 0.560	0.013 0.555	0.053 0.557
4.0 0.579	0.833 0.569	-0.351 0.560	-0.160 0.565	-0.038 0.560	0.013 0.555	0.053 0.557
4.0 0.579	0.833 0.569	-0.353 0.567	-0.160 0.565	-0.043 0.572	0.013 0.555	0.053 0.557
4.0 0.579	0.833 0.569	-0.360 0.572	-0.162 0.581	-0.043 0.572	0.011 0.577	0.049 0.581
4.0 0.579	0.833 0.569	-0.367 0.579	-0.162 0.581	-0.043 0.572	0.011 0.577	0.049 0.581
4.0 0.579	0.832 0.586	-0.367 0.579	-0.162 0.581	-0.047 0.584	0.011 0.577	0.049 0.581
4.0 0.579	0.832 0.586	-0.368 0.589	-0.162 0.581	-0.047 0.584	0.007 0.586	0.049 0.581
4.0 0.579	0.832 0.586	-0.368 0.589	-0.162 0.581	-0.049 0.591	0.005 0.591	0.049 0.581
4.0 0.579	0.827 0.600	-0.373 0.596	-0.167 0.598	-0.053 0.600	0.0 0.603	0.047 0.596
4.0 0.579	0.827 0.600	-0.373 0.603	-0.167 0.598	-0.053 0.600	0.0 0.603	0.043 0.608
3.5 0.617	0.827 0.600	-0.373 0.603	-0.173 0.605	-0.053 0.600	0.0 0.603	0.043 0.608
3.5 0.617	0.827 0.612	-0.378 0.610	-0.173 0.610	-0.054 0.615	0.0 0.603	0.043 0.608
3.5 0.617	0.827 0.612	-0.380 0.615	-0.178 0.617	-0.054 0.615	-0.005 0.617	0.043 0.608
3.5 0.617	0.822 0.620	-0.384 0.620	-0.178 0.617	-0.054 0.615	-0.005 0.617	0.040 0.620
3.5 0.617	0.816 0.624	-0.397 0.624	-0.182 0.629	-0.059 0.624	-0.007 0.629	0.038 0.632
3.5 0.617	0.813 0.634	-0.395 0.629	-0.180 0.629	-0.065 0.632	-0.007 0.629	0.038 0.632

3.0	0.646	0.813	0.634	-0.400	0.636	-0.180	0.629	-0.065	0.632	-0.007	0.629	0.038	0.632
3.0	0.646	0.813	0.634	-0.400	0.636	-0.184	0.639	-0.067	0.641	-0.011	0.648	0.038	0.632
3.0	0.646	0.811	0.648	-0.405	0.644	-0.187	0.648	-0.067	0.641	-0.011	0.648	0.033	0.651
3.0	0.646	0.811	0.648	-0.407	0.651	-0.187	0.648	-0.070	0.648	-0.011	0.648	0.023	0.651
3.0	0.646	0.811	0.648	-0.407	0.651	-0.187	0.648	-0.073	0.653	-0.011	0.648	0.003	0.651
3.0	0.646	0.805	0.660	-0.411	0.658	-0.189	0.663	-0.076	0.658	-0.011	0.648	0.033	0.651
2.5	0.679	0.805	0.660	-0.413	0.665	-0.189	0.663	-0.080	0.665	-0.013	0.667	0.032	0.665
2.5	0.679	0.800	0.672	-0.413	0.665	-0.189	0.663	-0.080	0.665	-0.013	0.667	0.032	0.665
2.5	0.679	0.800	0.672	-0.416	0.675	-0.193	0.672	-0.081	0.672	-0.013	0.667	0.027	0.675
2.5	0.679	0.800	0.672	-0.416	0.675	-0.195	0.677	-0.086	0.677	-0.020	0.682	0.027	0.675
2.5	0.679	0.793	0.682	-0.420	0.682	-0.200	0.682	-0.087	0.684	-0.020	0.682	0.027	0.684
2.5	0.679	0.789	0.691	-0.427	0.689	-0.200	0.691	-0.087	0.684	-0.020	0.682	0.027	0.684
2.5	0.679	0.789	0.691	-0.427	0.689	-0.200	0.691	-0.092	0.691	-0.022	0.691	0.022	0.701
2.5	0.679	0.789	0.691	-0.432	0.699	-0.200	0.691	-0.093	0.699	-0.027	0.699	0.022	0.701
2.0	0.708	0.784	0.701	-0.432	0.699	-0.205	0.703	-0.093	0.699	-0.027	0.699	0.022	0.701
2.0	0.708	0.773	0.708	-0.433	0.708	-0.205	0.703	-0.097	0.706	-0.032	0.706	0.022	0.701
2.0	0.708	0.773	0.708	-0.433	0.708	-0.207	0.713	-0.100	0.713	-0.033	0.711	0.022	0.701
2.0	0.708	0.773	0.715	-0.440	0.720	-0.207	0.713	-0.100	0.713	-0.038	0.715	0.016	0.718
1.8	0.725	0.768	0.720	-0.440	0.720	-0.211	0.722	-0.107	0.730	-0.040	0.725	0.016	0.718
1.8	0.725	0.767	0.732	-0.440	0.720	-0.211	0.722	-0.107	0.720	-0.040	0.725	0.013	0.725
1.8	0.725	0.767	0.732	-0.449	0.730	-0.213	0.732	-0.107	0.730	-0.040	0.725	0.011	0.730
1.7	0.734	0.767	0.732	-0.459	0.737	-0.213	0.732	-0.107	0.730	-0.043	0.734	0.007	0.737
1.6	0.739	0.767	0.732	-0.459	0.737	-0.216	0.739	-0.107	0.730	-0.047	0.746	0.007	0.737
1.5	0.754	0.760	0.749	-0.460	0.744	-0.220	0.746	-0.108	0.746	-0.047	0.746	0.005	0.758
1.5	0.754	0.760	0.749	-0.467	0.751	-0.220	0.746	-0.108	0.746	-0.047	0.746	0.005	0.758
1.5	0.754	0.760	0.749	-0.467	0.751	-0.222	0.754	-0.113	0.758	-0.047	0.746	0.005	0.758
1.5	0.754	0.753	0.758	-0.470	0.758	-0.227	0.758	-0.113	0.758	-0.049	0.761	0.005	0.758
1.5	0.754	0.746	0.763	-0.486	0.763	-0.227	0.763	-0.113	0.758	-0.049	0.761	0.005	0.758
1.4	0.770	0.741	0.768	-0.492	0.768	-0.233	0.768	-0.114	0.768	-0.053	0.768	0.005	0.758
1.4	0.770	0.740	0.773	-0.493	0.775	-0.238	0.773	-0.119	0.773	-0.059	0.775	0.005	0.758
1.2	0.782	0.735	0.778	-0.493	0.775	-0.247	0.778	-0.120	0.780	-0.059	0.775	0.0	0.778
1.2	0.782	0.733	0.785	-0.503	0.787	-0.249	0.782	-0.120	0.780	-0.060	0.782	-0.005	0.782
1.2	0.782	0.733	0.785	-0.503	0.787	-0.253	0.787	-0.127	0.787	-0.065	0.789	-0.011	0.789
1.0	0.816	0.730	0.794	-0.503	0.787	-0.254	0.792	-0.130	0.797	-0.065	0.789	-0.011	0.789
1.0	0.816	0.730	0.794	-0.508	0.797	-0.259	0.801	-0.130	0.797	-0.067	0.809	-0.013	0.799
1.0	0.816	0.727	0.809	-0.514	0.804	-0.259	0.801	-0.130	0.797	-0.067	0.809	-0.013	0.799
1.0	0.816	0.727	0.809	-0.514	0.804	-0.259	0.801	-0.140	0.809	-0.067	0.809	-0.016	0.811
1.0	0.816	0.727	0.809	-0.519	0.816	-0.260	0.813	-0.140	0.809	-0.067	0.809	-0.016	0.811
1.0	0.816	0.727	0.809	-0.519	0.816	-0.260	0.813	-0.146	0.821	-0.067	0.809	-0.015	0.811
1.0	0.816	0.724	0.825	-0.519	0.816	-0.267	0.821	-0.146	0.821	-0.067	0.809	-0.020	0.825
1.0	0.816	0.724	0.825	-0.520	0.825	-0.273	0.828	-0.146	0.821	-0.070	0.828	-0.020	0.825
1.0	0.816	0.724	0.825	-0.524	0.830	-0.273	0.828	-0.147	0.830	-0.070	0.828	-0.020	0.825
1.0	0.816	0.720	0.835	-0.535	0.835	-0.276	0.835	-0.151	0.840	-0.073	0.837	-0.027	0.835
1.0	0.816	0.714	0.844	-0.540	0.840	-0.280	0.844	-0.151	0.840	-0.073	0.837	-0.033	0.852
0.8	0.847	0.714	0.844	-0.541	0.847	-0.280	0.844	-0.151	0.840	-0.076	0.844	-0.033	0.852
0.8	0.847	0.714	0.844	-0.541	0.847	-0.280	0.844	-0.153	0.852	-0.080	0.852	-0.033	0.852
0.5	0.859	0.713	0.854	-0.547	0.854	-0.286	0.856	-0.153	0.852	-0.080	0.852	-0.033	0.852
0.5	0.859	0.707	0.859	-0.560	0.859	-0.286	0.856	-0.160	0.859	-0.081	0.859	-0.033	0.852
0.5	0.859	0.703	0.866	-0.562	0.864	-0.293	0.866	-0.162	0.864	-0.086	0.868	-0.033	0.852
0.0	0.933	0.703	0.866	-0.567	0.868	-0.293	0.866	-0.167	0.868	-0.086	0.868	-0.040	0.868
0.0	0.933	0.700	0.878	-0.568	0.876	-0.303	0.873	-0.168	0.876	-0.086	0.868	-0.043	0.873
0.0	0.933	0.700	0.878	-0.568	0.876	-0.308	0.878	-0.168	0.876	-0.087	0.883	-0.047	0.880
0.0	0.933	0.700	0.878	-0.573	0.885	-0.313	0.883	-0.173	0.885	-0.087	0.883	-0.047	0.880
0.0	0.933	0.687	0.888	-0.573	0.885	-0.314	0.888	-0.173	0.885	-0.087	0.883	-0.059	0.888
0.0	0.933	0.586	0.892	-0.518	0.892	-0.320	0.892	-0.173	0.892	-0.092	0.892	-0.060	0.895
0.0	0.933	0.573	0.897	-0.595	0.897	-0.324	0.897	-0.178	0.902	-0.093	0.900	-0.060	0.895
0.0	0.933	0.670	0.904	-0.600	0.902	-0.327	0.904	-0.178	0.902	-0.093	0.900	-0.065	0.904
0.0	0.933	0.670	0.904	-0.605	0.907	-0.327	0.904	-0.178	0.902	-0.103	0.907	-0.065	0.904
0.0	0.933	0.665	0.911	-0.611	0.911	-0.330	0.911	-0.184	0.911	-0.113	0.911	-0.067	0.911
0.0	0.933	0.649	0.916	-0.616	0.916	-0.333	0.919	-0.187	0.921	-0.124	0.919	-0.070	0.919
0.0	0.933	0.643	0.921	-0.622	0.921	-0.333	0.919	-0.187	0.921	-0.124	0.919	-0.070	0.919
0.0	0.933	0.627	0.926	-0.627	0.926	-0.340	0.926	-0.187	0.921	-0.130	0.928	-0.076	0.928
0.0	0.933	0.627	0.931	-0.627	0.931	-0.341	0.931	-0.193	0.933	-0.130	0.928	-0.076	0.928
0.0	0.933	0.622	0.938	-0.632	0.938	-0.357	0.938	-0.193	0.933	-0.133	0.935	-0.080	0.940
0.0	0.933	0.622	0.938	-0.632	0.938	-0.357	0.938	-0.195	0.943	-0.135	0.943	-0.080	0.940
0.0	0.933	0.613	0.945	-0.633	0.947	-0.362	0.945	-0.195	0.943	-0.135	0.943	-0.080	0.940
0.0	0.933	0.605	0.950	-0.633	0.947	-0.373	0.952	-0.205	0.950	-0.153	0.950	-0.086	0.952
0.0	0.933	0.600	0.957	-0.638	0.957	-0.373	0.952	-0.213	0.955	-0.157	0.955	-0.086	0.952
0.0	0.933	0.600	0.957	-0.638	0.957	-0.380	0.959	-0.222	0.962	-0.160	0.959	-0.097	0.959
0.0	0.933	0.595	0.964	-0.640	0.964	-0.389	0.964	-0.222	0.962	-0.168	0.967	-0.108	0.964
0.0	0.933	0.589	0.971	-0.649	0.969	-0.400	0.969	-0.233	0.969	-0.168	0.967	-0.113	0.969
0.0	0.933	0.589	0.971	-0.680	0.974	-0.400	0.974	-0.238	0.974	-0.173	0.974	-0.114	0.974
0.0	0.933	0.578	0.981	-0.703	0.978	-0.411	0.978	-0.243	0.978	-0.184	0.983	-0.124	0.978
0.0	0.933	0.578	0.981	-0.714	0.983	-0.465	0.986	-0.249	0.986	-0.184	0.983	-0.133	0.983
0.0	0.933	0.557	0.988	-0.762	0.988	-0.465	0.986	-0.249	0.986	-0.184	0.963	-0.135	0.988
0.0	0.933	0.541	0.993	-0.787	0.993	-0.476	0.993	-0.286	0.993	-0.207	0.993	-0.157	0.993
0.0	0.933	0.492	0.998	-0.795	0.998	-0.519	0.998	-0.300	0.998	-0.232	0.998	-0.195	0.998

193

MACH. NOZZLE. INLET .324

SHOT	T	TPK	PMAX	P1	P2	P3	P4	P5	HMAX	H1	H2	H3	H4	H5
335	1	10.0	1.35	0.68	1.03	1.35	1.01	0.44	0.730	-0.632	-0.319	-0.027	0.027	0.114
335	2	14.0	1.15	0.69	1.07	1.13	0.85	0.30	0.767	-0.540	-0.187	-0.047	0.047	0.120
336	1	9.0	1.32	1.04	1.04	1.30	0.70	0.39	0.714	-0.438	-0.314	-0.054	-0.141	0.086
336	2	2.0	1.00	0.99	0.93	0.93	0.75	0.42	0.667	-0.340	-0.280	-0.180	-0.020	0.200
337	1	10.0	1.25	1.08	1.10	1.25	1.11	0.40	0.676	-0.416	-0.281	-0.081	0.081	0.092
337	2	15.0	1.02	0.60	0.75	0.92	0.83	0.36	0.680	-0.600	-0.400	-0.187	0.033	0.160
338	1	6.5	1.69	0.90	1.63	1.50	1.20	0.14	0.914	-0.514	0.005	0.054	0.130	-0.049
338	2	6.5	1.25	0.70	1.22	1.11	0.79	0.36	0.833	-0.533	-0.087	-0.060	0.007	0.160
339	1	0.0	2.06	2.06	1.50	1.34	0.73	0.25	1.114	0.114	-0.065	-0.032	-0.124	0.011
339	2	16.0	0.94	0.73	0.82	0.83	0.89	0.32	0.627	-0.513	-0.353	-0.247	0.073	0.133
340	1	13.0	1.23	0.67	0.94	1.15	1.17	0.51	0.665	-0.638	-0.368	-0.135	0.114	0.151
340	2	8.5	1.07	0.89	0.98	1.05	0.72	0.41	0.713	-0.407	-0.247	-0.100	-0.040	0.193
341	1	22.5	1.22	0.85	0.76	0.96	1.20	0.52	0.659	-0.541	-0.465	-0.238	0.130	0.157
341	2	2.5	1.08	0.97	0.96	0.93	0.72	0.32	0.720	-0.353	-0.260	-0.180	-0.040	0.133
342	1	11.0	1.30	1.02	1.12	1.29	0.92	0.27	0.703	-0.449	-0.270	-0.059	-0.022	-0.005
342	2	5.0	1.21	0.93	1.21	1.09	0.69	0.11	0.807	-0.380	-0.093	-0.073	-0.060	-0.007
343	1	5.0	1.35	0.90	1.35	1.06	1.26	0.65	0.730	-0.514	-0.146	-0.184	0.162	0.227
343	2	10.0	1.13	0.49	0.98	1.13	0.95	0.65	0.753	-0.673	-0.247	-0.047	0.113	0.353
344	1	11.5	1.25	0.68	0.84	1.20	1.10	0.50	0.676	-0.632	-0.422	-0.108	0.076	0.146
344	2	6.5	1.37	1.33	1.35	1.32	0.84	0.14	0.913	-0.113	0.0	0.080	0.040	0.013
345	1	14.5	1.44	0.88	1.00	1.30	1.29	0.45	0.778	-0.524	-0.335	-0.054	0.178	0.119
345	2	7.0	1.03	0.51	0.98	1.00	0.85	0.54	0.687	-0.660	-0.247	-0.133	0.047	0.280
346	1	19.0	1.15	0.88	1.12	1.14	1.14	0.52	0.622	-0.524	-0.270	-0.141	0.097	0.157
346	2	10.0	0.99	0.38	0.93	0.99	0.86	0.28	0.650	-0.747	-0.280	-0.140	0.053	0.107
527	1	3.2	1.79	1.60	1.74	1.52	0.95	0.64	0.968	-0.135	0.065	0.065	-0.005	0.222
527	2	14.5	1.32	0.54	1.05	1.29	1.10	0.46	0.880	-0.640	-0.200	0.060	0.213	0.227
528	1	2.5	2.16	1.72	2.14	1.70	1.24	0.56	1.168	-0.070	0.281	0.162	0.151	0.178
528	2	4.5	1.10	0.85	1.09	1.00	0.93	0.48	0.733	-0.433	-0.173	-0.133	0.100	0.240
529	1	12.0	1.20	0.91	0.95	1.15	0.91	0.64	0.649	-0.508	-0.362	-0.135	-0.027	0.022
530	1	13.0	1.16	0.88	0.98	1.10	1.04	0.38	0.627	-0.524	-0.346	-0.162	0.043	0.081
530	2	6.0	1.27	0.80	1.26	1.26	0.91	0.26	0.847	-0.467	-0.060	0.040	0.087	0.093
531	1	10.0	1.15	0.86	0.94	1.15	1.13	0.25	0.622	-0.535	-0.368	-0.135	0.092	0.011
531	2	5.0	0.94	0.66	0.94	0.8?	0.84	0.36	0.627	-0.560	-0.273	-0.227	0.040	0.160
532	1	10.0	1.15	0.94	1.00	1.15	0.84	0.60	0.622	-0.492	-0.335	-0.135	-0.065	0.200
532	2	7.5	1.03	0.86	0.99	1.00	0.85	0.58	0.687	-0.427	-0.240	-0.133	0.047	0.307
533	1	7.0	1.84	1.56	1.76	1.78	1.10	0.21	0.995	-0.157	0.076	0.205	0.076	-0.011
533	2	3.0	1.29	1.19	1.19	1.16	0.80	0.28	0.860	-0.207	-0.107	-0.027	0.013	0.107
534	1	1.8	1.38	1.31	1.31	1.33	0.62	0.41	0.746	-0.292	-0.168	-0.038	-0.184	0.097
534	2	26.0	1.01	0.60	0.71	0.82	0.96	0.55	0.673	-0.600	-0.427	-0.253	0.120	0.287
535	1	10.5	1.14	1.01	0.86	1.13	0.97	0.21	0.616	-0.454	-0.411	-0.146	0.005	-0.011
535	2	6.5	1.31	0.84	1.26	1.24	0.87	0.20	0.873	-0.440	-0.060	0.027	0.060	0.053
536	1	11.0	1.51	0.95	1.16	1.45	1.15	0.25	0.816	-0.486	-0.249	0.043	0.103	0.011
536	2	4.3	1.45	1.33	1.43	1.29	0.76	0.35	0.967	-0.113	0.053	0.060	-0.013	0.153
537	1	8.7	1.55	1.10	1.46	1.52	0.91	0.43	0.838	-0.405	-0.086	0.065	-0.027	0.108
537	2	10.0	1.35	0.71	1.06	1.35	0.97	0.45	0.900	-0.527	-0.193	0.100	0.127	0.220
538	1	9.0	2.31	1.36	1.88	2.29	1.67	0.57	1.249	-0.265	0.141	0.481	0.384	0.184
538	2	14.0	1.26	0.92	1.14	1.22	1.10	0.63	0.840	-0.387	-0.140	0.013	0.213	0.340

HRMS = 0.793 0.475 0.260 0.144 0.111 0.169

F12	F13	F14	F15	F23	F24	F25	F34	F35	F45
0.8844	0.5176	-0.5263	-0.8189	0.7515	-0.2921	-0.6837	0.1078	-0.3969	0.5410

TPK	P(TPK)	HMAX	P(HMAX)	H1	P(H1)	H2	P(H2)	H3	P(H3)	H4	P(H4)	H5	P(H5)
26.0	0.011	1.249	0.011	0.114	0.011	0.281	0.011	0.481	0.011	0.384	0.011	0.353	0.011
22.5	0.032	1.168	0.032	-0.070	0.032	0.141	0.032	0.205	0.032	0.213	0.043	0.340	0.032
19.0	0.053	1.114	0.053	-0.113	0.064	0.076	0.053	0.162	0.053	0.213	0.043	0.307	0.053
16.0	0.074	0.995	0.074	-0.113	0.064	0.065	0.074	0.100	0.074	0.178	0.074	0.287	0.074
15.0	0.096	0.968	0.096	-0.135	0.096	0.053	0.096	0.080	0.096	0.162	0.096	0.280	0.096
14.5	0.128	0.967	0.117	-0.157	0.117	0.005	0.117	0.065	0.128	0.151	0.117	0.240	0.117
14.5	0.128	0.914	0.138	-0.207	0.138	0.0	0.138	0.065	0.128	0.130	0.149	0.227	0.138
14.0	0.170	0.913	0.160	-0.265	0.160	-0.060	0.170	0.06?	0.170	0.130	0.149	0.227	0.160
14.0	0.170	0.900	0.181	-0.293	0.181	-0.060	0.170	0.060	0.170	0.127	0.181	0.232	0.191
13.0	0.213	0.890	0.202	-0.340	0.202	-0.065	0.202	0.054	0.202	0.120	0.202	0.222	0.191
13.0	0.213	0.873	0.223	-0.353	0.223	-0.086	0.223	0.043	0.223	0.114	0.223	0.220	0.223
12.0	0.245	0.860	0.245	-0.380	0.245	-0.087	0.245	0.040	0.245	0.113	0.245	0.200	0.245
11.5	0.266	0.847	0.266	-0.387	0.266	-0.093	0.266	0.027	0.266	0.103	0.266	0.200	0.266
11.0	0.298	0.830	0.287	-0.405	0.287	-0.107	0.287	0.013	0.287	0.100	0.287	0.193	0.287
11.0	0.298	0.838	0.309	-0.407	0.309	-0.140	0.309	-0.027	0.309	0.097	0.309	0.184	0.309
10.5	0.330	0.833	0.330	-0.416	0.330	-0.146	0.330	-0.027	0.330	0.092	0.330	0.178	0.330
10.0	0.415	0.816	0.351	-0.427	0.351	-0.168	0.351	-0.032	0.351	0.087	0.351	0.160	0.372

10.0 0.415	0.807 0.372	-0.433 0.372	-0.173 0.372	-0.038 0.372	0.081 0.372	0.160 0.372
10.0 0.415	0.778 0.394	-0.438 0.394	-0.187 0.394	-0.047 0.404	0.076 0.404	0.160 0.372
10.0 0.415	0.767 0.415	-0.440 0.415	-0.193 0.415	-0.047 0.404	0.076 0.404	0.157 0.426
10.0 0.415	0.753 0.436	-0.449 0.436	-0.200 0.436	-0.054 0.447	0.073 0.436	0.157 0.426
10.0 0.415	0.746 0.457	-0.454 0.457	-0.240 0.457	-0.054 0.447	0.060 0.457	0.1?? 0.457
10.0 0.415	0.733 0.479	-0.467 0.479	-0.247 0.500	-0.059 0.479	0.053 0.479	0.151 0.479
9.0 0.511	0.730 0.511	-0.486 0.500	-0.247 0.500	-0.060 0.500	0.047 0.521	0.146 0.500
9.0 0.511	0.730 0.511	-0.492 0.521	-0.247 0.500	-0.073 0.521	0.047 0.521	0.133 0.532
8.7 0.543	0.720 0.543	-0.508 0.543	-0.249 0.543	-0.081 0.543	0.047 0.521	0.133 0.532
8.5 0.564	0.714 0.564	-0.513 0.564	-0.260 0.564	-0.100 0.564	0.043 0.564	0.120 0.564
7.5 0.585	0.713 0.585	-0.514 0.596	-0.270 0.596	-0.108 0.585	0.040 0.596	0.119 0.585
7.0 0.617	0.703 0.606	-0.514 0.596	-0.270 0.596	-0.133 0.623	0.040 0.596	0.114 0.606
7.0 0.617	0.687 0.638	-0.524 0.649	-0.273 0.628	-0.133 0.628	0.033 0.628	0.108 0.628
6.5 0.681	0.687 0.638	-0.524 0.649	-0.280 0.660	-0.135 0.628	0.027 0.649	0.107 0.660
6.5 0.681	0.680 0.670	-0.524 0.649	-0.280 0.660	-0.135 0.702	0.013 0.670	0.107 0.660
6.5 0.681	0.676 0.702	-0.527 0.691	-0.281 0.691	-0.135 0.702	0.007 0.691	0.097 0.691
6.5 0.681	0.676 0.702	-0.533 0.713	-0.314 0.713	-0.135 0.702	0.005 0.713	0.093 0.713
6.0 0.734	0.673 0.734	-0.535 0.734	-0.310 0.734	-0.135 0.702	-0.005 0.734	0.092 0.734
5.0 0.777	0.667 0.755	-0.540 0.755	-0.335 0.766	-0.140 0.755	-0.013 0.755	0.086 0.755
5.0 0.777	0.665 0.777	-0.541 0.777	-0.335 0.766	-0.141 0.777	-0.020 0.77?	0.081 0.777
5.0 0.777	0.660 0.798	-0.560 0.798	-0.346 0.798	-0.146 0.798	-0.022 0.798	0.053 0.798
4.5 0.819	0.659 0.819	-0.600 0.830	-0.353 0.819	-0.162 0.819	-0.027 0.830	0.013 0.819
4.3 0.840	0.649 0.840	-0.600 0.830	-0.362 0.840	-0.180 0.851	-0.027 0.830	0.011 0.862
3.2 0.862	0.627 0.862	-0.632 0.872	-0.368 0.872	-0.180 0.851	-0.040 0.872	0.011 0.862
3.0 0.883	0.627 0.894	-0.632 0.872	-0.368 0.872	-0.184 0.883	-0.040 0.872	0.011 0.862
2.5 0.915	0.627 0.894	-0.638 0.904	-0.400 0.904	-0.187 0.904	-0.060 0.904	-0.005 0.904
2.5 0.915	0.622 0.947	-0.640 0.926	-0.411 0.926	-0.227 0.926	-0.065 0.926	-0.007 0.926
2.0 0.947	0.622 0.947	-0.660 0.947	-0.422 0.947	-0.238 0.947	-0.124 0.947	-0.011 0.957
1.8 0.968	0.622 0.947	-0.673 0.968	-0.427 0.968	-0.247 0.968	-0.141 0.968	-0.011 0.957
0.0 0.989	0.616 0.989	-0.747 0.989	-0.465 0.989	-0.253 0.989	-0.184 0.989	-0.049 0.989

MACH, NOZZLE, INLET =334

SHOT	T	TPK	PMAX	P1	P2	P3	P4	P5	HMAX	H1	H2	H3	H4	H5
323	1	3.0	2.10	1.76	1.93	1.68	1.42	0.0	1.135	-0.049	0.168	0.151	0.249	-0.124
323	2	8.0	1.70	0.96	1.46	1.58	0.8	0.29	1.133	-0.360	0.073	0.253	0.060	0.113
324	1	0.0	2.82	2.82	1.77	1.44	0.63	-0.16	1.524	0.524	0.081	0.022	-0.178	-0.211
324	2	12.0	1.11	0.90	0.87	1.04	1.00	0.14	0.749	-0.400	-0.320	-0.107	0.147	0.013
325	1	20.0	1.10	1.04	0.94	1.07	1.10	0.55	0.595	-0.438	-0.368	-0.178	0.075	0.173
325	2	0.0	1.66	1.66	1.17	0.85	0.63	0.20	1.107	0.107	-0.170	-0.233	-0.100	0.053
326	1	0.0	1.20	1.20	1.13	1.05	0.82	0.34	0.649	-0.351	-0.265	-0.189	-0.076	0.059
326	2	4.5	1.47	1.26	1.47	1.23	0.63	-0.04	0.980	-0.160	0.080	0.020	-0.100	-0.107
327	1	2.0	2.19	1.75	1.88	1.62	1.05	0.22	1.184	-0.054	0.141	0.119	0.049	-0.005
327	2	0.0	2.34	2.34	1.68	1.26	0.80	0.05	1.560	0.560	0.220	0.040	0.013	-0.047
328	1	2.0	1.68	1.37	1.59	1.48	1.09	0.10	0.908	-0.259	-0.016	0.043	0.070	-0.070
328	2	7.5	1.24	1.17	1.17	1.10	0.80	0.27	0.827	-0.220	-0.120	-0.067	0.013	0.100
329	1	1.0	1.87	1.80	1.46	1.13	0.77	0.33	1.011	-0.027	-0.086	-0.146	-0.103	0.054
329	2	1.5	1.53	1.50	1.33	1.00	0.80	0.09	1.020	0.0	-0.013	-0.133	0.013	-0.020
330	1	12.0	2.50	1.00	1.37	2.45	1.70	0.10	1.351	-0.459	-0.135	0.568	0.400	-0.070
330	2	18.5	1.21	0.74	0.69	0.81	1.16	0.45	0.807	-0.507	-0.440	-0.250	0.253	0.220
331	1	0.0	3.70	3.70	2.34	2.09	1.35	-0.18	2.000	1.000	0.389	0.372	0.211	-0.222
331	2	0.0	1.71	1.71	1.33	1.22	0.95	0.27	1.140	0.140	-0.013	0.013	0.113	0.100
332	1	4.5	2.13	1.10	2.08	1.30	0.81	0.10	1.151	-0.405	0.249	-0.054	-0.081	-0.070
332	2	3.5	0.90	0.85	0.80	0.73	0.80	0.71	0.600	-0.433	-0.367	-0.313	0.013	0.393
333	1	5.0	2.55	1.10	2.55	2.13	1.60	0.70	1.378	-0.405	0.503	0.395	0.346	0.254
333	2	2.0	2.46	2.33	1.94	1.68	0.90	0.26	1.640	0.553	0.393	0.320	0.080	0.093
334	1	6.0	1.33	0.52	1.25	1.07	1.11	0.55	0.719	-0.719	-0.200	-0.178	0.081	0.173
334	2	0.0	1.58	1.53	1.45	1.14	0.75	0.18	1.053	0.020	0.067	-0.040	-0.020	0.340
515	1	20.0	1.95	0.89	1.15	1.32	1.95	0.49	1.054	-0.519	-0.254	-0.043	0.535	0.141
515	2	7.5	1.47	0.96	1.25	1.38	1.04	0.50	0.980	-0.360	-0.067	0.120	0.172	0.253
516	1	17.0	1.89	0.82	1.47	1.60	1.70	0.27	1.022	-0.557	-0.061	0.108	0.400	0.022
516	2	0.0	3.12	3.12	2.22	1.67	0.70	-0.36	2.080	1.080	0.580	0.313	-0.053	-0.320
517	1	1.2	1.36	1.31	1.24	1.28	0.84	-0.08	0.735	-0.292	-0.205	-0.065	-0.065	-0.168

```
517  2   0.0   1.05  1.05  0.74  0.77  0.86   0.30       0.700 -0.300 -0.407 -0.287  0.013  0.120
518  1   3.5   2.36  1.75  2.43  1.89  0.97   0.42       1.276 -0.054  0.38'  0.265  0.005  0.103
518  2   0.0   1.95  1.95  1.34  1.32  0.62   0.05       1.300  0.300 -0.007  0.080 -0.107 -0.047
519  1   3.5   1.78  1.65  1.76  1.68  0.90   0.0        0.962 -0.108  0.076  0.151 -0.032 -0.124
519  2   0.0   1.14  1.14  1.07  1.03  0.73   0.24       0.760 -0.240 -0.187 -0.113 -0.033  0.080
520  1  10.0   1.66  1.14  1.31  1.64  1.17   0.13       0.897 -0.384 -0.168  0.141  0.114 -0.054
520  2  12.5   1.40  0.46  0.94  1.30  1.22   0.53       0.933 -0.693 -0.273  0.067  0.293  0.273
521  1   2.5   1.35  1.27  1.34  1.21  0.72   0.31       0.730 -0.314 -0.151 -0.103 -0.130  0.043
521  2   5.0   1.33  1.00  1.33  1.07  0.65   0.52       0.887 -0.333 -0.013 -0.087 -0.087  0.267
522  1   5.5   1.32  1.12  1.30  1.27  1.06   0.40       0.714 -0.395 -0.173 -0.070  0.054  0.092
522  2   1.8   1.25  1.23  1.11  1.16  0.66   0.26       0.833 -0.180 -0.160 -0.027 -0.080  0.093
523  1   6.0   1.36  0.97  1.35  1.33  0.71   0.48       0.735 -0.476 -0.146 -0.038 -0.135  0.135
523  ?   0.0   1.46  1.46  1.32  1.06  0.66   0.62       0.973 -0.027 -0.020 -0.093 -0.080  0.333
524      1.2   1.70  1.57  1.66  1.51  1.00   0.40       0.919 -0.151  0.022  0.059  0.022  0.092
524  :   1.2   1.16  1.11  1.08  0.97  0.64   0.45       0.7'3 -0.260 -0.180 -0.153 -0.093  0.220
525  1   2.5   1.54  1.24  1.40  0.90  0.80   0.35       0.832 -0.330 -0.119 -0.270 -0.086  0.065
525  2   0.0   1.43  1.43  1.11  1.11  0.80   0.03       0.953 -0.047 -0.160 -0.960  0.013 -0.060
526  1  11.2   2.13  1.08  1.81  2.00  1.62   0.58       1.151 -0.416  0.103  0.324  0.357  0.189
526  2   9.0   2.35  2.29  1.99  2.33  1.00  -0.15       1.567  0.527  0.427  0.753  0.147 -0.180

                                    HRMS = 1.092  0.416  0.239  0.322  0.171  0.159


   F12     F13      F14      F15      F23      F24      F25      F34     F35      F45
  0.6642  0.3217 -0.3451 -0.6478   0.6976 -0.0259 -0.4514   0.4465 -0.3253  0.2364

 TPK P(TPK)  HMAX P(HMAX)    H1   P(H1)     H2   P(H2)     H3   P(H3)    H4   P(H4)     H5   P(H5)
20.0 0.021  2.080 0.010   1.080 0.010   0.580 0.010   0.753 0.010   0.535 0.010   0.393 0.010
20.0 0.021  2.000 0.031   1.000 0.031   0.503 0.031   0.568 0.031   0.400 0.042   0.333 0.031
18.5 0.052  1.640 0.052   0.560 0.052   0.427 0.052   0.395 0.052   0.400 0.042   0.273 0.052
17.0 0.073  1.557 0.073   0.553 0.073   0.393 0.073   0.373 0.073   0.357 0.073   0.267 0.073
12.5 0.094  1.560 0.094   0.527 0.094   0.389 0.094   0.324 0.094   0.346 0.094   0.254 0.094
12.0 0.125  1.524 0.115   0.524 0.115   0.384 0.115   0.320 0.115   0.293 0.115   0.253 0.115
12.0 0.125  1.378 0.135   0.300 0.135   0.249 0.135   0.313 0.135   0.253 0.135   0.220 0.146
11.2 0.156  1.351 0.156   0.140 0.156   0.220 0.156   0.265 0.156   0.249 0.156   0.220 0.146
10.0 0.177  1.300 0.177   0.107 0.177   0.168 0.177   0.253 0.177   0.211 0.177   0.189 0.177
 9.0 0.198  1.276 0.198   0.020 0.198   0.141 0.198   0.151 0.208   0.173 0.198   0.173 0.208
 8.0 0.219  1.184 0.219   0.0   0.219   0.103 0.219   0.151 0.208   0.147 0.229   0.173 0.208
 7.5 0.250  1.151 0.250  -0.027 0.240   0.081 0.240   0.141 0.240   0.147 0.229   0.141 0.240
 7.5 0.250  1.151 0.250  -0.027 0.260   0.080 0.260   0.120 0.260   0.114 0.260   0.135 0.250
 6.0 0.292  1.140 0.281  -0.047 0.281   0.076 0.281   0.119 0.281   0.113 0.281   0.120 0.281
 6.0 0.292  1.135 0.302  -0.049 0.302   0.073 0.302   0.108 0.302   0.081 0.302   0.113 0.302
 5.5 0.323  1.133 0.323  -0.054 0.333   0.067 0.323   0.080 0.323   0.080 0.323   0.103 0.323
 5.0 0.354  1.107 0.344  -0.054 0.333   0.022 0.344   0.067 0.344   0.076 0.344   0.100 0.354
 5.0 0.354  1.054 0.365  -0.108 0.365  -0.007 0.365   0.059 0.365   0.070 0.365   0.100 0.354
 4.5 0.396  1.053 0.385  -0.151 0.385  -0.013 0.406   0.043 0.385   0.060 0.385   0.093 0.396
 4.5 0.396  1.022 0.406  -0.160 0.406  -0.013 0.406   0.040 0.406   0.054 0.406   0.093 0.396
 3.5 0.448  1.020 0.427  -0.180 0.427  -0.013 0.406   0.022 0.427   0.049 0.427   0.092 0.438
 3.5 0.448  1.011 0.448  -0.220 0.448  -0.016 0.448   0.020 0.448   0.022 0.448   0.092 0.438
 3.5 0.448  0.980 0.479  -0.240 0.469  -0.020 0.469   0.013 0.469   0.013 0.521   0.080 0.469
 3.0 0.490  0.980 0.479  -0.259 0.490  -0.067 0.490  -0.027 0.490   0.013 0.521   0.065 0.490
 2.5 0.521  0.973 0.510  -0.260 0.510  -0.061 0.510  -0.038 0.510   0.013 0.521   0.059 0.510
 2.5 0.521  0.962 0.531  -0.292 0.531  -0.086 0.531  -0.040 0.531   0.013 0.521   0.054 0.531
 2.0 0.573  0.953 0.552  -0.300 0.552  -0.119 0.552  -0.043 0.552   0.013 0.521   0.053 0.552
 2.0 0.573  0.933 0.573  -0.314 0.573  -0.120 0.583  -0.054 0.573   0.013 0.521   0.043 0.573
 2.0 0.573  0.919 0.594  -0.330 0.594  -0.120 0.583  -0.060 0.594   0.005 0.594   0.040 0.594
 1.8 0.615  0.908 0.615  -0.333 0.615  -0.135 0.615  -0.065 0.615  -0.020 0.615   0.022 0.615
 1.5 0.635  0.897 0.635  -0.351 0.635  -0.146 0.635  -0.067 0.635  -0.032 0.635   0.013 0.635
 1.2 0.677  0.887 0.656  -0.360 0.667  -0.151 0.656  -0.070 0.656  -0.033 0.656  -0.005 0.656
 1.2 0.677  0.833 0.677  -0.360 0.667  -0.160 0.688  -0.087 0.677  -0.053 0.677  -0.020 0.677
 1.2 0.677  0.832 0.698  -0.384 0.698  -0.160 0.688  -0.093 0.698  -0.065 0.698  -0.047 0.708
 1.0 0.719  0.827 0.719  -0.395 0.719  -0.168 0.719  -0.103 0.719  -0.076 0.719  -0.047 0.708
 0.0 0.865  0.807 0.740  -0.400 0.740  -0.173 0.740  -0.107 0.740  -0.080 0.750  -0.054 0.740
 0.0 0.865  0.773 0.760  -0.405 0.771  -0.180 0.760  -0.113 0.760  -0.060 0.750  -0.060 0.760
 0.0 0.865  0.760 0.781  -0.405 0.771  -0.187 0.781  -0.133 0.781  -0.081 0.781  -0.070 0.802
 0.0 0.865  0.740 0.802  -0.416 0.802  -0.200 0.802  -0.146 0.802  -0.086 0.802  -0.070 0.802
 0.0 0.865  0.735 0.833  -0.433 0.823  -0.205 0.823  -0.153 0.823  -0.087 0.823  -0.070 0.802
 0.0 0.865  0.735 0.833  -0.438 0.844  -0.254 0.844  -0.178 0.854  -0.093 0.844  -0.107 0.844
 0.0 0.865  0.730 0.865  -0.459 0.865  -0.265 0.865  -0.178 0.854  -0.100 0.875  -0.124 0.875
 0.0 0.865  0.719 0.885  -0.476 0.885  -0.273 0.885  -0.189 0.885  -0.100 0.875  -0.124 0.875
 0.0 0.865  0.714 0.906  -0.507 0.906  -0.320 0.906  -0.233 0.906  -0.103 0.906  -0.168 0.906
 0.0 0.865  0.700 0.927  -0.519 0.927  -0.367 0.927  -0.260 0.927  -0.107 0.927  -0.180 0.927
 0.0 0.865  0.649 0.948  -0.557 0.948  -0.368 0.948  -0.270 0.948  -0.130 0.948  -0.211 0.948
 0.0 0.865  0.600 0.969  -0.693 0.969  -0.407 0.969  -0.287 0.969  -0.135 0.969  -0.222 0.969
 0.0 0.865  0.595 0.990  -0.719 0.990  -0.440 0.990  -0.313 0.970  -0.178 0.990  -0.320 0.990
```

MACH. NOZZLE, INLET =341

SHOT	T	TPK	PMAX	P1	P2	P3	P4	P5	HMAX	H1	H2	H3	H4	H5
478	1	6.5	1.74	0.66	1.63	1.68	0.90	0.19	0.941	-0.643	0.005	0.151	-0.032	-0.022
478	2	9.0	1.32	1.26	1.25	1.30	0.88	0.18	0.880	-0.160	-0.067	0.067	0.067	0.040
479	1	0.5	2.62	2.60	1.90	1.85	0.85	0.03	1.416	0.405	0.151	0.243	-0.059	-0.108
479	2	1.6	1.26	0.64	1.05	1.14	1.22	0.40	0.840	-0.573	-0.200	-0.040	0.293	0.187
480	1	1.0	1.74	1.72	1.30	1.30	1.27	0.10	0.941	-0.070	-0.173	-0.054	0.168	-0.070
480	2	4.0	1.36	1.12	1.34	1.07	0.62	0.21	0.907	-0.253	-0.007	-0.087	-0.107	0.060
481	1	3.0	1.55	1.32	1.40	1.15	0.79	0.30	0.838	-0.286	-0.113	-0.135	-0.092	0.038
481	2	9.0	2.00	1.23	1.84	1.93	0.95	0.40	1.333	-0.180	0.327	0.487	0.113	0.187
482	1	3.5	3.75	2.60	3.60	1.80	1.00	-0.01	2.027	0.405	1.070	0.216	0.022	-0.130
482	2	8.5	1.45	0.53	1.32	1.3_	0.84	0.67	0.967	-0.647	-0.020	0.080	0.040	0.367
483	1	1.5	2.75	2.50	2.40	2.53	0.89	0.11	1.486	0.351	0.422	0.611	-0.038	-0.065
483	2	3.5	1.16	0.97	1.15	1.15	0.93	0.30	0.773	-0.353	-0.133	-0.033	0.100	0.120
484	1	0.0	2.72	2.72	1.45	1.45	0.97	-0.03	1.470	0.470	-0.092	0.027	0.005	-0.141
484	2	10.0	1.15	0.88	1.00	1.15	1.08	0.25	0.767	-0.413	-0.233	-0.033	0.200	0.087
485	1	3.0	2.57	2.00	2.14	1.38	0.92	0.11	1.389	0.081	0.281	-0.011	-0.022	-0.065
485	2	10.0	1.33	1.31	1.21	1.35	0.90	0.36	0.887	-0.127	-0.093	0.097	0.080	0.160
486	1	2.0	2.80	2.40	2.45	1.74	0.79	-0.22	1.514	0.297	0.449	0.184	-0.092	-0.243
486	2	12.5	1.11	0.73	0.95	1.06	0.93	0.26	0.740	-0.513	-0.267	-0.093	0.100	0.093
487	1	9.0	1.74	0.90	1.52	1.70	1.15	0.44	0.941	-0.514	-0.054	0.162	0.103	0.114
487	2	10.0	2.00	0.70	1.13	2.00	1.20	0.11	1.333	-0.533	-0.147	0.533	0.280	-0.007
488	1	6.5	1.46	1.00	1.38	1.36	1.12	0.46	0.789	-0.459	-0.130	-0.022	0.086	0.124
488	2	0.0	1.68	1.68	1.30	1.04	0.89	0.14	1.120	0.120	-0.033	-0.107	0.073	0.013
489	1	6.5	1.76	1.16	1.55	1.70	1.60	0.60	0.951	-0.373	-0.032	0.162	0.346	0.200
489	2	8.5	1.50	1.07	1.33	1.36	0.85	0.37	1.000	-0.287	-0.013	0.107	0.047	0.167

HRMS = 1.139   0.393   0.291   0.223   0.138   0.142

F12	F13	F14	F15	F23	F24	F25	F34	F35	F45
0.4925	-0.0436	-0.5927	-0.7708	0.4709	-0.2701	-0.3862	0.2898	0.0303	0.5333

TPK	P(TPK)	HMAX	P(HMAX)	H1	P(H1)	H2	P(H2)	H3	P(H3)	H4	P(H4)	H5	P(H5)
12.5	0.021	2.027	0.021	0.470	0.021	1.070	0.021	0.611	0.021	0.346	0.021	0.367	0.021
10.0	0.104	1.514	0.065	0.405	0.083	0.449	0.063	0.533	0.063	0.293	0.063	0.200	0.063
10.0	0.104	1.486	0.104	0.405	0.083	0.422	0.104	0.487	0.104	0.280	0.104	0.187	0.125
10.0	0.104	1.470	0.146	0.351	0.146	0.327	0.146	0.243	0.146	0.200	0.146	0.187	0.125
9.0	0.229	1.416	0.188	0.297	0.188	0.281	0.188	0.216	0.188	0.168	0.188	0.167	0.188
9.0	0.229	1.389	0.229	0.120	0.229	0.151	0.229	0.184	0.229	0.113	0.229	0.160	0.229
9.0	0.229	1.333	0.292	0.081	0.271	0.005	0.271	0.162	0.292	0.103	0.271	0.124	0.271
8.5	0.354	1.333	0.292	-0.007	0.313	-0.007	0.313	0.162	0.292	0.100	0.333	0.120	0.313
8.5	0.354	1.120	0.354	-0.127	0.354	-0.013	0.354	0.151	0.354	0.100	0.333	0.114	0.354
8.5	0.354	1.000	0.396	-0.160	0.396	-0.020	0.396	0.107	0.396	0.086	0.396	0.093	0.396
6.5	0.479	0.967	0.438	-0.180	0.438	-0.032	0.438	0.087	0.438	0.080	0.438	0.087	0.438
6.5	0.479	0.951	0.479	-0.253	0.479	-0.033	0.479	0.080	0.479	0.073	0.479	0.060	0.479
6.5	0.479	0.941	0.563	-0.286	0.521	-0.054	0.521	0.067	0.521	0.067	0.521	0.040	0.521
4.0	0.563	0.941	0.563	-0.287	0.563	-0.067	0.563	0.027	0.563	0.047	0.563	0.038	0.563
3.5	0.604	0.941	0.563	-0.353	0.604	-0.092	0.604	-0.011	0.604	0.040	0.604	0.013	0.604
3.0	0.667	0.907	0.646	-0.373	0.646	-0.093	0.646	-0.022	0.646	0.022	0.646	-0.007	0.646
3.0	0.667	0.887	0.688	-0.413	0.688	-0.119	0.688	-0.033	0.708	0.005	0.688	-0.022	0.688
2.0	0.729	0.880	0.729	-0.459	0.729	-0.130	0.729	-0.033	0.708	-0.022	0.729	-0.065	0.750
1.6	0.771	0.840	0.771	-0.513	0.771	-0.133	0.771	-0.040	0.771	-0.032	0.771	-0.065	0.750
1.5	0.813	0.838	0.813	-0.514	0.813	-0.147	0.813	-0.054	0.813	-0.038	0.813	-0.070	0.813
1.0	0.854	0.789	0.854	-0.533	0.854	-0.173	0.854	-0.087	0.854	-0.059	0.854	-0.108	0.854
0.5	0.896	0.773	0.896	-0.373	0.896	-0.200	0.896	-0.093	0.896	-0.092	0.917	-0.130	0.896
0.0	0.958	0.767	0.938	-0.643	0.938	-0.233	0.938	-0.107	0.938	-0.092	0.917	-0.141	0.938
0.0	0.958	0.740	0.979	-0.647	0.979	-0.267	0.979	-0.135	0.979	-0.107	0.979	-0.243	0.979

MACH, NOZZLE, INLET =344

SHOT	T	TPK	PMAX	P1	P2	P3	P4	P5		HMAX	H1	H2	H3	H4	H5
464	1	20.0	1.92	0.44	0.80	1.23	1.92	0.64		1.038	-0.762	-0.443	-0.092	0.519	0.222
464	2	35.0	0.95	0.24	0.49	0.45	0.63	0.76		0.633	-0.840	-0.573	-0.500	-0.100	0.427
465	1	6.5	1.71	1.02	1.65	1.42	0.99	0.66		0.924	-0.449	0.016	0.011	0.016	0.232
465	2	7.0	1.54	1.25	1.47	1.30	0.60	0.70		1.027	-0.167	0.080	0.067	-0.120	0.387
466	1	8.5	2.95	0.74	2.40	2.76	1.92	-0.26		1.595	-0.600	0.422	0.735	0.519	-0.265
466	2	3.5	1.04	0.14	0.34	0.65	0.76	0.85		0.692	-0.907	-0.673	-0.367	-0.013	0.487
467	1	8.7	1.66	0.25	0.75	1.58	0.65	0.45		0.897	-0.865	-0.470	0.097	-0.168	0.119
467	2	5.0	1.20	0.30	1.20	0.84	0.65	0.65		0.800	-0.800	-0.100	-0.240	-0.087	0.353
468	1	10.0	1.60	0.35	0.88	1.60	1.06	1.04		0.865	-0.811	-0.400	0.108	0.054	0.438
468	2	5.5	1.31	0.40	1.30	1.26	0.91	0.83		0.873	-0.733	-0.033	0.053	0.087	0.473
469	1	18.0	1.28	0.78	1.23	1.04	1.10	0.93		0.692	-0.578	-0.211	-0.195	0.076	0.378
469	2	18.0	1.42	0.17	0.45	0.75	1.23	0.72		0.947	-0.887	-0.600	-0.300	0.300	0.400
470	1	13.0	1.45	0.32	0.88	1.10	1.44	0.60		0.784	-0.827	-0.400	-0.162	0.259	0.200
470	2	0.0	2.82	2.82	1.95	1.30	0.54	0.30		1.880	0.880	0.400	0.067	-0.160	0.120
471	1	16.0	1.63	0.65	1.10	1.20	1.27	0.80		0.881	-0.649	-0.281	-0.108	0.168	0.308
471	2	5.0	1.62	0.52	1.62	1.35	1.44	0.40		1.080	-0.653	0.180	0.100	0.440	0.187
472	1	26.0	2.22	0.70	1.04	1.15	1.33	0.96		1.200	-0.622	-0.314	-0.135	0.200	0.395
472	2	0.0	2.66	2.66	1.82	1.48	0.80	0.34		1.773	0.773	0.313	0.187	0.013	0.147
473	1	26.5	1.50	0.66	0.96	0.86	0.98	0.66		0.811	-0.643	-0.357	-0.292	0.011	0.232
473	2	8.0	2.02	0.35	1.10	1.78	0.98	0.48		1.347	-0.767	-0.167	0.387	0.133	0.240
474	1	16.5	1.71	0.60	1.33	1.33	1.24	0.34		0.924	-0.676	-0.157	-0.038	0.151	0.059
474	2	11.0	0.98	0.40	0.56	0.96	0.90	0.27		0.653	-0.733	-0.527	-0.160	0.080	0.100
475	1	14.0	1.43	0.15	0.70	1.15	0.80	1.19		0.773	-0.919	-0.497	-0.135	-0.086	0.519
475	2	2.0	2.62	2.30	2.20	1.70	0.87	0.15		1.747	0.533	0.567	0.333	0.060	0.020

HRMS = 1.096   0.731   0.388   0.262   0.216   0.313

F12	F13	F14	F15	F23	F24	F25	F34	F35	F45
0.7993	0.3240	-0.4821	-0.7400	0.6855	-0.1475	-0.6663	0.2222	-0.4346	0.1871

TPK	P(TPK)	HMAX	P(HMAX)	H1	P(H1)	H2	P(H2)	H3	P(H3)	H4	P(H4)	H5	P(H5)
35.0	0.021	1.880	0.021	0.880	0.021	0.567	0.021	0.735	0.021	0.519	0.042	0.519	0.021
26.5	0.063	1.773	0.063	0.773	0.063	0.422	0.063	0.387	0.063	0.519	0.042	0.487	0.063
26.0	0.104	1.747	0.104	0.533	0.104	0.400	0.104	0.333	0.104	0.440	0.104	0.473	0.104
20.0	0.146	1.595	0.146	-0.167	0.146	0.313	0.146	0.187	0.146	0.300	0.146	0.438	0.146
18.0	0.208	1.347	0.188	-0.449	0.188	0.180	0.188	0.108	0.188	0.259	0.188	0.427	0.188
18.0	0.208	1.200	0.229	-0.578	0.229	0.080	0.229	0.100	0.229	0.200	0.229	0.400	0.229
16.5	0.271	1.080	0.271	-0.600	0.271	0.016	0.271	0.097	0.271	0.168	0.271	0.395	0.271
16.0	0.313	1.038	0.313	-0.622	0.313	-0.033	0.313	0.067	0.333	0.151	0.313	0.387	0.313
14.0	0.354	1.027	0.354	-0.643	0.354	-0.100	0.354	0.067	0.333	0.133	0.354	0.378	0.354
13.0	0.396	0.947	0.396	-0.649	0.396	-0.157	0.396	0.053	0.396	0.087	0.396	0.353	0.396
11.0	0.438	0.924	0.458	-0.653	0.438	-0.167	0.438	0.011	0.438	0.080	0.438	0.308	0.438
10.0	0.479	0.924	0.458	-0.676	0.479	-0.211	0.479	-0.038	0.479	0.076	0.479	0.240	0.479
8.7	0.521	0.897	0.521	-0.733	0.542	-0.281	0.521	-0.092	0.521	0.060	0.521	0.232	0.542
8.5	0.563	0.881	0.563	-0.733	0.542	-0.314	0.563	-0.108	0.563	0.054	0.563	0.232	0.542
8.0	0.604	0.873	0.604	-0.762	0.604	-0.357	0.604	-0.135	0.625	0.016	0.604	0.222	0.604
7.0	0.646	0.865	0.646	-0.767	0.667			-0.135	0.625	0.013	0.646	0.200	0.646
6.5	0.688	0.811	0.688	-0.800	0.688	-0.400	0.667	-0.160	0.688	0.011	0.688	0.187	0.688
5.5	0.729	0.800	0.729	-0.811	0.729	-0.443	0.729	-0.162	0.729	-0.013	0.729	0.147	0.729
5.0	0.792	0.784	0.771	-0.827	0.771	-0.470	0.771	-0.195	0.771	-0.086	0.771	0.120	0.771
5.0	0.792	0.773	0.813	-0.840	0.813	-0.497	0.813	-0.240	0.813	-0.087	0.813	0.119	0.813
3.5	0.854	0.693	0.854	-0.865	0.854	-0.527	0.854	-0.292	0.854	-0.100	0.854	0.100	0.854
2.0	0.896	0.692	0.896	-0.907	0.896	-0.573	0.896	-0.300	0.896	-0.120	0.896	0.059	0.896
0.0	0.958	0.653	0.938	-0.907	0.938	-0.600	0.938	-0.367	0.938	-0.160	0.938	0.020	0.938
0.0	0.958	0.633	0.979	-0.919	0.979	-0.673	0.979	-0.500	0.979	-0.168	0.979	-0.265	0.979

MACH, NOZZLE, INLET =351

SHOT	T	TPK	PMAX	P1	P2	P3	P4	P5	HMAX	H1	H2	H3	H4	H5
491	1	1.5	1.65	1.50	1.43	1.45	1.04	0.29	0.892	-0.189	-0.070	0.027	0.043	0.032
491	2	0.0	2.15	2.15	1.47	1.32	0.85	-0.09	1.433	0.433	0.080	0.080	0.047	-0.140
492	1	1.3	1.73	1.66	1.62	1.49	1.06	0.20	0.935	-0.103	0.0	0.049	0.054	-0.014
492	2	0.0	1.54	1.54	1.36	1.29	0.84	0.16	1.027	0.027	0.007	0.060	0.040	0.027
493	1	0.5	2.04	2.02	1.56	1.57	0.90	0.12	1.103	0.092	-0.032	0.092	-0.032	-0.059
493	2	2.5	1.35	1.31	1.31	1.20	0.84	0.13	0.900	-0.127	-0.027	0.0	0.040	0.007
494	1	0.5	2.06	2.03	1.69	1.55	0.84	0.0	1.114	0.097	0.038	0.081	-0.065	-0.124
494	2	0.0	1.42	1.42	1.20	1.09	0.67	0.13	0.947	-0.053	-0.100	-0.073	-0.073	0.007
495	1	0.8	2.69	2.60	2.40	1.84	1.03	0.23	1.454	0.405	0.422	0.238	0.038	0.0
495	2	4.0	1.35	1.33	1.34	1.20	0.78	0.27	0.900	-0.113	-0.007	0.0	0.0	0.100
496	1	8.0	1.91	1.47	1.72	1.81	1.24	0.19	1.032	-0.205	0.054	0.222	0.151	-0.022
496	2	0.0	1.63	1.63	1.35	1.21	0.80	0.12	1.087	0.087	0.0	0.007	0.013	0.0
497	1	3.5	1.57	1.30	1.55	1.49	1.00	0.20	0.849	-0.297	-0.038	0.043	0.022	-0.016
497	2	3.0	1.49	1.45	1.40	1.32	0.86	0.15	0.993	-0.033	0.033	0.080	0.053	0.020
498	1	1.4	2.14	2.04	1.75	1.66	0.90	0.20	1.157	0.103	0.070	0.032	-0.032	-0.016
498	2	0.0	1.70	1.70	1.52	1.30	0.82	0.09	1.133	0.133	0.113	0.067	0.027	-0.020
499	1	1.8	2.21	2.00	1.92	1.80	1.28	0.40	1.195	0.081	0.162	0.216	0.173	0.092
499	2	0.8	1.69	1.68	1.49	1.29	0.80	0.31	1.127	0.120	0.093	0.060	0.013	0.127
500	1	1.4	2.15	2.05	1.82	1.70	1.11	0.29	1.152	0.108	0.108	0.162	0.081	0.032
500	2	0.0	1.61	1.61	1.50	1.28	0.82	0.12	1.073	0.073	0.100	0.053	0.027	0.0
501	1	1.2	1.57	1.47	1.51	1.49	0.85	0.23	0.849	-0.205	-0.059	0.049	-0.059	0.0
501	2	7.5	1.34	1.28	1.28	1.27	0.90	0.14	0.893	-0.147	-0.047	0.047	0.080	0.013
502	1	1.4	1.63	1.54	1.44	1.34	0.98	0.40	0.881	-0.168	-0.097	-0.032	0.011	0.092
502	2	0.0	1.53	1.53	1.38	1.22	0.86	0.10	1.020	0.020	0.020	0.013	0.053	-0.013

HRMS = 1.060 0.176 0.111 0.100 0.065 0.060

F12	F13	F14	F15	F23	F24	F25	F34	F35	F45
0.6992	0.3032	0.0022	-0.3209	0.7391	0.4169	-0.0030	0.7077	-0.0083	0.2546

TPK	P(TPK)	HMAX	P(HMAX)	H1	P(H1)	H2	P(H2)	H3	P(H3)	H4	P(H4)	H5	P(H5)
8.0	0.021	1.454	0.021	0.433	0.021	0.422	0.021	0.238	0.021	0.173	0.021	0.127	0.021
7.5	0.063	1.433	0.063	0.405	0.063	0.162	0.063	0.222	0.063	0.151	0.063	0.100	0.063
4.0	0.104	1.195	0.104	0.133	0.104	0.113	0.104	0.216	0.104	0.081	0.104	0.092	0.125
3.5	0.146	1.162	0.146	0.120	0.146	0.108	0.146	0.162	0.146	0.080	0.146	0.092	0.125
3.0	0.188	1.157	0.188	0.108	0.188	0.100	0.188	0.092	0.188	0.054	0.188	0.032	0.208
2.5	0.229	1.133	0.229	0.103	0.229	0.093	0.229	0.081	0.229	0.053	0.250	0.032	0.208
1.8	0.271	1.127	0.271	0.097	0.271	0.080	0.271	0.080	0.292	0.053	0.250	0.027	0.271
1.5	0.313	1.114	0.313	0.092	0.313	0.070	0.313	0.080	0.292	0.047	0.313	0.020	0.313
1.4	0.396	1.103	0.354	0.087	0.354	0.054	0.354	0.067	0.354	0.043	0.354	0.013	0.354
1.4	0.396	1.087	0.396	0.081	0.396	0.038	0.396	0.060	0.417	0.040	0.417	0.007	0.417
1.4	0.396	1.073	0.438	0.073	0.438	0.033	0.438	0.060	0.417	0.040	0.417	0.007	0.417
1.3	0.479	1.032	0.479	0.027	0.479	0.020	0.479	0.053	0.479	0.038	0.479	0.0	0.542
1.2	0.521	1.027	0.521	0.020	0.521	0.007	0.521	0.049	0.563	0.027	0.542	0.0	0.542
0.8	0.583	1.020	0.563	-0.033	0.563	0.0	0.583	0.049	0.563	0.027	0.542	0.0	0.542
0.8	0.583	0.993	0.604	-0.053	0.604	0.0	0.583	0.049	0.563	0.022	0.604	0.0	0.542
0.5	0.667	0.947	0.646	-0.103	0.646	-0.007	0.646	0.047	0.646	0.013	0.667	-0.013	0.646
0.5	0.667	0.935	0.688	-0.113	0.688	-0.027	0.688	0.032	0.688	0.013	0.667	-0.016	0.729
0.0	0.854	0.900	0.750	-0.127	0.729	-0.032	0.729	0.027	0.729	0.011	0.729	-0.016	0.729
0.0	0.854	0.900	0.750	-0.147	0.771	-0.038	0.771	0.013	0.771	0.0	0.771	-0.016	0.729
0.0	0.854	0.893	0.813	-0.168	0.813	-0.047	0.813	0.007	0.813	-0.032	0.833	-0.020	0.813
0.0	0.854	0.892	0.854	-0.189	0.854	-0.059	0.854	0.0	0.875	-0.032	0.833	-0.022	0.854
0.0	0.854	0.881	0.896	-0.205	0.917	-0.070	0.896	0.0	0.875	-0.059	0.896	-0.059	0.896
0.0	0.854	0.849	0.958	-0.205	0.917	-0.097	0.933	-0.032	0.938	-0.065	0.938	-0.124	0.938
0.0	0.854	0.849	0.958	-0.297	0.979	-0.100	0.979	-0.073	0.979	-0.073	0.979	-0.140	0.979

MACH, NOZZLE, INLET =354

SHOT	Γ	TPK	PMAX	P1	P2	P3	P4	F5		HMAX	H1	H2	H3	H4	H5
503	1	12.5	2.23	0.76	1.27	1.95	1.51	0.49		1.205	-0.589	-0.189	0.297	0.297	0.141
503	2	4.5	1.63	1.10	1.59	1.27	0.70	0.28		1.087	-0.267	0.160	0.047	-0.053	0.107
504	1	8.5	1.93	1.33	1.75	1.90	1.06	0.20		1.043	-0.281	0.070	0.270	0.054	-0.016
504	2	8.0	1.70	1.20	1.46	1.60	0.98	0.18		1.133	-0.200	0.073	0.267	0.133	0.040
505	1	16.5	1.67	1.17	1.27	1.33	1.59	0.10		0.903	-0.368	-0.189	-0.038	0.341	-0.070
505	2	3.0	1.29	1.20	1.10	0.94	0.75	0.34		0.860	-0.200	-0.167	-0.173	-0.020	0.147
506	1	2.2	2.09	1.93	1.93	1.65	0.92	0.33		1.130	0.043	0.178	0.135	-0.022	0.054
506	2	0.0	2.02	2.02	1.60	1.50	1.00	-0.10		1.347	0.347	0.167	0.200	0.147	-0.147
508	1	0.5	1.91	1.81	1.50	1.75	1.34	0.18		1.032	-0.022	-0.065	0.189	0.205	-0.027
508	2	0.0	1.65	1.65	1.15	1.26	1.00	0.27		1.100	0.100	-0.133	0.040	0.147	0.100
509	1	18.5	1.69	0.72	0.98	1.02	1.65	0.60		0.914	-0.611	-0.346	-0.205	0.373	0.200
509	2	2.9	2.42	1.82	1.91	1.20	0.98	0.34		1.613	0.213	0.373	0.0	0.133	0.147
510	1	6.5	2.22	0.70	1.80	1.93	1.06	0.20		1.200	-0.622	0.097	0.286	0.054	-0.016
510	2	2.5	2.36	1.85	1.94	1.23	0.60	-0.11		1.573	0.233	0.393	0.020	-0.120	-0.153
511	1	0.5	1.86	1.84	1.32	1.60	1.20	0.46		1.005	-0.005	-0.162	0.108	0.130	0.124
511	2	0.7	1.84	1.81	1.50	1.18	0.87	0.20		1.227	0.207	0.100	-0.013	0.060	0.053
512	1	2.0	2.15	1.97	1.80	1.65	1.05	0.15		1.162	0.065	0.097	0.135	0.049	-0.043
512	2	5.0	1.53	1.50	1.53	1.52	0.91	0.14		1.020	0.0	0.120	0.213	0.087	0.013
513	1	15.5	1.18	0.90	1.00	1.09	1.13	0.26		0.638	-0.514	-0.335	-0.168	0.092	0.016
513	2	12.5	1.18	0.71	0.91	1.12	1.02	0.43		0.787	-0.527	-0.293	-0.053	0.160	0.207
514	1	9.5	1.30	1.05	1.05	1.29	1.07	0.42		0.703	-0.432	-0.308	-0.059	0.059	0.103
514	2	4.0	1.92	1.64	1.75	1.31	0.70	0.34		1.280	0.093	0.267	0.073	-0.053	0.147

HRMS = 1.115   0.336   0.220   0.165   0.159   0.112

F12	F13	F14	F15	F23	F24	F25	F34	F35	F45
0.6302	-0.0728	-0.5699	-0.4991	0.3772	-0.4614	-0.3650	0.2434	-0.1008	0.4156

TPK	P(TPK)	HMAX	P(HMAX)	H1	P(H1)	H2	P(H2)	H3	P(H3)	H4	P(H4)	H5	P(H5)
18.5	0.023	1.613	0.023	0.347	0.023	0.393	0.023	0.297	0.023	0.373	0.023	0.207	0.023
16.5	0.068	1.573	0.068	0.233	0.068	0.373	0.068	0.286	0.068	0.341	0.068	0.200	0.068
15.5	0.114	1.347	0.114	0.213	0.114	0.267	0.114	0.270	0.114	0.297	0.114	0.147	0.159
12.5	0.182	1.280	0.159	0.207	0.159	0.178	0.159	0.267	0.159	0.205	0.159	0.147	0.159
12.5	0.182	1.227	0.205	0.100	0.205	0.167	0.205	0.213	0.205	0.160	0.205	0.147	0.159
9.5	0.250	1.205	0.250	0.093	0.250	0.160	0.250	0.200	0.250	0.147	0.273	0.141	0.250
8.5	0.295	1.200	0.295	0.065	0.295	0.120	0.295	0.189	0.295	0.147	0.273	0.124	0.295
8.0	0.341	1.162	0.341	0.043	0.341	0.100	0.341	0.135	0.364	0.133	0.364	0.107	0.341
6.5	0.386	1.133	0.386	0.0	0.386	0.097	0.409	0.135	0.364	0.133	0.364	0.103	0.386
5.0	0.432	1.130	0.432	-0.005	0.432	0.097	0.409	0.108	0.432	0.130	0.432	0.100	0.432
4.5	0.477	1.100	0.477	-0.022	0.477	0.073	0.477	0.073	0.477	0.092	0.477	0.054	0.477
4.0	0.523	1.087	0.523	-0.200	0.545	0.070	0.523	0.047	0.523	0.087	0.523	0.053	0.523
3.0	0.568	1.043	0.568	-0.200	0.545	-0.065	0.568	0.040	0.568	0.060	0.568	0.040	0.568
2.9	0.614	1.032	0.614	-0.267	0.614	-0.133	0.614	0.020	0.614	0.059	0.614	0.016	0.614
2.5	0.659	1.020	0.659	-0.281	0.659	-0.162	0.659	0.0	0.659	0.054	0.682	0.013	0.659
2.2	0.705	1.005	0.705	-0.368	0.705	-0.167	0.705	-0.013	0.705	0.054	0.682	-0.016	0.727
2.0	0.750	0.914	0.750	-0.432	0.750	-0.189	0.773	-0.038	0.750	0.049	0.750	-0.016	0.727
0.7	0.795	0.903	0.795	-0.514	0.795	-0.189	0.773	-0.053	0.795	-0.020	0.795	-0.027	0.795
0.5	0.864	0.860	0.841	-0.527	0.841	-0.293	0.841	-0.059	0.841	-0.022	0.841	-0.043	0.841
0.5	0.864	0.787	0.886	-0.589	0.886	-0.308	0.886	-0.168	0.886	-0.053	0.909	-0.070	0.886
0.0	0.955	0.703	0.932	-0.611	0.932	-0.335	0.932	-0.173	0.932	-0.053	0.909	-0.147	0.932
0.0	0.955	0.638	0.977	-0.622	0.977	-0.346	0.977	-0.205	0.977	-0.120	0.977	-0.153	0.977

APPENDIX D
DEVELOPMENT OF THE ASPIRATING PROBE SENSORS

The TSI anemometer units and a vacuum pump were used to drive several aspirating probes which were used as described in Reference 9 in an attempt to develop a sensor capable of measuring the boom signature pressures with a higher degree of fidelity than was possible using the B and K microphones. A total of six aspirating probes were used; four were custom built by Dr. A.B. Bauer and the other two were TSI models 1440E and 1440F. The custom-built probes had orifices approximately 0.024 inches in diameter; for record keeping they were numbered 520, 521, 522, and 523. In order to obtain maximum signal to noise ratio with these probes some experimentation was done with wire types. The hot-wire material used was 90 percent platinum and 10 percent rhodium. Pure platinum wire was available and theoretically would have given a larger signal-to-noise ratio because of a higher α, the temperature coefficient of resistance, but this was not tried because of the lesser tensile strength of pure platinum. Wire breakage was a problem with the platinum-rhodium wire possibly because of minute sand and/or dust particles aspirated through the probe. The wire length was varied between 0.023 inches, and 0.035 inches according to the probe used. The wire diameters used were 50, 70, and 100 microinches. The smaller wires had a larger theoretical signal-to-noise ratio but were also more fragile.

As discussed in Reference 9, the aspirating probe has the advantage of frequency response up to 500 kilohertz as compared with only 140 or so kilohertz for the B and K 4138 microphones. The disadvantage of the aspirating probe, as compared to the microphone, is a low signal-to-noise ratio. For example, Reference 9 predicts a noise level of 8.5×10^{-3} volts rms whereas the signal is 42×10^{-3} volts/psi. In table 1 of Reference 9 the overpressure for the large or "A" projectile is 0.69 psi; if this is reflected off a ground plane the amplitude is doubled and the signal level would be 58×10^{-3} volts for a signal-to-noise ratio N_{CT} of only 6.8, which is none too good. Furthermore, since Reference 9 was written the ground plane of the experiments was moved to 15 feet from the projectile path so that the N-wave

201

overpressure would be only about 0.27 psi instead of 0.69 psi. To make matters worse, the smaller projectiles have been of much more interest than the A projectiles because of their small overpressures. During November 1969, aspirating probe tests were run using 0.46 caliber bullets whose microphone signature is shown in figure Dla. Here the reflected N-wave pressure is only 0.28 psi so that the above implies a signal level 11.6×10^{-3} volts for an N_{CT} of only 1.4. This is for the leading edge of the N-wave; any perturbations or other features of the wave might be much smaller so that the signal would be almost undistinguishable from the noise.

Fortunately something can be done to greatly improve the situation. To fully understand this one must review the underlying theory. This had been worked out by Freymuth (References 10 and 11), but this needs to be discussed for the specific case of the aspirating probe. The heat transfer from the wire is

$$Q = I^2 R = \pi k \ell (T_w - T_R) Nu \tag{D1}$$

where the wire resistance R is

$$R = R_o + \alpha R_o (T_w - T_o) \tag{D2}$$

and where

I = wire current

k = fluid thermal conductivity
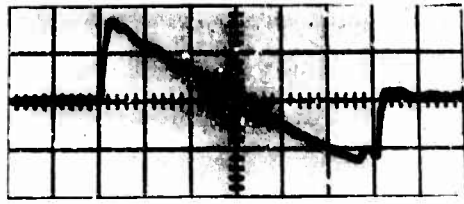
ℓ = wire length

T_w = wire temperature

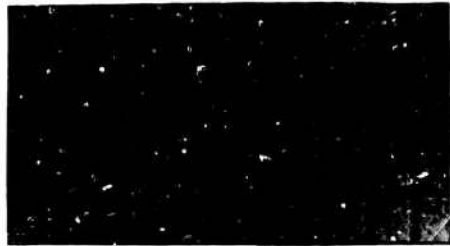T_R = wire recovery temperature for an unheated wire

T_o = a reference temperature, usually ambient
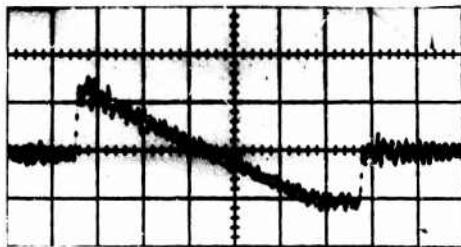
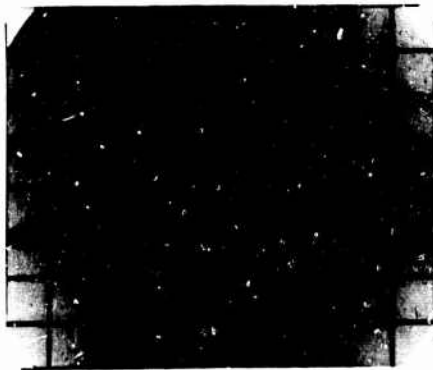R_o = wire resistance at temperature T_o

Nu = Nusselt number
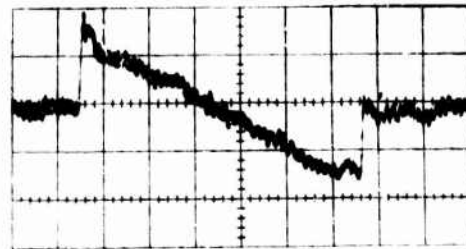
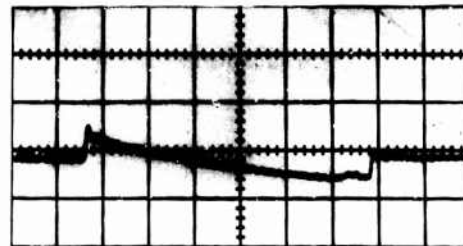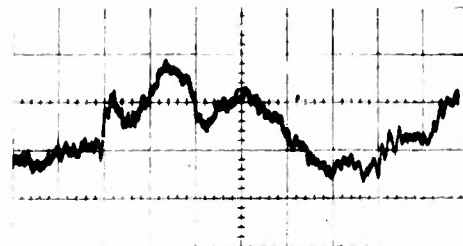Figure 31 Aspirating probe and microphone scnic boom signatures.
0.46 caliber bullets, M = 2.16.   The horizontal scales are 50 μsec/div.

also, Nu is given approximately by

$$Nu = a + bR_e^{1/2} \tag{D3}$$

where

$$R_e = \frac{\rho u d}{\mu} \tag{D4}$$

and where

ρ = fluid density

u = velocity past wire

d = wire diameter

μ = fluid viscosity

a = constant = 0.39

b = constant = 0.50

Freymuth defines U as the bridge voltage; hence U is the sum of the wire voltage IR and the voltage across the wire series resistor IR_3. The ratio R_3/R is called m. Then Freymuth gives the bridge noise output for a constant temperature anemometer system as

$$\Delta U_N = \frac{(1 + m)^3(1 + 1/m)}{2\alpha R_o} \left(\frac{R}{U}\right)^2 \omega c e_t \tag{D5}$$

Freymuth defines e_t as the noise generated by the bridge resistances and by the equivalent resistance of the anemometer amplifier. His ω is the bandwidth and c is the wire heat content, which may be written as

$$c = \rho_w c_w a_w \ell \tag{D6}$$

where $\rho_w c_w$ is the wire heat capacity per unit temperature and volume, and a_w is the wire cross sectional area $\pi d^2/4$. Then with a little manipulation we can write the noise level as

$$\Delta U_N = \frac{(1 + m)(1 + 1/m)}{2\pi k Nu} \left(\frac{R}{R - R_o}\right) \omega e_w \rho_w c_w e_t \tag{D7}$$

204

The aspirating probe is built with a sonic orifice just downstream of the wire so that the wire Mach number M remains constant. When a pressure wave of amplitude Δp hits the probe, changes are transmitted with the speed of sound past the wire and into the sonic orifice. For a sonic boom the changes across the shock wave are essentially isentropic so that

$$\frac{\partial T}{\partial p} = \frac{\gamma - 1}{\gamma} \left(\frac{T}{p}\right) \tag{D8}$$

$$\frac{\partial \rho}{\partial T} = \frac{1}{\gamma - 1} \left(\frac{\rho}{T}\right) \tag{D9}$$

$$\frac{\partial a_o}{\partial T} = \frac{1}{2} \left(\frac{a_o}{T}\right) \tag{D10}$$

where γ is the gas constant 1.4 for air, a_o is the speed of sound, p is the pressure, and T is the air temperature. Also, from Reference 12,

$$\frac{\partial \mu}{\partial T} = 0.76 \left(\frac{\mu}{T}\right) \tag{D11}$$

$$\frac{\partial k}{\partial T} = 0.80 \left(\frac{k}{T}\right) \tag{D12}$$

When a pressure wave passes the wire, changes occur in k, Nu, and T_R. Hence, from equation (D1)

$$\frac{dQ}{dT_R} = \pi \ell (T_w - T_R) Nu \frac{\partial k}{\partial T_R} - \pi k \ell Nu + \pi k \ell (T_w - T_R) \frac{\partial Nu}{\partial T_R} \tag{D13}$$

Since k is evaluated at the film temperature, $1/2(T_w + T_R)$,

$$\frac{\partial k}{\partial T_R} = \frac{1.60k}{T_w + T_o} \tag{D14}$$

also

$$\frac{\partial \mu}{\partial T_R} = \frac{1.52\mu}{T_w + T_o} \tag{D15}$$

and

$$u = Ma_o \tag{D16}$$

and

$$\frac{\partial Nu}{\partial T_R} = \frac{b}{2R_e^{1/2}}\left(\frac{\partial R_e}{\partial T_R}\right) \tag{D17}$$

$$\frac{\partial R_e}{\partial T_R} = \frac{R_e}{T_R}\left(\frac{T_R}{\rho}\frac{\partial \rho}{\partial T_R} + \frac{T_R}{a_o}\frac{\partial a_o}{\partial T_R} - \frac{T_R}{\mu}\frac{\partial \mu}{\partial T_R}\right) \tag{D18}$$

by putting together equations (D9) through (D18) we get, for air,

$$\frac{dQ}{dT_R} = -\pi k\ell Nu' \tag{D19}$$

where

$$Nu' = \left\{a + bR_e^{1/2}\left[1 - 1.60\left(\frac{T_w - T_R}{T_w + T_R}\right)\right] - bR_e^{1/2}\left[1.50\left(\frac{T_w - T_R}{T_R}\right) - 0.76\left(\frac{T_w - T_R}{T_w + T_R}\right)\right]\right\} \tag{D20}$$

Now, the change in bridge voltage U caused by a pressure change Δp is

$$\Delta U_S = \frac{dU}{dQ} \cdot \frac{dQ}{dT_R} \cdot \frac{dT_R}{dp}\Delta p \tag{D21}$$

and

$$\frac{dU}{dQ} = \frac{1 + m}{2I} \tag{D22}$$

$$I = \left[\frac{\pi k\ell(R - R_o)Nu}{\alpha R_o R}\right]^{1/2} \tag{D23}$$

and R_o can be written as

$$R_o = \frac{4\sigma_o\ell}{\pi d^2} \tag{D24}$$

where σ_o is the wire resistivity.

Then by substituting equations (D23) and (D24) into (D22), and (D8), (D19), and (D22) into (D21), we obtain

$$\Delta U_S = \left(\frac{1 - \gamma}{\gamma}\right)(1 + m)\left[\frac{\alpha\sigma_o Rk}{(R - R_o)Nu}\right]^{1/2}\left(\frac{\ell}{d}\right)\left(\frac{T_R}{p}\right)Nu'\Delta p \tag{D25}$$

Finally, taking equations (D7) and (D25) to form the signal-to-noise ratio, we get

$$N_{CT} = \frac{\Delta U_S}{\Delta U_N} = \frac{8(1-\gamma)}{\gamma(1+1/m)} \left[\frac{\alpha \sigma_o k^3 (R-R_o)\text{M}_1}{R}\right]^{1/2} \left(\frac{\ell}{d^3}\right)\left(\frac{T_R}{p}\right) \frac{\text{Nu}'\Delta p}{\omega \rho_w c_w e_t} \qquad \text{(D26)}$$

In the above equations a key parameter is Nu', which changes sign as a function of the wire temperature T_w. In Reference 9 it was assumed that T_w should be small so that Nu' was near its maximum positive value. Later it was found that N_{CT} could be greatly improved by increasing T_w to the highest possible temperature so that Nu' becomes negative. A numerical example will be helpful. Let $d = 100 \times 10^{-6}$ inches, $\ell = 0.033$ inches, use 90 percent Pt 10 percent Rh wire so that $R_o = 30.5$ ohms and $\alpha = 0.0017/^\circ K$, $M = 0.3$, $T_R = 300^\circ K$. Then $R_e = 16.8$, $bR_e^{1/2} = 2.07$, and Nu = 2.46.

Nu' will reach a positive maximum value of about 1.25 near $T_w = 400^\circ K$, Nu' will pass through 0 near $T_w = 500^\circ K$, and Nu' will be -3.9 at $900^\circ K$. For $T_w = 900^\circ K$, $R/R_o = 2.06$. Let the bandwidth be 500 kilohertz and m = 3.2. For a TSI 1050 anemometer e_t can be shown to be about 1.4×10^{-6} volts. Then $\omega \rho_w c_w e_t = 218$ joules volts/$^\circ$K sec. in.^{3}. Also, $k = 7 \times 10^{-4}$ watts/in.$^\circ$K. Then for the 0.460 caliber bullet, $\Delta p = 0.28$ psi and $\Delta U_S = 23 \times 10^{-3}$ volts. ΔU_N is 1.9×10^{-3} volts rms so that the signal-to-noise ratio is 12.

Results in reasonable agreement with the above calculations are shown in figures D1b, D1c, and D1d where the parameter R/R_o was 1.54, 1.64, and 1.79, respectively. In all three cases the custom-built probe 523 was used with a 100×10^{-6} inch diameter 90 percent Pt 10 percent Rh wire of resistance $R_o = 33$ ohms. The calculated values of T_w for the three cases are 618, 676, and $764^\circ K$, respectively. A fourth case was tried with $R/R_o = 1.17$. This resulted in a small negative N-wave shape, whereas the other three signatures show a positive and progressively-increasing amplitude as T_w is increased. These signature shapes are similar to those taken by microphones shown in figures D1a and D1d. The vertical scale on the aspirating probe pictures corresponds to a bridge output of 14×10^{-3} volts/division. This combination was obtained with a TSI model 1057 signal conditioner used in the 100X amplification mode to amplify the bridge signal. The amplified signal was fed into a Tektronix 555 oscilloscope set at one volt/division and shunted with a 50 ohm resistor.

207

The resistor reduced the amplification factor to 71. As a result, the N-wave amplitude of about 1.4 divisions on figure D1d corresponds to $\Delta U_S = 20 \times 10^{-3}$ volts, in reasonable agreement with the above calculations which were done for a somewhat different value of ℓ, m, R/R_o, and T_w. If the calculations are corrected for these parameters, we find $\Delta U_S = 16 \times 10^{-3}$ volts, in very good agreement with the measured 20×10^{-3} volts. The calculations assume that the flow past the wire is at M = 0.3; this, in practice, depends on the aspirating probe nozzle geometry. Since the nozzle cross section dimensions are very small — of the order of 0.030 inches — and since the nozzle dimensions could not be measured accurately during the probe construction, the experimental value of M at the wire could easily have been sufficient to result in the above difference between calculation and experiment.

The noise on figures D1b, D1c, and D1d has a peak-to-peak amplitude of about 0.25 division; the corresponding rms value is estimated to be 0.07 division which corresponds to a noise level of 1×10^{-3} volts rms. This is substantially less then the calculated value of 1.9×10^{-3} volts rms; the reason is probably because the bandwidth may have been substantially less than 500 kilohertz as assumed in the calculation. The bandwidth was not measured, but it was inferred from the process used in trimming the anemometer for good frequency response.

In figure D1e a somewhat ragged signature taken with probe 522 is shown. In this case d was again 100×10^{-6} inches, R_o was 27.5 ohms, and $R/R_o = 1.96$. This was taken near the upper limit on R/R_o, this limit is estimated to be near 2.1 because of wire burnout. Some wires were operated at R/R_o above 2.0, but no signatures were taken. The raggedness of the above signature was evidently the result of some leakage in the probe hose connection to the vacuum pump, which resulted in the probe orifice being subsonic.

In figure D1f is shown, a signature measured with probe 522 using a wire diameter of 50×10^{-6} inches and an oscilloscope sensitivity of 2 volts/division. Here R_o was 116 ohms and $R/R_o = 1.66$. Apparently ΔU is decreased from that given by the larger wires. Unfortunately the wire was broken before another shot could be made at a more appropriate value of oscilloscope sensitivity. According to equations (D7), (D25), and (D26), the smaller wire should result in a smaller noise level, a somewhat smaller signal, and a larger signal-to-noise ratio than with the 100×10^{-6} inch diameter wire.

208

The factor m in equations (D7), (D25), and (D26) varied with wire diameter inasmuch as R_3 remained fixed whereas R varied with wire diameter. For the experiments R_3 was 110 ohms. According to equation (D25), when d was decreased from 100×10^{-6} to 50×10^{-6} inches, ΔU_S was decreased by about 30 percent because of changes in m, Nu, and Nu' which overcame the factor of 2 increase in ℓ/d. A comparison of figures D1c and D1f seems to confirm this. (Recall that figure D1f has only half the amplitude of figure D1c for the same bridge voltage.) On the other hand, because of the factor (ℓ/d^3) in equation (D26) for N_{CT}, the change to the smaller wire size should increase N_{CT} by a factor of about 3. In practice some of this increase may be lost because of electrical noise picked up from such things as nearby radio stations. Therefore, the upper limits of the aspirating probe performance will require further research.

A persistent problem in the probe development was the lack of the capability of the TSI 1050 anemometer to be properly trimmed for the aspirating probes. This is illustrated in figure D2. In (a) is shown the proper anemometer response to a square wave input. The time τ is a measure of the upper limit of the system frequency response. In (b) is shown the closest to optimum that could be obtained using a 70×10^{-6} inch wire at $R/R_o = 1.50$. Part (c) shows that an almost proper response curve could be obtained with a 100×10^{-6} inch wire at $R/R_o = 1.47$, but when this was increased to 1.69 the overshoot again appeared as shown in (d). Increasing R/R_o to 2.00 made the overshoot worse, whereas decreasing R/R_o sufficiently always eliminated the problem. The difficulty was that reducing R/R_o reduced Nu' with a resulting large decrease in signal-to-noise ratio N_{CT}.

When probes 1440E and 1440F were ordered from TSI, the two TSI 1050 anemometer units were shipped to TSI for a change in the resistors R_3 of bridge 1 from 40 to 200 ohms. This resulted in a favorable increase in the parameter m by a factor of 5. The anemometer was then trimmed by TSI for proper operation at $R/R_o = 1.15$ as first suggested by Reference 9. Later the writer discovered the much greater N_{CT} available at $R/R_o = 1.50$ and above, but this brought along the overshoot problem. The problem was partially solved by the writer by decreasing R_3 to 110 ohms and certain other circuit modifications after consultation with TSI personnel. The best that could be

(a) PROPER RESPONSE TO THE SQUARE WAVE TEST (AMPLITUDE DEPENDS ON AMPLITUDE OF SQUARE WAVE INPUT)

(b) RESPONSE CURVE USING 70 MICROINCH WIRE ON PROBE 523 WITH $R/R_O = 1.50$

(c) RESPONSE CURVE USING 100 MICROINCH WIRE ON PROBE 522 WITH $R/R_O = 1.47$

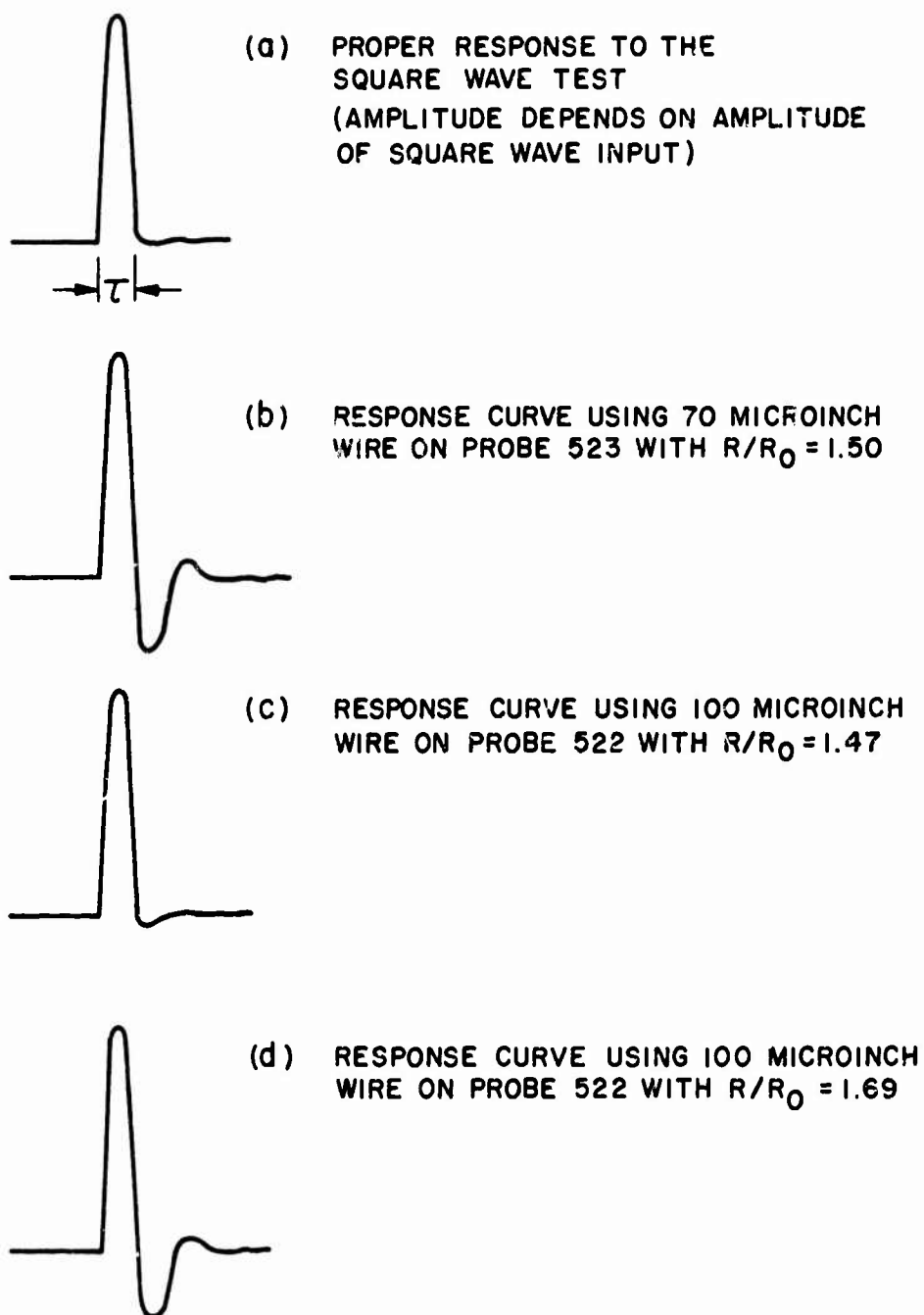(d) RESPONSE CURVE USING 100 MICROINCH WIRE ON PROBE 522 WITH $R/R_O = 1.69$

Figure D2 Oscilloscope patterns showing the response of the anemometer system to a square wave input.

accomplished is shown in figure D2. However, according to Freymuth (References 10 and 11), it is always possible to modify the circuit parameters so as to eliminate the overshoot problem. It is the writer's opinion that this cannot be done without some redesign of the TSI 1050 anemometer circuits for this specific job. It is pertinent to note that the standard sensors available from TSI have a cold resistance of the order of 10 ohms or less as compared to the 30 ohms to 120 ohms of the aspirating probes discussed here.

It may be noted that the overshoot problem is apparent in figures D1c and D1d and even more apparent in figure D1f. Figure D1b, which has the smallest R/R_o and the large wire, does not have the overshoot problem.

The time constant τ defined in figure D2 was of the order of 2 to 3 microseconds for the probes of figure D2, but about one microsecond should be subtracted from these figures for the finite rise times of the square-wave generator and the 500 kilohertz oscilloscope used for the tests. Thus, τ was only 1 to 2 microseconds. According to Freymuth, this corresponds to a system frequency response of 360 to 700 kilohertz. Because of lack of precision in the measurements, the 700 kilohertz is viewed with suspicion. About 500 kilohertz seems to be the upper limit.

The large frequency response of the aspirating probes can be confirmed by a careful inspection of figure D1. The time τ_1 required for the traces to jump to 2/3 full amplitude is only about 2 microseconds for the aspirating probes as compared to 5 microseconds for the microphones.

Figure D1g shows a signature taken using probe 523 with the 24-inch jet nozzle turned on to a speed of 80 feet/sec. The figure shows that the jet interacted with the aspirating probe to produce apparent pressure fluctuations before the arrival of the sonic boom. This interaction was confirmed for several different aspirating probes. Such an interaction phenomena was anticipated and was expected to have an amplitude of the order of only 0.5×10^{-3} volts. Instead the rms value of the fluctuations was of the order of 10×10^{-3} volts, or the same order as the boom N-wave signature. Because this problem could not be solved, and because of the much greater reliability and much lower noise level of the microphones, the boom experiments were run using the microphones rather than the aspirating probes.

211

It is the writer's belief that it is possible to develop the aspirating probe into a useful instrument by performing the following tasks:

1. The overshoot problem should be eliminated by redesign of the anemometer unit.

2. The jet interaction problem should be overcome by shielding the probe with a microscopic jet of laminar air or nitrogen gas.

3. The problem of wire breakage through ingestion of small particles should be solved by using the above laminar jet.

4. Wires smaller than 100×10^{-6} inches should be used for optimum signal-to-noise ratio.